LONDON'S GLOBAL UNIVERSITY

Development of Tethered Aligned Engineered Neural Tissue Containing Elongated Neurons for Peripheral Nerve Regeneration

Titinun Suannun

Thesis submitted in fulfilment of the requirements
for the degree of
Doctor of Philosophy

Eastman Dental Institute
University College London

March 2022

Declaration

I, Titinun Suannun, confirm that the work presented in this thesis is my own. Where information has been derived from other sources, I confirm that this has been indicated in the thesis.

Signed: _____

Date: _____

Acknowledgements

This research has been financially supported by the Royal Thai Government Scholarship Program offered by the Ministry of Science, Thailand. I gratefully acknowledge the use of the services and facilities of the Biomaterials and Tissue Engineering Department at UCL Eastman Dental Institute and School of Pharmacy.

All the experiments and analysis are made possible through a lot of help from my colleagues in James Phillips's Lab group, who provided inside the expertise that greatly assisted the research. The specialist microsurgery was performed by Dr Victoria Roberton, who carried out the guidance conduit transplantation into rat sciatic nerve and assisted me on nerve tissue harvesting. The SEM imaging was assisted by Dr Nicola Morden at Eastman Dental Institute. The DMA compression test was assisted by Despoina Eleftheriadou with a DMA hydrogel-specified protocol developed by Dr Richard Bartlett. The induction of neural cell culture and hydrogel techniques during the first year of this project were technically guided by Dr Caitriona O'Rourke. The 3D printer and materials were provided by UCL Institute of Making with tool training and guidance from technicians at the workshop.

I would like to express my sincere gratitude to Prof Jonathan Knowles, my secondary supervisor, for providing useful comments during our discussions and helping me solve some technical problems regarding the department facilities. Also, thank Dr Rachel Leeson for every documentary support and valuable encouragement during my writing up period.

My deep appreciation goes out to Dr James Phillips, my primary supervisor, the best supervisor I have ever met, who has been supporting me academically and emotionally since I started contacting him for pursuing my PhD degree a year before my research started. Without his thorough expertise, dedicated supervisory, and kind understanding, I could have not deal with many research difficulties and overcome the stress from the works.

Most importantly, I would like to express a heartfelt thank you to my family in Thailand, who always believe in me and encourage me to follow my passion. Thank dad and mom for taking care of me like the luckiest girl in the world. Thank Por and Parn for always being by my side and growing up together gracefully. Thank grandparents for staying healthy to see my success. I will never stop making all of you proud.

Thank you, all my supportive friends, for all the good memories in UK. 4 years in London was a very precious time that gave me many life-changing lessons.

Thank you, J, for coming at the right time and making everything better.

And finally, thank you to myself. You have been through lots of challenges and become a big girl. You did a great job! Be true to yourself, keep going, and trust the process.

Publications

Conference Proceedings:

SUANNUN, T., KNOWLES, J.C., PHILLIPS, J.B. (2019) Interaction between Exogenous and Endogenous Glial Cells in Engineered Neural Tissue. 5th International Symposium of Peripheral Nerve Regeneration, Porto (Portugal).

SUANNUN, T., KNOWLES, J.C., PHILLIPS, J.B. (2018) Development of Engineered Neural Tissue Containing Elongated Neurons for Peripheral Nerve Regeneration. UCL Neuroscience Symposium, London (UK).

SUANNUN, T., KNOWLES, J.C., PHILLIPS, J.B. (2017) Development of Engineered Neural Tissue Containing Elongated Neurons Supported by Aligned Glia for Peripheral Nerve Regeneration. 4th International Symposium of Peripheral Nerve Regeneration, Barcelona (Spain).

SUANNUN, T., KNOWLES, J.C., PHILLIPS, J.B. (2017) Development of Engineered Neural Tissue Containing Elongated Neurons for Peripheral Nerve Regeneration. European Chapter Meeting of the Tissue Engineering and Regenerative Medicine International Society, Davos (Switzerland).

Abstract

Following peripheral nerve injury, the axons in the distal nerve between the injury site and the muscle degenerate. When the injured site is very proximal, functional recovery from nerve repair is a clinical challenge since neuronal regeneration rate is limited, resulting in muscle atrophy due to the delay in reinnervation, even where the 'gold standard' autograft is used. Much research focuses on developing biomaterial scaffolds that mimic the autograft and promote host neurite regeneration from proximal to distal stump, whereas here, we aim to improve long distance repair by populating constructs with functional neurons and glial cells. With an engineered living scaffold populated with neurons exhibiting long neurite extensions supported by glial cells, the gap between proximal stump and muscle could potentially be reconnected promptly once the challenge of integration is overcome.

To test the concept, a method was developed using tethered aligned engineered neural tissue (TaeNT) formed from simultaneous self-alignment of Schwann cells and collagen fibrils in a fully-hydrated tethered gel resulting in an anisotropic tissue-like structure. The *in vitro* results showed neurite elongation and alignment in the co-culture of neurons and Schwann cells in TaeNT, indicating that TaeNT could be an appropriate substrate for growing long neurites with a view to generating therapeutic constructs containing long functional neurons. The implantation of TaeNT containing neurons and Schwann cells in a 10mm-gap rat sciatic nerve for 3 weeks provided information about host-transplant cell interaction including Schwann cell migration and alignment inside the conduit, and neurite elongation across the conduit interface. Furthermore, in an attempt to induce longer neurite growth, TaeNT was proposed as a substrate that could be combined with mechanical tension application using a 3D-printed mould developed to stretch the cellular gels in a controlled manner. A series of newly designed protocols for mechanical tension application to induce growth response for enhanced neural regeneration was developed and discussed correspondingly.

In summary, the findings represent the development and investigation of the regenerative potential for engineered living scaffolds containing neurons and Schwann cells suitable for stretch-growth to provide an elongated functional nerve graft. With a view to translation for clinical use, investigating the source of therapeutic cells in the conduit and the functional integration of host and transplanted cells is an important step towards optimising the regenerative potential of the engineered living scaffold.

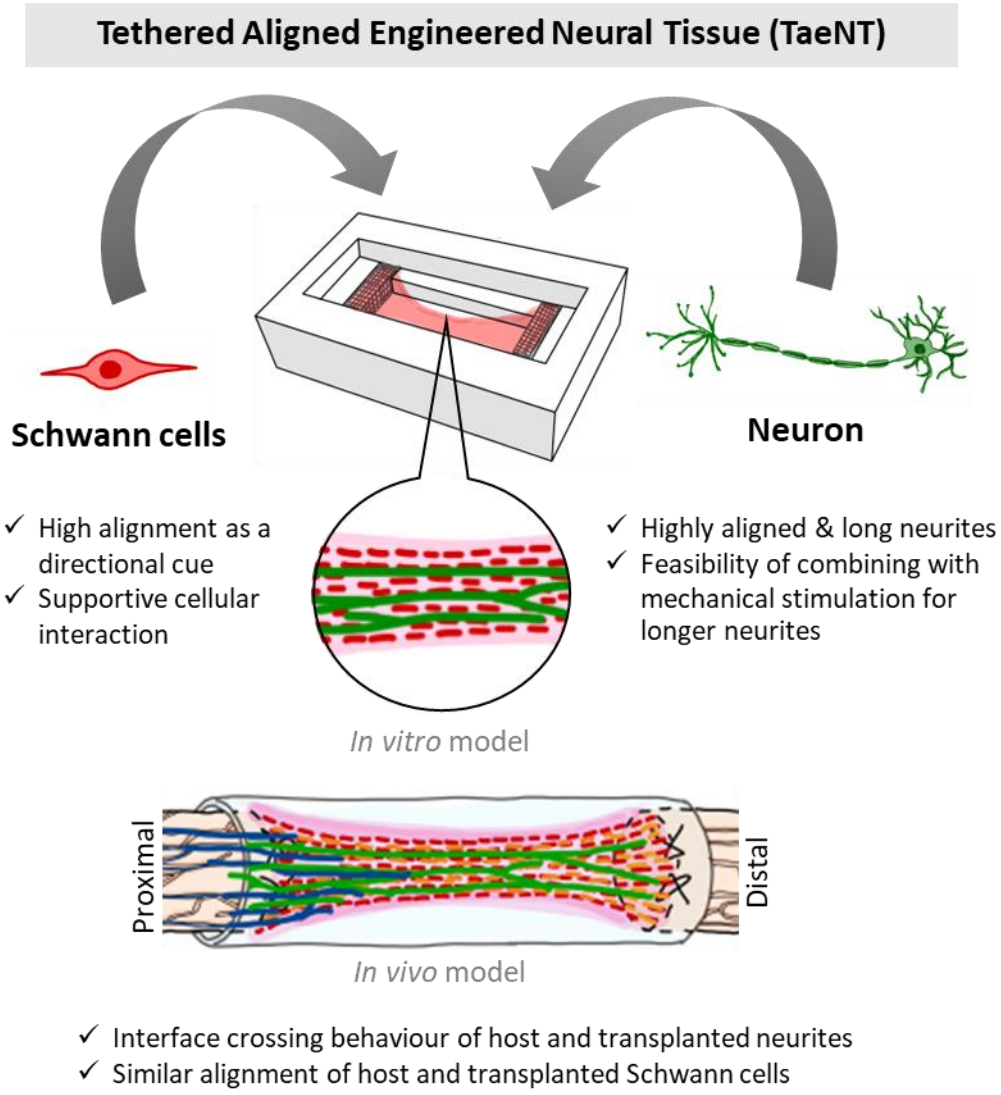

Figure 1 Summary of key findings on Tethered Aligned Engineered Neural Tissue (TaeNT) in the project.

Impact Statement

Traumatic peripheral nerve injury occurs when the injured site is very proximal, leaving a long distance from proximal stump to muscle to regenerate, resulting in muscle atrophy due to the delay in reinnervation, even where the 'gold standard' autograft is used. According to NHS England, traumatic peripheral nerve injury can lead to long-term disability, subsequent sick leave, and permanent disability pension. It also collectively affects the Gross Domestic Product (GDP) as the patients are often young adults at the peak of their employment productivity. The transplantation of nerve guidance conduit in patients would be an alternative treatment to improve the regeneration by reducing time for functional recovery and risk of muscle atrophy. Consequently, it would improve the quality of life for patients in the long term.

This research project was mainly focused on proposing a tethered aligned engineered neural tissue (TaeNT) as an alternative therapeutic strategy to improve functional recovery after long-distance peripheral nerve injury. The construct is intended to be an "off-the-shelf" transplanted construct populated with glial cells and neurons with elongated neurites. The initial development and investigation of TaeNT in this project reflect its potential in supporting nerve regeneration. Further research, including protocol optimisation, construct preservation, and functional integration analysis, are expected to push the TaeNT toward clinical use.

The study on TaeNT utilised multidisciplinary approaches from various fields, including cell biology, mechanical engineering, 3D material fabrication, biomaterials, and tissue engineering. The research brought about benefits inside academia by providing a better understanding of the transplantation of engineered neural tissue in peripheral nerves. TaeNT was used as a substrate to examine cell behaviour and interface integration. The results from this project filled the gap in previous literature both *in vivo* and *in vitro* about the interaction between host and transplanted cells during nerve regeneration. Understanding the interaction of host cells and transplanted cells is

essential for tissue engineering as it can guide us toward designing potential therapeutic options to improve peripheral nerve regeneration.

Besides, TaeNT with aligned Schwann cells and neurons was proposed as a 3D cellular hydrogel-based substrate to support mechanical tension application. The use of the fully-hydrated hydrogel system is beneficial in cell stretching approaches, providing a more natural tissue-like environment than monolayer systems and helping to retain cells and support cell viability. The stretching protocols for neurite elongation developed in this project were easy to set up and cost-reducing by minimising manufactured components. All aspects of the protocols are available in a typical cell culture laboratory enabling adoption and reproduction by other research groups, and suitable for future scale-up in a commercial or healthcare environment.

Abbreviations

2D	2-dimensional
3D	3-dimensional
ADSCs	Adipose-derived stem cells
Ara-C	Cytosine arabinoside
ATMPs	Advanced therapy medicinal products
BDGF	Brain-derived growth factor
bFGF	Basic fibroblast growth factor
cAMP	Cyclic adenosine monophosphate
CFM	Culture force monitor
CNS	Central nervous system
COX	Cyclooxygenase
dADSCs	Differentiated adipose-derived stem cells
DD	Distal device
DMA	Dynamic mechanical analysis
DMEM	Dulbecco’s modified eagle medium
DMSO	Dimethyl sulfoxide
DN	Distal nerve
DPS	Daedal positioning system
DRG	Dorsal root ganglion
ECM	Extracellular matrix
EGF	Epidermal growth factor
EngNT	Engineered neural tissue
FACS	Fluorescence activated cell sorting
FBS	Fetal bovine serum
FCS	Fetal calf serum
FDA	US Food and drug administration
GDNF	Glial cell-derived neurotrophic factor

GFAP	Glial fibrillary acidic protein
GFP	Green fluorescent protein
MACS	Magnetic-activated cell sorting
MAPs	Microtubule-associated proteins
MEM	Micro-electromechanical systems
Micro-TENNs	Micro-tissue engineered neural networks
NCAM	Neural cell adhesion molecule
NGF	Nerve growth factor
NHS	National Health Service
NMJ	Neuromuscular junction
NSCs	Neural stem cells
NT-3, NT-4	Neurotrophin-3, Neurotrophin-4
P/S	Penicillin and streptomycin
PBS	Phosphate-buffered saline
PCL	Polycaprolactone
PD	Proximal device
PDL	Poly-D-lysine
PDMS	Polydimethylsiloxane
PFA	Paraformaldehyde
PGA	Polyglycolide or poly(glycolic acid)
PGE2	Prostaglandin E2
PHB	Polyhydroxybutyrate
PLA	Polylactic Acid
PLGA	Poly(lactic-co-glycolic acid)
PLL	Poly-L-lysine
PN	Proximal nerve
PNS	Peripheral nervous system
PSCs	Perisynaptic Schwann cells

RA	Retinoic acid
RPNI	Regenerative Peripheral Nerve Interface
SCs	Schwann cells
SEM	Scanning electron microscope
Shh	Sonic hedgehog
TaeNT	Tethered aligned engineered neural tissue
TE	Trypsin/EDTA solution
TENGs	Tissue engineered nerve grafts
TMC/CL	Trimethylenecarbonate-co-epsilon-caprolactone

Contents

Index of Figures

CHAPTER 3

CHAPTER 4

CHAPTER 5

Index of Tables

CHAPTER 1

Introduction

1.1 Peripheral Nervous System

The nervous system is a highly complex part of an animal that coordinates to control, regulate, and communicate with all the parts of the body. In vertebrates, it can be functionally divided into two connecting systems: the central nervous system (CNS) and the peripheral nervous system (PNS). While the CNS, consisting of the brain and spinal cord, is mainly responsible for integrating and processing information, the PNS refers to parts of the nervous system outside the brain and spinal cord that communicate with the CNS by relaying signals back and forth from external stimuli and all parts of the body.

The peripheral nervous system can be divided into a sensory (afferent) division and a motor (efferent) division corresponding to the main function of each division. The sensory division connects sensory organs to the CNS, while the motor division connects the CNS to muscles and glands. The motor division is responsible for both the voluntary responses for the somatic nervous system, and the involuntary (visceral) responses for sympathetic and parasympathetic nervous systems.

In the human body, 12 pairs of cranial nerves from the brain and 31 pairs of spinal nerves from spinal cord segments connect the nervous system with other parts of the body (Figure 1.1). The longest nerve in the human body is the sciatic nerve which elongates from the lumbar region of the spine with branches leading to the tip of the toes. The length of the sciatic nerve and its branches in an average adult can be more than a metre.

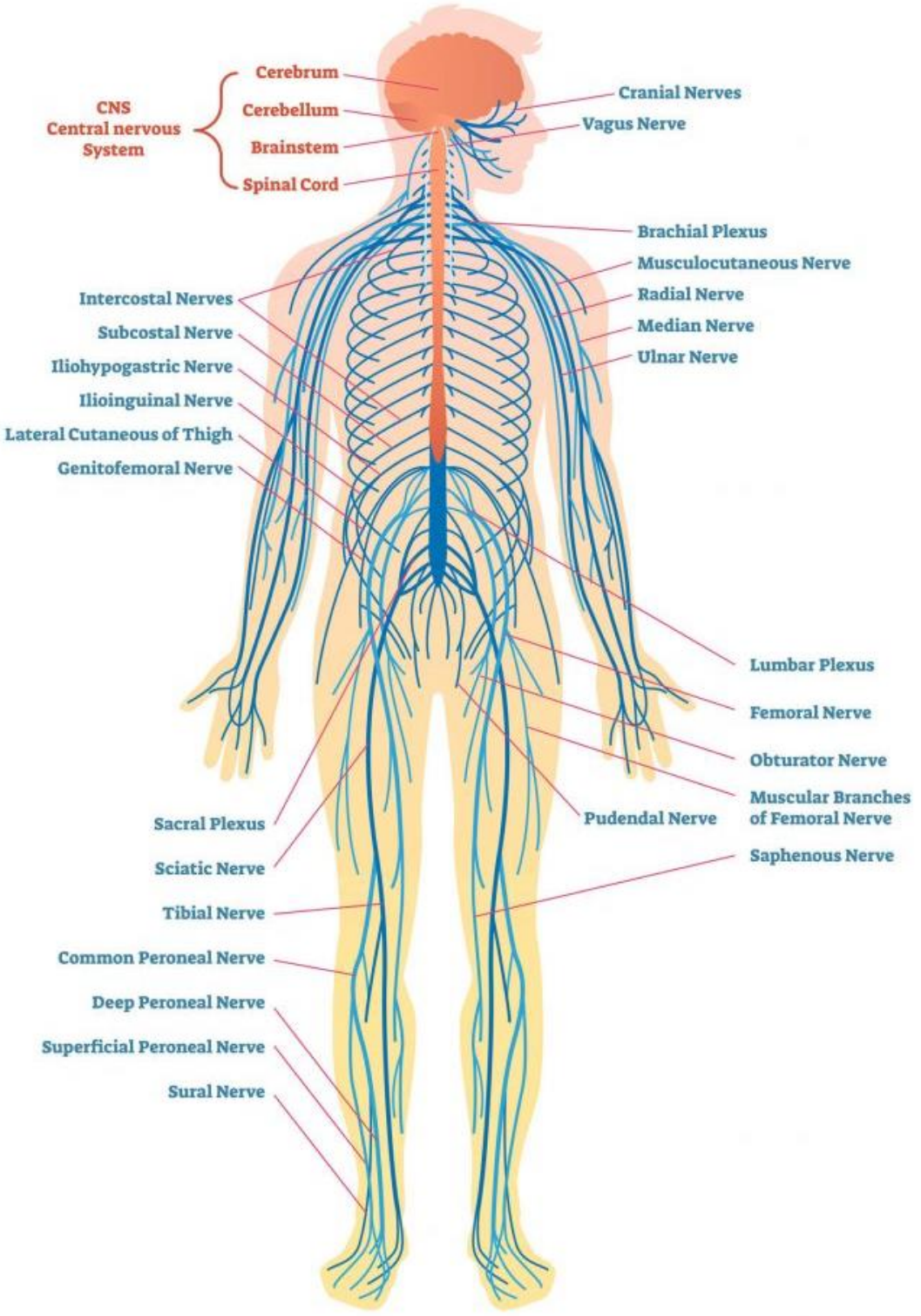

Figure 1.1 Nerves in the human body coordinating to communicate with all parts of the body. *It consists of cranial nerves from the brain and spinal nerves from the spinal cord (VectorMine/Depositphotos.com, 2018).*

Anatomically, the peripheral nerve structure is a bundle of fascicles consisting of many nerve fibres surrounded by connective tissue (Figure 1.2). An individual nerve fibre is covered with the layer of connective tissue called Endoneurium, and bundled together into a fascicle. The fascicle is wrapped with Perineurium. In the outermost layer, many fascicles are bundled and entirely coated with Epineurium which provides mechanical protection to nerve fibres. The area between fascicles and Epineurium layers has some blood vessels penetrating longitudinally along the nerve.

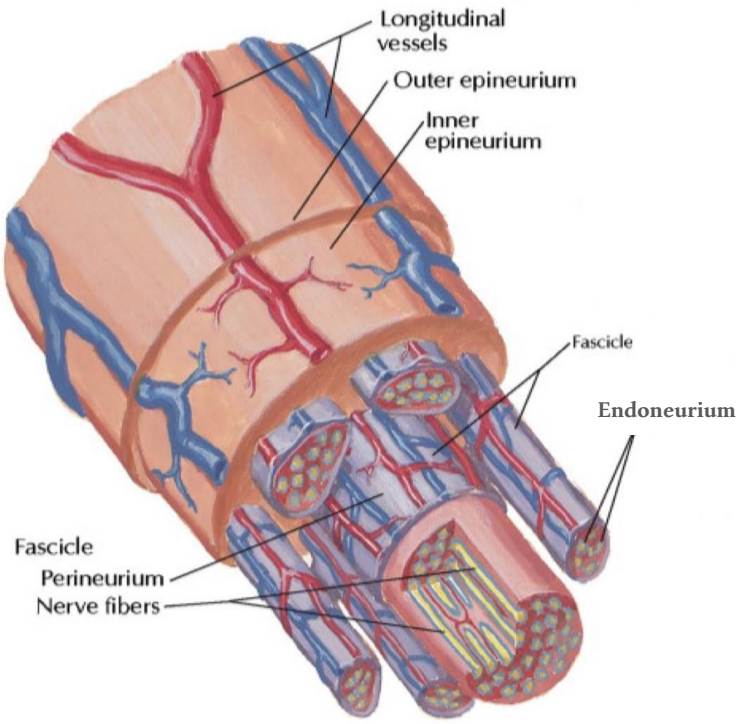

Figure 1.2 Peripheral nerve anatomy. *Fascicle bundle structure consists of many nerve fibres coated with connective tissue sheath: Endoneurium, Perineurium, and Epineurium (Thompson, 2016).*

1.1.1 Neurons

Neurons are the fundamental units of the nervous system which receive and transmit chemical and electrical signals between the system and the body. The signal transmission allows the brain to receive information from the external world and send signals to the target cells for the desired function (e.g., muscle movement). The electrical signals in neurons are regulated by the concentration balance of Sodium ions (Na+) and Potassium ions (K+) across the cell membrane. When the stimuli depolarise the ion concentrations and the signal reaches the threshold, an action potential occurs as the signal can pass along the nerve fibre, allowing cell communication.

The individual nerve fibres can be myelinated or unmyelinated. In PNS, myelin sheath is an extended and modified double-bilayer plasma membrane wrapping around the outer surface of some axons in a spiral fashion with periodic gaps called nodes of Ranvier (Liu et al., 2019). The myelin sheath functions as an insulation to minimise the dissipation of the electrical signal travelling along the axon. The transmitting electrical signal can travel along the axon by jumping from node to node resulting in the increasing speed of the signal conduction. In PNS, approximately 80% of motor axons are myelinated to accelerate signal transmission, enabling long-distance communication (Mackinnon, 1989).

There are 2 types of neurons in PNS with distinct functions: sensory neurons and motor neurons (Figure 1.3). The typical structure of sensory neurons is pseudo unipolar, as most of them have one axon that branches into two extensions. The sensory neurons receive information from internal organs or external stimuli through the receptor ending and convert it into an action potential which is then transmitted to the CNS. The cell body of motor neurons is located in the CNS with the neurites elongating into the PNS. Motor neurons are associated with the somatic nervous system controlling skeletal muscles, or the autonomic nervous system controlling involuntary muscles (e.g., smooth muscle and cardiac muscle). The typical structure of motor neurons is multipolar.

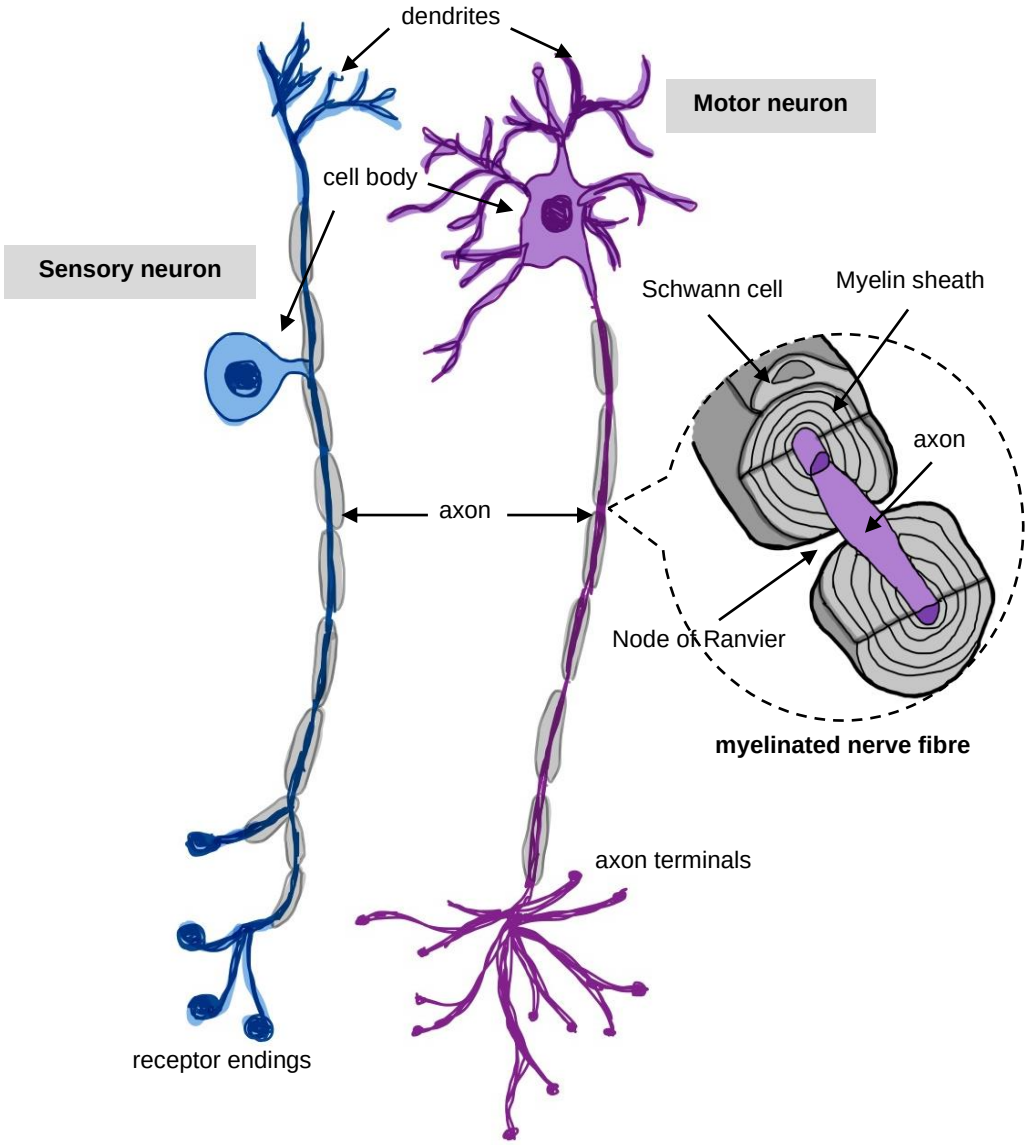

Figure 1.3 Sensory and motor neurons. *A sensory neuron receives the signal from external stimuli via receptor endings while a motor neuron sends the signal from CNS to target cells via axon terminals. Approximately 80% of motor axons are myelinated.*

1.1.2 Schwann cells

The Schwann cell is a type of glial cell in the PNS that plays an important role in neuronal survival and axon maintenance. Physical contact and communication between Schwann cells and adjacent axons influence each other in regulating development, function, and maintenance. For example, Schwann cells secrete several essential neurotrophins, such as brain-derived neural growth factor (BDGF), neurotrophins 3 and 4 (NT-3, NT-4), to support the survival of axotomised neurons (Birling and Price, 1995, Fu and Gordon, 1997, Raivich and Kreutzberg, 1993) and axon elongation (Davies, 2000). Furthermore, defects in Schwann cell development lead to sensory and motor neuron degeneration and neuromuscular junction defects (Kramer et al., 1996, Meyer et al., 1997, Wolpowitz et al., 2000).

There are four classes of Schwann cells found in different sites in the mature nervous system: myelinating Schwann cells, non-myelinating Schwann cells, perisynaptic or terminal Schwann cells, and satellite cells of peripheral ganglia (Corfas et al., 2004). Myelinating Schwann cells produce the myelin sheaths that surround axons of both sensory and motor neurons to increase electrical insulation and consequently accelerate neuronal signal transmission. Non-myelinating Schwann cells are involved in non-myelinated axon maintenance and wrap around axons to form Remak bundles. The other classes of Schwann cells are perisynaptic Schwann cells which cover the pre-synaptic terminal of motor axons at the neuromuscular junctions, and satellite cells which cover neurons in the sensory, sympathetic and parasympathetic ganglia. In peripheral nerve regeneration, myelinating Schwann cells and non-myelinating Schwann cells play an important role in responding to peripheral nerve injury by facilitating the inflammatory response and guiding axon elongation (Bhatheja and Field, 2006). The role of Schwann cells in peripheral nerve regeneration will be explained more extensively in Section 1.3.1.

1.1.3 Interconnection between neurons and muscle

Axons from motor neurons are structurally and functionally connected with skeletal muscle fibres through chemical synapses, called neuromuscular junctions. The neuron sending the signal and the stimulated muscle fibres are referred to as a pre-synaptic cell and post-synaptic cell, respectively. In synaptic transmission, neurotransmitter molecules are released from the pre-synaptic cell into the synapse and subsequently bind to specific receptors at post-synaptic cell membrane to stimulate muscle contraction for voluntary movement. The release of neurotransmitter molecules from pre-synaptic cells is triggered by the increase of local calcium ion concentration at the pre-synaptic active zone after the opening of voltage-gated calcium ion channels caused by the arrival of an action potential (Glitsch, 2008, Sudhof, 2012). Without signal transmission through neuromuscular junctions, there is no communication between the motor neuron and muscle; thus, the muscle loses its function.

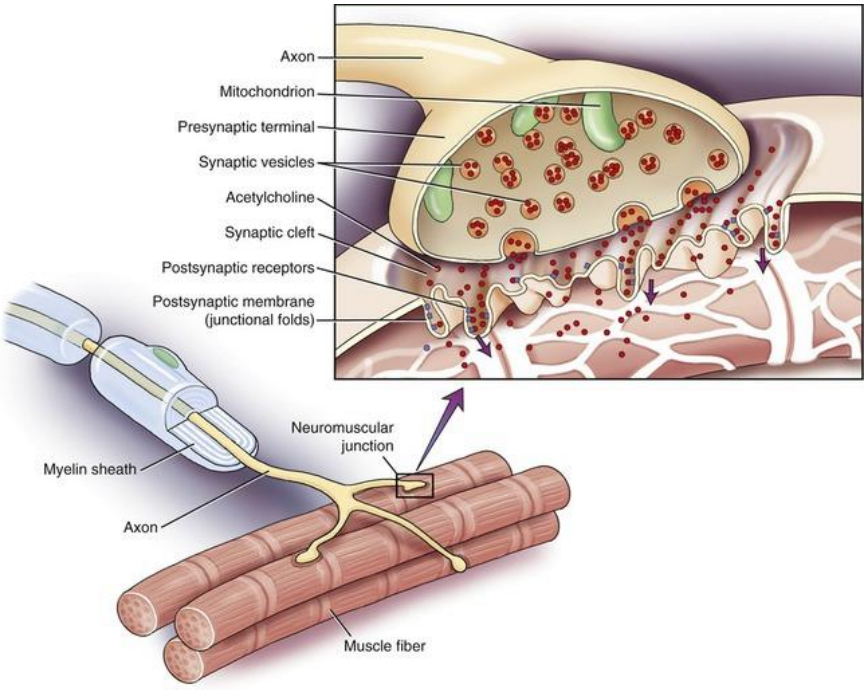

Figure 1.4 The neuromuscular junction (NMJ) connecting the axon terminal of a motor neuron and a muscle fibre*. (ClinicalGate, 2015). Perisynaptic Schwann cells (not shown in the figure) are also found at NMJ, playing roles in synaptogenesis, NMJ maintenance, and transmission.*

1.2 Peripheral nerve injury

Peripheral nerve injury causes damage to peripheral nerves preventing signal transmission between target organs and the CNS. The nerve damage can result from trauma nerve injuries or diseases that degenerate nerve cells such as viral infection and chronic diabetes. According to Operational Information for Commissioning NHS England, a total number of 136,335 diagnostic tests were undertaken for peripheral neurophysiology from October 2019 to October 2020, and 35.1% of patients with a nerve injury in October 2020 had to wait for more than 6 weeks to have the test during the COVID-19 pandemic (NHS England, 2020). The MarketScan Commercial Claims and Encounters Database from the MEDSTAT Group also reported that more than 5% of patients admitted to a level one trauma centre have a concurrent traumatic peripheral nerve injury (Taylor et al., 2008). These patients are often young adults at the peak of their employment productivity, and functional decline associated with nerve lesions is particularly significant (di Summa et al., 2011). Besides high healthcare costs corresponding to the lesion, nerve injury can lead to long-term disability, subsequent sick leave, and 30% of cases lead to permanent disability pension (Bergmeister et al., 2020). These statistical reports on the economic impact of nerve injury reflect the importance of efficient treatment for functional recovery following nerve injury.

Peripheral nerve injury is categorised into three major types: neurapraxia, axonotmesis, and neurotmesis (Seddon, 1942). Neurapraxia is a transient block caused by myelin sheath degeneration where axon continuity is preserved. Axonotmesis is a complete interruption of the axon where supporting structures and connective tissue elements are preserved. In this research, Neurotmesis condition, the most severe injury, has been studied since both nerves and all essential parts are disrupted and undergo distal degeneration subsequently. Without operative repairs, patients cannot recover spontaneously.

When the axon gets injured by crush or transection, the injured site has traumatic degeneration, and the distal part of the axon separated from the cell body undergoes Wallerian degeneration. The traumatic degeneration or axonal breakdown is mediated by calcium influx and involves the activation of axonal proteases (George and Griffin, 1994). The start of Wallerian degeneration is usually detectable within a day after nerve injury, and includes morphological and biochemical changes in axons, Schwann cells, and macrophages at the distal end of the axon resulting in a supportive environment for the subsequent nerve regeneration (Yi et al., 2017).

Yi et al. has suggested that Wallerian degeneration can be divided into 3 phases corresponding to transcriptional changes at different time points. Phase I begins when neurofilament and myelin disintegrate into fragments within an hour after the injury. Phase II occurs at around 6-24 hours afterwards as a pre-formation of Wallerian degeneration. Defence response, inflammatory response, immune response, apoptosis regulation, and cell death regulation were stimulated, resulting in the elevated expression of cytokine, growth factor, chemokines, and hormones. Wallerian degeneration finishes in phase III as the biological processes activated gradually decline to a homeostatic state. This phase takes 4 days to 3 weeks post-injury. Infiltrating macrophages remove myelin debris and clear the axon, while Schwann cells undergo proliferation.

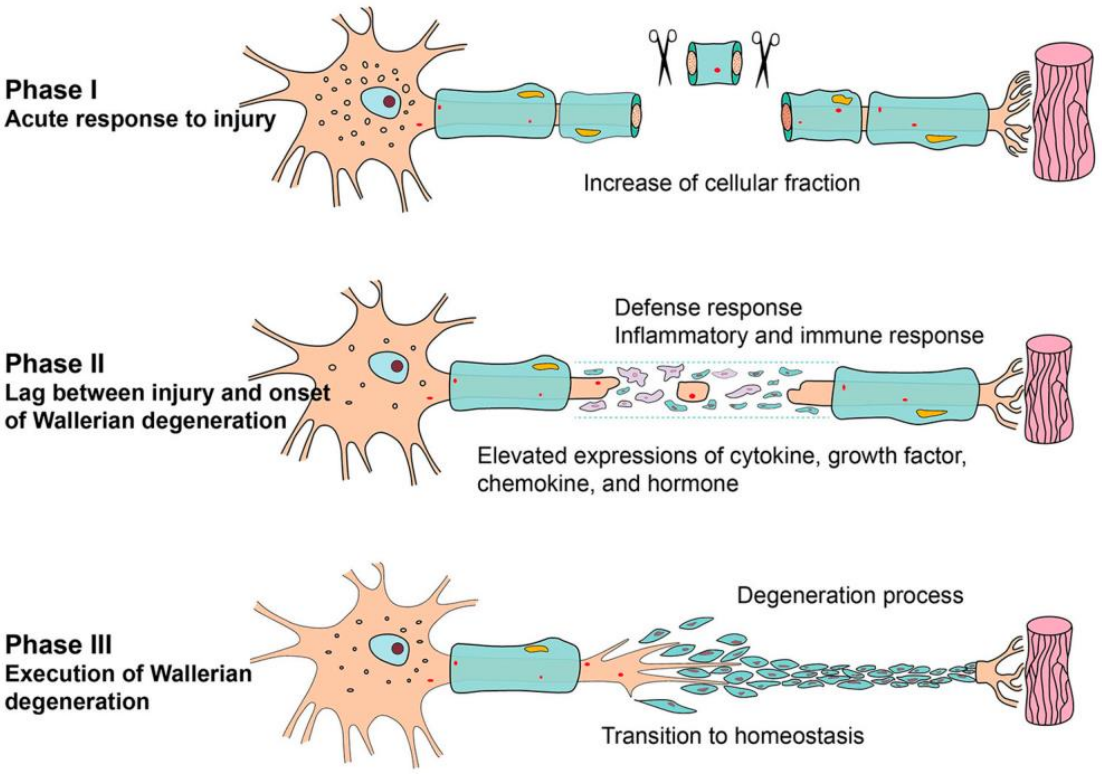

Figure 1.5 Phase changes during Wallerian degeneration. *Phase I is an acute response to injury with cellular fraction which referred to a disintegration of neurofilament and myelin into fragments. Phase II is a pre-formation of Wallerian degeneration with activation of stimulus response-associated biological processes. Phase III is a comprehensive execution of Wallerian degeneration (Yi et al., 2017).*

1.3 Peripheral nerve regeneration

While nerve regeneration in CNS is limited by the inhibitory influences of glial cells and the extracellular environment, the peripheral nerve has the ability to regenerate in a limited extent determined by the regeneration rate, plasticity, and degree of injury (Mokarram and Bellamkonda, 2011). After Wallerian degeneration, most cellular debris is removed from the site by Schwann cells and macrophages. Neurons change function from cell-cell signaling to a regenerative state (Blesch et al., 2012, Doron-Mandel et al., 2015), forming axon sprouts to elongate from the proximal stump toward the original targets at the distal site. After nerve transection, peripheral regeneration occurs when the regenerating axons cross the nerve gap and grow through the distal nerve segment. When the regenerating axons reach the target, reinnervation consequently occurs to obtain a functional recovery. The direction of regenerating axon outgrowth is guided by the remaining endoneurium of the original nerve and aligned Schwann cells. Schwann cells align to form bands of Büngner along the endoneurial tube to protect and preserve the longitudinal column structure. Several neurotrophic factors are also released to enhance axon regeneration. For example, nerve growth factor (NGF), neurotrophin-3 (NT-3), and BDNF are essential for the survival, differentiation, and maintenance of both neuronal and non-neuronal cells during regeneration.

Since the more distal part of an injured axon is entirely degenerated, leaving a distance between proximal stumps and muscles after nerve injury, there is a limitation in nerve regeneration when the injured site is very proximal. Since the spontaneous rate of axonal regeneration in humans is approximately up to 1 mm per day in small nerves and 5 mm per day in large nerves across the site of injury (Burnett and Zager, 2004), complete long-distance nerve repair takes months or even years. Due to the delay, chronic denervation of the distal nerve leads to a decline of Schwann cell repair-ability, and the loss of axonal communication results in muscle atrophy. Improving functional recovery following proximal injuries with a large regeneration distance is, therefore, a clinical challenge. In contrast, more distal injuries take less time for regeneration to reach

target organs and, therefore, have a higher chance of recovering muscle function successfully.

1.3.1 Role of Schwann cells in nerve regeneration

Following axonal damage, myelinating Schwann cells and non-myelinating Schwann cells lose contact with the axon and are triggered to reprogram morphologically and functionally to adopt a new repair-supportive phenotype which is different to their developmental phenotype (Jessen and Mirsky, 2016) (Figure 1.7A). The repair Schwann cells exhibit more branching and elongate to 2-3 folds longer than the original phenotype (Figure 1.6) and can transition back to remyelinating Schwann cells after the regeneration (Gomez-Sanchez et al., 2017). The adaptive cellular reprogramming is mainly controlled by the up-regulation of the transcription factor c-Jun whose pathway regulation is highly dependent on the physical conditions in the microenvironment surrounding Schwann cells (Arthur-Farraj et al., 2012, Fazal et al., 2017). Pro-myelin factor Krox20 and cholesterol synthesis are down-regulated, while the transcription factors associated with immature Schwann cells (e.g., Sox-2, Pax-3, Notch, L1, NCAM, and GFAP) are up-regulated (Jessen and Mirsky, 2008, Leblanc et al., 2005). In non-myelinating Schwann cells, N-cadherin and integrin a1b1 are also up-regulated in the cell reprogramming (Stewart et al., 1997, Thornton et al., 2005).

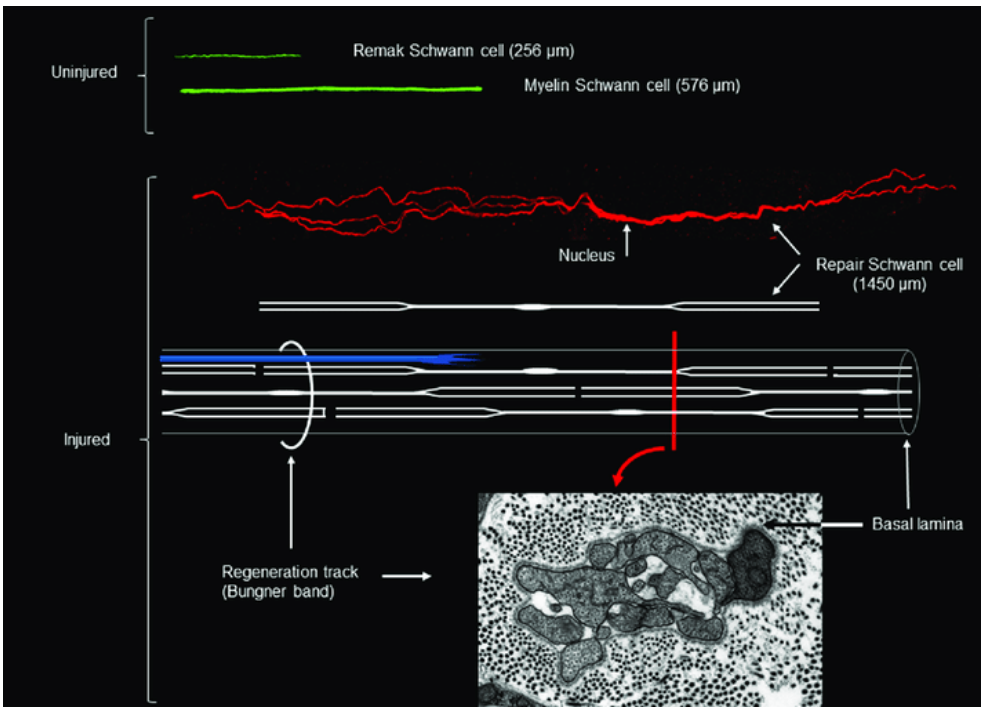

Figure 1.6 Morphological change of Schwann cells to repair-supportive phenotype. *The repair Schwann cell phenotype is relatively long and branching and can align to form a band of Büngner along the endoneurial tube (Gomez-Sanchez et al., 2017).*

Repair Schwann cells proliferate, migrate, and elongate at the lesion site and this supports nerve regeneration. Firstly, myelin fragments are cleared by Schwann cell phagocytosis, autophagy, and the action of infiltrating macrophages. Several neurotrophic factors and angiogenic factors are released into the extracellular matrix (ECM) to prepare a new environment that promotes axon regeneration (Fornaro et al., 2021). Highly aligned tubular structures, called Bands of Büngner, are formed from the Schwann cells and the basal lamina structures in the nerves, where growth cones of regenerating neurons elongate along the guidance track toward the muscle (Arthur-Farraj et al., 2012, Jessen et al., 2015). The efficiency of nerve regeneration is highly dependent on Schwann cell migration and alignment to provide directional guidance for regenerating axons.

As the regenerating axons elongate along the Bands of Büngner, the physical contact between Schwann cells and regenerating axons induces a morphological

change in the repair Schwann cells to initiate remyelination, and the size of Schwann cells is shortened to about 1/7 (Gomez-Sanchez et al., 2017). Repair Schwann cells reorganise their cytoskeleton and produce a thin myelin sheath at the interface with the axon. The remyelination can promote functional recovery once the regenerating nerve reaches the target organ.

Besides, perisynaptic Schwann cells (PSCs), located at the neuromuscular junction, also take part in the remodeling and regeneration of damaged neuromuscular junctions. After peripheral nerve transection, PSCs extend and temporarily maintain processes in the absence of innervation. The PSC processes align with nerve terminal branches and become substrates for axon outgrowth (O'Malley et al., 1999). During reinnervation, axons continue to grow along the aligned Schwann cell bridge and cross the boundary of a denervated neuromuscular junction (Kang et al., 2003).

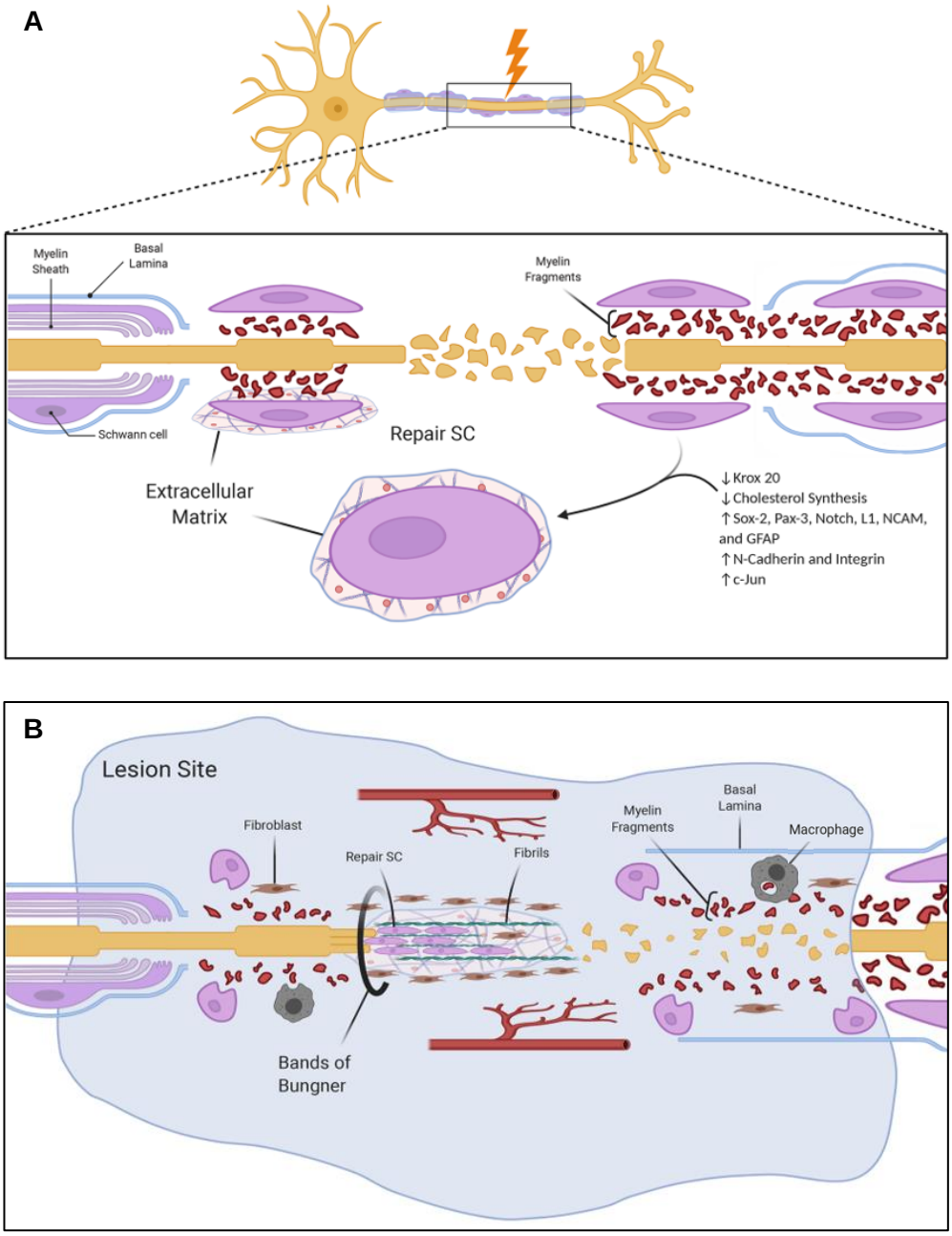

Figure 1.7 Role of Schwann cells and other relevant cells in peripheral nerve regeneration. *(A) Schwann cells lose contact with the axon and reprogram to repair-supportive phenotype. Several signaling pathways are regulated. (B) Following myelin fragment clearance by Schwann cells and infiltrating macrophages, repair Schwann cells align to form Bands of Büngner that directionally guide the regenerating axon from the proximal site (Fornaro et al., 2021).*

1.3.2 Current therapeutic strategies for peripheral nerve regeneration

Treatment for Neurotmesis, a peripheral nerve transection, is mainly determined by the length of the damaged gap and proximity to the distal muscle. The direct end-to-end suture of separated nerve ends back to healthy-appearing fascicles, so-called a primary repair, is suitable in the absence of tension. Alternative methods are required for a longer nerve gaps where tension would result from an attempt at direct primary repair (Siemionow and Brzezicki, 2009). The current gold standard for long gap nerve injury is a nerve autograft. A nerve section from another part of the body, such as the sural nerve is transferred to fill the nerve gap. The autografts contain pro-regenerative trophic support with haptotactic and chemotaxic cues to accelerate axon regeneration across the graft. However, autografts have several limitations due to mismatches in the size of nerves, donor site morbidity, and neuroma formation (M et al., 2014). Also, the autograft is commonly taken from sensory nerves to repair motor nerve damage, so the result is not optimal (Ali et al., 2019).

Nerve guidance conduits are biomaterial tubes connecting the two injured nerve stumps to confine regenerating axons and protect them from scar tissue and trauma. Several studies have illustrated that scaffolds that are similar to the natural extracellular environment can be used to support and improve neural regeneration (Balgude et al., 2001, Bhang et al., 2007, Dillon et al., 1998, Yang et al., 2004, Yannas et al., 2010). Available nerve guidance conduit can be categorized into 3 generations. The first generation of nerve guidance conduit is a non-resorbable, synthetic tube made of silicone or polytetrafluoroethylene with the length up to 4 cm for transplantation in humans. The non-resorbable conduit has a disadvantage in its requirements for additional surgery for conduit removal, so the second generation of nerve guidance conduit was developed to be resorbable and made of various types of biocompatible materials. Most commercially available hollow nerve conduits are made of polyglycolic acid (PGA), collagen, or polycaprolactone (PCL) (Arslantunali et al., 2014, Isaacs and Browne, 2014). Although the resorbable conduit does not require a second surgery, it

has the key limitation in the degradability of the conduits which might result in an instable barrier for surrounding tissue. The third generation of conduit includes a surface or luminal modification or an addition of neurotrophic factors, electroconductive material, stem cells or supportive cells (e.g., Schwann cells), and extracellular matrix proteins. For instance, NeuraGen® is the first nerve guidance conduit comprising a 3D luminal filler that was approved by FDA. The conduit contains collagen type I and glycosaminoglycan chondroitin-6-sulfate, and has been reported with the potential to support regeneration as much as autograft (Lee et al., 2012a). However, the modified conduits have a regenerative limitation as they were reported to be comparable to the gold standard only in a limited defect size range. The longest nerve guidance conduits which are commercially available and FDA-approved was Salutunnel (Salumedica LLC, US) with the length of 6.35 cm (Pedrosa et al., 2017). Further development of nerve guidance conduits is still required for a long-distance nerve regeneration.

A similar concept is applied to decellularised nerve allografts which have the advantages of being a natural scaffold from the remaining ECM and provide an instantly available source of graft material (Cheng et al., 2014). Nevertheless, nerve conduits and decellularised allografts have limited ability to support effective regeneration for nerve gaps longer than 3 cm (Karabekmez et al., 2009). In the transplantation of acellular nerve guidance conduits, endogenous trophic support is reduced compared with autografts due to the absence of transplanted cells (Maggiore et al., 2020). Simple tubular guidance conduits also lack directional guidance cues (e.g., alignment pattern inside the conduit), so axonal outgrowth can be disorganised, reducing regenerative capacity.

Neural tissue engineering arises from the difficulty of promoting neural regeneration after severe damage in the nervous system. It combines approaches from the fields of biomaterials and neuroscience, considering material selection, scaffold fabrication, cellular composition, and mechanisms for nerve regeneration. Bioengineered scaffolds containing living cells are a relatively new approach to use for

nerve regeneration, often developed by adding living cells to conventional biomaterial guidance conduits. Similar to an autograft, the presence of transplanted cells provides pro-regenerative and trophic support to the regenerating axons to improve neuron behaviour and overall capacity for regeneration. Principles and examples of using living scaffolds in nerve repair will be discussed in the following section.

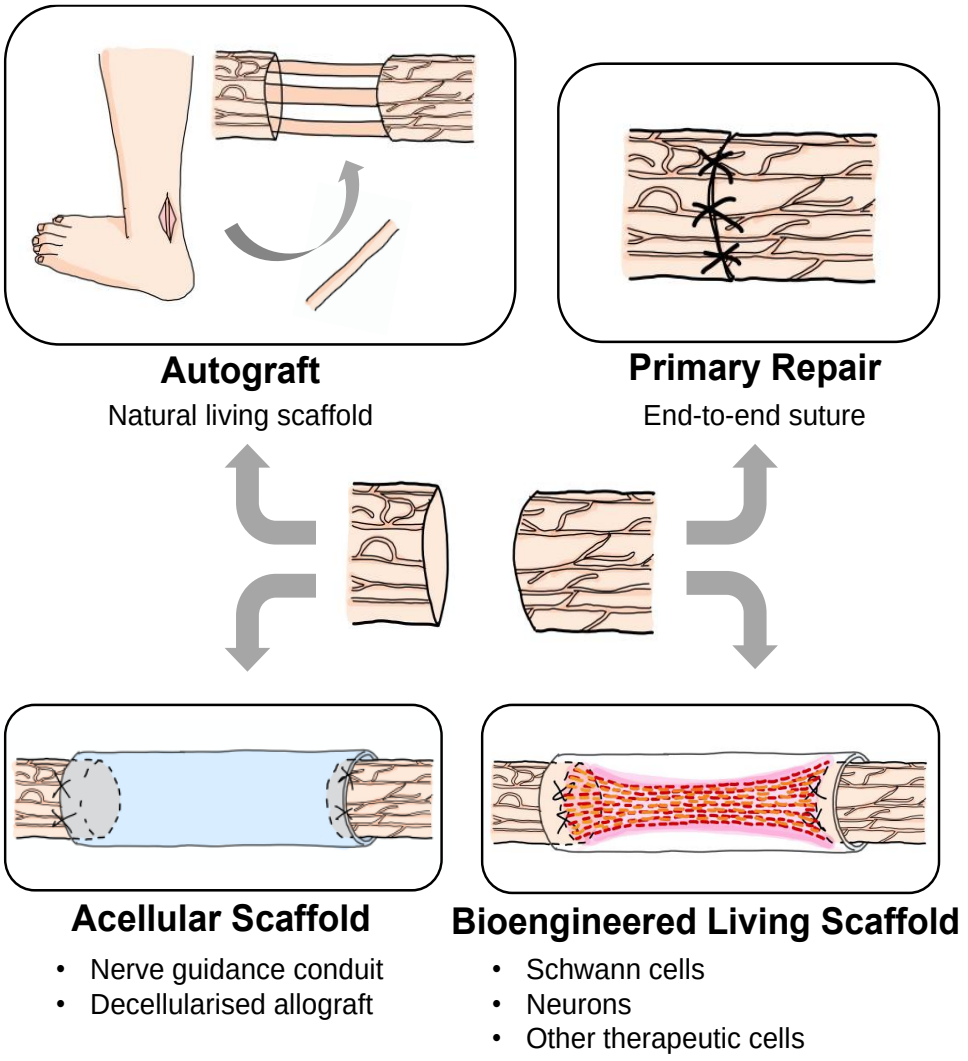

Figure 1.8 Current therapeutic strategies for peripheral nerve regeneration. *Primary repair is a direct end-to-end suture of separated nerve ends in the absence of tension. Natural living scaffold or autograft is the current gold standard for long gap nerve injury. Acellular scaffolds utilise biomaterial technologies to synthesise a physical barrier to surround the repair site. Bioengineered living scaffolds containing living cells are a relatively new approach to use for nerve regeneration, often developed by adding living cells to conventional biomaterial guidance conduits.*

1.4 Engineered living scaffold for peripheral nerve regeneration

As briefly mentioned in the previous section, a bioengineered living scaffold is a cell-based therapy to improve functional recovery after nerve injury. The living scaffold can be fabricated through various processes depending on the types of biomaterials and cells inside. The cells can be a single population or a combination of Schwann cells, neurons, and other supportive cells such as endothelial cells (Georgiou et al., 2013, Li et al., 2018, May et al., 2016, Muangsanit et al., 2021, Muangsanit et al., 2020).

The most widely established approach to make living scaffolds for peripheral nerve regeneration is a biomaterial conduit containing Schwann cells. The presence of Schwann cells is critically supportive to regenerating neurites, as described in Section 1.3.1. It was also considered that Schwann cell transplantation is the gold standard of cellular-based therapies for peripheral nerve repair because it mimics the key cellular component of the nerve autograft (Pearse et al., 2018). Schwann cells can align and provide a cellular guidance substrate and trophic support to axonal regeneration and myelination. The alignment of Schwann cells can be spontaneous or induced by various engineering techniques. For example, engineered neural tissue (EngNT) formed from simultaneous self-alignment of Schwann cells and collagen fibrils in a tethered gel, followed by stabilisation with plastic compression resulting in an anisotropic tissue-like structure (Figure 1.9), and gel aspiration-ejection (GAE) using a cannula to fabricate a dense, injectable, anisotropic cellular collagen gel scaffold with controllable fibrillar densities. The transplantation of these tissue engineered constructs into the rat sciatic nerve model showed their feasibility in supporting neuronal regeneration comparable to an autograft, (Georgiou et al., 2013, Marelli et al., 2015, Muangsanit et al., 2020).

For clinical translation, a suitable source of therapeutic cells must be identified for nerve tissue engineering because autologous Schwann cells can only be obtained by damaging nerves and therefore carries the same limitations associated with the autograft. One approach is to convert a more accessible cell type such as stem cells to

become Schwann cells, with approaches reported using embryonic stem cells, induced pluripotent stem cells, bone marrow stem cells, adipose-derived stem cells, human umbilical-cord stem cells, skin-derived precursors, and dental pulp stem cells (Cui et al., 2008, Uemura et al., 2014, Mohammadi et al., 2012, Matsushita et al., 2012, Georgiou et al., 2015, Matsuse et al., 2010, Park et al., 2012)

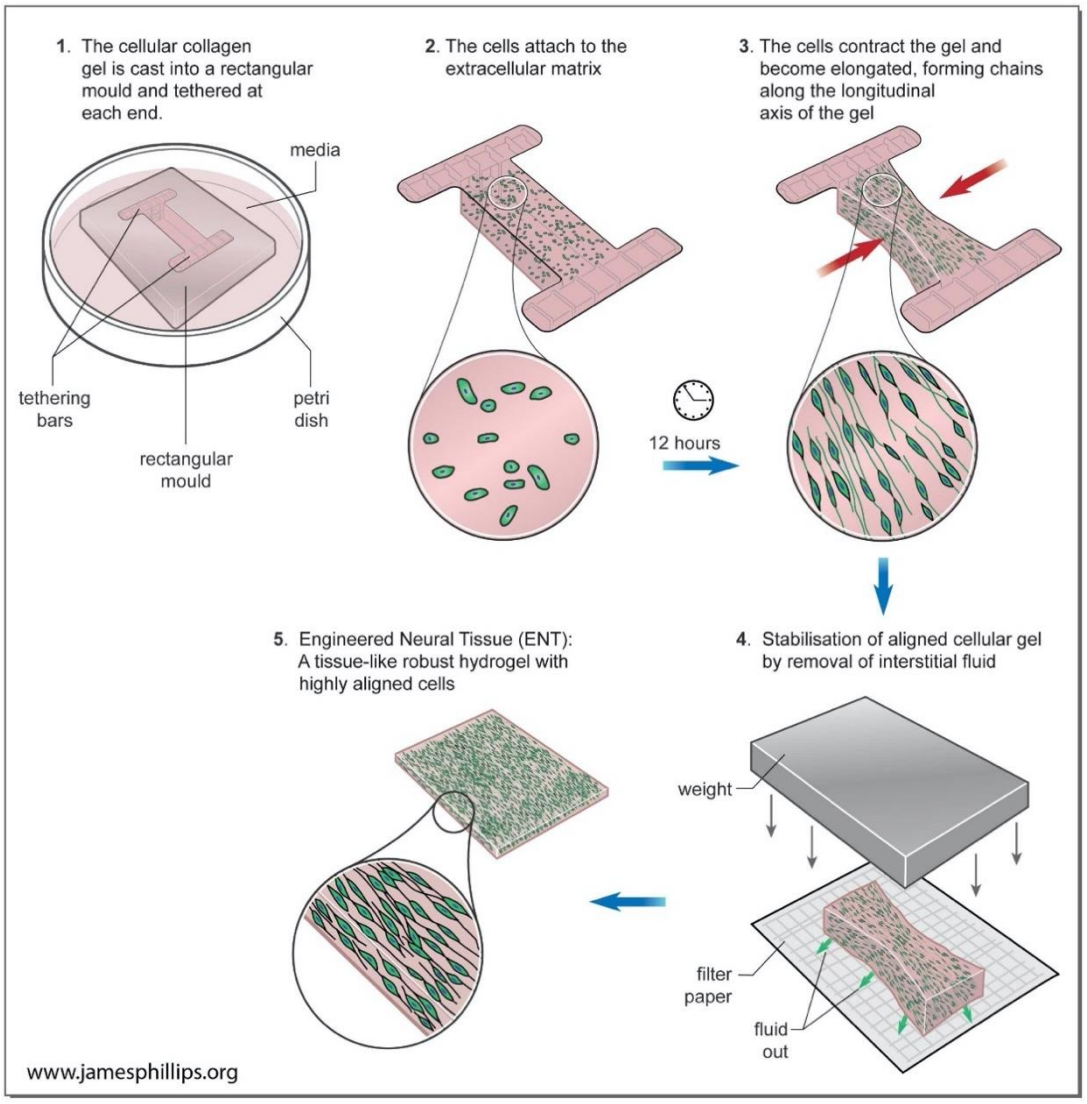

***Figure 1.9 Production of Engineered Neural Tissue (EngNT)**. Highly aligned Schwann cells in EngNT provides a cellular guidance substrate and trophic support to axonal regeneration and myelination (Georgiou et al., 2013).*

Despite these tissue engineering approaches to mimic the autograft in bridging the nerve gap, when nerve injury occurs at a more proximal location, leaving a long distance of neural degeneration with insufficient guidance and inhibitory factors between the injury site and the target muscle, axonal regeneration takes a long time and functional recovery is reduced. In order to address this issue, an alternative approach for tissue engineered living scaffolds can be developed which involves populating constructs with living neurons as well as supporting Schwann cells. The concept is partly based on the axon elongation along pioneer axons that takes place during embryonic development (Figure 1.10). The pioneer axon is the first developing axon that reaches the end target, and this subsequently guides other following axons in the right direction. Similarly, engineered living axons can mimic the guiding ability of the pioneer axon to guide host axons to regenerate successfully (Struzyna et al., 2015a).

There are examples of living neuronal scaffold constructs applied in both the PNS and CNS. In the CNS, implantable micro-tissue engineered neural networks (Micro-TENNs) consisting of cerebral cortical neurons with long axonal tracts in biocompatible micro-columns have been developed to reconstruct neuronal circuits and modulate activities and connectivity in the brain (Struzyna et al., 2015a). Similarly, tissue engineered nerve grafts (TENGs), consisting of dorsal root ganglia and axonal tracts, were shown to repair sciatic nerve lesions in rats effectively. Neurons in TENGs was found to have anatomic integration with the host nerve tissue and axon myelination after 16 weeks post-transplantation in rat sciatic nerve (Huang et al., 2009).

Additionally, previous research has reported the transplantation of living cells to induce the formation of neuromuscular junctions following peripheral nerve injury. Myoblasts were cultured in a scaffold to provide a regenerative peripheral nerve interface (RPNI) implanted on a divided peroneal nerve end in rats (Urbanchek et al., 2016). Electrophysiological tests showed electromyographic activity and stimulated compound muscle action potentials from the RPNIs, and there was axonal regeneration with synaptogenesis after RPNI transplantation. Embryonic spinal cord neurons were

transplanted on the tibial nerve in rats and subsequently resulted in neuromuscular junction formation, as well as motor neuron regeneration and axon elongation (Zhang et al., 2017).

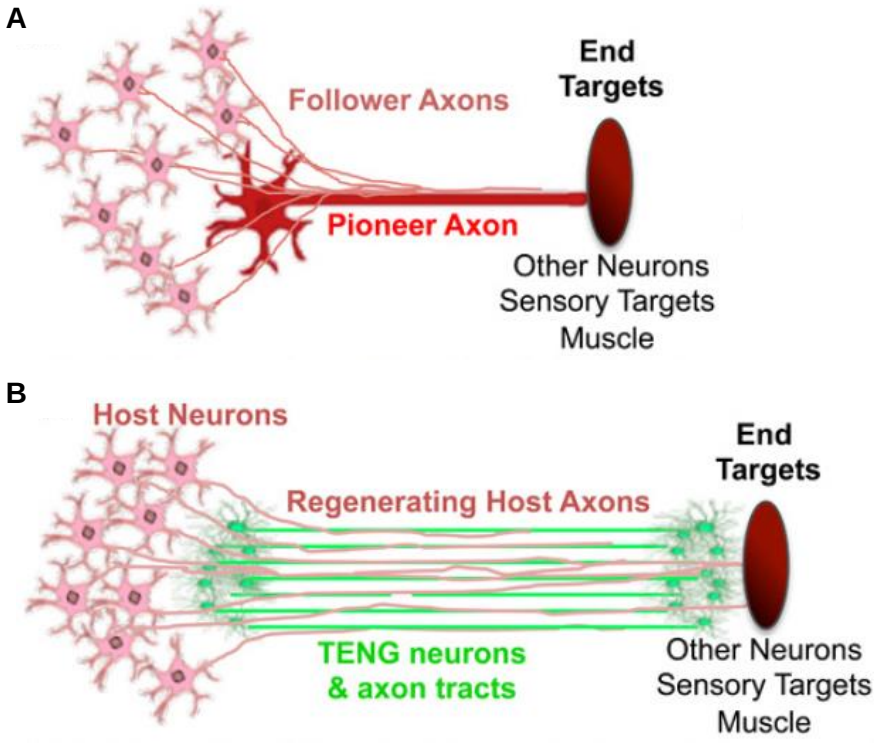

Figure 1.10 Principle of axon elongation from the cell body to the end target. *(A) During development, a pioneer axon forms a pioneer tract to reach the target firstly, and following axons are subsequently guided in the right direction. (B) Living scaffolds (e.g. TENG) mimic the guiding ability of the pioneer axon to guide host axons to regenerate successfully. The guidance tracts can be multiple to facilitate functional recovery (Struzyna et al., 2015a).*

1.5 Tethered aligned engineered neural tissue (TaeNT)

This project has investigated the combination of the tethered aligned collagen gel technique and the living neuronal scaffold concept, which can potentially be a promising solution to improve regeneration in long nerve gaps. The term "Tethered Aligned Engineered Neural Tissue (TaeNT)" will be used to describe this new combined approach: an anisotropic cellular construct formed from a 3D co-culture of highly aligned Schwann cells and neurons in fully-hydrated tethered collagen gels. Neurons derived from therapeutically suitable cells will be cultured in the TaeNT, where aligned Schwann cells are present to guide axon elongation. The intention is that TaeNT can be prepared in advance in the laboratory to become an off-the-shelf construct populated with glial cells supporting neurons with elongated neurites. As well as providing a suitable microenvironment to guide regenerating host axons from the proximal stump, axons from transplanted neurons in TaeNT could functionally reconnect the proximal nerve stump and downstream muscle, and potentially interact positively with the muscle as the regeneration progresses.

The transplantation of TaeNT was aimed to bypass the distal stump and connect proximal stump directly to muscle. The method could potentially reduce the delay in muscle reinnervation following nerve repair. 2 possible mechanisms are hypothesised to occur at the long nerve distance between a proximal nerve stump and distal muscle after TaeNT transplantation (Figure 1.11). In the first hypothesis, the neurites in TaeNT could permanently replace the injured neurons. The elongated neurites inside the transplanted conduit would promptly interact with cells at proximal stump of the nerve gap and the muscle, forming functional networks for signal transmission. Muscle cells would be reinnervated via this bridge, without requiring regenerating axons from host tissue. Alternatively, the neurites in TaeNT could be hypothesised to temporarily reinnervate the muscle during the period when host neuronal regeneration from the proximal stump is progressing. The signal transmission through the temporary route might be sufficient to maintain the cellular interaction to muscle cells, so that the muscle

atrophy would delay while the actual regenerating axons are elongating from the proximal stump. The temporary relay could also behave like a pioneer route for cellular directional guidance.

This project included both *in vitro* and *in vivo* models to investigate aspects of using the TaeNT approach. For *in vitro* models cellular constructs were generated in tethering moulds (Phillips and Brown, 2011) whereas for *in vivo* studies cellular gels were tethered within medical-grade silicone tubing with perforations to facilitate collagen tethering (Muangsanit et al., 2021, Phillips et al., 2005).

The important attributes of neurons in TaeNT are long-term survival, long neurite elongation, and the ability to functionally connect with the proximal nerve stump and to form neuromuscular junctions with the distal muscle. The neurites from neurons in TaeNT should form a tract long enough to bridge the distance from injury site to muscle and effectively transmit signals from the proximal stump to the muscle. Thus, previous research on generating long and aligned axon tracts has utilised mechanical stimulation or ‘stretch-growth’ in bioreactors, with a recent study providing evidence that the resulting constructs can be effective in animal models of nerve repair (Katiyar et al., 2020).

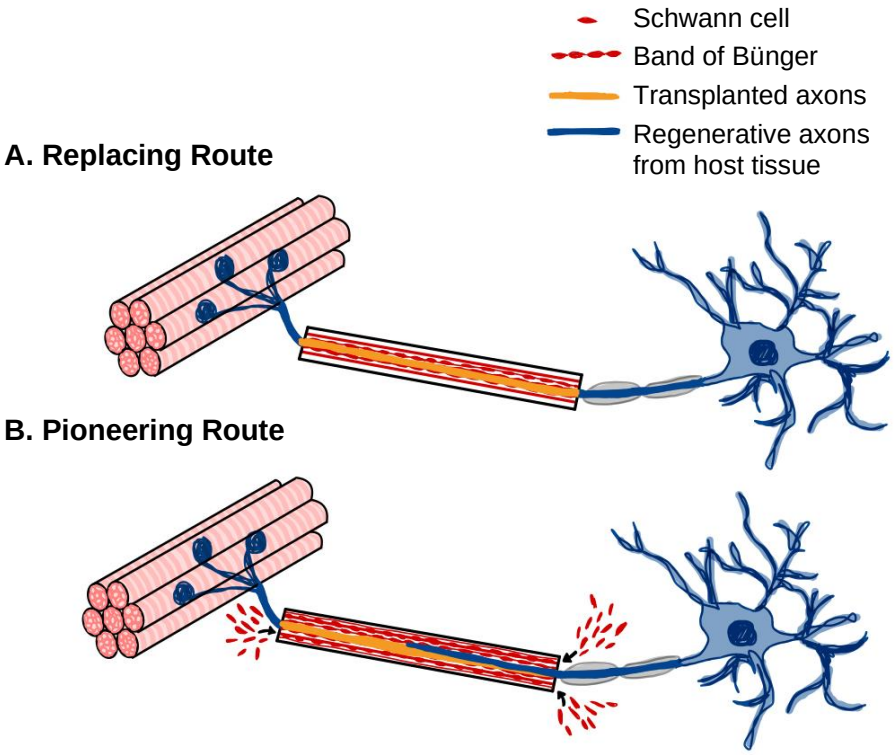

Figure 1.11 Possible mechanisms hypothesised to occur in the long nerve distance between a proximal nerve stump and distal muscle after TaeNT transplantation. *Schwann cells align longitudinally and form bands of Büngner to guide regenerative neurites elongating from the proximal to distal stump. The presence of living neurons with elongated neurites in TaeNT could potentially reduce the time required for muscle reinnervation following nerve injury. The neurites in TaeNT could become either (A) a permanent nerve replacing the injured one as soon as the cellular network is completely formed at the interface between the conduit and the nerve stump, or (B) a pioneer route to temporarily restore and maintain muscle reinnervation while the regenerating host axons are elongating from the proximal stump and entering the conduit to follow the pioneer route formed by the transplanted neurites.*

1.6 Mechanical tension application for stretch growth in neural cells

The common use of mechanical tension application in neuronal cells can be generally categorised into two main aims: (1) to create neurodegenerative disease or neuronal injury models for biochemical and physiological investigations of nerve damage, and (2) to induce growth response for nerve regeneration and therapeutic study. Here, the concept of using mechanical tension to gradually stretch processes of cells was studied as it replicates some aspects of axon growth during animal development, where axons respond to mechanical tension both before and after synaptogenesis. The stretch growth begins during embryogenesis after axons sprouting from neurons form synapses with their target cells. As the size of an animal's body expands, neuronal cell bodies and their target cells move further from each other, exerting tensile forces on the axons (Weiss, 1934).

Paul Weiss suggested that stretching a plasma clot; a sponge of fibrin fibres containing embedded neurons, eventually guides the direction of the outgrowing axon grown in the stretched plasma (Weiss, 1941). The later observation in the lateral line organ of zebrafish showed that the migration of post-synaptic cells generates towing force to the axon during synaptogenesis (Gilmour et al., 2004). This result was consistent to Bray's *in vitro* experiment in sympathetic neuron cultures, concluding that growth cones of neurons pull out the neurite while migrating away from the neuron cell body (Bray, 1979).

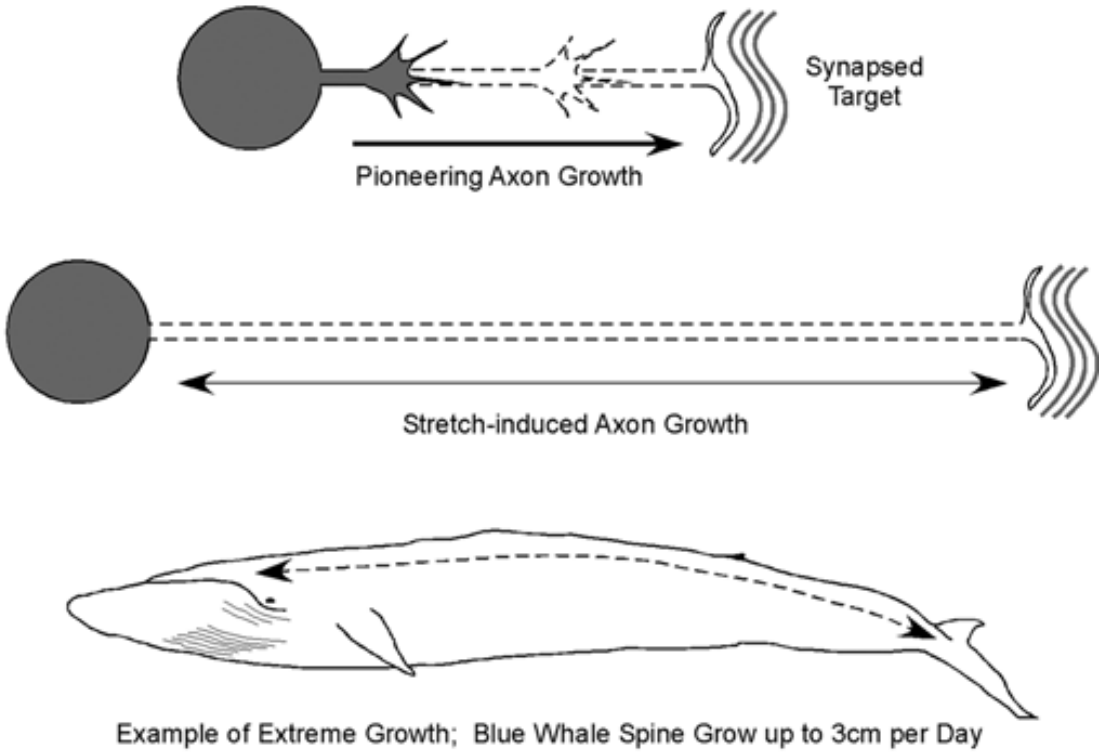

Figure 1.12 Stretch growth of neurons in a biological system. *In early development, pioneering axons use their growth cones to navigate to the right target. After the growth cones reach the target and form synapses, mature axons are under mechanical tension as the size of an animal's body expands, so their axon length gradually increases. The spontaneous tension can stretch the nerve to grow in length with an average rate of 3 cm per day in the blue whale, whose average length of the whole body is 25 m (Pfister et al., 2007).*

With a suitable strain range, it has been shown that axons can respond positively to mechanical tension, but how neurons regulate the strain after the mechanical perturbation remains unclear. Experiments in Drosophila embryos revealed that the behaviour of neurons follows viscoelastic solid principles, exhibiting both viscous and elastic characteristics under deformation (Rajagopalan et al., 2010). According to the study, neurons maintain a resting tension in the absence of external force and elongate in linear response to external force during rapid perturbation. When the applied force is withdrawn, reducing the mechanical tension, neurons restore resting tension by contracting axons. This finding is consistent with the *in vitro* stretch of individual CNS glial cells and neurons, where viscoelasticity properties were observed (Lu et al., 2006).

The mechanical tension can also induce axon initiation and stabilisation. Generally, neuronal cells extend several immature neurites out of the cell bodies and selectively polarise the neurites to become axons and dendrites. When the orientation of elongating neurites loses symmetry, a single immature neurite becomes an axon, and the other neurites retract or turn to be dendrites (Axon-dendrite polarisation), then the axon grows longer rapidly while dendrites branch out (Polleux and Snider, 2010). With suitable tension magnitude above some threshold, externally-applied strain stimulates axon initiation, inducing the neurons to emit new axons (Bray, 1984, Chada et al., 1997, Zheng et al., 1991). The mechanical tension caused by the attachment of the growth cone to target cells also influences neuron branching dynamics by promoting stabilisation of selective axons and eliminating the other neurites (Anava et al., 2009). In a unipolar neuron with only one extending axon, mechanical stimulation can eventually induce the formation of multiple axons (Lamoureux et al., 2002).

Mechanical tension application to growth cones of axons has been observed to increase axon length and volume of neurite cytoplasm in culture (Bray, 1984, Chada et al., 1997, Dennerll et al., 1989, Zheng et al., 1991). In regenerating neurons, the rate of axonal elongation is approximately 1 mm per day or slower across the site of injury (Burnett and Zager, 2004). Previous research demonstrated that dorsal root ganglion

(DRG) neurons with an original axon length of 100 μm could respond to tensile elongation by growing to a remarkable 10 cm in length in 28 days without disconnection (Pfister et al., 2004). Moreover, transplantation of stretched DRG neurons in PGA Neurotube^{TM} to a 1 cm excised segment of the sciatic nerve in adult male transgenic rats for 10 days showed survival and integration of transplanted engineered nervous tissue constructs with host tissue (Katiyar et al., 2020).

Even when axons are stretched to increase the length by 35% of the original length, the morphology and density of cytoskeleton constituents are maintained (Pfister et al., 2004). It is hypothesised that the cytoskeleton is regulated to facilitate axon elongation, so that the length of the axon is extended without any loss of function. Heidemann and Bray suggested a mechanism of tension-driven axon assembly describing microtubule rearrangement as a response to the pulling force on axons (Figure 1.13). In summary, in a stable condition without external mechanical force, axons align in the longitudinal direction parallel to several segments of microtubules with various lengths. The short microtubule segment is mobile and rapidly transported in the retrograde and anterograde direction along the axon region. When the nerve is stretched by pulling proximal and distal ends away from each other, the nerve is adjusted by decreasing its thickness and restricting the microtubule transport. The thinner nerve physically pulls the long segment of the microtubule to move apart toward both ends longitudinally and simultaneously induces the short segment to aggregate at the middle instead. In order to restore normal transport of the short microtubule segment after the stretch, the short microtubule segments rearrange to fill occurring gaps, and then the new transport route is stabilised by associated proteins, and the nerve returns to the normal thickness and regular transport. Therefore, the axon becomes longer as its cytoskeleton elements are rearranged, with transport being maintained (Heidemann and Bray, 2015).

The model proposed by Heidemann and Bray is consistent with other models claiming that microtubule arrangement is related to axon elongation (Athamneh et al.,

2017, de Rooij et al., 2017, Suter and Miller, 2011), and it is considered to be a fundamental of mechanobiology for neurite stretching. Likewise, neurite retraction is also regulated by microtubules but in a different manner. The orderly retrograde shortening of the microtubule coordinated with the surface area of plasma membrane retrieval by submembrane actin dynamics is proposed to be a mechanism for neurite shortening (Prager-Khoutorsky and Spira, 2009). Hence, the dynamics of microtubules directly modulate the cytoarchitecture of neuronal cells and neurites and consequently play a critical role in determining the strain range in which neurites can still maintain a normal function.

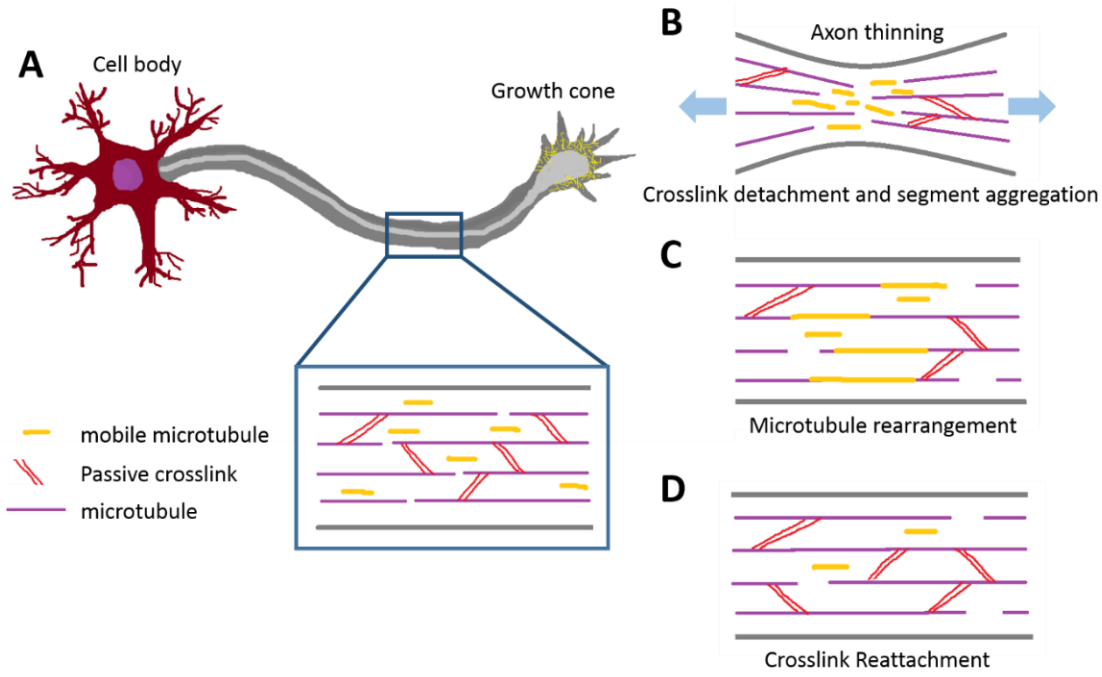

Figure 1.13 Possible mechanism of tension-driven axon growth. *(A) The arrangement of long microtubules and short mobile segments in axon before mechanical tension application. (B) The separation of long microtubules and aggregation of short segments when the nerve is pulled apart at both ends. (C) The rearrangement of microtubules resulting in axon elongation with normal transport. (D) The passive crosslink reattachment. The illustrating figure was adapted from Heidemann and Bray's suggestion (Heidemann and Bray, 2015).*

Research Objectives of this PhD Project

The overall aim of the research project is to develop and investigate tethered aligned engineered neural tissue (TaeNT) containing neurons and Schwann cells for long-gap peripheral nerve regeneration. The living neurons in TaeNT are hypothesised to improve functional recovery by restoring muscle innervation more rapidly than treatments that simply provide a bridge for host neuron regeneration (e.g., autograft, conduit, previous EngNT).

The TaeNT approach requires different types of cellular interactions as it contains both transplanted neurons and Schwann cells and also interfaces with Schwann cells and elongating neurites and other components in the host tissue. The cellular interactions between the different cell populations will underpin the regenerative properties of TaeNT. Here, important attributes to determine an effective cellular engineered construct for peripheral nerve repair include: (1) the ability to resemble the structure of Bands of Büngner containing aligned Schwann cells to support axon elongation, (2) biocompatibility with host tissue such that the interaction of host and transplanted cells leads to a supportive environment for regeneration, (3) the feasibility to further develop the construct for mechanical tension application to induce longer neurites in the construct. Therefore, the main hypotheses to be tested in the project were whether the TaeNT has the 3 attributes stated above which reflect its potential as an alternative transplanted construct to improve peripheral nerve regeneration.

Quantifying host and transplanted neurons and Schwann cell interaction, neurite elongation, and interface integration of host and transplanted cells could provide experimental evidence to determine whether the TaeNT has the required attributes mentioned above (Figure 1.14). In this project, experimental approaches were divided into three chapters, each of which tacked a specific objective corresponding to particular components in the TaeNT, as follows:

Objective 1: To investigate the elongation of neurons within TaeNT and at the interface with host tissue.

The regenerative potential of TaeNT containing neurons and Schwann cells was investigated in terms of supporting neurite elongation within the transplant and across the host/graft interface. To test the hypothesis whether the neurite elongation of neurons was supported by the co-culture of Schwann cells in TaeNT, both *in vitro* and *in vivo* experiments were carried out. The length, alignment, and interface-crossing of neurites were quantified to provide preliminary experimental evidence about TaeNT containing neurons and Schwann cells in peripheral nerve regeneration.

Objective 2: To understand the nature and consequences of the interaction between host and transplanted glial cells in nerve repair.

In the transplantation scenario, Schwann cells from host tissue migrated into the conduit, and interacted with cells in the conduit. The interactions between two cell populations were hypothesised to be supportive to the regeneration by their mobility to cross the interface and alignment pattern. TaeNT was used to study the interaction between host and transplanted glial cells when the TaeNT was transplanted into a rat sciatic nerve injury model. The distribution, migration, and alignment of both glial cell populations were examined to understand whether glial cells from within and outside the engineered tissue influence each other in a supportive or disruptive way.

Objective 3: To develop a protocol for mechanical tension application to induce stretch growth of neurons in engineered tissue.

TaeNT with aligned Schwann cells and neurons was proposed as a 3D cellular hydrogel-based substrate that can be modified and combined with a stretching system to induce longer neurites in the construct prior to transplantation. This chapter mainly contained engineering development of stretching protocol on TaeNT with preliminary tests on cell morphology to test the hypothesis that the TaeNT has a feasibility to provide an alternative platform to apply mechanical tension to neural cells for growth response.

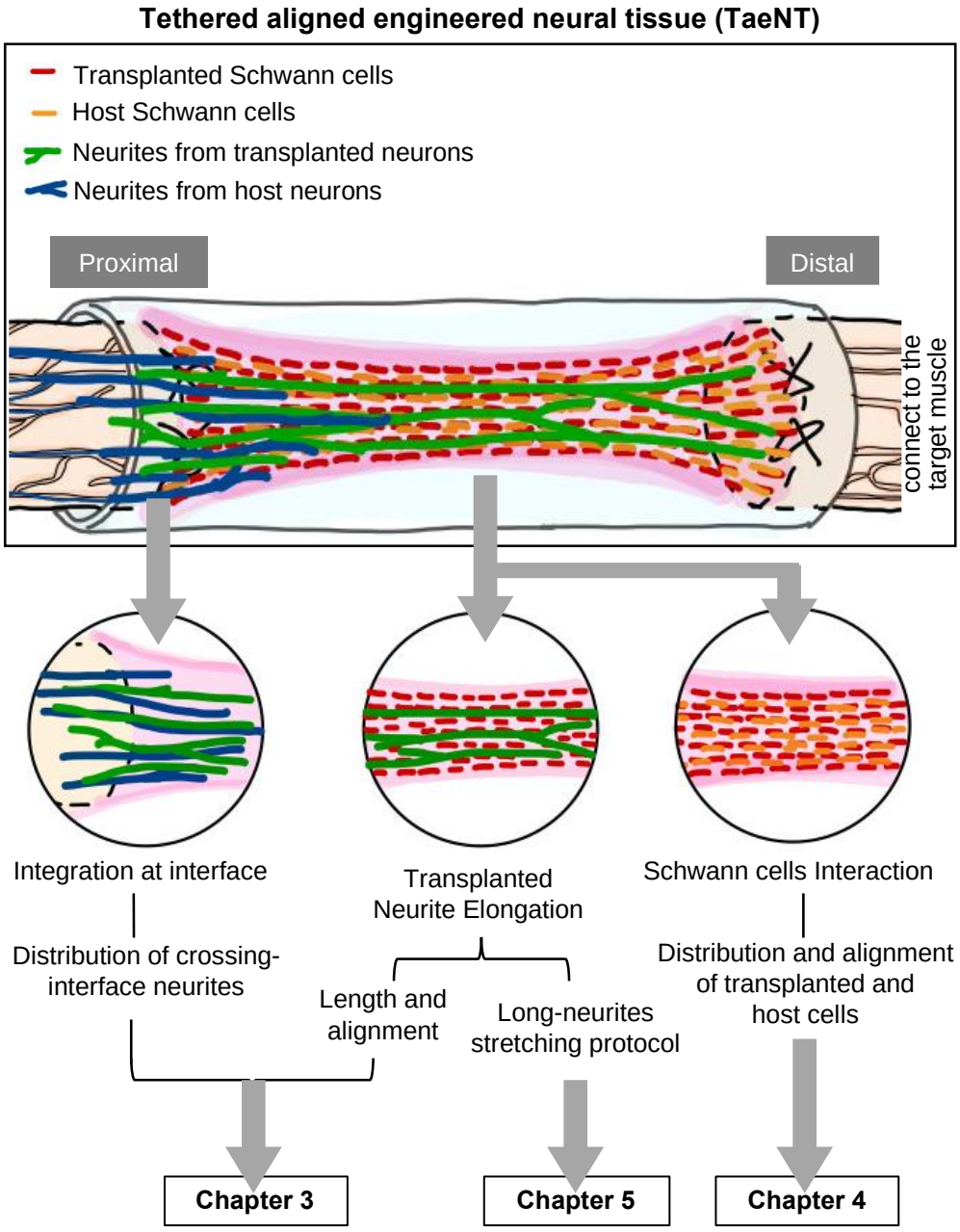

Figure 1.14 Overview of the key topics related to the use of TaeNT for long-gap nerve regeneration. *When TaeNT containing elongated neurons and Schwann cells is transplanted into the nerve gap, many cell populations are included in the regenerative scenario, therefore various cell behaviours and interactions were investigated. Regenerative neurites from host neurons are elongating into the proximal end of the conduit toward the distal end while host Schwann cells are migrating into the conduit. The investigation of each particular topic contributes to the main objectives of experimental chapters in this project.*

CHAPTER 2

Materials and Methodology

2.1 Materials

Cell lines	Origin	Supplier	Catalogue number
NG108-15	Mouse neuroblastoma x Rat glioma hybrid	ATCC, US	HB-12317™
SCL4.1/F7	Rat Schwann cells	ECACC	93031204

Table 2.1 Cell line used in the experiments.

Primary antibody	Target	Species	Dilution	Supplier	Catalogue Number	Secondary antibody
Polyclonal anti-β-Tubulin III	Neurons	Rabbit	1:400	Sigma-Aldrich, UK	T3952	Anti-Rabbit 488
Monoclonal anti- β-Tubulin III	Neurons	Mouse	1:400	Sigma-Aldrich, UK	T8660	Anti-mouse 488
Polyclonal anti-S100	Glial cells	Rabbit	1:400	Dako	Z0311	Anti-rabbit 549
Neurofilament-H	Axons	Mouse	1:1000	Euroge-ntec	SMI-35-050	Anti-mouse 488

Table 2.2 Primary antibodies used in the experiments.

Secondary antiboy	Species	Dilution	Supplier	Catalogue number
DyLight 488, anti-rabbit IgG (H+L)	goat	1:300	Vector Laboratories, US	DI-1488
DyLight 549, anti-rabbit IgG (H+L)	goat	1:300	Vector Laboratories, US	DI-1549
DyLight 488, anti-mouse IgG (H+L)	horse	1:300	Vector Laboratories, US	DI-2488
DyLight 549, anti-mouse IgG (H+L)	horse	1:300	Vector Laboratories, US	DI-2549

Table 2.3 Secondary antibodies used in the experiments.

Reagent/solution/material/other	Supplier	Catalogue number
Dulbecco's modified Eagle's medium (DMEM)	Sigma-Aldrich, UK	D6429
Foetal Bovine Serum (FBS)	Sigma-Aldrich, UK	26140079
Penicillin-streptomycin (P/S)	Sigma-Aldrich, UK	P0781
Trypsin-EDTA solution (TE)	Fisher-Scientific, UK	R001100
Poly-L-lysine	Sigma-Aldrich, UK	P6282
Collagen type I from rat tail	First Link, UK	60-30-810
Phosphate buffered saline (PBS)	Sigma-Aldrich, UK	P4417
Paraformaldehyde (PFA)	Fisher-Scientific, UK	P/0840/53
Dimethyl Sulfoxide (DMSO)	Sigma-Aldrich, UK	D5879
Hoechst 33342 (Bisbenzimide)	Sigma-Aldrich, UK	B2261
Triton X-100	Sigma-Aldrich, UK	T9284
Normal goat serum	Dako, Denmark	X0907

Reagent/solution/material/other	Supplier	Catalogue number
Normal horse serum	Vector Laboratories, UK	S-2000
Isoflurane anaesthetic	Minrad Inc, UK	From the pharmacist
Rimadyl analgesic	Pfizer, US	From the pharmacist
Lacri-lube	Allergan, UK	From the pharmacist
Battles veterinary wound powder	Fearing, UK	AH07045
10-0 sutures	eSutures	2830G
Sucrose	Fisher-Scientific, UK	S/8600/60
Medical-grade stainless steel wire 0.25 mm	KC Smith Ortho Ltd	R600H00.250PC7
Medical-grade stainless steel wire 0.9 mm	KC Smith Ortho Ltd	R600H00.900L30
Polysiloxane filler	R&S Dental Product	16-120
Medical-grade silicone tube	Syndev, US	228-0235
Glass slide for frozen sections	Superfrost™ Plus, Thermo Fisher Scientific	12-550-15
Parafilm® M sealing film	Sigma-Aldrich, UK	BR701611
4-0 sutures	Ethicon	1667G
PLA filament for 3D printing (2.85mm)	PolyMax™	-

Table 2.4 Materials used in the experiment.

2.2 Methods

2.2.1 Cell culture and preparation

NG108-15 is a somatic hybrid cell line originally formed from rat C6-BU-1 glioma cells and mouse N18TG2 neuroblastoma. The immortalized cell line exhibits characteristics of motor neurons with neurite outgrowth and has been widely used in various *in vitro* neuronal studies including the mechanisms of neuronal development and differentiation.

SCL4.1/F7 rat Schwann cell line is an immortalised Schwann cell line derived from neonatal Wistar rat Schwann cells being cultured from long periods and cloned by limiting dilution to establish its proliferation without mitogens. The cell line displays an identity and molecular markers similar to Schwann cells, such as calcium-binding cytosolic protein S100, differentiation-related p75, and GFAP in non-myelinating phenotype *in vitro*, so it has been widely used as a tool to study biochemical and cellular basis of Schwann cells in peripheral nerve.

NG108-15 rat glioma cells and SCL4.1/F7 rat Schwann cells were maintained in a DMEM-complete medium which was made of high glucose Dulbecco's Modified Eagle's Medium culture medium (DMEM) supplemented with 10% v/v fetal bovine serum, penicillin, and streptomycin (100 U/ml and 100 mg/ml, respectively) in standard cell culture flasks. The sub-confluent cultures were split when reaching 70-80% confluence. F7 cells were detached by incubation with 0.25% trypsin-EDTA solution for 7-10 minutes at 37°C, 5% CO_2, while NG108-15 were detached from the flask surface by gently knocking the flask without adding trypsin since the cells are lightly attached. Then, cells were centrifuged with a round bucket rotor at 400 G for 5 minutes and then resuspended in a DMEM-complete medium for use in experimental studies.

Dorsal root ganglion (DRG) is one of the most widely used sources of primary neural cells as it contains pseudo-unipolar neurons, glial cells (a mixture of Schwann cells and satellite glial cells), and other cells such as fibroblasts and endothelial cells. It

is located in a dorsal root of a spinal cord and can be purified and prepared to obtain each particular cell type. The DRG culture can be used to study molecular mechanisms, cellular survival and physiology, electrophysiology, signal transduction, or neural development.

Dorsal root ganglion (DRG) neurons were obtained from postnatal 2 (P2) day-old Sprague Dawley rats as a source of primary neurons. To obtain the DRGs, the spinal column was excised from P2 Sprague-Dawley rats that were culled using decapitation. The spinal column was divided in half in the sagittal plane to expose the spinal cord, and the cord tissue was removed to expose the DRGs and roots in the intervertebral foramen. Using the Olympus SZ40 dissecting microscope with Volpi, Intralux® 6000 optical fibre light source, the DRGs were removed and placed in a universal tube containing DMEM supplemented with penicillin and streptomycin. Approximately twenty DRGs were collected from each animal's thoracic and lumbar regions. The DRGs were transferred to a petri dish and incubated in 2.5 ml 0.125% collagenase type IV – prepared in serum-free DMEM media supplemented with 100µg/ml penicillin and streptomycin solution – at 37°C, 5% CO_2 for 90 minutes. The collagenase-treated explants were mechanically dissociated by trituration with a 1ml Gilson pipette. Collagenase was removed by two 20ml spin washes in DMEM-complete at 400 G for 5 minutes. For experimental studies, cells were resuspended in a DMEM-complete medium as 'crude' DRG preparations.

To obtain enriched cultures of DRG neurons by depletion of satellite glial cells and any fibroblasts, the crude cell pellet was resuspended in 10 ml DMEM-complete supplemented with 0.01mM cytosine arabinoside and plated in a poly-D-lysine coated flask (cells from 2-3 pups per flask) and incubated at 37°C, 5% CO_2 for 24 hours before use. DRG neurons were detached by incubation with 0.25% trypsin-EDTA solution for 7-10 minutes at 37°C, 5% CO_2. Cells were recovered by centrifugation at 400 x g for 5 minutes and then resuspended in a DMEM-complete medium for experimental studies.

Primary glial cell cultures were prepared by subculturing the crude DRG culture in a DMEM-complete medium for extended days to increase the proportion of proliferating glial cells in the culture. The duration of subculturing that optimised glial cell culture preparation was investigated in Section 4.2.1.

2.2.2 Media testing for the co-culture of NG108-15 and F7 Schwann cells

Three media solutions were investigated: DMEM-complete medium, serum-free DMEM medium, and conditioned medium taken from F7 culture at 70-80% confluence. Each medium was added on top of two different substrates: glass surface coated with poly-D-lysine and collagen gels in 24-well plates. The collagen gels were prepared from 80% v/v type I rat tail collagen, 10% v/v 10 x minimum essential medium, and 10% v/v DMEM with FBS. Before adding the cell suspension, drops of sodium hydroxide diluted 1:10 in PBS were slowly added to the gel mixture to adjust pH for gel neutralisation. 400 µl of the collagen gel mixture was added to each well and allowed to set at 37°C, 5% CO_2 for 10 minutes. 10,000 NG108-15 cells were seeded on top of each collagen gel or glass surface, and subsequently, 800 µl of one medium was added into each well. Therefore, in each experiment, there were 6 culture conditions: three different media and two different surfaces. NG108-15 were incubated at 37°C, 5% CO_2 for 72 hours. The number of cells per field and neurite length of each cell in each condition was measured.

2.2.3 Contraction profile to identify cell contractibility

Contraction Profile is a cell-matrix interaction assay system for determining the ability of cells to contract free-floating collagen gels, providing information about the optimal number of cells and ratio of neurons and Schwann cells required to create alignment in self-organising guidance conduit. NG108-15 and F7 Schwann cells were co-cultured in 6 conditions: 3 different NG108-15/F7 ratios (1/2, 1/4, and 1/8), and 2

different F7 densities: 4 x 10^6, 2 x 10^6 cells/ ml collagen gel. The collagen gels were prepared from 80% v/v type I rat tail collagen (2 mg/ml in 0.6% acetic acid), 10% v/v 10x minimum essential medium, and 10% v/v cell suspension containing cells in FBS-supplemented DMEM. Before adding the cell suspension, drops of sodium hydroxide diluted 1:10 in PBS were slowly added to the gel mixture to adjust pH for gel neutralisation. 75 µl of the collagen gel mixture was added to each well in a 96-well plate and allowed to set at 37°C, 5% CO_2 for 10 minutes before 200 µl media was added. The gels were incubated at 37°C, 5% CO_2 for 15 minutes and detached from well plates using a needle. The free-floating gels were then incubated at 37°C, 5% CO_2 for up to 24 hours. Then, the media was removed, and the gels photographed. The contraction (% change in gel size compared to initial dimensions) was measured using ImageJ software.

2.2.4 Fabrication of collagen gels in tethered aligned system

Collagen gel mixture was prepared from 80% v/v type I rat tail collagen (2 mg/ml in 0.6% acetic acid), 10% v/v 10x minimum essential medium, and 10% v/v cell suspension containing neurons and Schwann cells at a required density. Before adding the cell suspension, drops of sodium hydroxide diluted 1:10 in PBS were slowly added to the gel mixture to adjust pH for gel neutralisation. An approximate amount of 43 µl per 1 ml of gel mixture was sufficient to neutralise the gel mixture at 4 °C as the yellow colour of the phenol red indicator in the gel mixture was observed to change to a faint pink. The cell suspension was added to the neutralised gel mixture and slowly resuspended for cell distribution. The complete cellular gel mixture at a required volume was gently added to a specific mould (described in 2.2.5 and 2.2.6) at 4 °C. In order to obtain consistent gel contraction, tethering meshes or holes were thoroughly soaked in the gel for optimal gel integration. The cellular gel in the mould was then incubated at 37 °C in a humidified chamber with 5% CO_2 and 95% air for 15 minutes to allow gel setting before adding DMEM-complete medium to the mould. After incubating for at least 24 hours, gel

contraction was observed consistent with formation of a self-aligned cellular hydrogel system as demonstrated previously (Sanen et al., 2017, Georgiou et al., 2013).

2.2.5 Tethered Aligned Engineered Neural Tissue (TaeNT)

An *in vitro* fully-hydrated cellular hydrogel system mainly consists of a rectangular nylon culture mould with the dimension of 3 x 3.8 x 0.5 cm and 4 pieces of tethering mesh with the dimension of 6 x 17 x 0.3 mm (Figure 2.1). The mould has an H-shape cavity cut through the middle to accommodate the gel and tethering meshes. To prepare the materials, the culture mould, tethering meshes, and pieces of parafilm were sterilised by soaking in 70% ethanol for at least an hour and leaving to completely dry inside the tissue culture hood. A piece of sterile parafilm was used to seal the mould base before it was placed in a petri dish. 2 pieces of tethering mesh were placed at each end of the mould cavity.

1 ml of the gel mixture containing F7 Schwann cells at the density of 4 x 10^6 cells/ml prepared by methods in Section 2.2.4 was added to the assembled mould at 4 °C and integrated with tethering mesh at both ends. To optimise the gel integration, approximately 100 µl of the gel mixture was firstly added to the tethering mesh to soak it thoroughly before adding the remaining gel mixture into the mould. After setting for 15 min at 37°C, tethered gels were incubated in DMEM with FBS at 37°C with 5% CO_2 and 95% air for 24 hours to allow Schwann cell contraction and alignment to take place, then 0.1 x 10^6 NG108-15 in 50 µl DMEM supplemented with 10% FBS was seeded on top of the gels and incubated to promote cell attachment on gels at 37°C, 5% CO_2 for 1 hour. Then, the TaeNT was topped up with FBS-supplemented DMEM and maintained for 3 days.

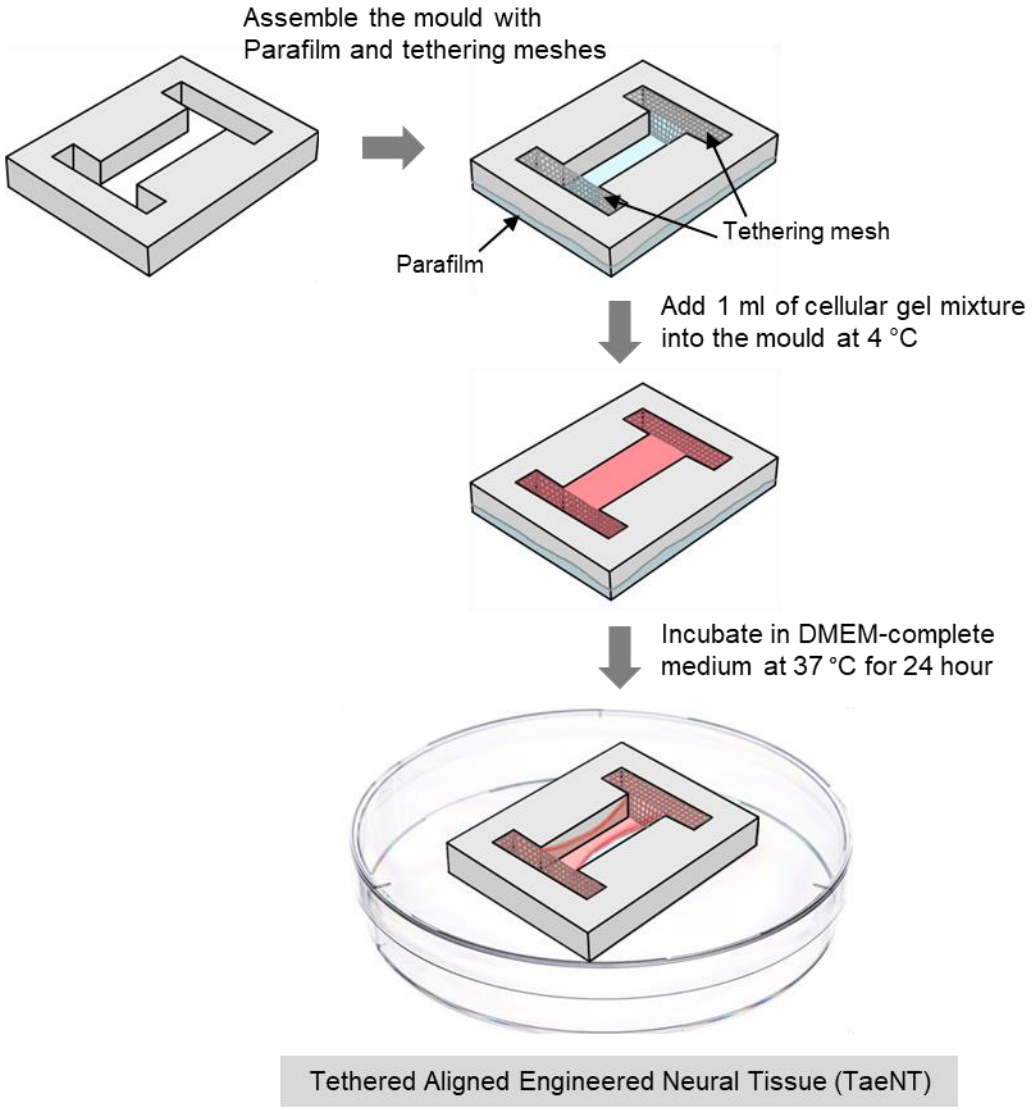

Figure 2.1 Fabrication of tethered aligned engineered neural tissue (TaeNT)

2.2.6 Fabrication of self-organising collagen guidance conduit for transplantation

The self-organising collagen guidance conduit is an implantable engineered living scaffold which was used here for *in vivo* studies. It is like a tethered aligned collagen-based culture system containing living cells for nerve regeneration similar to TaeNT, but modified to be in a conduit shape compatible with the nerve geometry (Figure 2.2). Medical-grade silicone tubes with an internal diameter 1.98 mm and an external diameter 3.17 mm were cut into 10 mm in length. 16 square holes were made at both ends of the silicone tube with a side length of approximately 0.9 mm each. At each end of the tube, 2 rings of 8 holes were made, using a 19-gauge hypodermic needle under a dissection microscope (Figure 2.2). The holes were analogous to the tethering mesh in TaeNT, which allowed collagen gels to become tethered at the end of the tubes during the contraction.

50 µl of collagen gel mixture containing DRG neurons and F7 Schwann cells prepared by methods in Section 2.2.4 was injected into the perforated silicone tube. Two densities of F7 Schwann cells (2 and 4 x 10^6 cells per ml) and 3 different ratios of neurons to Schwann cells (1:2, 1:4, and 1:8) were examined prior to the transplantation to optimise by contraction profile the optimal ratio considered to provide reliable contraction. To maximise gel integration, another 50 µl of the cellular collagen gel mixture was added to the perforated holes on the external surface of the tube to bridge the gel between each tethering hole. After incubating in DMEM with FBS at 37°C with 5% CO_2 and 95% air for 24 hours, gel contraction can be clearly observed with the gel under tension between the attachment points, leaving an approximately 1 mm gap at each end of the conduit to accommodate insertion of the nerve stumps.

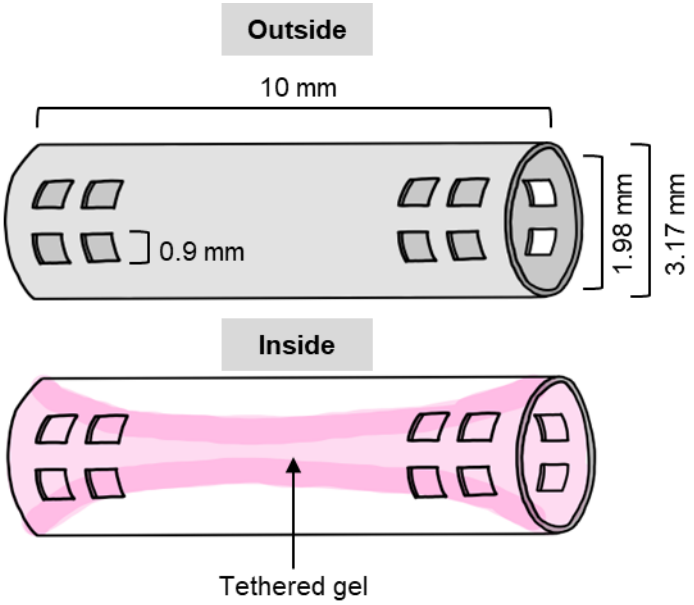

Figure 2.2 Size and dimension of a medical-grade silicone conduit for transplantation

2.2.7 Freeze-and-thaw process

The freeze-and-thaw process was selected to kill neural cells within TaeNT to examine exogenous cell behaviours when cultured with TaeNT in the absence of endogenous cell in the construct. Previous experiments using this method with stabilised tethered collagen gel containing F7 Schwann cells reported that approximately 96% of cells were dead (Georgiou et al., 2013). For fully-hydrated collagen-based tissue, 60% of fibroblasts were dead right after being frozen at a cooling rate of 40°C/min without cryoprotective agents, and the percentage of dead cells continued increasing to 90% at 24 hours after the freeze-and-thaw process (Devireddy et al., 2003, Jain et al., 2014).

TaeNT was made with the procedure explained previously. After incubating in a DMEM-complete medium for 24 hours, the medium was removed. TaeNT was detached from the mould using a surgical blade to cut both ends of the gel from the tethering meshes. The detached TaeNT was placed longitudinally inside a 1.5 ml conical cryotube. The tube containing TaeNT was rapidly frozen in liquid nitrogen at -196 °C without cryoprotective agents for 5 minutes and subsequently thawed in a water bath at 37°C for 10 minutes.

To investigate glial cell behaviour, the frozen-and-thawed TaeNT was placed in the petridish. 100 µl of DMEM-complete medium containing DRG glial cells with the density of approximately 100,000 cells was seeded on top of the frozen-and-thawed TaeNT and incubated for 1 hour to allow cell attachment to the hydrogel. The petridish with the frozen-and-thawed TaeNT was filled with DMEM-complete medium, and then fixed and immunostained for quantitative analysis after incubated for 3 days.

2.2.8 3D culture interface model

The 3D interface cultures were prepared by casting in a stainless steel mould with dimensions of 3 x 3.5 x 0.4 cm^3 (Figure 2.3). The mould has a rectangular cavity divided into 4 adjacent channels by inserting 0.1 mm-thick stainless steel dividers into the frame. The casting mould, stainless steel dividers, and a piece of parafilm were sterilised by soaking in 70% ethanol for at least an hour and leaving to completely dry inside the tissue culture hood. The sterile parafilm was used to seal the mould base which was then placed in a 60 mm diameter petridish. Since the experiment aimed to examine 2 cell populations and an acellular hydrogel, a total of 3 channels were used to cast the gel, and 2 sterile dividers were inserted into the frame. Each divided channel was filled with 400 µl of collagen gel mixture prepared with the method explained in Section 2.2.4 (80% v/v type I rat tail collagen, 10% v/v 10x minimum essential medium, and 10% v/v cell suspension or culture media without cells, neutralised with sodium hydroxide diluted 1:10 in PBS). F7 Schwann cells and primary glial cells from DRG cultures with a density of 2 million cells per ml were mixed into the collagen mixture in different channels. The mixture was filled into each channel promptly and maintained at 4°C until the dividers were removed. After removal of dividers to let the gels integrate, the collagen gel in the mould was incubated at room temperature for 10 minutes to allow setting before adding medium and being maintained at 37 °C for 3 days.

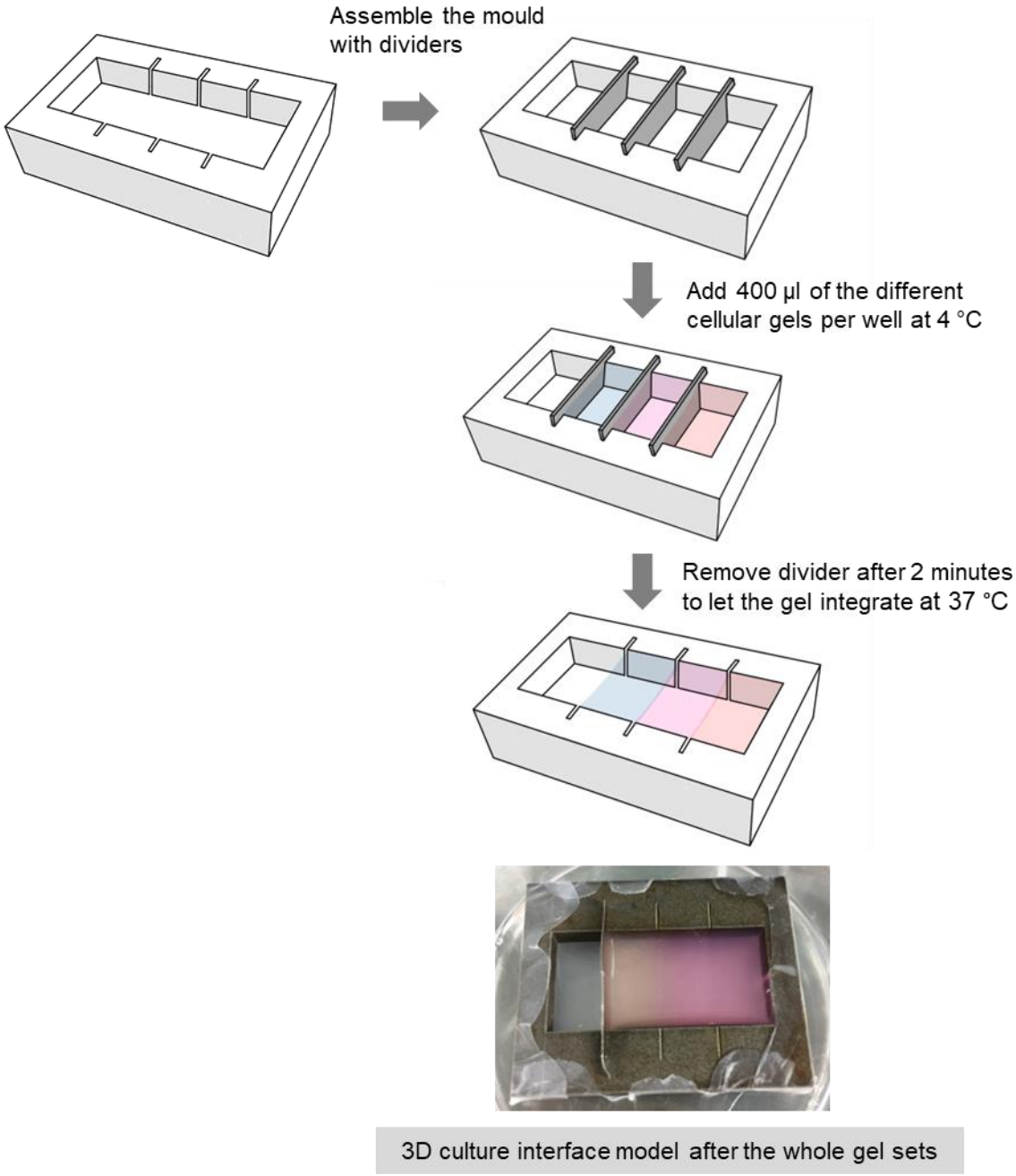

Figure 2.3 Materials for 3D interface model. *4 cavities in the mould where different cultures were divided using dividers while making the gel. Each cavity can contain approximately 400 µl of collagen. By controlling the rate of setting, gels in adjacent compartments can integrate mechanically without the cell populations mixing at the start of the experiment.*

2.2.9 Transplantation of self-organising collagen guidance conduit containing neurons and Schwann cells in rat sciatic nerve model

All surgical procedures were performed in accordance with the UK Animals (Scientific Procedures) Act (1986), the European Communities Council Directives (86/609/EEC) and approved by the UCL Animal Welfare and Ethics Review Board. Adult Wister rats (250-300 g) were housed randomly into groups in plastic cages with soft bedding and free access to food and water. After being deeply anaesthetised with isoflurane inhalation, each rat was placed under the microscope (Zeiss CL 1500 ECO), then using aseptic procedures the left sciatic nerve was exposed by making a 3-cm incision parallel to the femur between the knee and hip, where muscle layers were then separated. The sciatic nerve was released from the surrounding tissue to prepare it for a nerve transection. Neurotmesis was conducted using sharp scissors to transect the sciatic nerve at approximately 1.5 cm distal to the hip.

A self-organising collagen guidance conduit containing living cells was transplanted by placing it between the transected nerve stumps (Figure 2.4). The proximal and distal nerve stump was inserted into each end of the conduit and two 10-0 epineurial sutures were used to secure each nerve stump. The overlying muscle layers, and the skin were then closed using two 4-0 sutures and stainless steel wound clips, respectively. The rats were allowed to recover and maintained for 3 weeks post-transplantation.

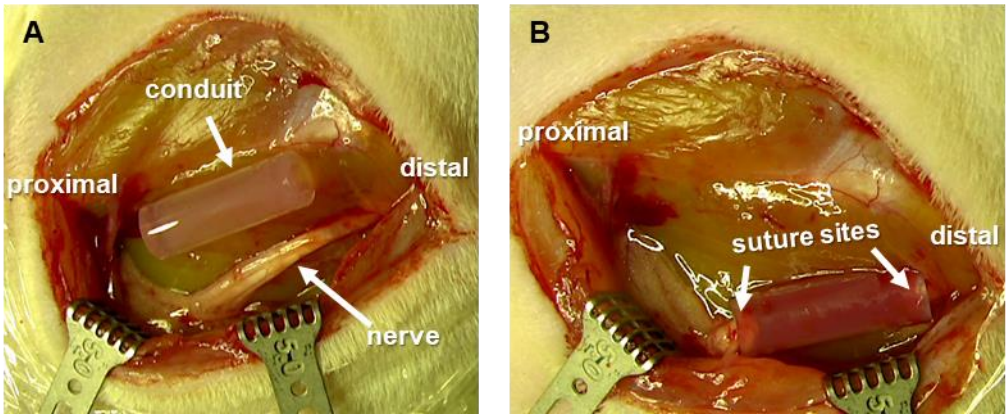

Figure 2.4 Transplantation of self-organising collagen guidance conduit in rat sciatic nerve. *(A) The nerve was exposed after release from surrounding tissue. (B) Following nerve transection, the transplanted conduit physically connected the nerve gap by suturing proximal and distal stump to each end of the conduit.*

2.2.10 Nerve tissue preparation for analysis

To harvest nerve tissue, each rat was culled by CO_2 asphyxiation (as guided by local regulations). The left sciatic nerve with transplanted conduit was immersion-fixed in 4% (w/v) PFA in PBS at 4 ºC overnight. The silicone tube was carefully removed from the tissue inside, along with approximately 3-5 mm of nerve tissue at both ends.

For cryo-sectioning preparation, the fixed nerve was dissected using a surgical blade to divide it into 5 different areas: PN (proximal nerve), PD (proximal device), middle, DD (distal device), DN (distal nerve), from proximal to distal, respectively (Figure 2.5). The length of nerve tissue in the middle was approximately 4 mm, leaving 3-mm tissue at both ends to be PD and DD. The 3-mm tissue outside the conduit next to PD and DD were PN and DN, respectively. Note that the interface between nerve and conduit was identified by the suture site, as shown in Figure 2.5C. The tissue division was subjected to different sectioning for two different analyses: PN, PD, DD, and DN was subjected to cross-sectioning for neurite distribution and interface investigation in Chapter 3, and the middle tissue was for longitudinally sectioned for cell interaction analysis in Chapter 4.

Following the harvesting and fixation, the tissue segment was incubated in 30% sucrose overnight before undergoing snap freezing in 1:1 of FSC 22 Frozen Section Media (Leica) and 30% sucrose. Either longitudinal or cross-section at 15 µm thickness was prepared by a cryostat (Leica CM1860) and then adhered to glass slides for histological analysis.

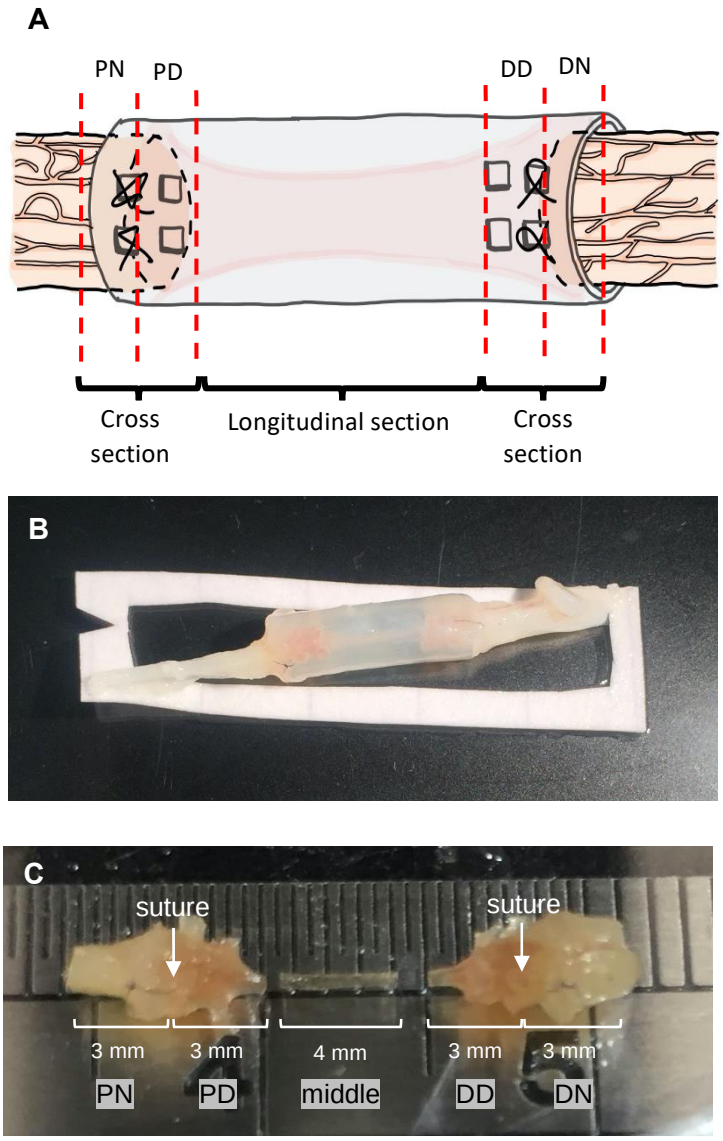

Figure 2.5 Tissue harvesting and division for different analyses. *(A) Area identification of self-organising collagen guidance conduit in rat sciatic nerve after transplanting in rat sciatic nerve for 3 weeks. Both 3-mm ends of the conduit were cross-sectioned, while the tissue in the middle part inside the conduit was for longitudinal sectioning. (B) Rat sciatic nerve with transplanted conduit harvested after 4 weeks post-transplantation. (C) Nerve tissue after conduit removal. The white arrow indicates a suture site at both ends of the conduit.*

2.2.11 Immunocytochemical labelling

For *in vitro* experiments in the monolayer cell culture, after incubating cells for a specific time, media was removed, and the culture substrate was gently washed with PBS and fixed with 4% paraformaldehyde in PBS overnight. Each well was incubated with 0.5% (v/v) Triton-X at room temperature for 15 minutes to permeabilise the cells, and blocked with 5% goat or horse serum at room temperature for 15 minutes before washing and primary antibody addition. For collagen gels, fixing, permeabilising, and blocking protocol were similar with double incubating time (30 minutes), and the gels were released from the mould and placed in a well plate after fixation.

Monoclonal anti-βIII-tubulin antibody and anti-S100 antibody were used to immunostain neurites and F7 Schwann cells, respectively. These primary antibodies were diluted to 1/400 in PBS and added to each well to incubate overnight. Then, the samples were washed for 6 times (15 minutes each) and incubated in corresponding anti-mouse or anti-rabbit (secondary antibody) diluted to 1/300 in PBS at room temperature for 45 minutes in the 2D substrate and 90 minutes in the 3D substrate. To stain nucleic acid, Hoechst 33342 was added and incubated at room temperature for 15 minutes.

For the tissue sections from *in vivo* experiments (Section 2.2.9), nerve sections mounted on glass slides were washed with PBS and then permeabilised and blocked with 10% goat or horse serum and 0.3% Triton-X diluted in PBS at room temperature for 2 hours. The tissue sections were gently washed and incubated with the primary antibody in 10% goat or horse serum in PBS inside a humidified box at 4 ºC overnight. Anti-neurofilament and anti-S100 antibodies were used to immunostain neurites and F7 Schwann cells, respectively. After incubating with primary antibodies, the sections were washed with PBS before incubating with corresponding secondary antibodies in 10% goat or horse serum in PBS at room temperature for 2 hours. The sections were washed with PBS and mounted using Vectashield HardSet mounting medium.

2.2.12 Dynamic mechanical analysis (DMA)

Although tensile testing can also provide similar mechanical measurement to determine viscoelasticity properties of the specimen (i.e., storage modulus, loss modulus, tan delta), there is a difficulty in gripping both end of the gel as the gel is very soft and easy to break. In this project, uniaxial mechanical compression test was more suitable to analyse the mechanical properties of the whole fully-hydrated collagen gel.

The DMA compression test was performed using a Bose Electroforce (3200 Series II, TA Instruments) and WinTest 7 software. TaeNT and frozen-and-thawed TaeNT were prepared and measured their dimensions using a vernier caliper (Figure 2.6). The gel was placed between two metal platens where the load and displacement values were zeroed. To ensure the gel-platen contact, platens were adjusted to slowly brought together until a small initial deflection in platen displacement was observed in the WinTest 7 software. An initial ramp of 15% pre-strain was applied with a 1 Hz pre-conditioning cycle. DMA cycle was then measured by setting 2% dynamic amplitude and 1-70 Hz ascending frequency sweep. Storage modulus (E') and loss modulus (E'') at frequency from 1 to 70 Hz were plotted into the graphs. Tan delta was calculated from the ratio of loss modulus to storage modulus. The gel was considered to be in a rectangular shape with the dimension of L 16.6 x W 3.6 x H 1.3 mm^3 for the calculation. All specimens were tested at room temperature and fully hydrated in DMEM.

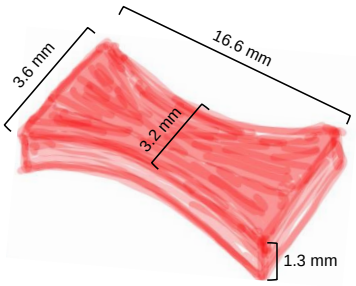

Figure 2.6 Dimensions of TaeNT in fully-hydrated condition after removing from the mould. *The measurement was done using a vernier caliper, and each dimension was an average value of 3 samples prepared independently.*

2.3 Image analysis and quantification

2.3.1 Scanning electron microscopy (SEM)

The alignment of the collagen matrix in Chapter 4 was visualised using scanning electron microscopy (Philips XL30 FEG or FEI Quanta 200F) operating at 5 kV. Prior to the imaging, the sample was fixed with PFA and dehydrated in a series of graded ethyl alcohols at room temperature. The sample was immersed in 70% and 90% ethyl alcohol for 15 minutes each, respectively, and then soaked 3 times in 100% ethyl alcohol for 10 minutes each. The sample preparation was completed with a further drying process by immersing the sample in Hexamethyldisilazane (HMDS) in a metal foil container for 5 minutes and placing on filter paper to dry in the fume hood for at least an hour. The 3D collagen gel was mounted onto metal specimen stubs with double-sided adhesive tape, then vacuum coated with a platinum film. Images at various resolutions were taken for quantification analysis by Volocity™ 6.4 (PerkinElmer) software.

2.3.2 Fluorescence microscopy

The immunostained samples were soaked in PBS and visualised under Leica DM IRB fluorescence microscope starting with 4X objective lens for scanning and then 10X objective lens for imaging. The number of cells, neurite length and angle between neurite and aligned cells in Chapter 3 were measured by ImageJ software (Schneider et al., 2012). The angle of deviation was calculated from the angle between the alignment of each individual neurite and the main longitudinal axis of the construct.

2.3.3 Confocal microscopy

LSM confocal microscopy (Zeiss LSM 710) was used to visualise immunostained cells in 3D collagen scaffolds after longitudinal or transverse sectioning. The images

were then analysed using Volocity™ 6.4 (PerkinElmer) software with automated image analysis protocols.

Cells immunostained for S-100 and GFP were automatically detected in different channels and then characterised as either host glial cells or transplanted glial cells by an intersecting or subtracting protocol. Host glial cells were positive in both S-100 and GFP channels, while transplanted glial cells were positive only in the S-100 channel and not the GFP channel (Figure 2.7). Likewise, cells immunostained for neurofilament and GFP were characterised as either host neurites or transplanted neurites by the similar method. Host neurites were positive in both neurofilament and GFP channels, while transplanted neurites were positive only in the neurofilament channel and not the GFP channel.

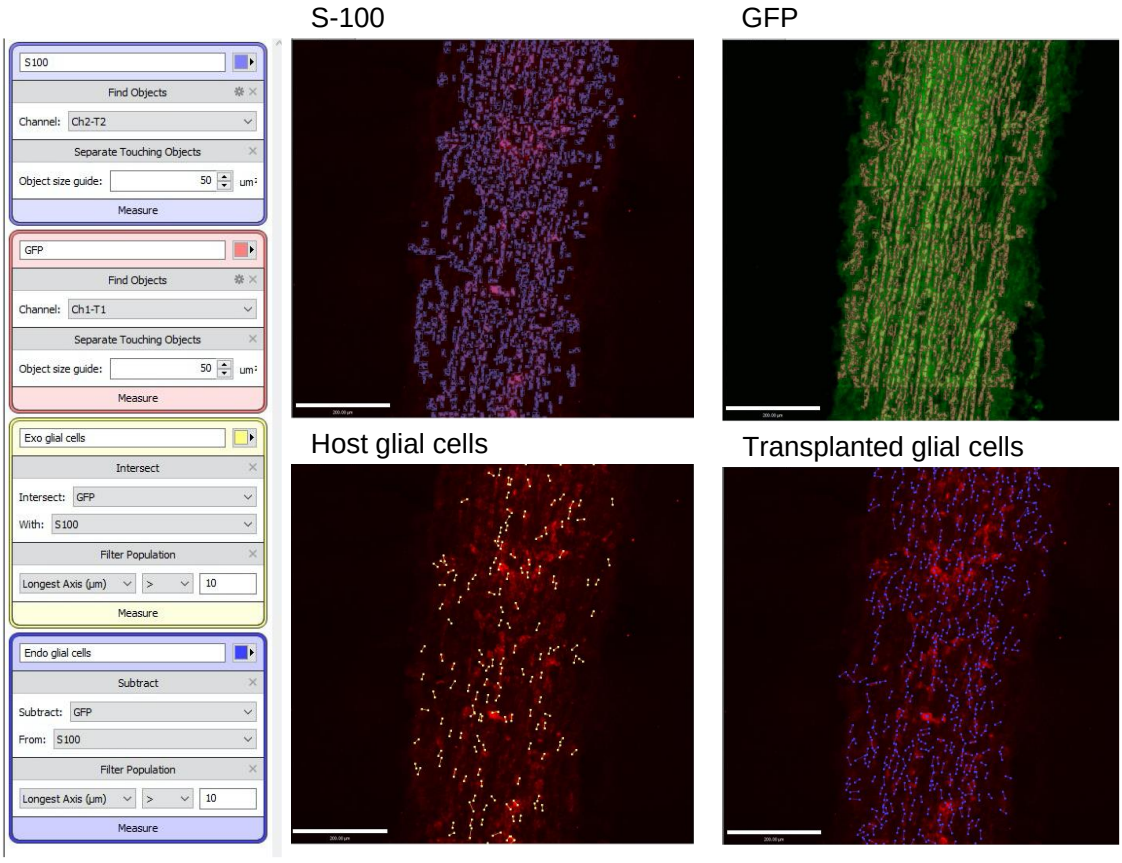

Figure 2.7 Example of localisation analysis protocol from Volocity™ software. *Cells immunostained for S-100 and GFP were detected in different channels and then characterised as either host glial cells or transplanted glial cells by an intersecting or subtracting protocol.*

2.3.4 Statistical analysis

For the statistical tests to determine differences between groups, either analysis of variance (ANOVA) or t-tests were performed as appropriate. A one-way ANOVA was followed by Tukey's multiple comparison post hoc test to compare every mean to every other means where *p<0.05, **p<0.01, ***p<0.001 and ****p<0.0001 were considered to be significant. Retrospective power and sample size analysis were also computed to determine whether group sizes in particular *in vivo* experiments had enough power.

Box-and-whisker plots were used to display descriptive statistics, depicting groups of numerical data through their quartiles. These represent data with 5 values as a summary of a data set: minimum, first quartile, median, third quartile, and maximum. A box was plotted from the first quartile to the third quartile, with a median value in between. The whiskers at both sides of the box go from the first and third quartile to the minimum and maximum value, respectively.

CHAPTER 3

Tethered Aligned Engineered Neural Tissue (TaeNT) containing neurons and Schwann cells as a substrate for neurite elongation

3.1 Introduction

3.1.1 Motor neurons in nerve regeneration

The preliminary experiments of the research were focused on identifying the appropriate source of neurons to be used in the engineered construct. Many previous PNS studies have been done with sensory neurons from dorsal root ganglia (DRGs) as a conventional model in peripheral neuropathies because it is easy to culture and purify. However, sensory neurons from DRGs might not be the most suitable source of neuron to be used for peripheral nerve interface because of the lack of ability to form neuromuscular junctions in the body, while motor neurons can innervate skeletal muscle fibres and form neuromuscular junctions (Gutmann, 1945, Langley and Anderson, 1904, Weiss, 1945, Zalewski, 1970). Since this project is aimed to develop engineered neuron-containing tissue for peripheral nerve regeneration, motor neurons would be one of the better sources for functional recovery of muscle.

Motor neurons carry signals from the CNS to control effector parts of the body by projecting axons from their cell body in the spinal cord to the target muscle cells. The morphological features of motor neurons are varied in size, branching patterns, and axon length. In humans, some motor neurons have projecting axons which can be as long as 1 metre elongating from spinal cord to the lower limb. For *in vitro* studies, there are 3 main sources of motor neuron used in cell culture studies: primary cells, immortalised cell lines, and stem cell-derived cells.

Primary cells are purified populations of cells isolated from specific organs or tissues, thus are expected to be more representative of natural motor neurons in biological systems. Compared to the use of immortalised cell lines, aspects such as neuronal morphology, neurotoxicity, disease modelling, and various neuronal activities can sometimes be more reliably explored in primary cultures as they are derived directly from *in vivo* tissue. A number of protocols have been developed to overcome difficulties in culture and purification of motor neurons (Beaudet et al., 2015, Gingras et al., 2007, Graber and Harris, 2013) enabling us to use primary motor neurons in peripheral nerve research. However, primary cells have limited expansion capacity, and it is difficult to obtain purified populations due to contamination with other cell types (Gordon et al., 2013). To obtain healthy cultures and good morphology, isolation and purification of primary neurons requires various additional media and supplements which are specifically customised for each cell type. The use of primary cells can increase the cost, time, and complexity of research. Hence, many researchers only use primary cells to verify and refine experimental results following investigations with model cell lines.

An immortalised cell line is a population of mutant cells which can be passaged under certain conditions for a long period of time *in vitro*. When a population of cells mutate either spontaneously in nature or experimentally induced in the laboratory, cells can undergo indefinite division due to the absence of cellular senescence. The prolonged proliferating cells are commonly used in preliminary *in vitro* research due to their reproducibility and similar characteristics to primary cells. NG108-15 cell line is a somatic cell hybrid of mouse neuroblastoma clone N18TG-2 and rat glioma clone C6 Bv-1, and has been widely used for *in vitro* studies as it has similar characteristics to motor neurons; it is cholinergic in nature and can form neuromuscular junctions when co-cultured with muscle cells (Busis et al., 1984). It also responds to electrical stimulation by accelerating its neuromuscular junction formation (Fukazawa et al., 2013). However, since immortalised cell lines are produced from mutation, some genetic and phenotypic characteristics are different from cells in the body, so they do not maintain important

functions and markers that are normally seen *in vivo* (Pan et al., 2009). Many investigations have also reported a frequent occurrence of misidentification and contamination in cell lines leading to unreliable results. At least 15 percent of cell lines sent from laboratories in United states, Europe, and Asia have been found to be misidentified or contaminated (Lorsch et al., 2014). Cultured cell lines can be contaminated by other microorganisms or phenotypically altered by chromosomal duplications, mutation, and epigenetic changes after a large number of passages.

Moreover, functional motor neurons can also be derived from embryonic and induced pluripotent stem cells by reprogramming and direct differentiation. Under suitable culture conditions, stem cells are self-renewing progenitors that can form either expanded stem cells or differentiated cells for specific functions. Several researchers have previously reported the successful motor neuron differentiation from stem cells by adding or withdrawing growth factors such as fibroblast growth factor (bFGF), epidermal growth factor (EGF), retinoic acid (RA), and Sonic hedgehog (Shh) (Goncalves et al., 2005, Lee et al., 2007, MacDonald et al., 2003, Thonhoff et al., 2009). Although the derived motor neurons could be less physiologic compared to primary cells, it is expandable and provides better purity of motor neurons in the culture. In the translational stage, the use of stem cell-derived motor neurons enables personalised transplantation to patients with a low risk of immune rejection. However, the culturing and differentiation method of stem cell-derived motor neurons involves a number of parameters, such as media composition, and requires optimisation for co-culture in specific biomaterials. Therefore, to simplify the protocol for a proof-of-concept study on transplanted conduits, the use of stem cells with complex culture conditions was eliminated and will be included in further research.

3.1.2 Source of cells for neurite elongation study

For preliminary *in vitro* modelling in this chapter, a simple, reliable, and cheap cell line would allow the engineered tissue experiments to be conducted easily. Here, NG108-15 was chosen to be an *in vitro* model cell line as it exhibits characteristics of motor neurons with neurite outgrowth (Smalheiser, 1989). Many previous studies have reported methods to optimise neurite length of NG108-15 *in vitro*. Table 3.1 presents the results of a systematic literature review of NG108-15 culture protocols, providing average neurite length at particular time points. The longest neurite lengths of NG108-15 in the review were from co-culture with Schwann cells (Armstrong et al., 2008, Kingham et al., 2007).

According to ATCC (American type culture collection), the base medium for NG108-15 cell line is Dulbecco's Modified Eagle's Medium (DMEM) with 10% fetal bovine serum (FBS). FBS is a standard supplement of cell culture medium containing a number of growth factors and other necessary ingredients to facilitate sustained cell growth and activities (Gstraunthaler, 2003). However, many studies also used defined medium or serum-free DMEM to culture NG108-15 for neurite elongation as the removal of FBS from DMEM was reported to induce differentiation and neurite outgrowth of neuroblastoma cells (Ghahary et al., 1989, Harkins et al., 1972, Krystosek, 1989). It was established that NG108-15 cultured in a defined medium exhibited morphology, proliferation, and viability similar to those of cells cultured in medium supplemented with 5% fetal calf serum (Griffin et al., 1985). For electrophysiological studies, serum-free medium is suggested to be suitable as excitability of NG108-15 depends on the amount of serum supplement in the medium, and regenerative action potentials spontaneously occur more frequently when cells are cultured in serum-free medium (Kowtha et al., 1996, Kowtha et al., 1993).

However, the *in vitro* experiment in this chapter included co-culture of NG108-15 with F7 Schwann cells whose culture medium was FBS-supplemented DMEM. Also,

previous experiments have commonly used FBS-supplemented DMEM to co-culture F7 Schwann cells and neurons (Georgiou et al., 2013, Muangsanit et al., 2020, Rayner et al., 2018, Santiago-Toledo et al., 2019). Therefore, different co-culture conditions for NG108-15 were tested at the beginning of this chapter to verify a suitable condition to support both cell populations in term of proliferation and neurite outgrowth, compared to other culture conditions.

Reference	Culture Method	Duration (day)	Neurite length (μm)	
			Control	Induced
(Kraus et al., 2015)	3D-Schwann cell-neuron spheroid model (embedded in collagen)	10	65	176
(Palazzolo et al., 2012)	incubated in C3 transferase and flavonoid isoquercitrin	2	30	210
(Paviolo et al., 2013)	Laser exposure of gold nanorods	3	70	90
(Tomita et al., 2013)	co-cultured with human dADSCs	1	10	33
(Tong et al., 2010)	co-cultured with differentiated NSCs	1	n/a	242.3
	co-cultured with undifferentiated NSCs			78.9
	co-cultured with SCs			260.8
(Kingham et al., 2007)		1	67.5	309.8
(Kingham et al., 2009)	co-cultured with dADSCs	1	41	147.72
(Kingham et al., 2007)		1	67.5	205.2
(Kingham et al., 2009)	co-cultured with ADSCs + DAPT	1	41	133.48
(Armstrong et al., 2008)	co-cultured with SCs seeded on laminin	1	n/a	238.74
		3		321.89
	co-cultured with SCs seeded on PDL	1		157.57
(Armstrong et al., 2007)	co-cultured with SCs seeded on fibronectin	1	40.5	283.8
	co-cultured with SCs seeded on collagen	1		111.9
(Wu et al., 2007)	cross-linking of GM1 ganglioside with multivalent ligands	2	199	292

Reference	Culture Method	Duration (day)	Neurite length (μm)	
			Control	Induced
(Ehrlicher et al., 2007)	Valproic acid	6	75	150
(Kim et al., 2003)	Dexamethasone	1	20	100
	cAMP	1		135
	Dexamethasone+ indomethacin+ PGE2	1		100
(Kadoyama et al., 2001)	cyclooxygenase-2 (COX) enzyme	-	40	85
(Tohda and Jacobowitz, 1999)	Sproutin (neurite growth factor) by transfection	7	25	47.7
(Zhong et al., 1999)	Overexpression of Adhesion Molecule L1 and cAMP by transfection	4	94.2	142.5
(Lozano et al., 1995)	plated on Poly-L-Lysine (PLL)	1	n/a	78
(Krystosek, 1989)	1-β-d-Arabinofuranosylcytosine in N2 Medium (Ara-C) after serum-free	3	183	198

Table 3.1 Systematic literature review of NG108-15 neurite length with various in vitro induction for neurite elongation from 1989-2016. *A literature search was performed on PubMed database in September 2016 with the keywords "NG108-15" and "neurite". This initial literature search identified 149 articles for further review and analysis. In the elimination process, the search was limited to articles with quantification of NG108-15 neurite length in vitro culture. The average neurite length incubated in the controlled and induced condition from each literature was reviewed. The controlled and induced neurite length refers to an average length of neurites measured without and with the specific induction in the culture at a similar duration, respectively.*

3.1.3 Interface between host tissue and transplanted neurons

Several studies using a hollow or acellular biomaterial conduit for peripheral nerve transplantation aimed to focus on behaviour and interaction of cells inside the transplanted conduit. Following conduit transplantation into the nerve gap, the biological system responds to the transplant by various cells and cellular components entering the transplanted conduit. The infiltration of Schwann cells, fibroblasts, mast cells, and macrophages to the site have been previously studied, as well as the morphology of regenerating neurites across the conduit (Fogli et al., 2019, Fornasari et al., 2020, Mokarram et al., 2012, Quigley et al., 2013, Suzuki et al., 2000).

Nevertheless, when a conduit containing neurons is transplanted into the injured site, focusing only on cells from host tissue entering the conduit is not enough to understand the regeneration scenario, because the presence of transplanted cells inside the conduit might affect the organisation and interaction of cells and consequently influence the regeneration. The interface between host tissue and transplanted conduit is an important region to investigate as it is the first area where host and transplanted cells are spatially colocalised with each other. Understanding how the presence of other cell populations influences the interface-crossing behaviour, cell distribution and integration of host and transplanted cells will help to determine the potential of cellular transplanted conduits in peripheral nerve regeneration.

Some previous studies have reported the interaction of host and transplanted cells at the interface after transplantation. In CNS research, micro-tissue engineered neural networks (micro-TENNs) containing primary cerebral cortical neurons with long-distance axonal tracts designed to rebuild disrupted axonal pathways by directly replacing and modulating neural circuitry have been investigated. The 4 mm micro-TENNs was injected into rats to bridge the deep thalamus to the cerebral cortex. The transplanted neurites survived for at least 1 month, and penetrated into the host cortex with synapse formation. The axons from transplanted micro-TENNs elongated into host

cortex and became part of a long-distance axonal pathway in the brain (Struzyna et al., 2015b). In the PNS, Huang et al. found that DRG neurons transplanted inside a 12 mm conduit survived and integrated with host tissue by penetrating neurites into the host sciatic nerve despite the absence of immunosuppressive therapy (Huang et al., 2009). After 16 weeks, the transplanted axons mediated host axonal regeneration across the injured site and formed intimate contacts by intertwining with each other. Tightly packed tracts of both host and transplanted neurites were observed inside the transplanted conduits indicating that host neurites also elongated into the transplanted area.

It is noticeable that previous studies on the neurites at the interface have tended to use longitudinal sections of nerve tissue (Figure 3.1) to observe neurite elongation throughout the transplanted conduit. That approach provides a number of immunostained images that can be arranged into a continuous image of the whole nerve segment from proximal to distal stump. Although the advantage of this approach is that intertwined neurites can be followed through the repair site, it is difficult to quantify neurites that grow through different planes, so precise distribution of host and transplanted neurite at the interface and in other parts of the conduit remains unknown.

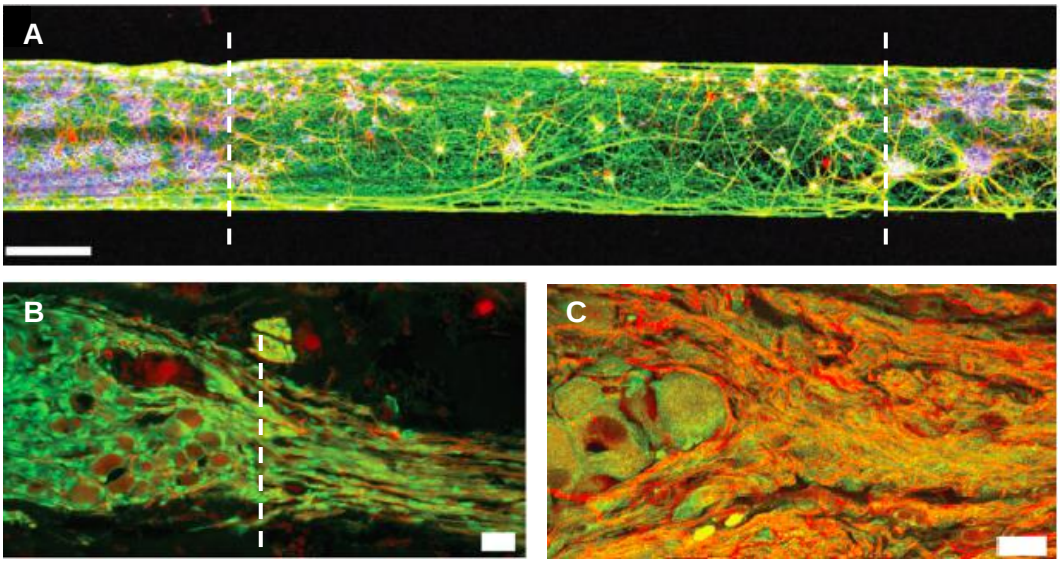

Figure 3.1 Longitudinal sections of nerve tissue at a transplanted region from previous studies. *Host and transplanted neurites elongated across the interface to another region indicating the spatial integration of neurite after cellular conduit transplantation. White lines represent an interface between host tissue and transplanted conduit. (A) micro-TENNs in cerebral cortex (MAP-2 [red]; β-tubulin III [green]; Hoechst [blue]). The dense cluster of neurons were found the both end of the conduit extending neurites across the interface. (B, C) Engineered nervous tissue construct consisted of DRG neurons in rat sciatic nerve (NF-200 [red]; GFP+ [green] for transplanted cells). The packed track of neurites elongated across the interface (B) and inside the transplanted conduit (C). Scale bar (A) = 200 μm; (B, C) = 20 μm. (Huang et al., 2009, Struzyna et al., 2015b).*

3.1.4 Objectives of this chapter

The main objective of this chapter was to investigate the potential of tethered aligned engineered neural tissue (TaeNT) containing neurons and Schwann cells in terms of supporting neurite elongation within the transplant and across the host/graft interface. Both *in vitro* and *in vivo* experiments were carried out. The length, alignment, and interface-crossing of neurites were quantified to provide preliminary experimental evidence about TaeNT containing neurons and Schwann cells in peripheral nerve regeneration.

Initially, an *in vitro* experiment measured neurite length and alignment of the motor neuron cell line (NG108-15) seeded on top of TaeNT containing aligned Schwann cell line (F7). The neurite length of NG108-15 in the co-culture system was then compared with other studies to evaluate the potential of the culture system in supporting neurite elongation. The preliminary experiments included substrate and medium testing for NG108-15 to compare TaeNT culture with other culture conditions by measuring cell density and percentage of cells with neurite elongation.

In vivo experiments then aimed to examine and quantify the distribution of neurites from different sources after transplantation of TaeNT, and to investigate interface-crossing behaviours of neurites elongating from the proximal stump into the transplanted conduit and of transplanted neurites elongating from the conduit into the host tissue. TaeNT was modified to be in the form of a self-organising collagen guidance conduit to allow a compatible shape with the nerve geometry. The optimal ratio and number of cells in the transplanted construct was determined prior to transplantation through a contraction profile experiment using collagen gels containing both neurons and Schwann cells. The self-organising collagen guidance conduit was transplanted into a 10-mm rat sciatic nerve gap for 3 weeks. To assess the distribution and interface-crossing of neurites after the transplantation, the number and density of both host and transplanted neurites at different area along the conduit interface were quantified.

In the *in vivo* studies, the source of neurons chosen for the construct transplantation was changed from NG108-15 to primary therapeutic cells because transplanting immortalised cell lines had several limitations, such as uncontrollable changes in phenotype and functional alterations, resulting in the comparatively low relevance of immortalised cell line transplantation in *in vivo* research. Primary DRG neurons were thus chosen to be used as a suitable source of neurons for the *in vivo* studies in this research project. Although DRG neurons were not motor neurons, which were likely to be more suitable for functional recovery of muscles (Section 3.1.1), it was considered to be a useful model cell source which was sufficient to provide preliminary evidence on neurite behaviour after cell transplantation. More sophisticated engineered protocols for TaeNT (e.g., the use of motor neurons purified from primary cell culture) could be optimised and examined later in the future work.

3.2 Results

3.2.1 Culture medium for the co-culture of NG108-15 and F7 Schwann cells

Prior to *in vitro* co-culture experiments, the effect of medium and substrate on NG108-15 cell density and neurite outgrowth was justified through testing 3 different culture media (FBS-supplemented DMEM, serum-free DMEM, and conditioned medium from F7) on 2 different substrates (collagen gel and PDL-coated glass surface) (Figure 3.2). FBS-supplemented DMEM (condition A, D) and serum-free DMEM (condition B, E) were common culture conditions for F7 and NG108-15, respectively. Conditioned medium from F7 in FBS-supplemented DMEM (condition C, F) represented a co-culture condition of NG108-15 with F7. PDL-coated glass surface was a culture substrate for general monolayer culture, and collagen gel was a substrate used to fabricate TaeNT. In this way, the co-culture condition of NG108-15 with F7 Schwann cells in TaeNT was represented by condition C.

NG108-15 cells were cultured on different substrates and incubated in different medium for 3 days with the initial density of 10,000 cells per well. Immunofluorescence images showed differences in number of cells, cell aggregation and neurite outgrowth corresponding to different types of medium and substrates (Figure 3.2). According to immunostaining images, cell clumps were observed in collagen gel condition, and neurites were noticeably found to elongate from a single cell than aggregating cells.

Five immunofluorescence images from each culture condition were quantified to determine the total number of cells per image and the proportion of cells with neurite elongation (Figure 3.2). The cell density and neurite outgrowth of NG108-15 in all culture conditions was statistically compared to those in conditioned medium on collagen gel (condition C) which represented culture condition of NG108-15 in TaeNT. The ordinary one-way ANOVA test with Dunnett's post-hoc test showed no difference in cell density in all comparisons. However, the percentage of NG108-15 with neurite outgrowth in serum-free DMEM and conditioned medium on PDL-coated substrate (condition E and

F) were significantly higher than that in the TaeNT condition. Almost 50% of NG108-15 cells cultured in serum-free DMEM on PDL-coated glass surface elongated at least one neurite, while approximately 10% of NG108-15 cells in TaeNT condition had neurites.

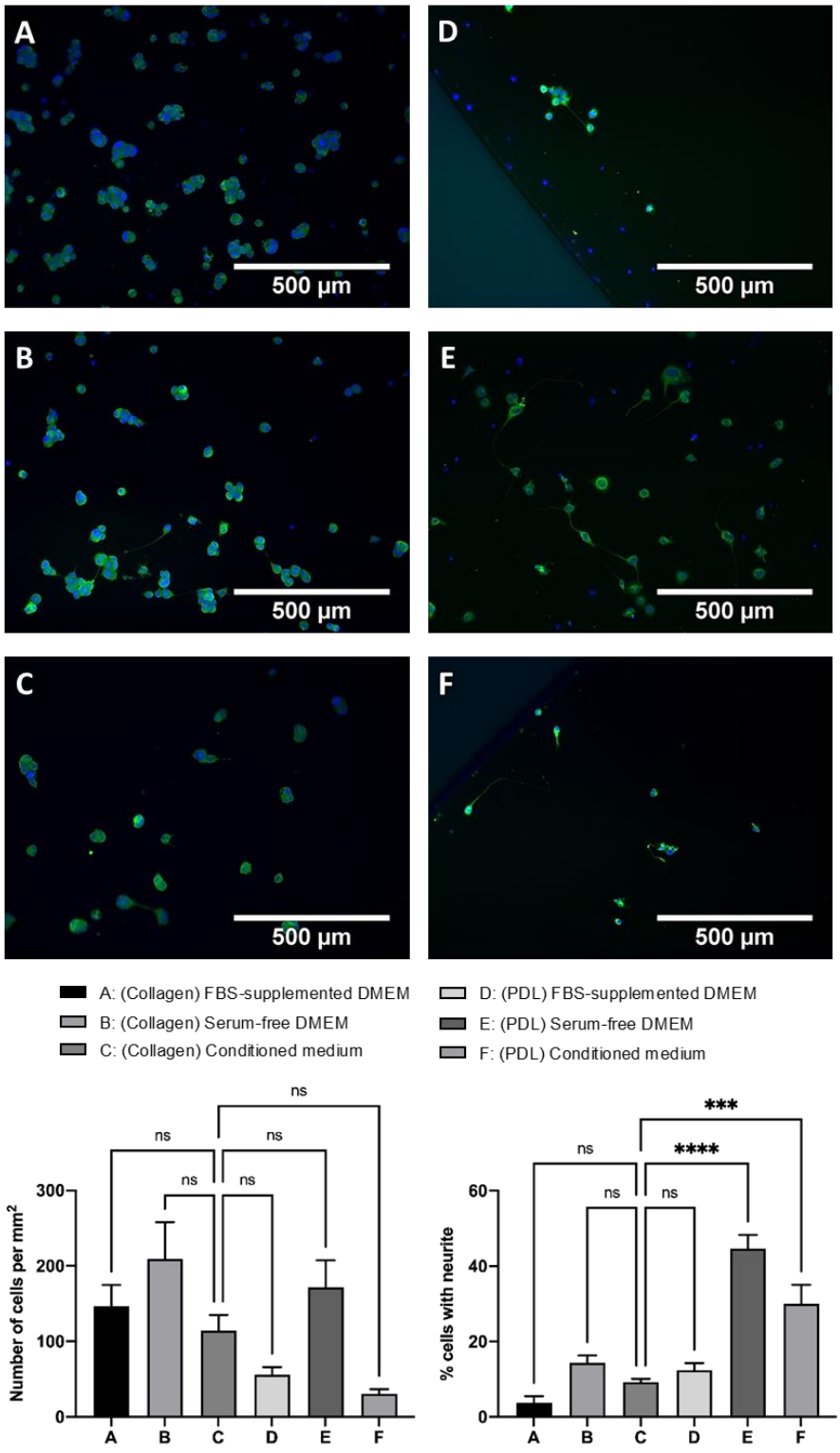

Figure 3.2 Immunostaining for β-tubulin (green) and Hoechst33342 (blue) of NG108-15 cell line cultured on different substrates and medium cultures after incubating in 24-well plate for 3 days. *Scale bar = 500 µm. Below graphs showed the number of cells and the percentage of cells that had neurites elongating from cell bodies counted on a surface area of 1 mm^2. All of the culture conditions were statistically compared with condition C which represented a co-culture of neurons and Schwann cells in TaeNT. Data shown as mean with SEM of 5 independent experiments. Ordinary one-way ANOVA with Dunnett post-hoc test. ***p = 0.002, ****p < 0.0001*

3.2.2 Neurite Length of NG108-15 in co-culture with TaeNT containing aligned F7 Schwann cells

Neurite length and alignment angle of NG108-15 in the gel was assessed by immunostaining followed by fluorescence microscopy and image analysis. Figure 3.3 showed the alignment of NG108-15 and F7 along the longitudinal axis of the gel, and some NG108-15 had at least one neurite elongated from the cell bodies. The result showed that the mean neurite lengths of NG108-15 after incubating with F7 in TaeNT for 4 and 7 days were not significantly different with the mean of 193 ± 13 μm and 196 ± 7 μm respectively. However, maximum neurite length increased with time in culture, reaching the mean of maximum length of 379 ± 27 μm after 7 days.

The neurite alignment angle was measured by firstly identifying each individual neurite outgrowing from its cell body and then drawing a straight line starting from the center of the cell body to the end of the neurite. The angle of the straight line was considered to be the alignment angle of the neurite. The angle of deviation was calculated between alignment of each individual NG108-15 neurite and the gel's longitudinal axis. In both incubating days, NG108-15 neurites co-cultured with F7 in TaeNT aligned parallel to the longitudinal orientation of the gel, with 85% of neurites exhibiting less than 30-degree deviation from the alignment axis. More highly aligned neurites were found after a longer time in culture as the proportion of neurites with angle deviation less than 10 degree changed from 23.22% to 38.89% when increasing the incubating time from 4 days to 7 days (Figure 3.3- right graphs).

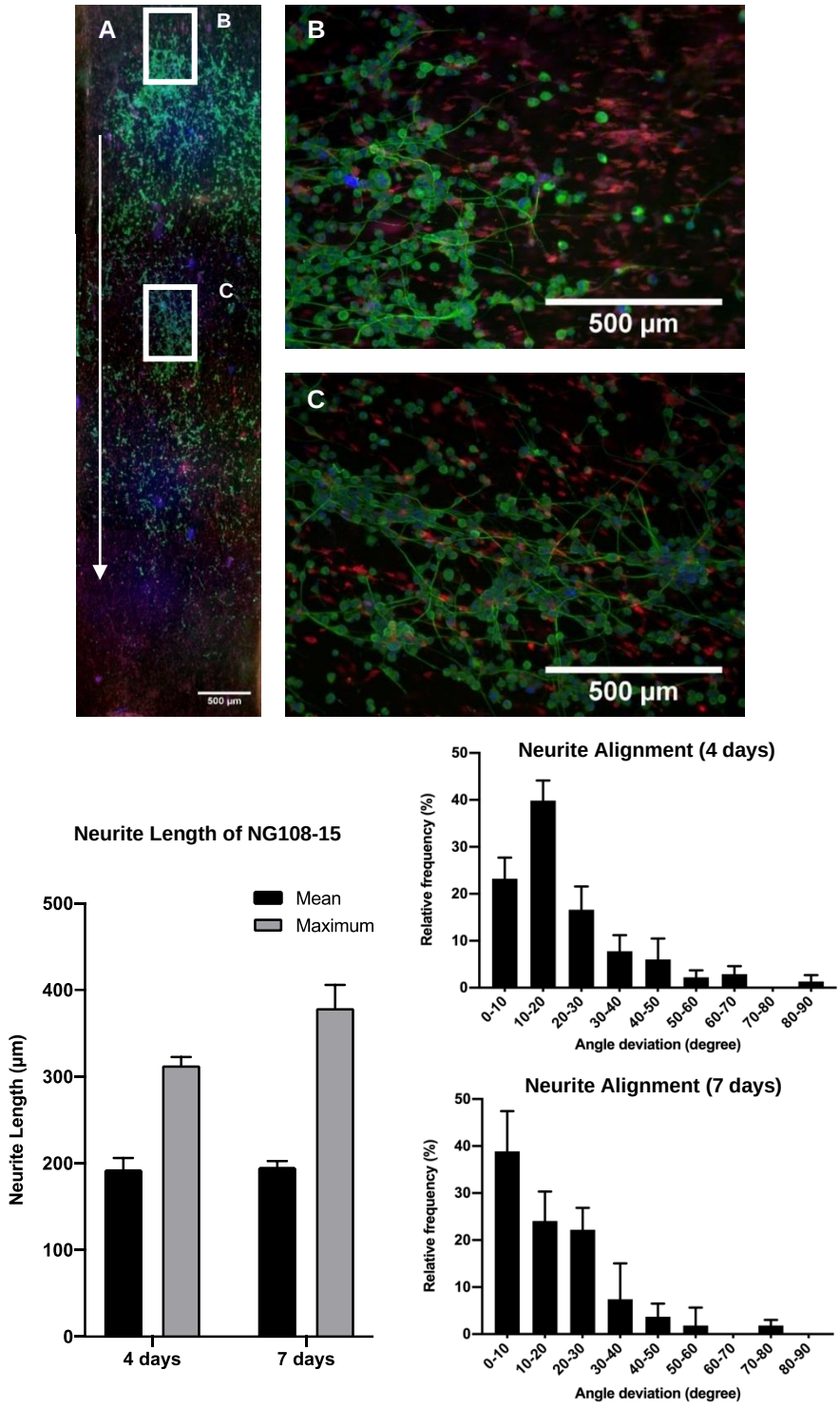

Figure 3.3 NG108-15 neurite elongation after seeding on top of TaeNT for 4 and 7 days. *Immunostaining for β-tubulin (green), S100 (red), and Hoechst 33342 (blue) of NG108-15 cell line co-cultured with F7 cell line in TaeNT after 4 incubating days. White arrows indicated the longitudinal direction from one tethered end to the other of the (A) whole TaeNT and (B), (C) selected area expanded from the white rectangles in (A). Scale bar = 500 µm. Below graphs showed quantification of mean and maximum length of NG108-15 neurite (left) and relative frequency of each angle deviation range from the longitudinal axis of gel after incubating with serum-free DMEM for 4 and 7 days, respectively (right). Data shown as mean with SEM of 4 independent experiments.*

The NG108-15 neurite length measured in this experiment was compared to the NG108-15 neurite length reported in other literature in order to justify the comparative potential of TaeNT in neurite elongation among other culture protocols. The neurite length of NG108-15 after 4- and 7-days co-culture with TaeNT was plotted alongside the results taken from the literature review in Table 3.1 (Figure 3.4). The mean of the reported NG108-15 neurites length induced by various culture methods from previous literature from 1989 to 2015 (n=26) was calculated. The mean of neurite length cultured in controlled and induced culture condition was 70 ± 14 µm and 166 ± 16 µm, respectively. The neurite growth of NG108-15 from co-culture with Schwann cells in TaeNT was greater than the mean of the controlled and induced neurite length cultured in the reviewed culture protocols. Besides, at day 4 and 7, the average neurite length of NG108-15 in the experiment was greater than those in other protocols at the same culture duration.

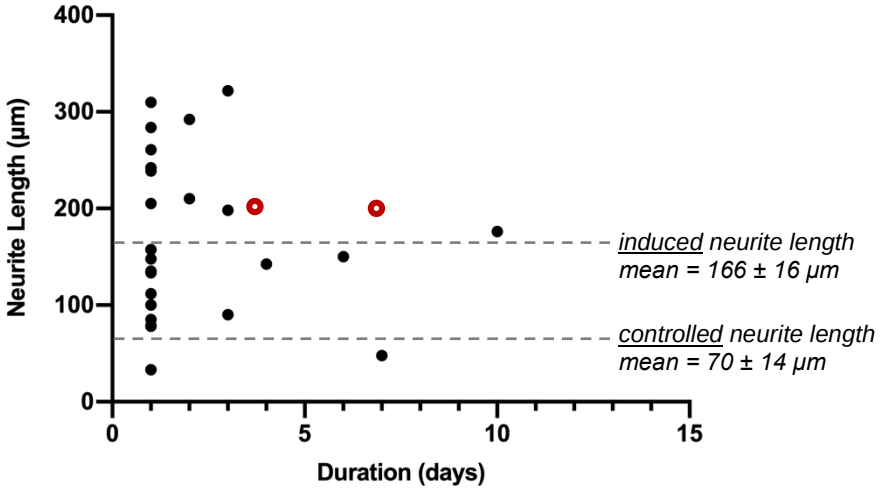

Figure 3.4 NG108-15 neurite length co-cultured with TaeNT plotted alongside results taken from systematic literature review in Table 3.1 at different incubating time. *The literature search was performed on PubMed database in September 2016 with the keywords "NG108-15" and "neurite" from publications in 1989 to 2015. The average neurite length incubated in controlled and induced condition at different times was reviewed. The black dots represented the length of NG108-15 neurites induced by various culture methods at specific incubating time from each reviewed literature (n=26). The dotted lines indicated the calculated mean of NG108-15 neurite length incubated in control and induced culture condition reported from the literature review. The red open circles represented the mean of NG108-15 neurites length with TaeNT measured from the experiment in this chapter, as shown in Figure 3.3.*

3.2.3 Optimisation of co-cultured F7 Schwann cells and neurons in self-organising collagen guidance conduit

Moving toward the *in vivo* experiment, TaeNT was modified to be in form of a self-organising collagen guidance conduit to allow a compatible shape with the nerve geometry. The holes at both end of the conduit were analogous to the tethering mesh in TaeNT, which allowed collagen gels to become tethered at the end of the tubes during the contraction. Without the tethering holes, the cellular gel would contract without tension so that cells in the gel would not align to form an anisotropic structure.

Neurons and Schwann cells were co-cultured in the conduit with tethered holes at both ends. When the cellular gel was set in the self-organising collagen guidance conduit, the collagen gel completely filled the tube (Figure 3.5A). After 24 hours, the gel detached from the tube wall and contracted toward the middle of the conduit leaving gel attached via the tethering holes at both ends of the conduit (Figure 3.5B).

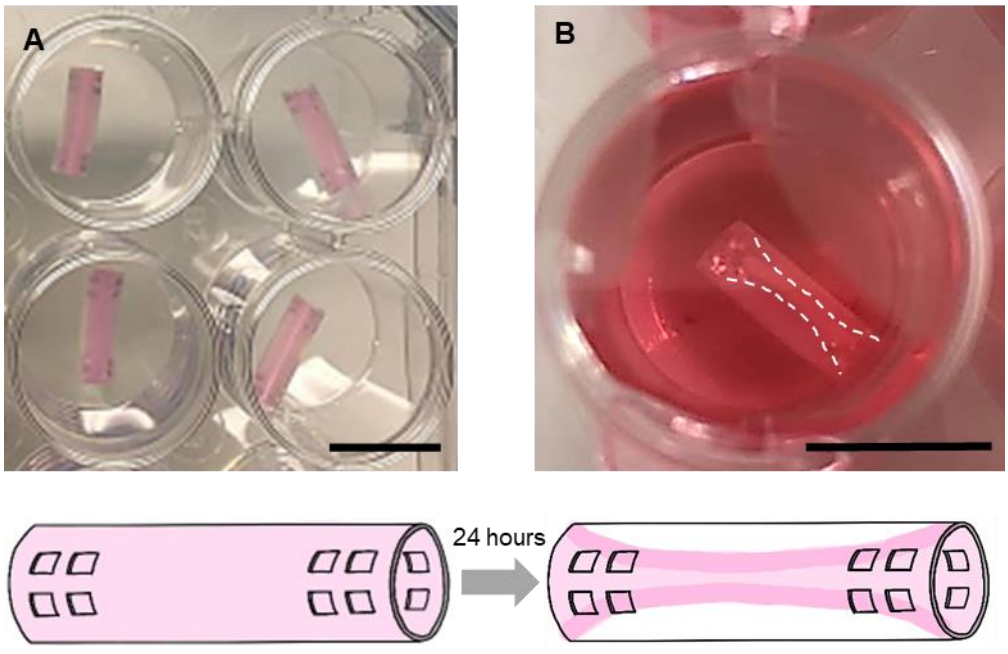

Figure 3.5 Self-organising collagen guidance conduit contain NG108-15 and F7 cell lines. *(A) collagen guidance conduits at preparation time in 24-well plate (B) Contraction of cellular collagen hydrogel in the conduit after incubating in culture medium for 24 hours. The white dotted line in Figure 3.5B indicated the shape of contracted gel inside the tube. Scale bar = 10 mm.*

The self-alignment of cells in the longitudinal axis of the gel was a result of cellular contraction being opposed by the tethering and generating tension in the gel. To verify cell alignment in the guidance conduit, F7 and NG108-15 cell lines in the self-organising collagen guidance conduit were immunostained and compared with F7 and NG108-15 cell lines co-cultured inside a normal silicone tube (silicone tube without holes). Fluorescence microscopy showed cell alignment along longitudinal orientation in the guidance conduit while no alignment was observed in the normal silicone tube without tethering holes at both ends (Figure 3.6). At 24-hour incubation, the neurite outgrowth of NG108-15 was slightly observed but with very short length. More neurites with longer length would be more noticeable at increasing incubation time.

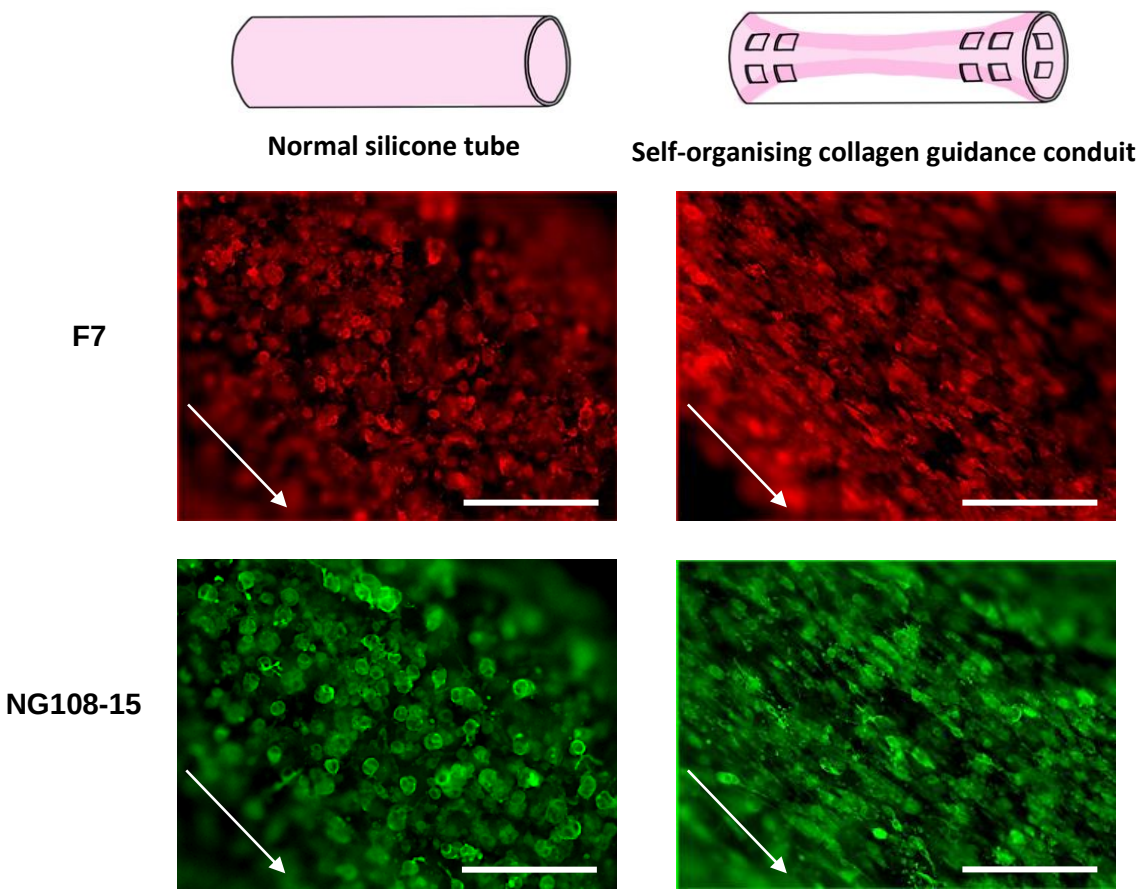

Figure 3.6 Alignment of F7 and NG108-15 co-cultured in collagen gel inside normal silicone tube and self-organising collagen guidance conduit under fluorescence microscope. *Immunostaining for β-tubulin (green) and S100 (red) of NG108-15 and F7 cell line co-cultured at ratio 1:1 with a density of 2 millions cells per ml for 24 hours. White arrows indicated longitudinal orientation of the cellular tube. Scale bar = 200 μm.*

The optimal ratio and number of cells in the construct was determined prior to transplantation through a contraction profile experiment using collagen gels containing both neurons and Schwann cells. To determine the optimal ratio and seeding density of neurons and Schwann cells in self-organising collagen guidance conduits for sciatic nerve transplantation, cells were co-cultured in collagen gel with 3 different ratios and 2 different Schwann cell densities. The quantified degree of contraction was different at different ratios and cell densities. Figure 3.7 showed that a higher ratio of neurons in the co-culture resulted in lower % contraction, and the cellular gels with Schwann cell density at 4 million cells per ml contracted more than the gel with Schwann cell density at 2 million cells per ml. With the ratio of NG108-15 to Schwann cells at 1/8, which was the ratio with the highest contraction compared to other ratios, there was no significant difference in contraction when Schwann cells were seeded at densities of 2 or 4 million cells/ml.

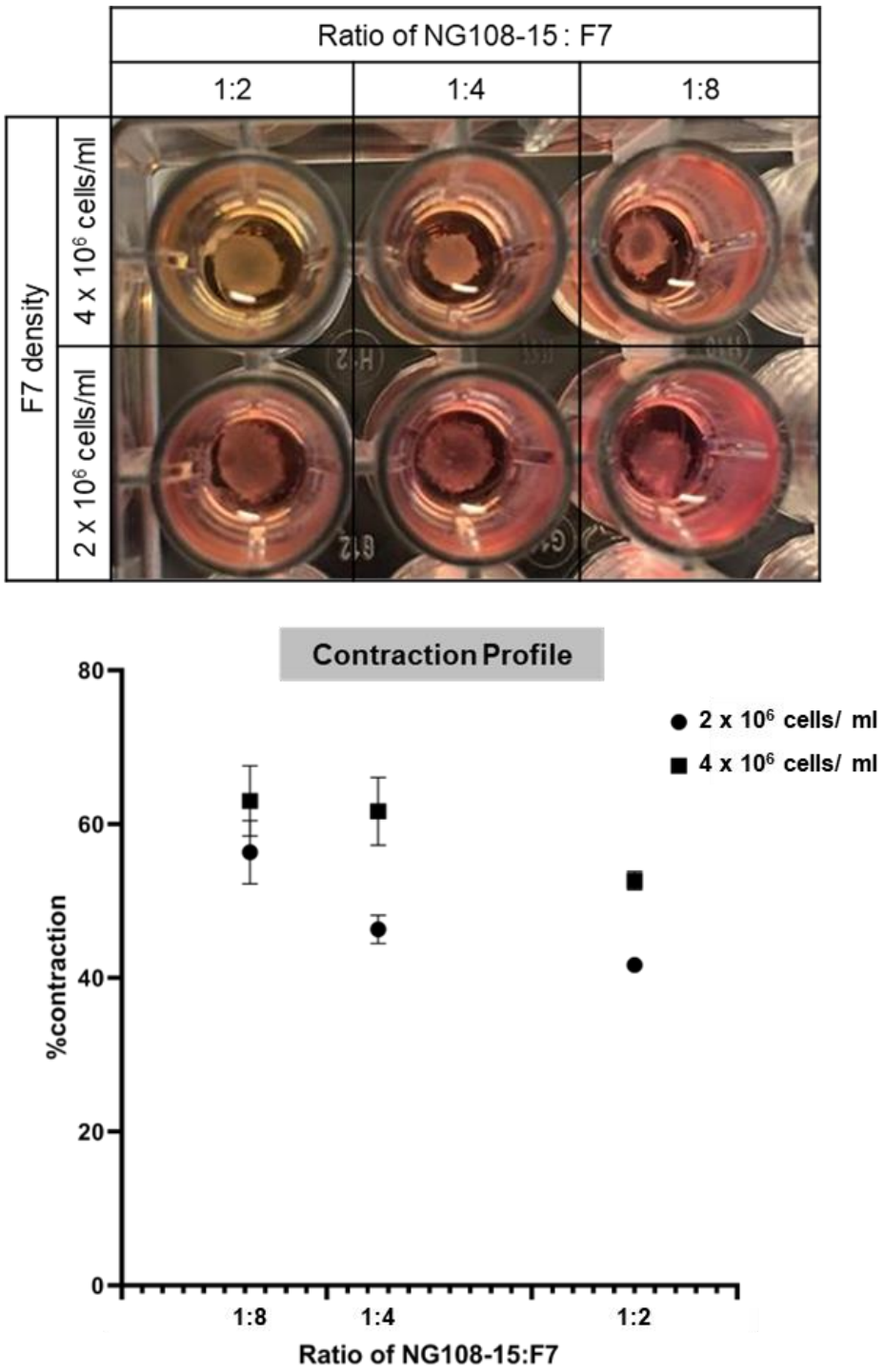

Figure 3.7 Contraction profile of neurons and Schwann cells co-cultured at different cell densities and ratios. *The area of free-floating gels after incubation in culture medium in a 96 well-plate for 24 hours were measured and calculated for % change in gel size compared to initial dimensions. The below graph represented % contraction of gels at different ratios of NG108-15: F7 (x-axis) and F7 densities (graph legend). Data shown as mean with SEM of 4 independent experiments.*

3.2.4 Quantification of transplanted and regenerating neurites in self-organising collagen guidance conduit

In order to investigate neurite growth at the interface between transplant and host tissue, an *in vivo* experiment was conducted by transplanting self-organising collagen guidance conduits containing DRG neurons and F7 Schwann cells into a rat sciatic nerve gap model for 3 weeks. The interface between transplant and host tissue was defined as the suture site between each end of the conduit and each nerve stump. The tissue within the transplant or the nerve stumps 3 mm away from the interface was cross-sectioned at 4 positions: (from most proximal to most distal) proximal nerve (PN), proximal device (PD), distal device (DD), and distal nerve (DN) (Figure 3.8). The middle of the conduit was sectioned longitudinally for glial cell immunostaining and analysis in Chapter 4.

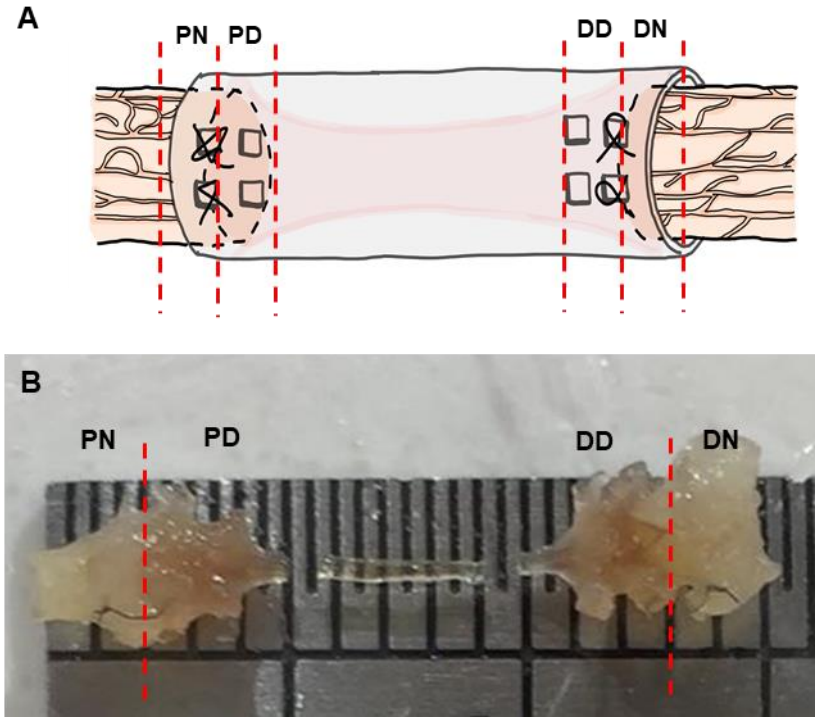

Figure 3.8 Area identification of self-organising collagen guidance conduit in rat sciatic nerve after transplanting in rat sciatic nerve for 3 weeks. *Transplant and host tissue were sampled at 4 positions for cross-section: (from left to right) proximal nerve (PN), proximal device (PD), distal device (DD), and distal nerve (DN). (A) Schematic diagram showing analysis positions (B) tissue after conduit removal on mm-ruler scale.*

With immunostaining and image co-localisation processing, transplanted and host neurites at each position were distinguished and analysed. Neurites immunostained for neurofilament and GFP were automatically detected in different channels and then characterised as either host or transplanted neurites (Figure 3.9). Host neurites were positive in both neurofilament and GFP channels, while transplanted neurites were positive only in the neurofilament channel and not the GFP channel.

Both transplanted and host neurites were present at all 4 positions, distributed throughout the tissue (Figure 3.9). In the proximal nerve (PN), transplanted neurites were noticeably dense at the rim of the tissue. The host and transplanted neurites at proximal and distal device within the construct distributed evenly throughout the cross-sectioned tissue.

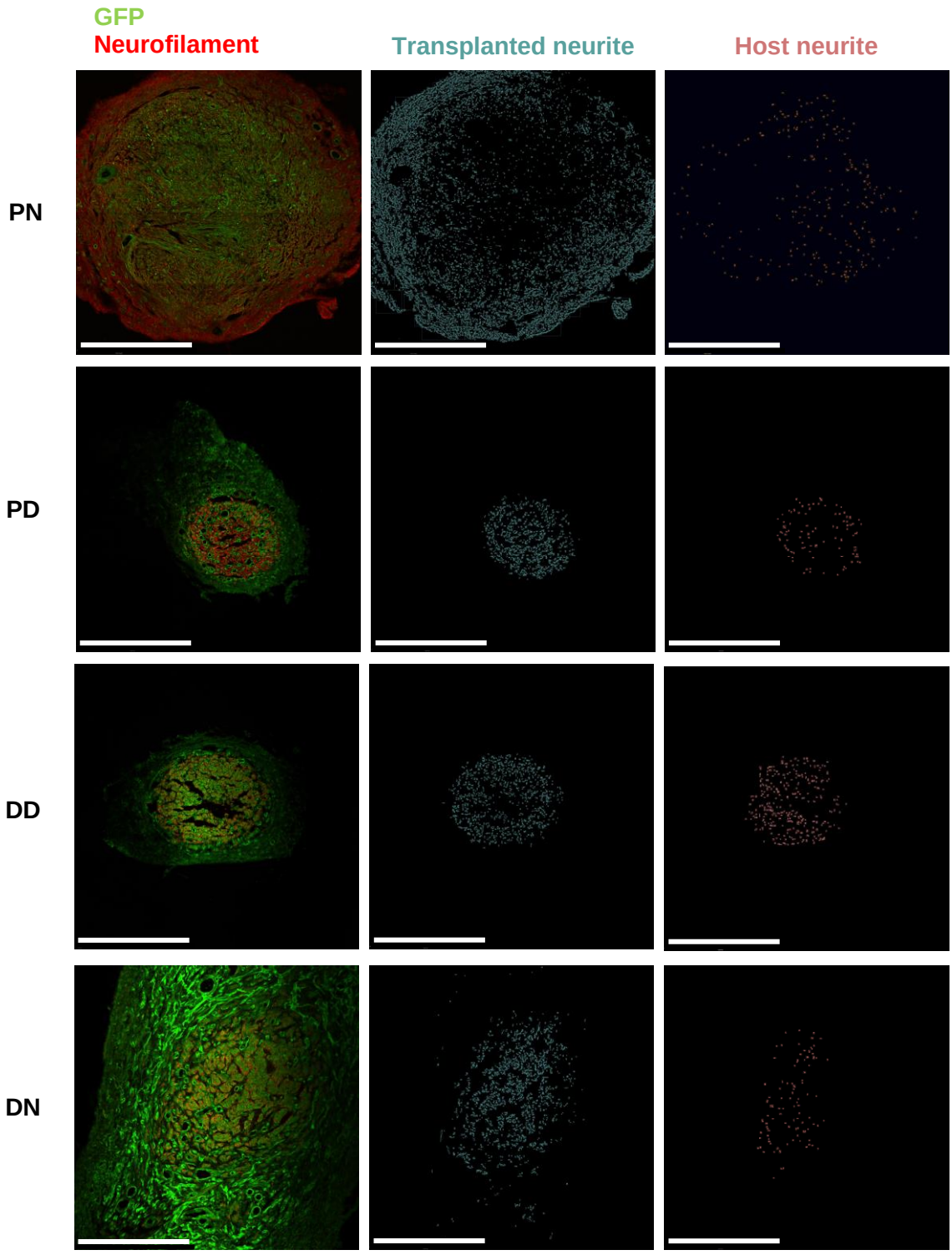

Figure 3.9 Immunostaining for neurofilament (red) in cross-sectioned GFP-positive tissue (green) at both ends of transplanted guidance conduit at 3 weeks after transplantation. *Neurons and neurites from all sources were positively stained by neurofilament, and all cell types from host tissue were GFP-positive. Transplanted neurites (blue) and host neurites (orange) were distinguished by co-localisation analysis at each particular area. Host neurites were positive in both neurofilament and GFP channels, while transplanted neurites were positive only in the neurofilament channel and not the GFP channel. (A) Proximal Nerve (B) Proximal Device (C) Distal Device (D) Distal Nerve. Scale bar = 500 μm.*

Figure 3.10 shows the quantification of neurite staining in the cross-sections at different positions as represented in Figure 3.9. The number of both host and transplanted neurites across both interfaces remained steady as the number of neurites at the proximal nerve (PN) and distal nerve (DN) were similar to the number of neurites at proximal device (PD) and distal device (DD), respectively. Besides, the number of transplanted neurites in each position was higher than the number of host neurites. The number of host neurites at each position was similar at both proximal and distal interfaces, while the number of transplanted neurites was higher at the proximal than the distal side (Figure 3.10A).

The number of host neurites expressed as a proportion of total neurites at the proximal stump was approximately 20%, which was slightly greater (30-40%) at the distal stump (Figure 3.10B). The density of stained neurites per area was also calculated to account for the different size of the tissue at different positions: the cross-sectional area of the proximal stump was larger than distal stump (Figure 3.10D). The density of host neurites was constant at around 500 neurites per mm^2 where the density of transplanted neurites was varied from 1,500 to 2,500 neurites per mm^2 (Figure 3.10C).

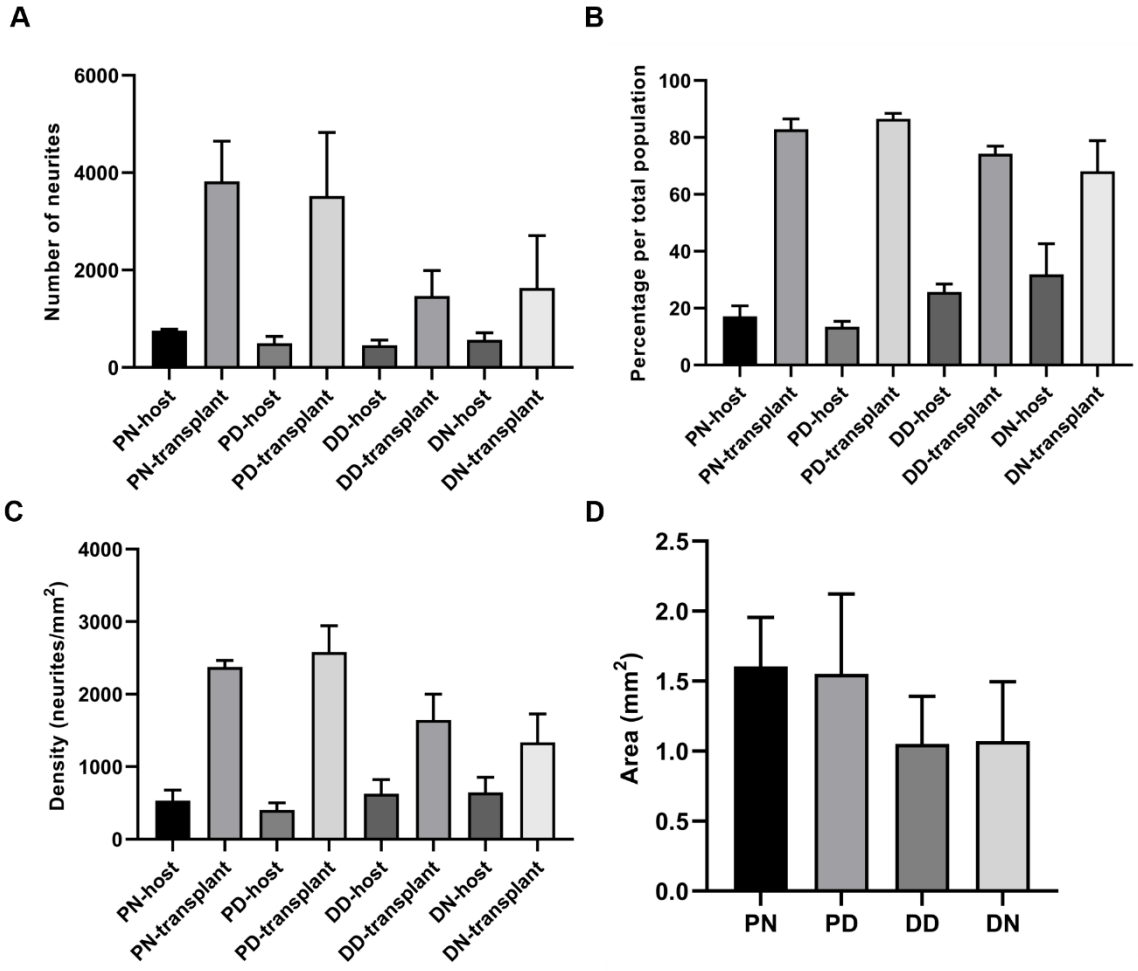

Figure 3.10 Quantification of host and transplanted neurites in cross sections at different positions in the rat sciatic nerve gap model after 3 weeks. *(A) Number of neurites at each particular area. (B) Percentage of host or transplanted neurite out of the total neurites in each particular area. (C) Density of neurite per area of each cross-sectioned tissue containing all neurites. (D) Area of cross-sectioned tissue containing neurites. Data shown as mean with SEM of triplicate tissue slices and are representative of 3 individual rats (n=3).*

3.3 Discussion

Before investigating the cell line with the engineered construct, various culture conditions for NG108-15 were examined by measuring the number of cells and neurite outgrowth. Culturing NG108-15 in conditioned medium from F7 in FBS-supplemented DMEM on collagen gel (condition C in Figure 3.2) represented a co-culture condition of NG108-15 with F7 Schwann cells in TaeNT. According to the comparison in the results, there was no statistical difference in the number of NG108-15 between the culture system with and without Schwann cells. This implies that NG108-15 in TaeNT condition can still proliferate and expand with a similar rate to NG108-15 in a culture flask with a common culture condition.

On the other hand, the neurite outgrowth of NG108-15 in TaeNT condition was significantly lower than in serum-free DMEM and conditioned medium in PDL-coated substrate (condition E and F in Figure 3.2, respectively). The highest neurite outgrowth in condition E was likely to be due to the higher stiffness of PDL-coated glass compared to collagen gel and the absence of serum in the medium. It was previously reported that the higher stiffness of glass provides greater support for growing axons than the lower stiffness of collagen gels (Greco and Rameshwar, 2008). Other studies have reported a consistent neurite-elongating effect of serum-free medium in rat neuroblastoma B104 cell line where the serum-free medium increased the number of neurites and the presence of serum in the medium caused a reduction in the percentage of neurons bearing neurites (Bottenstein and Sato, 1979, Davis et al., 1984).

Besides, although condition F had serum in the medium, the higher neurite outgrowth in condition F implies that NG108-15 neurite outgrowth on PDL-coated substrate could also increase by the co-culture with Schwann cells. It was consistent with the previous literature where the presence of Schwann cells in the co-culture did not increase cell proliferation rate, but supported survival and neurite outgrowth in neurons

(Guenard et al., 1992, Hadlock et al., 2000, Kwiatkowski et al., 1998, Ramon-Cueto et al., 1998).

The alignment of NG108-15 neurites was induced by co-culture with aligned F7 Schwann cells in the tethered gel. Many previous experiments in peripheral nerve research have also tried to promote directional axonal guidance by Schwann cell alignment on an engineered substrate such as laminin, bioresorbable glass fibres, and hydrogels (Bozkurt et al., 2009, Bunting et al., 2005, Martens et al., 2014, Rosner et al., 2005, Thompson and Buettner, 2006). Schwann cells are sufficient to guide neurite outgrowth in the absence of other directional cues (Thompson and Buettner, 2006). More highly-aligned neurons were observed following a longer incubation time, implying that the neurite alignment was continuously induced to be aligned in parallel with Schwann cells. In other words, the directional guidance from the aligned Schwann cells affected the neurite alignment not only when the neurites sprouted from the cell bodies, but also when the neurites continued elongating in the culture.

According to a literature search to compare the neurite length results with previous studies reporting neurite length of NG108-15 cells *in vitro*, neurite growth from co-culture with Schwann cells was longer than neurite growth in control cultures, and greater than that reported previously using other culture conditions. The neurite length of NG108-15 in TaeNT measured in our experiment were among the longest ones in other culture protocols. It is consistent with previous literature where the presence of aligned Schwann cells in similar cultures increased neurite growth *in vitro* (Georgiou et al., 2013, Georgiou et al., 2015, Martens et al., 2014). The longer neurite growth is likely to be due to the trophic support and directional guidance provided by the highly oriented Schwann cells in the TaeNT. The trophic support from Schwann cells includes producing ECM components, such as laminin, and secreting several essential neurotrophins, such as BDGF, NT-3, and NT-4, to support the survival of neurons and axon elongation (Birling and Price, 1995, Fu and Gordon, 1997, Raivich and Kreutzberg, 1993). These results indicate that TaeNT may be an appropriate substrate for generating long neurites

in vitro with a view to generating therapeutic constructs containing long functional neurons.

Interestingly, culture duration affected the neurite length by increasing the maximum length, but not the mean length of the neurite elongation. It can be hypothesised that either the difference between the 2 culture durations in the experiment, 4 and 7 days, might not be long enough to observe a change in length of the whole population of neurites, or perhaps NG108-15 might have an upper limit on neurite elongation where most of neurites could stop elongating at a particular time or length. If the latter is true, NG108-15 might not be a good source of model motor neurons to be used in the development of neurite elongation protocols required here. The experimental engineered neural tissue being developed in this project is intended to yield better recovery than current treatments following long gap nerve injury. This will need to be suitable for testing in the rat sciatic nerve model, where a long gap can be up to 2-3 cm (Isaacs et al., 2014). Since the longest length of NG108-15 measured in the experiment was less than 0.5 mm, another source of cells should be considered to replace the use of NG108-15 in order to obtain the longer neurites required in the later experiments.

The investigation in the regenerative potential of a guidance conduit containing Schwann cells and neurons was consequently carried out with a preliminary *in vivo* experiment. Since the thick sheet-like shape of TaeNT was not suitable to be transplanted into rat sciatic nerve, the self-organising collagen guidance conduit was selected as a similar fully-hydrated tethered collagen scaffolds for living cells. The holes at both ends of the conduit functioned similarly to tethering meshes of the TaeNT where uniaxial tension was generated by cells in the gel resulting in hydrogel contraction and cell alignment (Eastwood et al., 1998, Mudera et al., 2000, Phillips et al., 2005).

The seeding density of Schwann cells was correlated with the extent of hydrogel contraction: increasing the number of F7 cells resulted in greater contraction, similarly to previous studies using a C6 glioma cell line, primary rat astrocytes, and fibroblasts

(Nirmalanandhan et al., 2006, O'Rourke et al., 2015, Redden and Doolin, 2003). In addition, the presence of neurons in the culture altered the contraction: an increasing ratio of neurons resulted in a decreasing degree of contraction. The contraction profiles of the co-cultured cells correlated to the alignment behaviour of the cells. O'Rourke et al. demonstrated that the degree of gel contraction required to produce reliable cellular alignment should be above 60%. Therefore, the optimised cell number and ratio was 2 millions/ml of Schwann cells with 1/8 neurons in the culture.

The use of self-organising guidance conduits in this chapter provides an approach to examine the spatial interaction of host and transplanted cells after cellular guidance conduit transplantation. It has been established that regenerating neurites from host tissue could enter an acellular hydrogel conduit (Du et al., 2017, McGrath et al., 2010, Meyer et al., 2016, Wu et al., 2017), as well as into a guidance conduit containing Schwann cells, neurons or neural stem cells (Huang et al., 2009, Georgiou et al., 2013, Lee et al., 2017b, Flachsbarth et al., 2014). This chapter has expanded the understanding of neurite elongation in the transplanted conduit by investigating whether the presence of transplanted neurons disrupted the host regenerating neurite elongation. The presence of neurons in the transplanted conduit did not reduce the number of host neurites crossing the interface and entering the conduit, and the host neurites could elongate throughout transplanted conduit and cross the distal interface to the distal nerve.

The transplanted neurites could also penetrate into host tissue without disruption as the number of neurites across both interfaces remained consistent. However, the number and density of both host and transplanted neurites at the distal stump was lower than those at proximal stump. It is noticeable that although the number of transplanted neurites significantly dropped at the distal stump, the difference in the percentage of transplanted neurites per total neurites at proximal and distal interfaces was comparatively smaller. The reduced number of transplanted neurites correlated with the distribution of migrating Schwann cells along the transplanted conduit. Schwann cells

migrated into the conduit from both ends, but the number of migrating Schwann cells at the distal part was about a half those at the proximal part (Chen et al., 2019a).

There were limitations of the *in vivo* experiment reported in this chapter. Firstly, the transplantation duration was only 3 weeks, selected because it was a minimum time point sufficient for regenerating neurites to reach the distal stump in a 10-mm nerve gap (Williams et al., 1983). The approach to investigate host and transplanted neurites at the interface was a snapshot in time, so any temporal changes could not be examined. With longer transplantation duration, the distribution and spatial interaction of host and transplanted neurites might change, therefore further experiments with different time points will be required in the future.

The *in vivo* work presented here was an initial experiment conducted with a minimal number of animals so the statistical analysis should be treated with caution as there was insufficient information about the likely variability and effect size to allow a power calculation to be performed in advance. A retrospective power analysis (Figure 3.14) indicates that the total number of animals used in the experiment should be at least 16 rats in order to confidently detect a medium effect size with 5% error probability and a statistical power of 0.8. Although the sample size of 3 in this initial experiment was not enough to detect an effect with a given degree of confidence, the results from 3 experimental animals can preliminarily demonstrate a trend of data with a statistical power of 0.1-0.2. The *in vivo* results in this chapter will be useful in future experimental design to investigate and quantify neurite elongation at transplant interface.

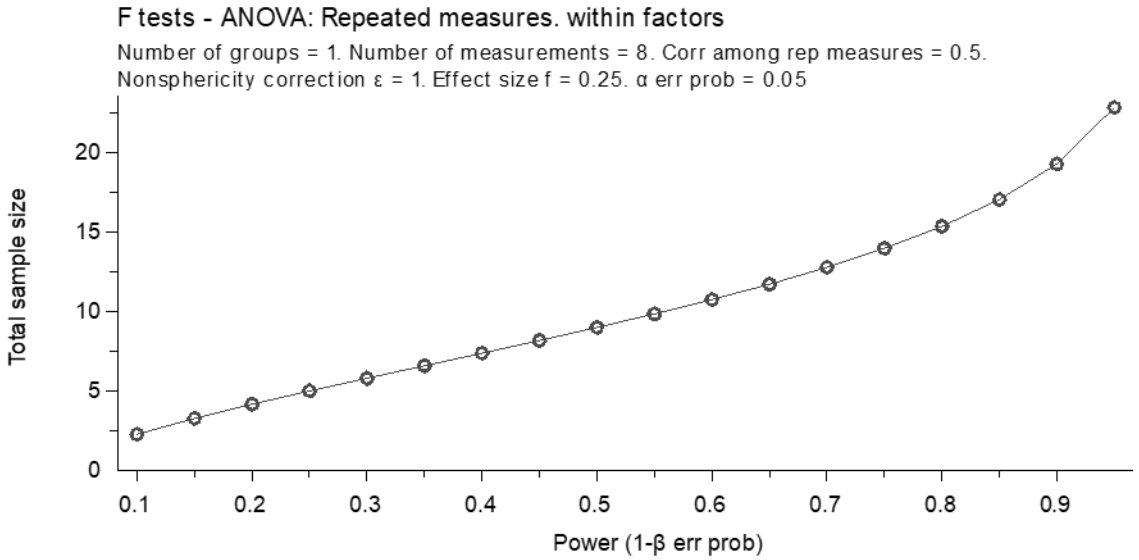

Figure 3.11 Total sample sizes corresponding to the power from 0.1 to 1 for a one-way ANOVA test with repeated measures, within factors in cell number quantification. *The analysis was calculated with effect size of 0.25 (medium) with 5% error probability and plotted by G*Power software.*

Overall, this chapter has demonstrated a supportive role of TaeNT in terms of neurite elongation within the transplant and across the host/graft interface. From the *in vitro* studies, NG108-15 cell lines cultured on TaeNT could elongate and align with the longitudinal axis of the gel. The *in vivo* experiments with the transplanted modified version of TaeNT showed that the host neurites could elongate from the proximal stump into the transplanted conduit reaching the distal stump, and transplanted neurites could elongate from the conduit into the host tissue, without disruption of each other. The elongation, alignment, and interface-crossing behaviour of neurites in TaeNT reflects the regenerative potential of TaeNT which may contribute to functional recovery following peripheral nerve injury.

CHAPTER 4

Interaction between transplanted Schwann cells and infiltrating host Schwann cells in nerve repair

4.1 Introduction

Communication between cells in response to the dynamic of their environment is crucial in nerve regeneration. The behaviours of cells are chemically and/or physically influenced by environmental cues and signals from other cells in the surrounding region, and these transient and dynamic interactions are associated with different stages of degeneration and regeneration. In peripheral nerve tissue after injury, many types of cells migrate to the injured site in response to the damage and along with the resident cells they become involved in regeneration processes. Macrophages, mast cells, and T lymphocytes are activated at the damaged nerve site and play a role in clearing cellular debris, then a fibrin deposit containing erythrocytes, neutrophils, platelets, and macrophages is formed, before the migration of fibroblast, endothelial cells, and Schwann cells (Cattin et al., 2015, Ellis and Bennett, 2013, Mosser and Edwards, 2008). Schwann cells reprogramme to a repair phenotype and proliferate along the nerve tract to form Bands of Bünger to guide nerve regeneration (Arthur-Farraj et al., 2012, Jessen et al., 2015). The regenerating axons can elongate and successfully reach the distal stump through this support from many types of cells functioning in parallel and signalling to each other (Figure 4.1).

The interaction between different types of cells has been extensively researched in order to increase understanding of the complex mechanisms in nerve injury and regeneration. Schwann cells and other associated cells communicate and influence on each other through various types of kinase, cytokines, and integrins. Signalling pathways in the Schwann cells can activate and regulate activities of other cells in the

system. For examples, the associated neurons increase neurite outgrowth in response to the activation of Erk1/2 in Schwann cells, and macrophages are recruited and activated by the upregulation of cytokine MCP-1 in Schwann cells, leading to Wallerian degeneration (Martini et al., 2008, Namgung, 2014, Stratton and Shah, 2016). Likewise, other types of cells also play an important role in regulating regenerative activities of neurons and Schwann cells. Infiltrating fibroblasts take part in tissue debris clearance, Schwann cell migration, vascularisation, and neurite extension modulation through the upregulation of extracellular matrix tenascins (Dun and Parkinson, 2020, Meiners et al., 1999, Sorrell and Caplan, 2009, Zhang et al., 2016). Endothelial cells, which vascularise the injured nerve, release glial cell line-derived neurotrophic factor (GDNF) to support neurite growth while nerve growth factors (NGF) produced by local fibroblasts stimulate angiogenesis (Shvartsman et al., 2014).

One way to investigate these types of cell interactions is to model cell behaviour *in vitro*. Since the biological system *in vivo* contains various types of cells and complex extracellular matrix, multiple environmental factors simultaneously influence cell behaviour, so minimising these variables can provide useful information about the interaction between cells and specific factors. *In vitro* models offer isolated and controlled environmental conditions, so can provide useful information about specific responses before examining the cell behaviour *in vivo* to understand the results in a more complex environment.

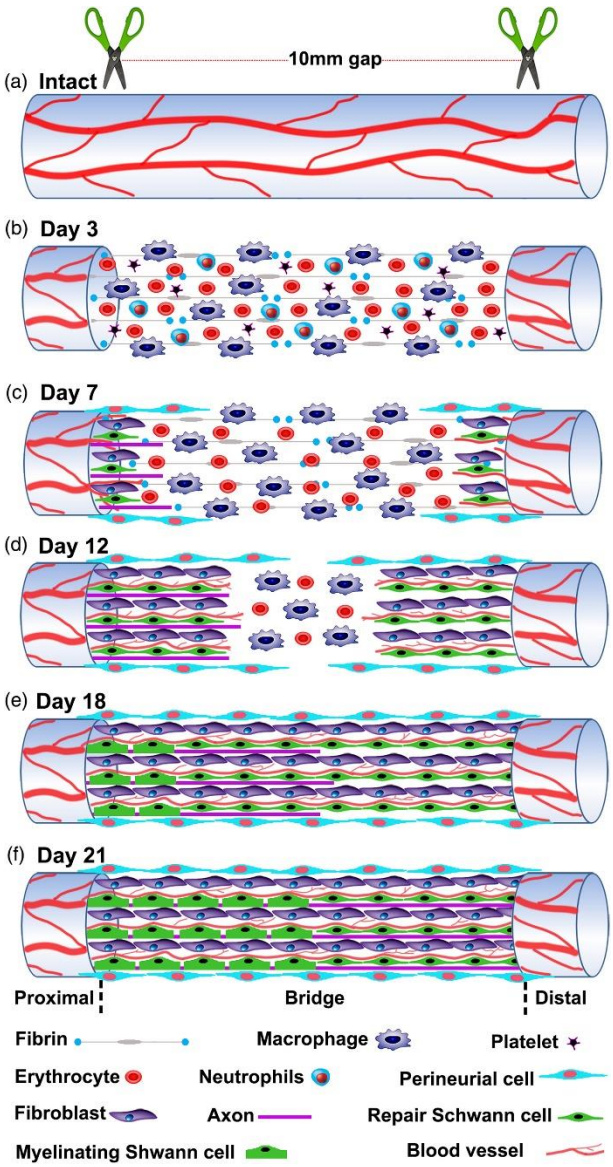

Figure 4.1 Nerve bridge formation and axon regeneration with specific time frame studied in 10-mm rat sciatic nerve gap with a hollow nerve conduit. *Many types of cells are involved through the process as they interact with each other to form a successful nerve bridge to support axon elongation. The interactions are transient and dynamic depending on stages of degeneration and regeneration (Min et al., 2021).*

4.1.1 Schwann cell transplantation for PNS regeneration

Transplanting Schwann cells as a component to enhance the performance of nerve guidance conduits has become a widely-studied method in nerve regeneration research. Many different cell types are involved in the response to transplanted cells and some of these interactions, such as host neurons being supported and guided by donor Schwann cells, are well-studied *in vitro* and in animal models (Karimi et al., 2014, Lago et al., 2009, Levi et al., 2016, Strauch et al., 2001). The response of other cell populations to transplantation of Schwann cells is less well studied, but are likely to be important in supporting successful integration and function.

A systematic literature review was conducted on Schwann cell transplantation experiments to gather an understanding of what interactions have been reported; Table 4.1 summarises common measurements that previous research quantified after cell transplantation in peripheral nerve repair models. The earlier work mainly focused on using primary Schwann cells, and then later studies increasingly used differentiated stem cells and precursor cells for transplantation. Note that stem cell experiments were excluded unless the transplanted cells were induced to differentiate into a Schwann cell phenotype prior to the transplantation, because it is not certain that stem cells can spontaneously differentiate into Schwann cells after being transplanted into the injured nerve. For example, the main effect of mesenchymal stem cell transplantation in PNS regeneration is likely to be releasing factors that promote host Schwann cell proliferation rather than differentiating to be Schwann cells (Erba et al., 2010, Yamamoto et al., 2016, Carlson et al., 2011).

To understand the efficacy of nerve regeneration after cell transplantation, a range of outcome measures were quantified: morphology and myelination of regenerating nerve fibres, vascularisation, electrophysiology, behavioural analysis, immune response, and gastrocnemius muscle restoration. It is noticeable that most studies in Table 4.1 have mainly focused on understanding the morphology and

behaviour of regenerating neurons in the presence of Schwann cells, but the behaviour of the transplanted Schwann cells and their interaction with host Schwann cells remains unclear. Only the viability of transplanted Schwann cells was quantified in early experiments (Berrocal et al., 2013, Fansa et al., 1999, Mosahebi et al., 2003, Tohill et al., 2004). There is a lack of studies reporting whether transplanted Schwann cells and infiltrating Schwann cells from host tissue could facilitate or disrupt each other's function and alignment in the context of a cellular tissue engineered graft.

Understanding how endogenous and exogenous glial cells respond to each other, particularly at the interface with the proximal and distal nerve stump, will thus help to optimise tissue engineering protocols and other medical treatments for nerve injury that involve transplantation of cellular materials. Studying the physical response of one population of cells to another is a starting point to understand cell-cell interaction. The cell-cell interaction could be preliminarily investigated by measuring morphological and behavioural change correlating to the existence of the interaction.

Reference	Model	Source of cells	Repair distance (mm)	Transplantation method	Quantified Measurement						
					Regenerated nerve	Schwann cells	Vasculari-zation	Electro-physiology	Behavioural analysis	Immune response	Muscle weight
(Mirfeizi et al., 2017)	mouse	adult skin-derived precursor cells	crush	injection	✓						
(Lee et al., 2017a)	mouse	differentiated NSCs	3	PLA conduit	✓			✓	✓		
(Levi et al., 2016)	human	primary SCs	75	sural nerve graft					✓		
(Wang et al., 2016)	rat	skin-derived precursor cells	10	chitosan with silk fibroin fibres			✓				
(Bozkurt et al., 2016)	rat	primary SCs	20	collagen conduit	✓				✓		

Reference	Model	Source of cells	Repair distance (mm)	Transplantation method	Quantified Measurement						
					Regenerated nerve	Schwann cells	Vasculari-zation	Electro-physiology	Behavioural analysis	Immune response	Muscle weight
(Stratton et al., 2016)	rat	Skin-derived precursor SCs	crush	injection	✓			✓		✓	✓
(Kappos et al., 2015)	rat	differentiated ADSCs	10	fibrin conduit	✓				✓		✓
(Das et al., 2015)	rat	primary SCs	10	silk based gold nano-composite conduit	✓			✓	✓		
(Georgiou et al., 2015)	rat	differentiated ADSCs	15	NeuraWrap conduit	✓						
(Tremp et al., 2015)	rat	Schwann cell-like from ADSCs	10	fibrin conduit	✓						

Reference	Model	Source of cells	Repair distance (mm)	Transplantation method	Quantified Measurement						
					Regenerated nerve	Schwann cells	Vasculari-zation	Electro-physiology	Behavioural analysis	Immune response	Muscle weight
(Karimi et al., 2014)	rat	primary SCs	30	PHBA conduit					✓		
(Georgiou et al., 2013)	rat	cell lines	5 and 15	NeuraWrap conduit	✓						
(Berrocal et al., 2013)	rat	primary SCs	13	collagen conduit	✓	✓			✓		
(Biazar and Heidari Keshel, 2013)	rat	primary SCs	30	PHBV conduit	✓						✓
(Liu et al., 2012)	rat	primary SCs	8	collagen conduit	✓					✓	
(You et al., 2011)	rat	primary SCs	20	PLGA conduit	✓			✓	✓		✓

Reference	Model	Source of cells	Repair distance (mm)	Transplantation method	Quantified Measurement						
					Regenerated nerve	Schwann cells	Vasculari-zation	Electro-physiology	Behavioural analysis	Immune response	Muscle weight
(Lago et al., 2009)	rat	primary SCs	10	silicone conduit	✓						
(Kim et al., 2007)	rat	primary SCs	10	silicone conduit	✓				✓		✓
(Sinis et al., 2005)	rat	primary SCs	20	TMC/CL conduit	✓			✓	✓		✓
(Tohill et al., 2004)	rat	primary SCs	10	PHB conduit	✓	✓					
(Mosahebi et al., 2003)	rat	primary SCs	10	PHB conduit	✓	✓					
(Strauch et al., 2001)	rabbit	primary SCs	60	gluteal vein graft	✓						

Reference	Model	Source of cells	Repair distance (mm)	Transplantation method	Quantified Measurement						
					Regenerated nerve	Schwann cells	Vasculari-zation	Electro-physiology	Behavioural analysis	Immune response	Muscle weight
(Fansa et al., 1999)	rat	primary SCs	20	acellular muscle graft	✓	✓		✓			

Table 4.1 Systematic literature review on Schwann cell transplantation in peripheral nerve injury in the PubMed database from 1976 to 2018. *The electronic search was performed using search term: ("Schwann cell") AND (("nerve conduit") OR ("nerve guide") OR ("transplant")) NOT ("spinal cord") NOT ("CNS"). In January 2021, 133 results were obtained and further screened by reading abstracts and research methods. In vitro experiments, PNR-unrelated research, transplantation of undifferentiated stem cells, and review articles were excluded.*

4.1.2 Cell migration in collective cellular system

Cell migration is the processes in which a single cell or collective cells coordinately translocate to different target locations as a response to the external environment such as chemical or mechanical stimulation. It can be observed in many types of cells during development and regeneration stages, and induced by chemical stimulus (chemotaxis), substrate stiffness of extracellular matrix (durotaxis), or gradient of cellular adhesion sites (haptotaxis). Collective cell migration reflects the interaction of cells in the same population and/or between other types of cells in the environment (Mishra et al., 2019, Trepat et al., 2012, Yamada and Sixt, 2019). In collective cellular systems where more than one type of cell is included, cells can either attract or repel each other. For example, highly migratory neural crest cells repel each other by retracting their projections and altering direction of movement once they are in contact with the same type of cell, but can migrate into an area with different types of cells (Carmona-Fontaine et al., 2008).

One available method to monitor the migration of cells is to culture them in a 3D hydrogel which imitates the extracellular matrix of cells in biological systems and allows cells to possess natural morphologies and translocate in all spatial directions. In order to examine the interaction of two populations of cells in migration studies, 3D tissue culture systems can involve cellular interfaces where one cell population interacts with another cell population in close proximity. East et al (2012) developed a 3D collagen hydrogel system to study the interaction between different neural cell populations in the absence of confounding factors like mechanical cues (East et al., 2012). By allowing adjacent gels to integrate mechanically during setting without the cell populations mixing, the cellular interface in the model can initially segregate one cell population from the adjacent cell population without a mechanical barrier while maintaining integration of the whole hydrogel system. The model was previously used to explore the interaction between neurons and astrocytes by measuring neuronal length and orientation at the cellular interface. In this chapter, the migration of cell populations across the cellular interface

was quantified using the same type of model, in order to examine the interaction of Schwann cells from different sources.

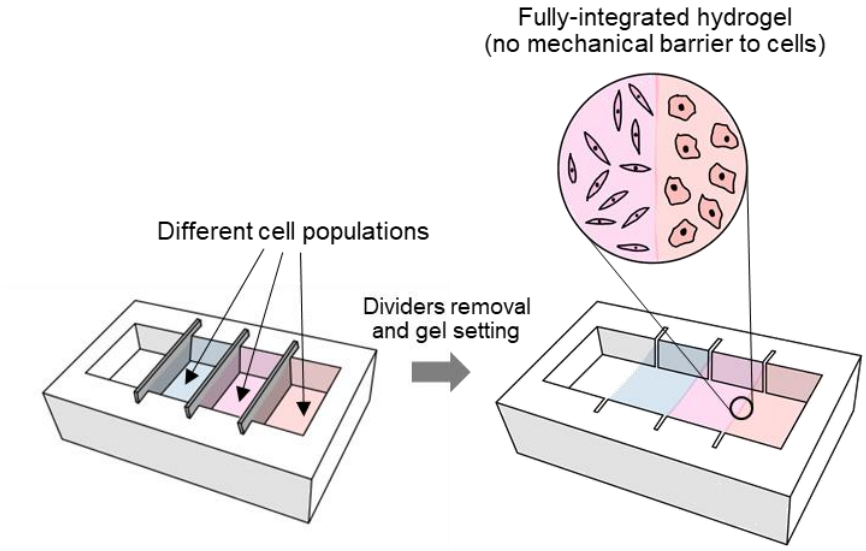

Figure 4.2 An integrated cellular interface in 3D hydrogel culture for cell interaction studies. *Hydrogels in adjacent compartments can integrate mechanically without the cell populations mixing at the start of the experiment*, *and then allow different cell populations to interact. The interaction of cells can be examined by measuring cell morphological change and migration across the interface.*

4.1.3 Mechanical properties of hydrogels

Mechanical properties refer to the physical characteristics of a material when external force is applied to it, and can be described using measurements such as elasticity, viscosity, and stiffness. Viscoelasticity refers to time-dependent mechanical properties and is relevant here because nervous system tissues and hydrogels have viscoelastic properties, exhibiting both viscous and elastic behaviour (Chaudhuri, 2017, Fung, 1993, Levental et al., 2007). Mechanical change affects neuronal cell behaviours in many aspects; for example, Schwann cells are highly sensitive to mechanical stiffness of substrates during PNS development, myelination, and regeneration as they can alter their morphology and behaviour following change of their microenvironment stiffness (Evans et al., 2018, Rosso et al., 2014, Zhang et al., 2014). Thus, it is important to take

into consideration the mechanical properties of the extracellular matrix when discussing cell behaviour and interaction.

Dynamic mechanical analysis (DMA) is a suitable analytical technique for measurement of viscoelastic materials because it can provide mechanical information as a function of time, temperature, or frequency. It applies repeatable compression or tension resulting in sinusoidal stress to the materials, and then the corresponding strains at different frequencies are measured. The relationship between the oscillating stress and strain is useful to determine viscoelasticity of materials. Storage and loss modulus are commonly measured to determine the elastic and viscous behaviour of materials respectively. The storage modulus or Young's modulus indicates an ability to store energy until deformation and relates to the stiffness of a solid material while the loss modulus represents energy lost to heat during the stress. Tan delta is also calculated as a ratio of the loss energy to the storage energy as a loss factor.

4.1.4 Freeze-and-thaw process

A freeze-and-thaw process is a tissue preparation process where a tissue or biological sample is frozen, and subsequently thawed to return to an initial temperature. The cooling rate of freeze-and-thaw protocols can be varied depending on the usage purpose. For cryopreservation, the process is aimed to diminish living cell metabolism and preserve the extracellular structure while optimising a percentage of cell viability in the tissue, so that the tissue can be stored for long time for further scientific research or medical applications (Bojic et al., 2021). The slow cooling rate and the addition of cryoprotective agents, such as DMSO and Glycerol, are necessary in minimising cell damage due to the intracellular ice forming (Gao and Critser, 2000, Jang et al., 2017).

On the other hand, freeze-and-thaw processes can be used to kill cells in the tissue while preserving the tissue geometry for decellularised applications. In the absence of cryoprotective agents, as the temperature decreases to below freezing point

at fast cooling rates, large ice crystal are rapidly formed in both intracellular and extracellular space in the tissue causing cell damage. The slow thawing causes further damage to the cells as the extracellular ice melts before the intracellular ice resulting in an imbalance of osmotic conditions. The osmotic gradient forces extracellular melting water to flow into the cells causing cytolysis. The freeze-and-thaw process can be repeated for multiple cycles to optimise cell destruction (Moutinho et al., 2017). The process produces a non-viable construct with a similar structure to the original one, and allows the decellularised construct to be recellularised with other types of cells (Hadjipanayi et al., 2011, Xiao et al., 2011, Georgiou et al., 2013).

Previous experiments with stabilised tethered collagen gel containing F7 Schwann cells reported that approximately 96% of cells were dead (Georgiou et al., 2013). For fully-hydrated collagen-based tissue, 60% of fibroblasts were dead right after being frozen at cooling rate of 40°C/min without cryoprotective agents, and the percentage of dead cells continued increasing to 90% at 24 hours after the freeze-and-thaw process (Devireddy et al., 2003, Jain et al., 2014).

4.1.5 Sources of glial cells in this study

There are two types of glial cells found in the peripheral nervous system (PNS): Satellite glial cells and Schwann cells. Both of them are originally derived from the neural crest during embryonic development and then separated into different sites as the nervous system develops. Satellite glial cells are mainly found in dorsal root ganglia (DRG). They surround sensory, sympathetic, and parasympathetic neurons to support neuronal function and regulate the chemical environment through their receptors and signalling pathways. Schwann cells are also located in DRG and throughout the rest of the PNS. They wrap around neuronal axons, and, in the case of myelinated fibres, form the myelin sheath. Even though one cell type surrounds cell soma while the other one surrounds axons, both have similar functions, producing extracellular matrix and

modulating the neural activity in healthy tissue and activating in response to nerve injury. Following nerve injury, the activation of Schwann cells and satellite glial cells influences activities of neighbouring neurons and their environment, for example, the expression of neurotrophin receptor p75 is dramatically upregulated in both satellite glial cells and Schwann cells (Nascimento et al., 2014, Richner et al., 2014, Vaegter, 2014). Satellite glial cells also possess Schwann cell-like properties such as expressing intermediate filament nestin and transcription factor Sox2 which are related to regenerative capabilities (Tongtako et al., 2017).

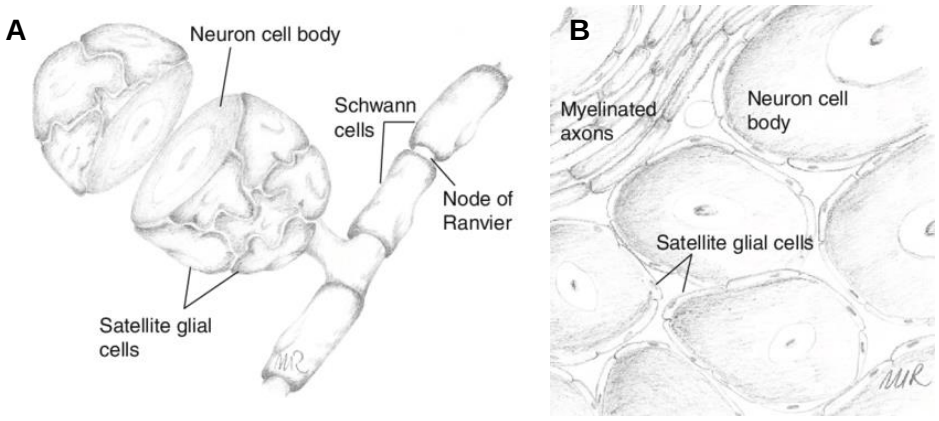

Figure 4.3 Satellite glial cells and Schwann cells in the peripheral nervous system. *(A) DRG neuron cell bodies surrounded by satellite glial cells and elongated axons ensheathed by Schwann cells. (B) Cross-section of DRG showing a layer of satellite glial cells around sensory neuron cell bodies (Richner et al., 2014).*

Instead of using the term ‘Schwann cells’, this chapter expands the terminology to “glial cells” to avoid confusion since both Schwann cells and satellite glial cells were present in the cultures from DRG. To simulate the interaction that would occur between host glial cells and Schwann cells implanted in an engineered nerve graft, glial cells from GFP-labelled rat dorsal root ganglia (DRG) and SCL4.1/F7 Schwann cell lines were co-cultured and phenotypically quantified. Additionally, preparing primary glial cells from DRG culture may be easier than purification of primary Schwann cells from the peripheral nerve (e.g. sciatic nerve) because many available methods for Schwann cell isolation

and purification from nerve tissue have limitations with fibroblast contamination, or are costly and time-consuming (Jin et al., 2008, Wei et al., 2009, Zhao et al., 2014).

The terminology to identify different types of glial cells has been adjusted for *in vitro* and *in vivo* experiments. In the *in vitro* experiment, TaeNT is a substrate for glial cell interaction. Cells originally cultured inside the gels are referred to as 'endogenous' while those later seeded on top of the gels are 'exogenous'. To avoid confusion these terms 'endogenous' and 'exogenous' were used only in the *in vitro* experiment, and then changed to 'transplanted' and 'host' for the *in vivo* experiment.

4.1.6 Protocols to prepare primary glial cells

Optimisation of primary glial cell preparation aims to overcome common challenges to maximise yield and minimise preparation time. According to previous protocols, neonatal rat sciatic nerve (or Brockes' method) is the most widely used source for Schwann cells (Brockes et al., 1979), providing a rapid method for generating purified populations. Some researchers have changed the cell source to adult rat sciatic nerve to acquire higher amounts of Schwann cells from fewer animals; however, it takes more than a week to complete the whole preparation, proliferation, and purification process (Komiyama et al., 2003, Mauritz et al., 2004, Morrissey et al., 1991). Another alternative source for Schwann cell preparation is DRGs which contain neurons, glial cells (a mixture of Schwann cells and satellite glial cells), and other cells such as fibroblasts and endothelial cells. Kim et al. proposed a method to isolate glial cells from single neonatal mouse DRGs which takes approximately 2 weeks to complete the preparation process (Kim and Kim, 2018). Adult rat DRGs offer another source to prepare peripheral nerve glial cells providing advantages over the use of neonatal DRGs in terms of easier dissection, but importantly also reflecting the adult stage of development that is more relevant in models aimed at studying nerve injury and repair. In this preparation method, incubating the crude DRG culture for 2-5 days increases the proportion of glial cells in

culture because glial cells continue proliferating *in vitro* after DRG dissection and compete for survival with neurons when nutrients in the culture are limited. On the other hand, neurons, which are highly differentiated cells, rarely proliferate *in vitro*, so the proportion of neurons decreases. (Castillo et al., 2013, Tongtako et al., 2017, Liu et al., 2012).

Besides incubation time, substrate coatings also influence the purity of glial cells in DRG culture because different types of cells have different adhesion characteristics. Some culture protocols seed the crude DRG culture in uncoated plastic flasks or on coverslips in order to further reduce the number of neurons in the culture (Capuano et al., 2009, England et al., 2001, Lemes et al., 2018, Villa et al., 2010). The attachment of glial cells to the substrate surface tends to be sufficient in uncoated culture flasks while neurons require PLL, PDL, or laminin coating. However, although uncoated culture surfaces were reported to effectively deplete neurons, yielding highly glial-enriched cultures, it could also reduce the survival rate of glial cells as they take a longer time to attach (Honkanen et al., 2007, Wang et al., 2019). It was also reported that the expression of some types of receptors in glial cells was significantly affected in the absence of neurons; for example, purinergic metabotropic P2Y receptors were undetectable in the purified culture (Villa et al., 2010). In this study, culture flasks were coated with PDL to facilitate rapid adhesion of adult rat DRG cells and the percentage of glial cells was increased by extending the incubation time.

4.1.7 Objective of this chapter

The main objective of this chapter was to understand the nature and consequences of the interaction between host and transplanted glial cells in nerve repair. The distribution, migration, and alignment of both glial cell populations were examined to understand whether glial cells from within the engineered tissue or from outside influence each other in a supportive or disruptive way.

Both *in vitro* and *in vivo* experiments were included starting with the study of glial cell migration in a 3D fully-hydrated hydrogel model containing 2 cell populations in adjacent chambers with a connecting interface. The number of cells and their ability to cross an interface to infiltrate another cell population were measured. Then, the alignment of endogenous therapeutic glial cells and exogenous infiltrating host glial cells was examined through TaeNT *in vitro* and then using a self-organising collagen guidance conduit *in vivo*. The guidance conduit containing aligned Schwann cells was transplanted into a 10 mm-gap rat sciatic nerve model for 3 weeks. The behaviour and interaction of transplanted therapeutic glial cells in a self-organising collagen guidance conduit and infiltrating glial cells from host tissue were explored.

Apart from the main experiments to investigate cell interaction, a number of other experiments were included to verify the protocols used and provide additional evidence for further investigation. Firstly, the protocol to prepare primary glial cells from DRG culture was examined for a percentage of glial cell population. Secondly, in addition to investigating the interaction of exogenous glial cells and endogenous glial cells in TaeNT, an additional experiment was carried out to examine the behaviour of exogenous glial cells on TaeNT when the aligned Schwann cells were killed using a freeze-and-thaw method. The preservation of collagen fibril alignment and mechanical properties of frozen-and-thawed TaeNT were also tested. The viscoelastic characterisation of TaeNT and frozen-and-thawed TaeNT were compared using DMA to determine whether the freeze-and-thaw process alters the mechanical properties of TaeNT, which may have influenced cell behaviour.

4.2 Results

4.2.1 Enrichment of glial cell population in DRG culture

To increase the number of primary glial cells in DRG cultures without any additional chemicals, 20-25 DRG explants were obtained from an adult rat. The percentage of glial cells in the cultures increased from DRG preparation over days by approximately 60% to 80%.

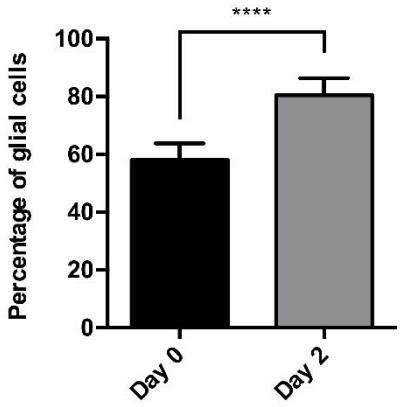

Figure 4.4 Enrichment of glial cell population in DRG culture. *The percentage of glial cells per total cells in DRG culture increased from approximately 60% to 80% in 2 days. Data shown as mean with SEM of 3 independent experiments; Unpaired t-test with two-tailed, **** $p < 0.0001$*

4.2.2 Migration of DRG glial cells and F7 Schwann cells in a 3D culture interface model

Two cell populations which are similar cell types from different sources, DRG glial cells and F7 Schwann cells, were investigated by visualising their migration behaviour in a 3D cell culture model containing these separate cell populations in close proximity. Acellular hydrogel compartments were also added in the hydrogel system for an interface observation, and the border-crossing behaviour of glial cells were quantified only at the cellular interface (i.e., the interface between two cell populations). After casting the gels, the stainless steel dividers separating the compartments were carefully removed without

disrupting the cell populations, enabling the adjacent gels to form one continuous gel with no mechanical interfaces (Figure 4.5).

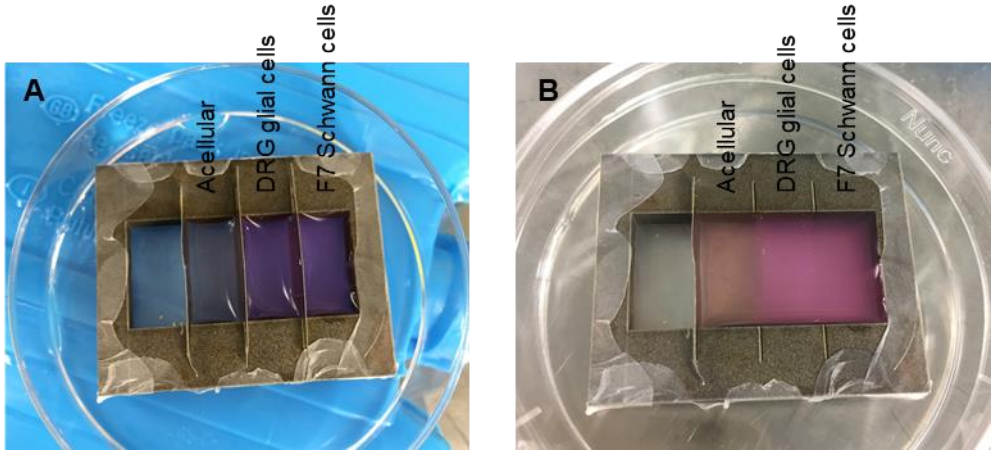

Figure 4.5 Experimental setup for 3D cell culture model to examine cell behaviour and interaction. *The cell culture construct consists of a stainless steel mould with 3 occupied chambers separated by removable dividers. Each chamber contains acellular, primary glial cells and F7 Schwann cells, respectively (from left to right). (A) Cell culture during casting process. The mould with gels was maintained at 4ºC to delay gelation before removing the dividers. (B) Gel setting. Dividers were removed after 2 minutes to allow gel integration without mixing of cell populations.*

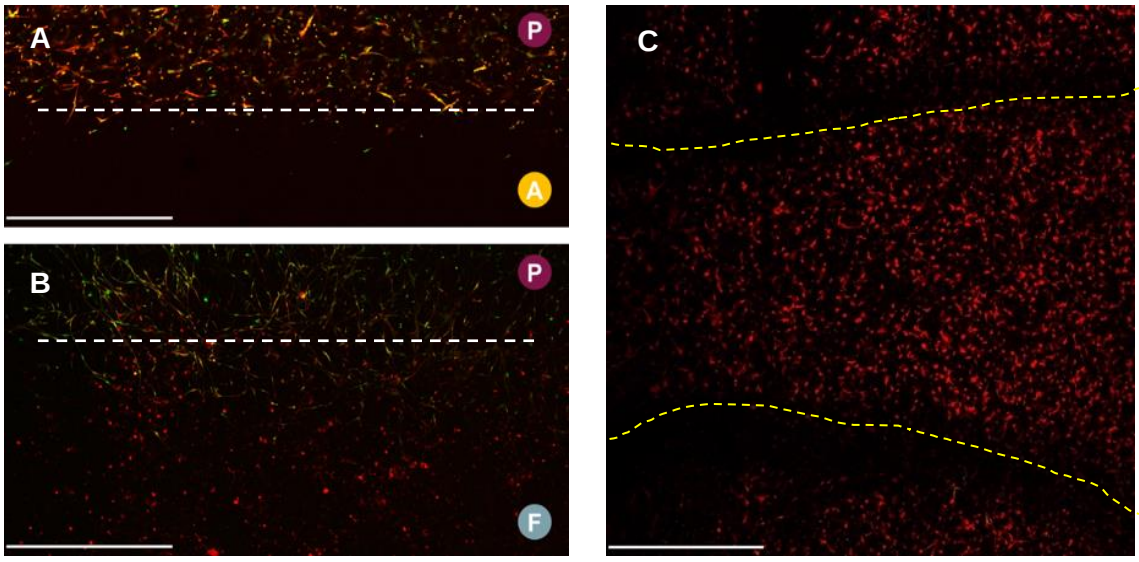

Figure 4.6 Location of glial cells in the 3D culture model after 3 days. *The white dotted lines indicated interface of two cell populations (A) Interface between primary DRG glial cells and acellular collagen gel. (B) Interface between primary DRG glial cells and F7 Schwann cells. (C) In 1 sample out of total 3 samples, a small degree of contraction was observed in the middle of the chamber containing F7 Schwann cells. The yellow dotted line showed the deformation of interface due to the cell contraction. All glial cells are shown in red (S-100) and primary cells (GFP+) are shown in green. Letters A, F, and P in circles represent the cell population in the particular area; A- acellular, F- F7 Schwann cells, P- primary DRG glial cells. Scale bar = 200 µm*

The migration of cells across the interface between the two cell populations was measured. After 3 days, the majority of cells remained in their original area, and approximately 2-20% of glial cells moved across the interface to another cellular area. The interfaces between cell populations were still detectable under a confocal microscope (Figure 4.6). In one out of a total of 3 trials, a small degree of gel contraction was observed within the F7 Schwann cells area and some of the F7 Schwann cells congregated towards the middle of the contracted gel. Nevertheless, the crossing behaviour of the F7 Schwann cells in the contracted sample was consistent with the other gels.

The crossing behaviour of glial cells was quantified by measuring the number of cells that had crossed the interface and the distance migrated into the adjacent area containing another cell population (Figure 4.7). F7 Schwann cells showed more migrating cells and greater displacement when compared to DRG glial cells. 20% of F7 Schwann cells crossed the interface whereas less than 5% of the DRG glial cells did. The longest distance that F7 Schwann cells migrated from the interface into the adjacent area was around 8 times more than that of the DRG glial cells.

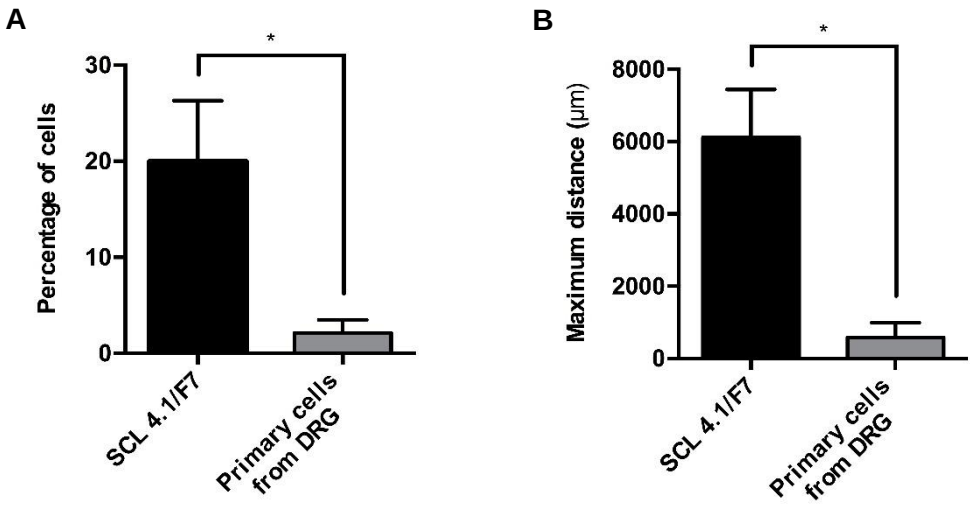

Figure 4.7 Quantification of glial cell migration across cell population interface in 3D culture model. *(A) Percentage of cells in the population found in another cell population area. (B) Maximum migration distance of cells away from their population interface into another cell population. Data shown as mean with SEM of 3 independent experiments. Unpaired t-test with two-tailed, *p<0.05.*

4.2.3 Interaction of endogenous and exogenous glial cells in an engineered tissue *in vitro* co-culture model

Having explored the extent to which glial cell populations invade adjacent regions in 3D collagen gels, a co-culture model was established to simulate the interaction of exogenous glial cells with the F7 Schwann cells in an implanted cellular material. The cell distribution and alignment were measured as features contributing to nerve regeneration.

Primary glial cells from GFP-labelled rat dorsal root ganglia, (defined as 'exogenous' glial cells), were seeded onto TaeNT constructs containing aligned (defined as 'endogenous' glial cells) F7 Schwann cells. After 3 days in co-culture, the images were analysed using a co-localisation protocol where areas that were both GFP and S-100 positive identified as exogenous glial cells, and areas that were GFP-negative and S-100 positive identified as endogenous glial cells (Figure 4.8).

All exogenous glial cells, as well as DRG neurons, were found only on the top surface of TaeNT without penetration into the collagen gels. The proportion of endogenous cells and exogenous cells in each image were not significantly different with an average of 54% and 46%, respectively (Figure 4.8D). After 3 days in co-culture, the exogenous glial cells seeded on top had become aligned with the endogenous Schwann cells in the TaeNT. The alignment of each cell population was quantified by calculating the difference between the angle of the longest axis of each cell and the longitudinal axis of the gel to obtain the angle of deviation of each cell. (Figure 4.9). The angle of deviation of each glial cell was categorised into 9 groups ranging from 0 to 90°, and the relative frequency of each group was compared to determine the degree of alignment. Both endogenous and exogenous glial cells were highly aligned after 3 days, with average angle of deviation less than 20%, and approximately 40% of cells deviating less than 10 degrees from the longitudinal axis (Figure 4.9A, B). According to the box-and-whisker graph, endogenous glial cells were aligned slightly better than exogenous glial cells. The

angle of deviation of glial cells in different areas (edge and middle of TaeNT) were similar, especially those of endogenous glial cells where the mean angles of deviation were very close (Figure 4.9C, D).

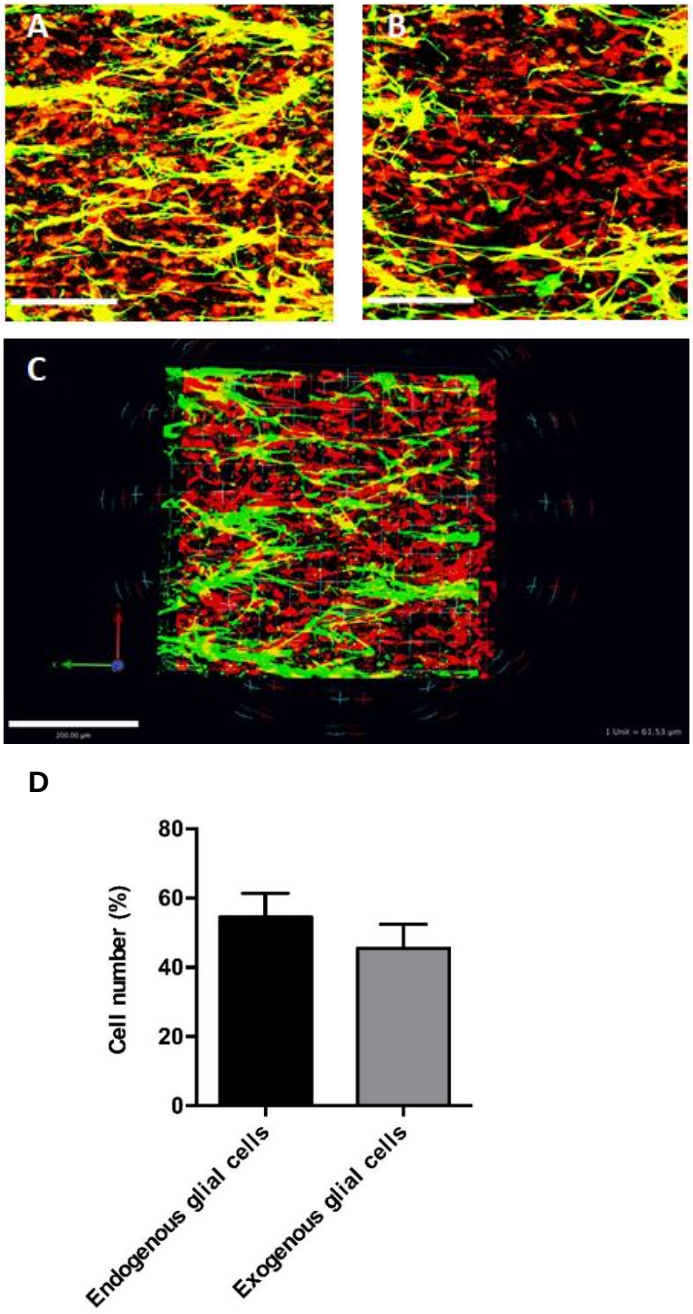

Figure 4.8 Proportion of endogenous and exogenous glial cells after 3 days of TaeNT co-culture. *Confocal micrographs showing a single slice (A) in the middle area, and (B) at the edge area of TaeNT. (C) 3D opacity images (confocal Z-stack) in the middle area of TaeNT. Glial cells are shown in red (S-100) and GFP+ cells are shown in green. Exogenous glial cells are areas of both red and green and endogenous glial cells are those of red only. Scale bar = 200 µm. (D) Percentage of endogenous and exogenous glial cells in co-culture after 3 days. Data shown as mean with SEM of 4 independent experiments with 4 images taken from each experiment. Paired t-test with two-tailed, p = 0.2859. No statistical difference.*

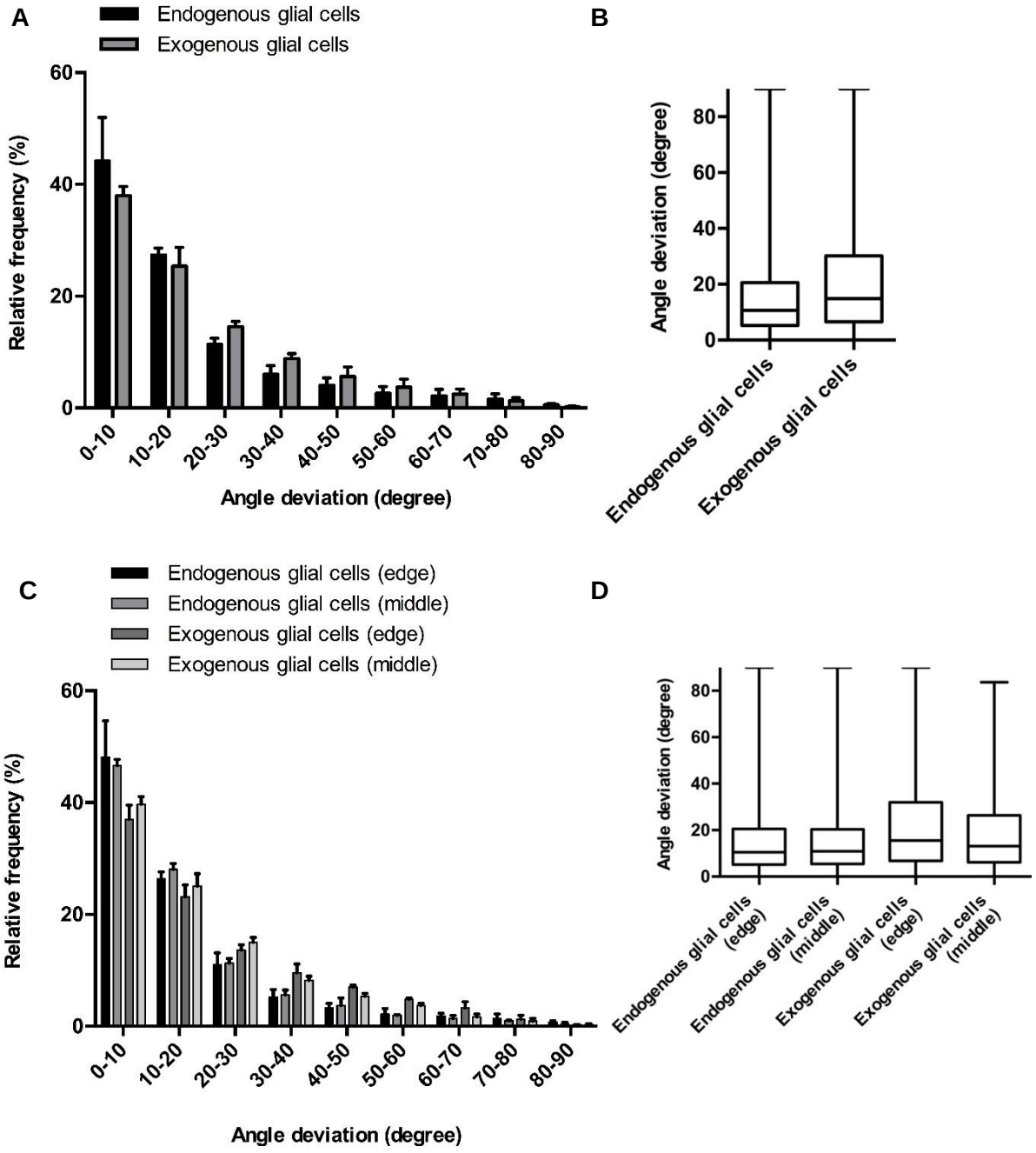

Figure 4.9 Quantification of glial cell alignment after 3 days of co-culture. *Angle of deviation of cells was measured relative to the longitudinal axis of TaeNT. Data shown as mean with SEM of 4 independent experiments. (A) Relative frequency of each angle deviation range. (B) Box-and-whisker plot of angle deviation of different populations of glial cells. (C) Relative frequency of each angle deviation range of cells in different areas in TaeNT. (D) Box-and-whisker plot of angle deviation of all data in different area in TaeNT. Data shown in (A) and (C) as mean with SEM of 4 images from each 4 independent experiments. Data shown in (B) and (D) as minimum, lower quartile, median, upper quartile, and maximum of all data measured from 4 images representing 4 independent experiments.*

4.2.4 The effect of freeze-and-thaw process on collagen matrix of TaeNT

Although the result in previous experiment (Section 4.2.3.) showed the alignment of exogenous glial cells on TaeNT 3 days after seeding them in co-culture with aligned endogenous glial cells, it was not clear whether the aligned endogenous glial cells themselves or the anisotropic extracellular matrix environment induced the exogenous glial cells to align. An additional experiment in Section 4.2.5. was thus carried out to investigate the alignment of exogenous glial cells in the absence of endogenous glial cells. When acellular TaeNT was prepared for the experiment, the preservation of TaeNT extracellular matrix and mechanical properties after the freeze-and-thaw process were tested. With alignment of collagen matrix and mechanical properties as controlled variables, the alignment of exogenous glial cells in the absence of endogenous glial cells could be compared with that in the presence of endogenous glial cells.

To examine exogenous cell behaviours when cultured with TaeNT in the absence of endogenous cell within TaeNT, the freeze-and-thaw process was selected as an approach to kill the endogenous cells in the construct while preserving extracellular matrix in the tethered gel. After snap-freezing TaeNT in liquid nitrogen at -80°C, the frozen hydrogels became stiffer, opaque, and brittle. Subsequently-thawed TaeNT had a similar shape to the gel before undergoing the whole freeze-and-thaw process. The contracted gel shape and collagen fibril alignment were preserved after the freezing and thawing cycle. Scanning electron microscopy revealed that the extracellular matrix of frozen-and-thawed TaeNT resembled that in the control TaeNT. The collagen fibrils in TaeNT were dense and aligned with elongated cells (Figure 4.8A, C). A number of porous spaces were observed throughout the aligned matrix of both TaeNT and frozen-and-thawed TaeNT, but were more noticeable in frozen-and-thawed TaeNT (Figure 4.10B). Although frozen-and-thawed TaeNT had around 5% reduction in fibrils within the highest alignment range and a small increase in angle deviation mean, 60% of fibrils in both conditions still aligned with angle deviation less than 30 degrees (Figure 4.11).

Mechanical properties were also compared by compressive DMA testing to obtain storage modulus, loss modulus, and tan delta value at different frequencies. The storage and loss modulus increased with increasing frequencies. Responses of normal TaeNT had a similar trend to those of frozen-and-thawed TaeNT, but with smaller standard deviation making the variability range narrower (Figure 4.12). The mean of storage and loss modulus slightly increased following freeze-and-thaw treatment and the variability was greater, mostly at high frequencies. Both TaeNT and frozen-and-thawed TaeNT has similar tan delta (phase shift) reflecting preserved viscoelastic properties of the materials.

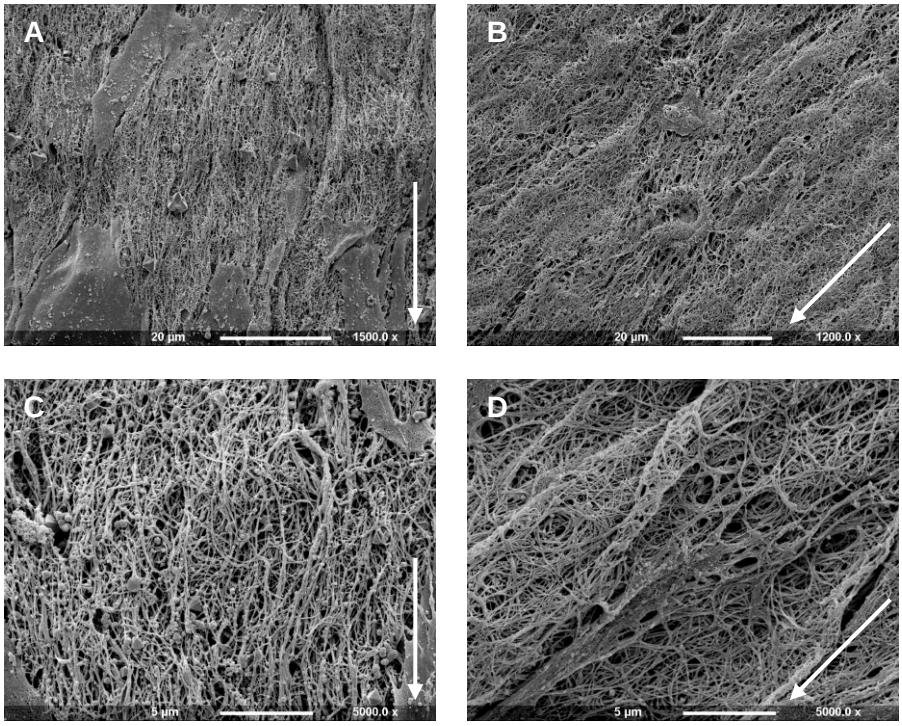

Figure 4.10 Alignment of collagen matrix under SEM after 24 hours in (A),(C) TaeNT, and (B),(D) frozen-and-thawed TaeNT. *The white arrows indicate the main orientation of alignment (longitudinal axis). Scale bar = (A),(B) 20 µm, (C),(D) 5 µm.*

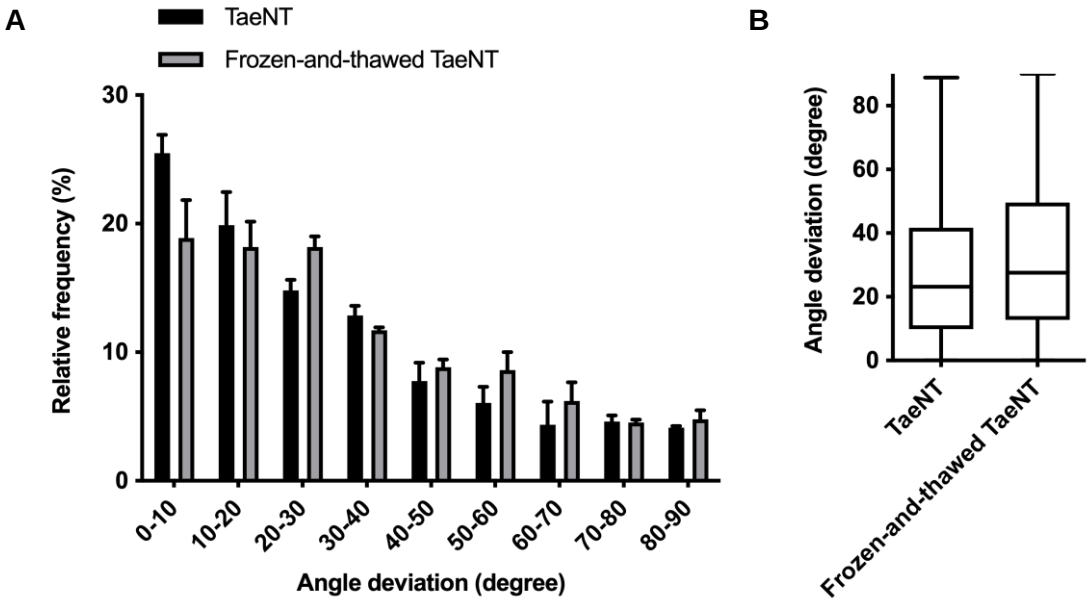

Figure 4.11 Freeze-and-thaw process had minimal effect on collagen matrix alignment in TaeNT. *(A) Relative frequency of each range of angle deviation. Data shown as mean with SEM of 4 images from 4 independent experiments. (B) Box-and-whisker plot of angle deviations. Data shown as minimum, lower quartile, median, upper quartile, and maximum of all data measured from 4 images representing 4 independent experiments.*

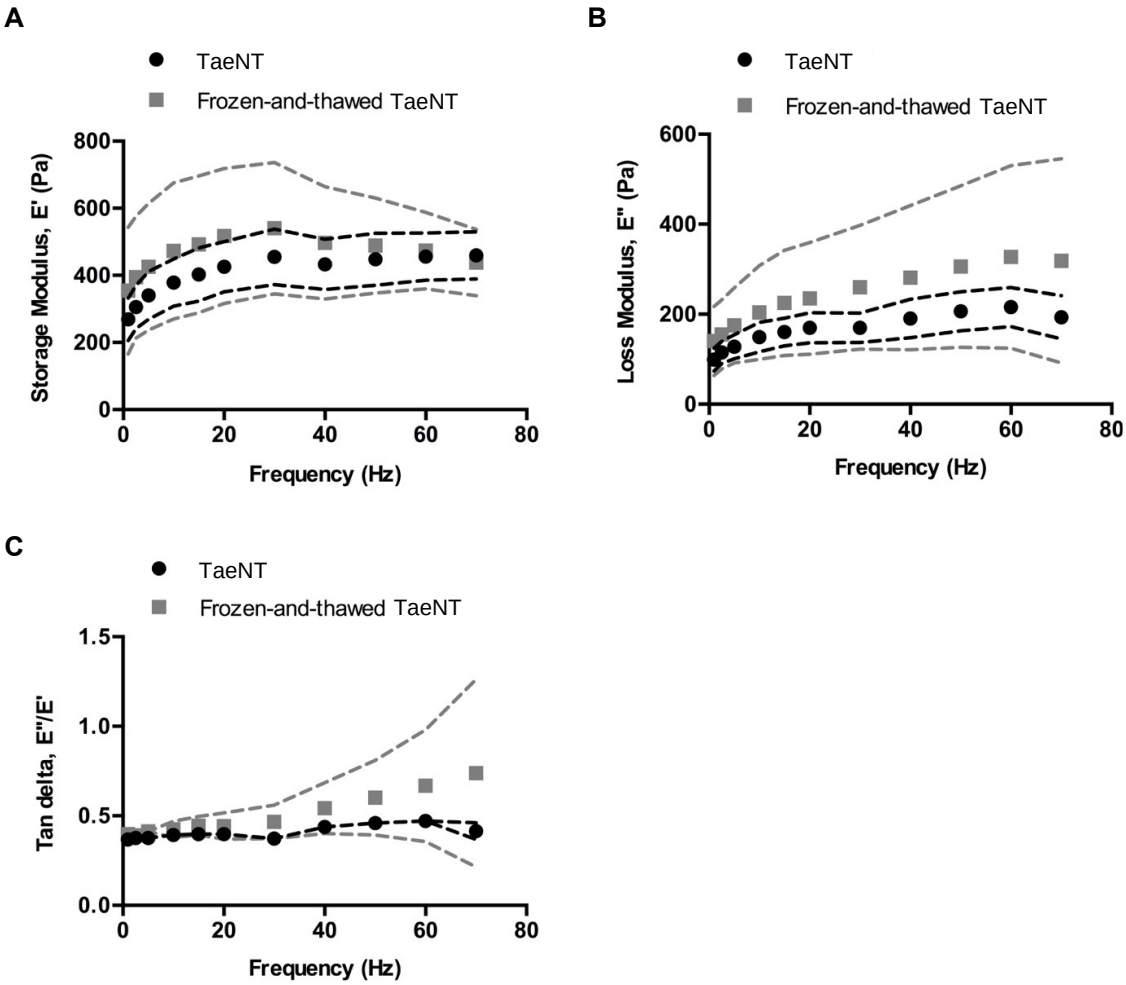

Figure 4.12 Compressive DMA testing on TaeNT and frozen-and-thawed TaeNT with similar viscoelastic behaviour. *(A) Storage modulus. (B) Loss modulus. (C) Tan delta. Data shown as mean with SEM of 4 independent experiments. Black dots with dotted-line and grey boxes with dotted-line represent mean with SEM of TaeNT and Frozen-and-thawed TaeNT, respectively.*

4.2.5 Alignment of Exogenous glial cells cultured on freeze-and-thawed TaeNT

The alignment of exogenous glial cells in the absence of aligned endogenous glial cells was investigated to test whether the preserved alignment of collagen matrix could also induce the alignment of exogenous glial cells. In this section, TaeNT was prepared in the usual way then frozen-and-thawed before exogenous glial cells were seeded onto it, and the alignment of exogenous glial cells was measured and compared with that of exogenous glial cells on TaeNT in Section 4.2.3.

Immunostaining images showed that many exogenous glial cells in frozen-and-thawed TaeNT congregated and aligned to the longitudinal axis (Figure 4.13). The congregation of cells, forming a long continuous tract along the middle area of gels, was highly aligned resulting in a low mean angle of deviation from the longitudinal axis. The quantified result showed that the number of exogenous cells present on the frozen-and-thawed TaeNT was significantly less than those on the cellular material. The alignment of exogenous glial cells in frozen-and-thawed TaeNT (without endogenous glial cells) was comparatively higher than that in TaeNT (with endogenous glial cells). More than 90% of the exogenous glial cells showed less than 10 degrees angle of deviation from the longitudinal axis (Figure 4.14).

Although glial cells from two different sources interacted and influenced each other to align in the similar pattern as demonstrated in Section 4.2.3, the result in this section implied that glial cells eventually aligned better in the absence of glial cells from the other source at a similar incubating time. The decellularised TaeNT by freeze-and-thaw technique provided the better substrate for glial cell alignment, but not for cell attachment as number of glial cells to the substrate was much lower.

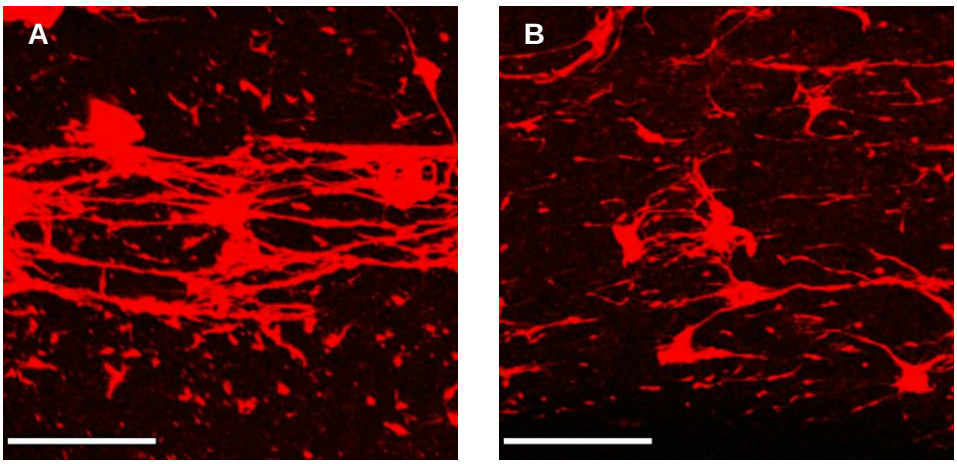

Figure 4.13. Alignment of exogenous glial cells after 3 days of co-culture on freeze-and-thawed TaeNT. Glial cells are shown in red (S-100). (A) alignment of co-culture in freeze-and-thawed TaeNT at middle area, and (B) edge area. Scale bar = 200 μm

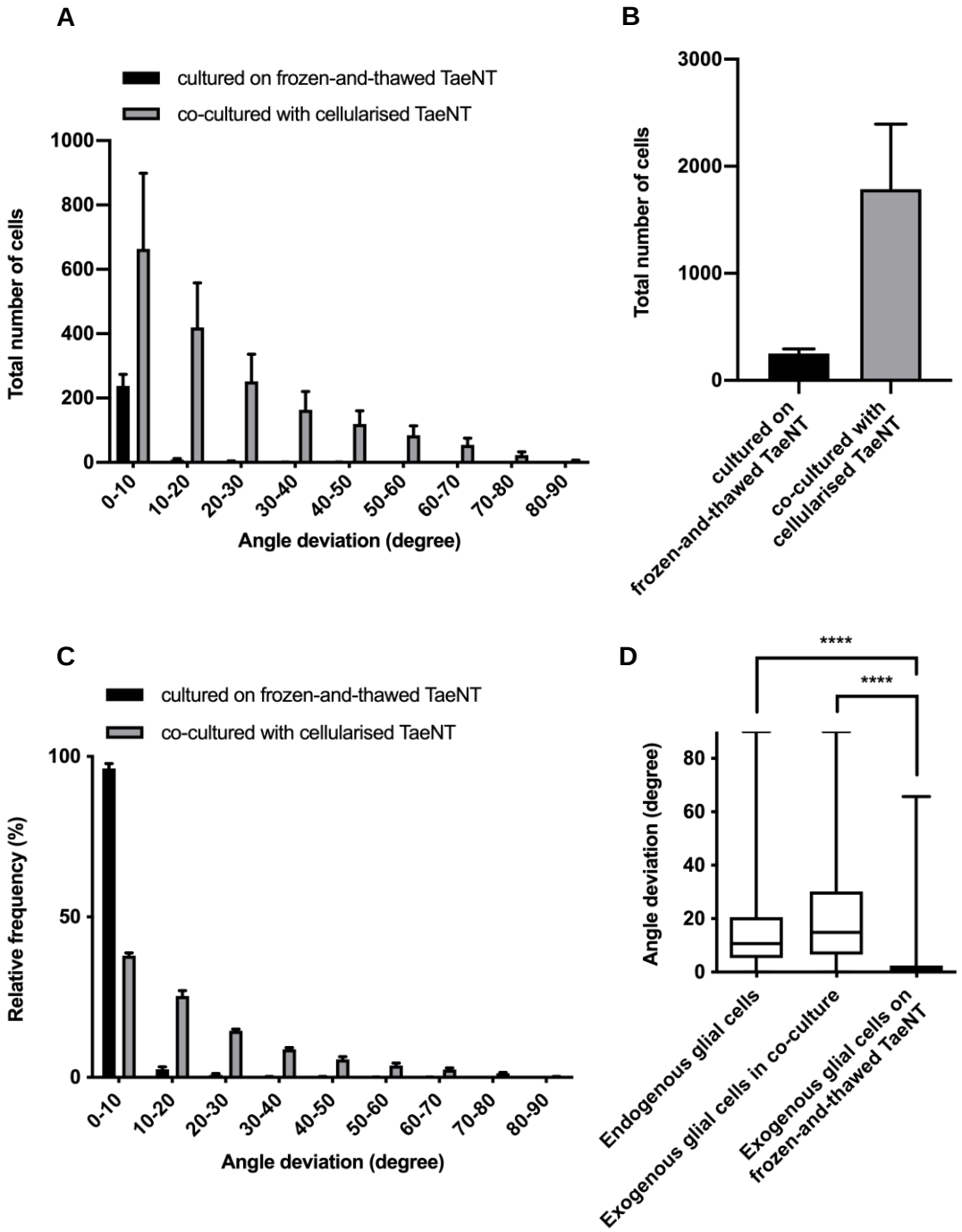

Figure 4.14 Quantification of exogenous glial cell alignment after 3 days of co-culture on freeze-and-thawed TaeNT, compared to exogenous and endogenous glial cells on normal TaeNT. *Angle deviation was measured from the longitudinal axis of TaeNT. Exogenous glial cells on frozen-and-thawed TaeNT showed higher alignment with significantly lower angle deviation. (A) Number of cells with each range of angle deviation. (B) Total number of cells counted from samples in the analysis. (C) Relative frequency of each angle deviation range. (D) Box-and-whisker plot of angle deviation of different glial cells when cells on frozen-and-thawed TaeNT was compared with cells on cellular TaeNT from Section 4.2.3. Data shown in (A) and (C) as mean with SEM of 4 images from each 4 independent experiments. Paired t-test with two-tailed, p = 0.0913. No statistical significance. Data shown in (D) as minimum, lower quartile, median, upper quartile, and maximum of all data measured from 4 images representing 4 independent experiments.*

4.2.6 Interaction of transplanted and host glial cells *in vivo*

After investigating the distribution, migration and alignment of glial cells as a consequence of cell-cell interaction *in vitro*, an *in vivo* experiment was carried out to test interactions in a more complex model. Since the TaeNT requires tethering to maintain alignment, the self-organising collagen guidance conduit was prepared by tethering collagen gels containing aligned F7 Schwann cells in 10-mm silicone tubes.

The experimental setup was the same transplantation into a 10-mm sciatic nerve gap of GFP-expressing transgenic rats for 3 weeks as performed in Chapter 3 but with different sectioning, immunostaining, and quantification analysis. Here, 4-mm longitudinal middle sections were stained with anti-S100 antibody DyLight^{TM} 549 for glial cell identification. (Note that the remaining 3-mm length at each end of transplanted conduit was cross-sectioned and analysed in Chapter 3 for neurite identification). Images were captured of longitudinal sections through the transplanted conduits using confocal microscopy to visualise cell populations along the construct. Image analysis for co-localisation was similar to the previous *in vitro* experiment (Section 4.2.3). The areas positive for both GFP and S-100 were identified as host glial cells, and areas negative for GFP and positive for S-100 were identified as transplanted glial cells. Figure 4.15 shows examples of how cells of each different type were identified, and skeletal length lines assigned by the software.

According to Figure 4.15, transplanted and host glial cells were found distributed throughout the transplanted conduit at 3 weeks post-transplantation. Glial cells were slightly less dense at the rim of the gel along the longitudinal axis. More transplanted cells were observed. Approximately 70% of total glial cell population along the longitudinal section of the conduit was transplanted cells, and the remaining 30% was infiltrating glial cells from host tissue (Figure 4.16).

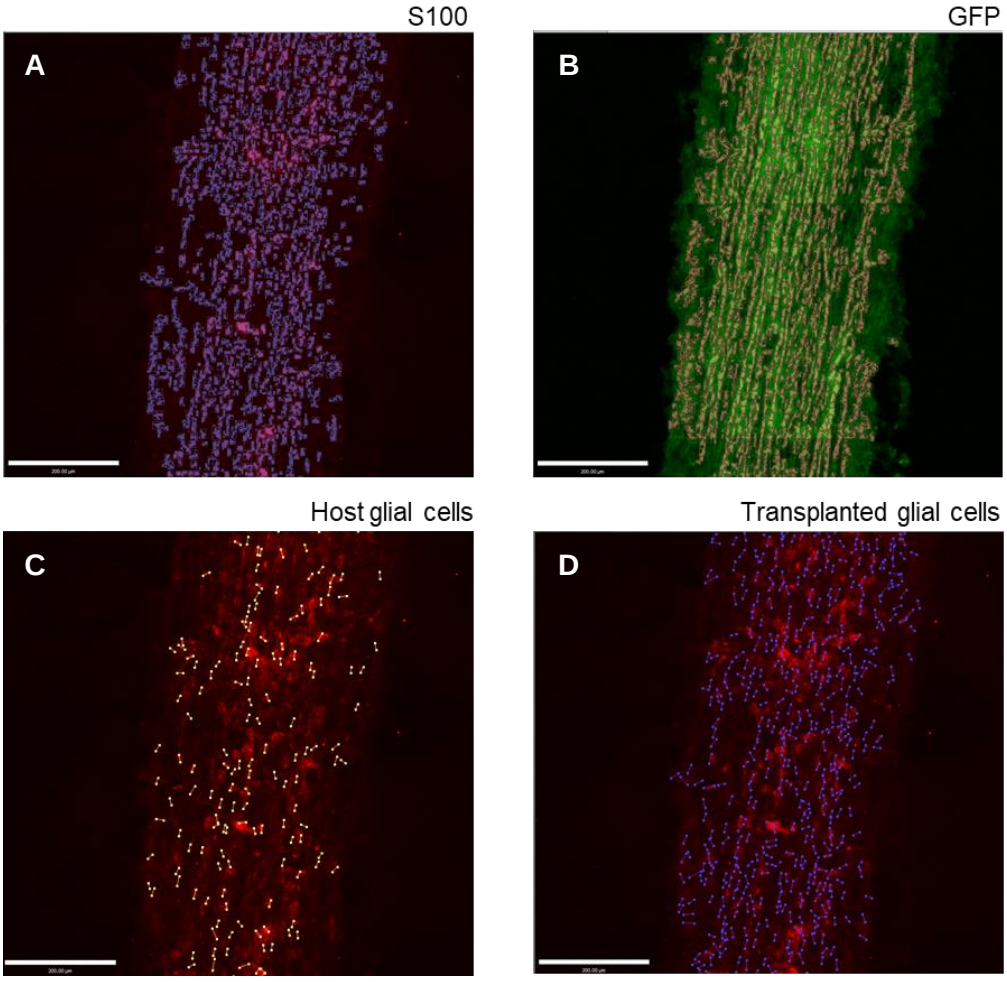

Figure 4.15 Alignment of host and transplanted glial cells in self-organising collagen guidance conduit at 3 weeks post-injury following transplantation into a 10-mm rat sciatic nerve gap. *All glial cells are shown in red (S-100), and host cells (GFP+) are shown in green. (A, B) Volocity™ software detected glial cells in red and green channels, and then (C, D) identified host and transplanted cells using the 'overlap' and 'exclude' functions. Yellow and blue arrows in the bottom figures indicate the skeletal length lines assigned to host and transplanted glial cells, respectively. Scale bar = 200 µm*

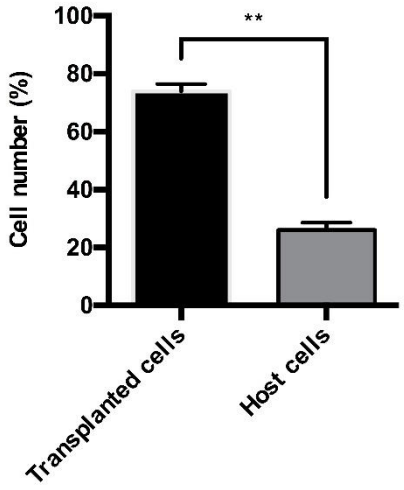

Figure 4.16 The percentage of host and transplanted glial cells per total glial cells inside 3.3-mm longitudinal middle section of self-organising collagen guidance conduit *containing aligned F7 Schwann cells at 3 weeks post-injury following transplantation into a 10mm rat sciatic nerve gap. Data shown as mean with SEM from 3 samples; 3 sections from each rat. Paired t-test with two-tailed, **p < 0.005*

To measure the longitudinal distribution of each glial cell population, the number of glial cells was counted at every 100 μm starting from proximal to distal end of the section (Figure 4.17A). Both transplanted and host glial cells had a similar pattern of distribution along the conduit. The highest percentage of glial cells were located within the first 500 μm away from the proximal end, and the percentage of glial cells gradually decreased to a plateau at more distal positions. The longitudinal distribution of the glial cells was also assessed by categorising the tissue into 3 equal- length parts (1,100 μm each): proximal, middle, and distal (Figure 4.17B). 50% of the total glial cell population in the conduit was found at the proximal sites while approximately 27% and 23% of the population was found at the middle and distal sites, respectively. There was a significant difference in the percentage of glial cells at the proximal part when compared to those at the middle and distal parts.

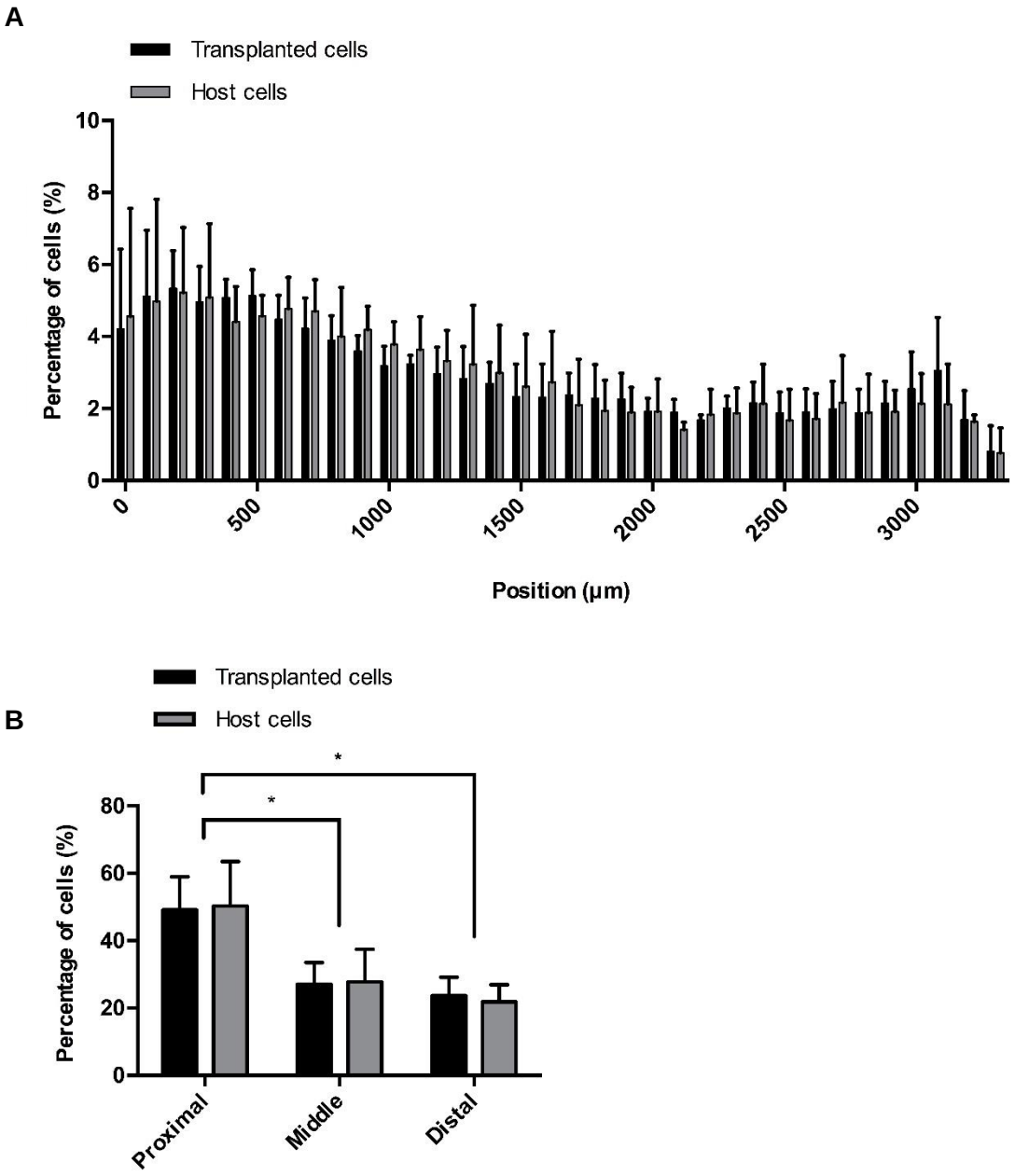

Figure 4.17 The proportion of glial cells at different positions along the transplanted conduit. *The data showed the percentage of host and transplanted glial cells out of the total number of glial cells in the same population. (A) shows detailed information captured every 100 µm along the length whereas (B) shows summary information from categorising each longitudinal section into 3 parts with equal length of 1100 µm: proximal, middle, and distal. Data shown as mean with SEM from 3 samples; 3 sections from each rat.*

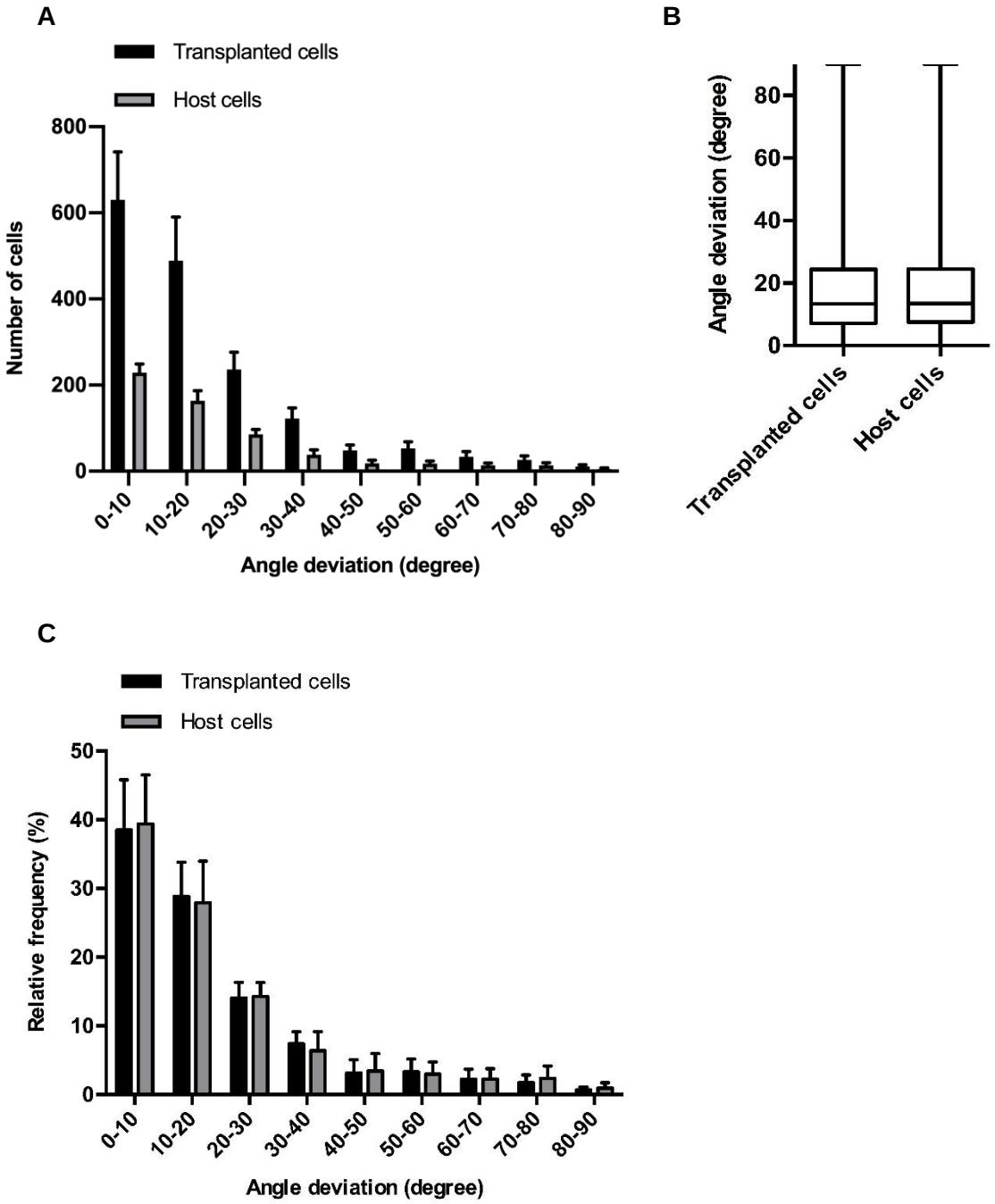

Figure 4.18 Quantification of glial cell alignment in self-organising collagen guidance conduit at 3-week post-transplantation in a 10 mm rat sciatic nerve gap. *Angle deviation was measured from whole longitudinal length of the conduit. Transplanted and host cells were highly aligned in a similar pattern. (A) Number of glial cells at each angle deviation range. (B) Box-and-whisker plot of angle deviation of different populations of glial cells. (C) Relative frequency of glial cells with each angle deviation range per total glial cells in the same population. Data shown in (A) and (C) as mean with SEM from 3 samples; 3 section from each rat. Data shown in (B) as minimum, lower quartile, median, upper quartile, and maximum of all data measured from 3 samples; 3 sections from each rat.*

Both transplanted and host glial cells aligned in a similar pattern with approximately 40% of cells deviating less than 10 degrees deviating from the longitudinal axis (Figure 4.18). According to the box-and-whisker plot (Figure 4.18B), the angle deviation of both glial cell population had similar minimum, lower quartile, median, upper quartile, and maximum implying that their behaviours in spatial orientation were synchronised into the similar pattern after 3 weeks of transplantation. The *in vivo* experiment was consistent with the *in vitro* experiment, showing that glial cells from different sources interact and align in a similar pattern. The interaction between the host and transplanted glial cells is supportive to axon regeneration providing a directional cue for the neurite elongation from the proximal stump.

4.3 Discussion

In the first experiment, the preparation method of DRG culture, usually used as a source of primary neurons, was modified to enrich the glial cell population for use as a primary glial cell source in this chapter. The initial percentage of glial cells in the adult rat DRG measured by S-100 immunostaining analysis was approximately 50-60% which was higher than previous estimation by FACS sorting where the percentage of Schwann cells and satellite glial cells counted from mouse dissociated DRG were 10% and 30%, respectively, making the summation of 40% (Avraham et al., 2020). The difference between the previous report and the result measured from this experiment might be due to the difference in measurement method and a low number of counted samples from both methods. Additional experiments with sufficient number of animals would possibly increase consistency in the glial cell ratio obtained from different measurement methods.

Preparation of glial cells from DRG by culturing for extending time has been considered to be a simple way to optimise glial cells from DRG without digestion. The glial cells continue proliferating *in vitro* after DRG dissection while neurons, which are highly differentiated cells, rarely proliferate *in vitro* (Castillo et al., 2013, Tongtako et al., 2017, Liu et al., 2012). The method was demonstrated in neonatal rats where the percentage of glial cells seeded on a coated flask reached 95% after 3 days in culture (Wang et al., 2019). The comparison between glial cells ratio at different time points measured in this chapter also showed the increase of glial cells from adult rat DRG with incubating time. The glial cells from adult rat DRG proliferated and reached the ratio of 80% enabling further experimental uses of glial cells after 2 days without complicated culture preparation.

Another limitation of this method is that it did not attempt to remove fibroblasts from the culture. Further refinements could therefore be considered to remove fibroblasts such as antimitotic treatment, immunodepleting with Thy1-antibody, magnetic activated cell sorting (MACS), fluorescence-activated cell sorting (FACS), or replacement of L-

valine with D-valine in culture medium (Assouline et al., 1983, Brockes and Raff, 1979, Hongpaisan, 2000, Manent et al., 2003, Spiegel and Peles, 2009).

The main experiments in this chapter aimed to understand the nature and consequences of the interaction between host and transplanted glial cells in nerve repair by measuring the distribution, migration, and alignment of both glial cell populations. While the early experiments quantified only the viability of transplanted Schwann cells in the conduit (Fansa et al., 1999, Mosahebi et al., 2003, Tohill et al., 2004, Berrocal et al., 2013), this chapter provided an in-depth experiment reporting whether transplanted Schwann cells and infiltrating Schwann cells from host tissue could facilitate or disrupt each other's function and alignment in the context of a cellular tissue engineered graft. The overall results indicate that the interaction of host and transplanted glial cells maintains the initial pattern of spatial organisation.

The *in vitro* migration of glial cells when interacting with another cell population was investigated in a 3D collagen hydrogel system. With the same 3D culture system, an inhibitory interface was observed in astrocytes when cultured adjacent to DRG cells (East et al., 2012). Here, DRG glial cells and F7 Schwann cells did not repel each other at the interface, since there was no evidence of cell segregation persisting at the interface and cells migrated into adjacent gel compartments. The ability to cross the interface and mix with the other cell population indicates the absence of inhibitory interfaces at the boundary between the two different glial cell populations.

To investigate the effect on alignment of glial cell interaction on cells in engineered tissue, DRG glial cells and F7 Schwann cells were co-cultured in TaeNT by seeding DRG glial cells from GFP-labelled rat dorsal root ganglia (exogenous glial cells) onto TaeNT containing aligned F7 Schwann cells (endogenous glial cells). The endogenous glial cells in fully-hydrated collagen gels attached to the fibrillar collagen network which was tethered to facilitate cell alignment in parallel to longitudinal orientation (Phillips et al., 2005). In other studies, tethered aligned cellular collagen gels,

used as a substrate for neurite elongation, have been stabilised by the removal of interstitial fluid to increase cell and matrix density and enable tethering to be removed without loss of alignment (East et al., 2010, Georgiou et al., 2013). Here, TaeNT was left in a fully hydrated state, and not stabilised in order to allow Schwann cells to freely migrate and align in 3-dimensional space while embedded in the hydrogel. Thus, it was a suitable tool to examine the spatial behaviour and interaction of cells.

Exogenous glial cells become aligned with the endogenous Schwann cells in the TaeNT over 3 days in co-culture while the alignment of endogenous glial cells remained undisrupted, with alignment persisting throughout different areas in the TaeNT. The alignment of exogenous glial cells observed in co-culture implies that the fully-hydrated cellular tethered collagen gels provided directional guidance cues to exogenous glial cells. It also indicates that endogenous glial cells can still preserve their highly-aligned topography in the presence of another cell population, which is an important consideration for therapeutic transplantation of these types of engineered tissues. The proportion of DRG glial cells aligned on TaeNT with angle deviation less than 20 degrees was approximately 65% which was similar to that reported previously for DRG neurons on top of stabilised TaeNT gels containing F7s *in vitro* (Georgiou et al., 2013).

To investigate the role of the presence of endogenous cells in conferring alignment on exogenous cells *in vitro*, an investigation was carried out on TaeNT in the absence of endogenous glial cells. SEM images showed that the collagen fibrils in TaeNT remained aligning after a cycle of freeze-and-thaw. This result in engineered tissue is consistent with the extracellular matrix preservation reported after freeze-and-thaw in other tissues such as arteries, bone, and tendon (Suto et al., 2012, Delgadillo et al., 2010). After freeze-and-thaw process had removed the endogenous cells, the aligned extracellular matrix was still enough to induce alignment of glial cells cultured on top of the surface (Dubey et al., 1999, Ribeiro-Resende et al., 2009, Rosner et al., 2005, Maturana et al., 2011). Interestingly, these experiments showed better alignment of exogenous glial cells on frozen-and-thawed TaeNT compared with those seeded on the

normal TaeNT. Importantly, other factors such as the mechanical properties and collagen fibril alignment remained equivalent between the two conditions, indicating that any differences in the behaviour of the exogenous glial cells was likely to be due to a direct effect of the presence of endogenous cells. Further research could be conducted to explore differences in the cell alignment on frozen-and-thawed TaeNT compared with on TaeNT. One hypothesis to consider is that endogenous glial cells killed by freeze-and-thaw method left unoccupied pores within the collagen matrix, which may have accommodated and aligned the exogenous glial cells.

When self-organising cellular collagen guidance conduits were transplanted into 10-mm rat sciatic nerve gaps, at 3-weeks post-transplantation both transplanted and host Schwann cells were found inside the conduit. This implies that transplanted glial cells had survived for at least 3 weeks in the transplanted conduit, and host glial cells migrated into the conduit from the nerve stumps. The migration of glial cells from host tissue has been found previously in acellular conduit transplantation, where glial cells are crucial in forming cellular guidance for regenerating neurites (Bryan et al., 1999, Chen et al., 2019b, Parrinello et al., 2010, Cattin et al., 2015, Dun and Parkinson, 2020). This experiment demonstrated that the presence of aligned transplanted glial cells did not prevent host glial cell migration into the conduit. A further question remains about whether the presence of transplanted glial cells induces any change in migration rate or time frame, compared to glial cells entering acellular conduits, which are normally found after 2-3 days in rodent models (Chen et al., 2019b, Torigoe et al., 1996).

The similar distribution pattern of host and transplanted glial cell populations throughout the conduit at 3-weeks post-transplantation implies the glial cells from both sources respond to the regional environment in a similar way. The alignment patterns of transplanted and host glial cells in the *in vivo* experiment were more similar to each other than those in the *in vitro* experiment. This may be due to the longer time point and presence of additional biological signals involved in inducing the alignment of Schwann cells to form Bands of Büngner *in vivo* (Min et al., 2021, Wanner and Wood, 2002).

Although more glial cells were found in the proximal area than in the middle and the distal area, it cannot be concluded from this experiment whether cells in the middle and distal area had a lower survival rate, or cells in the proximal area proliferated more than cells in other areas. The distribution difference of glial cells from the proximal to distal area might be caused by cell environment that influences cell survival, and/or the morphology of individual aligned cells that influences cell quantification. The proximal stump has been previously reported to have more activation of the transcription factor STAT3 which was necessary for the morphology maintenance and survival of repair Schwann cells in chronic denervation (Benito et al., 2017, Jessen and Mirsky, 2016, Sheu et al., 2000). Besides, the remyelination of Schwann cells shortened the length of the cells and more myelinated Schwann cells were found at proximal side of the regenerating nerve (Gomez-Sanchez et al., 2017). The activation of STAT3 and the higher number of shortened Schwann cells at the proximal stump were possibly contributed to the result where more Schwann cells were counted at the proximal area, compared to the middle and distal area with similar tissue length.

The *in vivo* work presented here was an initial experiment conducted with a minimal number of animals so the statistical analysis should be treated with caution as there was insufficient information about the likely variability and effect size to allow a power calculation to be performed in advance. A subsequent power analysis (Figure 4.19) indicates that the total number of experimental animals should be at least 18 rats in order to confidently detect a medium effect size with 5% error probability and a statistical power of 0.8. Although the sample size of 3 in this initial experiment was not enough to detect an effect with a given degree of confidence, the results from 3 experimental animals can preliminarily demonstrate a trend of data with a statistical power of 0.1-0.2. The result from this chapter will be useful in future experimental design for example to compare migrating behaviour of host glial cells into acellular and cellular conduits.

A

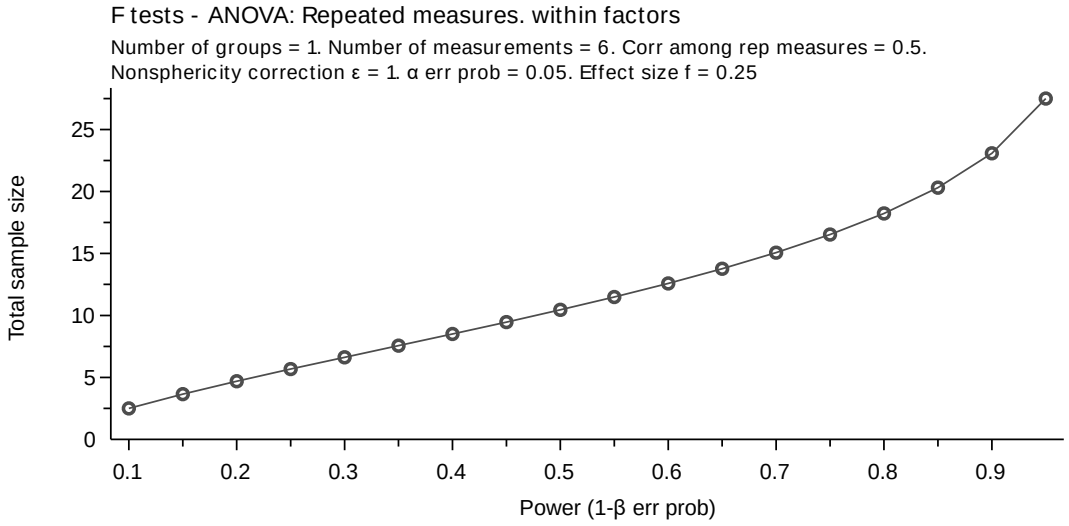

B

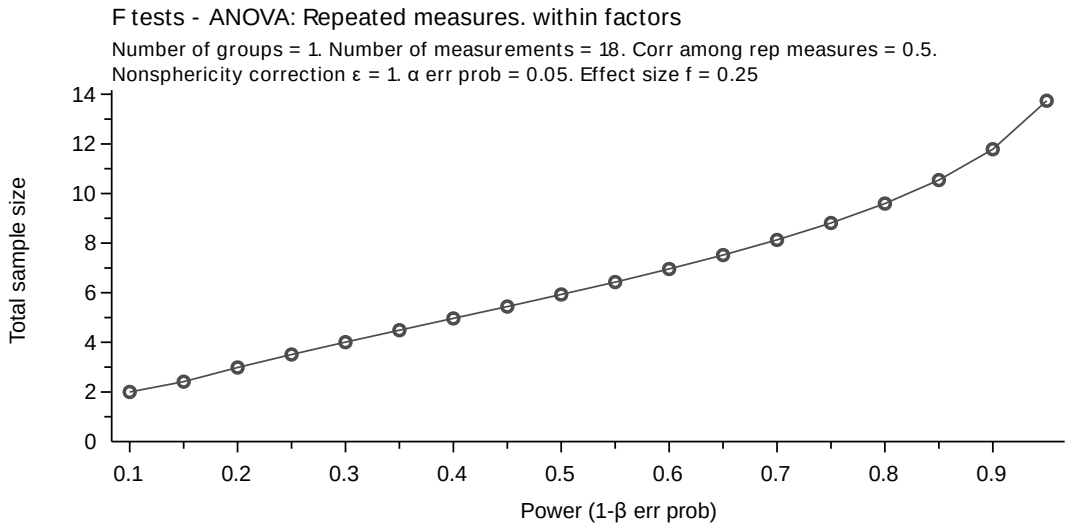

Figure 4.19 Total sample sizes corresponding to the power from 0.1 to 1 for one-way ANOVA test with repeated measures*, within factors in (A) alignment, and (B) distribution quantification. The analysis was calculated with effect size of 0.25 (medium) with 5% error probability and plotted by G*Power software.*

In summary, this chapter attempted to investigate the interaction of host and transplanted glial cells in fully-hydrated TaeNT. Firstly, a method to prepare primary glial cells from adult rat DRGs was tested to confirm an increasing percentage of glial cells in the culture with increased incubation time. Secondly, *in vitro* experiments showed that endogenous and exogenous glial cells did not disrupt the migration and orientation of each other in co-culture. Finally, transplanting a self-organising collagen guidance conduit containing aligned Schwann cells gave similar results in terms of cell alignment to the *in vitro* experiment. The distribution of host and donor Schwann cells after transplantation were subjected to further investigation and discussion.

The results from this chapter filled the gap in previous literature both *in vivo* and *in vitro* about the interaction between endogenous and exogenous glial cells during nerve regeneration. Understanding the interaction of host cells and transplanted cells is important for tissue engineering as it can help us know how to design therapeutic options for to improve peripheral nerve regeneration.

CHAPTER 5

Protocol design and development of mechanical tension application for stretch growth of neuronal cells in regenerative medicine

5.1 Introduction

Previous chapters have demonstrated the potential of TaeNT in supporting neurite elongation where the main player was Schwann cells providing trophic factors and directional cues to the neurites with supportive cell interactions. To develop an engineered neural tissue with long neurites for long distance nerve regeneration, additional cues might be necessary to further induce longer neurites in the construct. Previous research has investigated various approaches to induce long neurites, such as growth factor addition in culture media, drug treatment, magnetic fields, and electrical stimulation (Adams et al., 2014, Lestanova et al., 2016, Mahmood Alabed et al., 2019, Rayner et al., 2018). Mechanical tension application for growth response is another tissue engineering approach with a novel concept to induce long axons by gradually stretching processes of cells. Additionally, since TaeNT is a fully-hydrated tethered collagen gel containing elongated neurons, it might be a suitable 3D substrate with a feasibility in applying mechanical tension to extend neurite length.

5.1.1 Mechanical tension application for cell growth and development

Mechanical stimulation through external force application to cells plays a significant role in regulating cell behaviour. For example, skeletal and smooth muscle cells can mature and align in a controllable direction following stretching (Liu et al., 2008, Boonen et al., 2010, Weinberger et al., 2017). Stem cells and mature cells, such as vascular endothelial cells and smooth muscle cells, can be induced to differentiate or

reprogrammed with mechanical stimulation (Jiang et al., 2016, Kim et al., 2017, Liu et al., 2017). Increasing research on mechanical stimulation in cells has aimed to understand mechanobiology and mechanotransduction of various types of cells. The mechanobiology of cells is examined by observing how cells respond to mechanical force (i.e., changes in behaviour, organisation, interaction), where mechanotransduction is a process to explain how mechanical force is converted into biomolecular events. Extracellular matrix, integrins, and cytoskeleton are currently in the spotlight of mechanotransduction studies, including various signaling pathways and gene expression changes (Brown et al., 2014, Shao et al., 2014, Weng et al., 2016).

Stretching parameters, such as force magnitude, the direction of strain, frequency, and time interval, influence cell behaviours differently depending on each specific type of cell. Different stretching systems can be selected depending on particular experimental requirements, and the design considerations and available system components are varied. However, the main component, commonly considered essential for most *in vitro* stretching systems, is an actuator that supplies an external force to the cell culture.

Various actuation approaches have been engineered to study mechanobiology and mechanotransduction with different advantages and disadvantages (Table 5.1). The most common actuation design was a pneumatic actuator which uses external pressure to generate homogenous strain to cells seeded on a flexible membrane (Shimizu et al., 2011, Heo et al., 2013, Huang and Nguyen, 2013, Kreutzer et al., 2014). The indirect contact between cell culture and pressure supply contributes to a low risk of contamination in the simple setup. The actuation also allows biaxial stretching using a multi-layered membrane to apply tension to cells horizontally and vertically (Tremblay et al., 2014). Flexcell stage flexer was an example of a commercialised actuator used widely by tissue engineers to apply mechanical tension to various types of cells (Liu et al., 2008, Brown et al., 2014, Andrews et al., 2016, Loperena and Harrison, 2017, Kim et al., 2017)

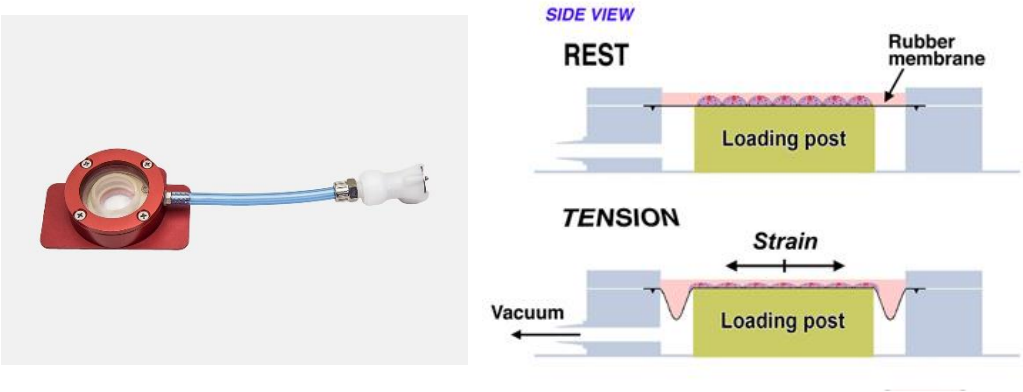

Figure 5.1 An example of commercialised actuator for cell growth. *Stage flexer utilises a pneumatic actuation system to induce strain to cells seeded on loading membrane (Frazier et al., 2017).*

Type of Actuator	Principle	Advantages	Disadvantages
Pneumatic actuator	Gas or air pressure used to control deformation of a thin membrane where cells were cultured on top	• Simple setup • Homogenous strain application • No direct contact with the cell and medium resulting in low risk of contamination	• Concerns related to cell-membrane adhesion
Piezoelectric actuator	Piezoelectric manipulator controlled by a computer to stretch cells in micro- or nano- chamber	• High displacement resolution (suitable for on-chip cell stretching) • Broad range of controllable strain • No heat induction	• Limitation in strain consistency when using porous and gas-permeable substrate • Risk of contamination in culture medium
Electromagnetic actuator	Uses electromagnetic motors to pull movable plate or holder away from fixed clamping	• Simple setup (suitable for custom-made cell stretching devices) • High precision and controllability	• Risk of contamination through lubrication process and possible device erosion
Optical actuator	Uses optical tweezers to produce high power diode laser with a wavelength width smaller than those of cells to induce force onto the cells along the axis of the laser	• No direct contact with the cell and medium resulting in low risk of contamination • Suitable for in-situ single-cell stretching • No need to concern about cell-substrate adhesion	• Low precise controllability of the flow in the microchannel • Possibility of non-uniform stretching and undesired optical stimuli induction to cells • Limitation in cell quantification

Type of Actuator	Principle	Advantages	Disadvantages
Electro-thermal actuator	Use a V-shape beam to stretch cells through thermal expansion along the apex	• Suitable for micromanipulation in micro-electromechanical systems (MEMS) • Application in using shape memory alloy to stretch cells cyclically	• Limitation concerns related to cell sensitivity in high temperature as heat and high voltage involved
Dielectrophoretic actuator	Use high-frequency electric field to induce electrostatic force causing cell deformation	• Suitable for in-situ single-cell stretching • Application in cell separation and positioning	• Loading limitation • Low magnitude of force induction
Electrostatic actuator	Use comb drive consisted of movable finger and fixed finger to stretch cell connected with linkages	• Suitable for micromanipulation in MEMS technologies • Application in biaxial stretching (vertical and horizontal stretching)	• Loading limitation • Concerns related to cell sensitivity in high temperature as heat and high voltage involved • Possibility of undesired electrical stimuli induction to cells

Table 5.1 Summary of different types of actuators for mechanical tension application in cells. *The principle, advantage, and disadvantage of each actuator type (Kamble et al., 2016, Zhang et al., 2020, Arold et al., 2007, Chan et al., 2008, Christopher et al., 2010, Cui et al., 2015, Huh et al., 2010, Roth et al., 2015).*

5.1.2 Models of mechanical tension application for inducing growth response in neuronal culture

Neuronal culture models for investigating mechanical tension application should be designed to maintain neuronal morphology and function (e.g., survival, network formation, and cell interaction, both before the application of mechanical tension and during force application in the long term). There are various confounding issues such as the consistency of small magnitude forces, magnitude control, attachment of cell culture substrate and towing, and the contamination of cultured cells with the exogenous tools. Table 5.2 summarises the main characteristics of previously reported *in vitro* models used to test the effect of applying mechanical forces to neurons, with maximum reported axon length as a result of stretching. Some studies did not report axon length because their main objectives for tension application were not for axon elongation, but some other aspects such as model optimisation, intracellular response, and strain accumulation (Table 5.2).

According to the previous mechanical tension application models in Table 5.2, two predominant approaches have been reported for cell-substrate attachment in the stretching of neurons in culture. The first approach is to attach neurites to a movable coated microelectrode tip to apply mechanical tension to neurons and measure strain generated as a response by the cells (Dennerll et al., 1989, Smith et al., 2001, Zheng et al., 1991). The early-introduced mechanical tension application model, the so-called Cell Puller, was developed by Bray using microelectrodes to attach an individual embryonic DRG growth cone at the tip (Bray, 1984). With the model, axon elongation was successfully induced at the stretch rate up to 100 μm/hr to reach the length of 960 μm in a day, and generated neurite initiation in a neuron with mechanical tension application. The use of a microneedle to attach and stretch the growth cone allows a force to be applied to only a single neuron at a time which limits the usefulness of this approach in studying populations of neurons within engineered tissues. The more widely used

approach is to attach neuronal cell bodies to a movable substrate and stretch them apart from their stationary neurite (Bray, 1984, Smith et al., 2001, Pfister et al., 2004, Huang et al., 2009, Loverde et al., 2011b, Xu et al., 2014). By attaching neurons with axons growing over the interface between two overlapping coated membranes and then moving them apart, multiple neurons can be stretched at once, enabling collective axon elongation (Figure 5.2). In both approaches, neurons were stretched directly as either cell bodies or neurites were longitudinally pulled away from the other part. Besides, the existing stretching model for neuronal growth response utilised either an electromagnetic or optical actuator to induce the mechanical tension. The electromagnetic uses a stepper motor to pull a movable plate or holder away from fixed clamping, and it has an advantage in simple setup and controllability.

In terms of cell types used in studies to explore the response of neural cells to mechanical tension, PNS cells are more frequently selected than CNS cells, and embryonic neurons in particular have been commonly used (Table 5.2). Embryonic axons could be stretched to reach the length of 4 cm within 2 weeks, while adult axons required more than 3 weeks with tension to reach the same length (Loverde et al., 2011a). Dorsal root ganglion (DRG) neurons are a commonly used source of cells for these kinds of studies due to the relative ease with which they can be cultured reliably. However, for translational purposes, motor neurons may be of more interest than DRG neurons which are sensory since restoration of muscle function is an important objective.

Reference	Stationary substrate	Towing characteristics	Type of neurons	Stretch rate range	Maximum resulted axon length
(Bray, 1984)	Coverslip coated with silicon monoxide under electron microscope	Microelectrode coated with rat-tail collagen and polylysine type II	Embryonic chick DRG (E10-12)	40-170 um/hr	960 um in 1 day
(Chada et al., 1997, Dennerll et al., 1989, Lamoureux et al., 1992, Zheng et al., 1991)	Corning tissue culture dishes covered with mineral oil	Calibrated needle coated with polylysine, collagen type IV and laminin	PC12, embryonic chick DRG, and embryonic chick forebrain neurons	25-150 udynes	150 um in 1 hour
(Smith et al., 2001)	Aclar membrane	Machined plastic block	Primary rat cortical neurons, and differentiated human neurons from the N-tera2 (NT2) cell line	42-84 um/hr	1 cm in 10 days
(Huang et al., 2009, Pfister et al., 2004)	Two overlapping Aclar membrane coated with PLL and rat-tail collagen type I		Embryonic rat DRG (E15)	42-330 um/hr*	10 cm in 28 days

Reference	Stationary substrate	Towing characteristics	Type of neurons	Stretch rate range	Maximum resulted axon length
(Haq et al., 2006)	PDMS mould	Mobile clamp coated with PLL	Rat pheochromocytoma cell line (PC12)	up to 16% strain rate (cyclic strain)	70 µm in 1 day
(Loverde et al., 2011a, Loverde and Pfister, 2015, Loverde et al., 2011b)	Aclar membrane or coverslip	Sanded Aclar membrane coated with PLL	Embryonic rat DRG (E16)	42 - 250 µm/hr**	4 cm in 2 weeks
(Xu et al., 2014)	Aclar membrane	Towing block coated with silicon	Embryonic rat DRG	600 µm/hr	n/a***
(Li et al., 2016)	Two overlapping substrates coated with rat-tail collagen and PDL		Embryonic rat DRG	330 µm/hr	5.94 mm in 7 days
(Abraham et al., 2019)	PDMS stretching chamber		Primary rat cortical neurons	up to 28% strain rate (cyclic strain)	150 um in 1 day****

Reference	Stationary substrate	Towing characteristics	Type of neurons	Stretch rate range	Maximum resulted axon length
(De Vincentiis et al., 2021)	Biosynthesised magnetosome adhered to cell membrane		Mouse hippocampal neurons	-	400 μm in 4 hours

**The towing membrane moved with displacement step of 2-4 μm at each different interval, and the total stretch rate was between 1-8 mm/day. The calculation is to convert 1-8 mm/day to μm/hr unit by multiplying by 42.*

***The calculation is to convert 1-6 mm/day to μm/hr unit by multiplying by 42.*

****Although there was no measurement for axon elongation, the paper is for model design and optimisation. Only the accuracy and repeatability of the model were quantified.*

*****Axon elongation was recorded in the unit of summed-up length of all branches per cell.*

Table 5.2 Systematic literature review on models for mechanical tension application protocols for neuronal cells with main characteristics and experimental results on axon length in the PubMed database from 1978 to 2021. *The electronic search was performed using the search term: ("axon") AND ("stretch growth") NOT ("neurodegenerative disease"). In September 2021, 153 results were obtained and further screened by reading research methods and results. The redundancy of protocols was eliminated by combining papers with the same model protocols and methodology. Injury Induction study, computational stimulation, review articles, and irrelevant papers that did not aim to study or measure neurite elongation were excluded.*

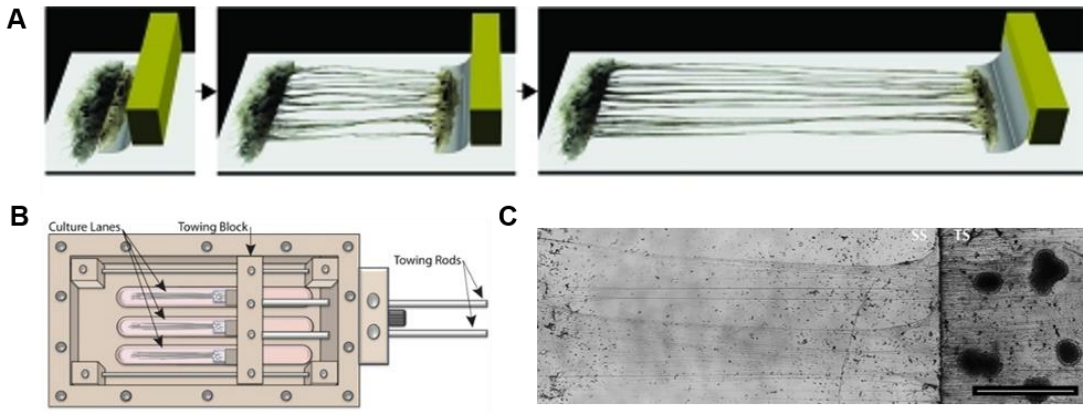

Figure 5.2 Examples of designs for mechanical tension application. *Constructs generally consist of longitudinally aligned axons. Neurons were plated on adjacent membranes that were gradually displaced to induce stretch-growth in the axonal tracts. (A) Model concept from Huang et al., 2009 with axonal tract spanning two populations of DRG neuron. One population was fixed while the other one was gradually pulled away. (B) Model concept of Bioreactor Chamber from Loverde et al., 2011 with multiple stretching tracks, and (C) Axonal tract of embryonic DRG explant seeded on towing substrate with one end fixed on the stationary substrate. Scale bar = 2 mm*

5.1.3 Magnitude of applied tension in neural cells

Elongation rate is critical to cell viability and morphology as neurons respond to different magnitudes of the force differently. Axons elongate when the applied tension is more than a particular threshold, and the elongation rate of neurites is proportional to the magnitude of external tension (Bray, 1984, Dennerll et al., 1989). Higher magnitude of applied tension can lead to increased steady state tension of the membrane (Purohit and Smith, 2016). However, rapid stretching can result in process degeneration or outright breakage, and, contrarily, too slow stretching can lead to adaptive motility that causes failure in process elongation (Mazzuoli-Weber and Schemann, 2015).

The length-dependent effect of neuron extension under applied tension reflects a Newtonian fluid characteristic where viscous stresses are linearly proportional to the rate of change of velocity vector. When there is a pulling force produced by the growth cone in nature or by external strain application *in vitro*, the axon exhibits a fluid-like manner by elongating more or longer axons to disperse the force (O'Toole et al., 2008). In Drosophila, axons exhibit the linear-force deformation relationship only when stretched, and then relax to a steady state when the magnitude of the force is maintained constantly. When the stretch magnitude is reduced, axons restore the tension to a resting value (Rajagopalan et al., 2010). There are 3 units of magnitude widely used to evaluate mechanical tension application: stretching velocity (μm/hr or mm/day), force magnitude (dyne), and strain (%). The unit selection depends on the tools used to apply the force, measurement method, and purpose of experiments.

In most research aiming to quantify axon elongation, velocity is simply used to indicate displacement of towing materials attached without disconnection to the axon per unit of time regardless of the original length of the axon. The optimal stretching rate for healthy astrocytes with long processes is 12.5 μm per hour (Katiyar et al., 2016). DRG

neurons can withstand an increasing stretching rate from 42 to 166 μm per hour without axonal disconnection (Pfister et al., 2004, Bray, 1984), The optimal velocity that can stretch the axon without disconnection and loss of function is consistent with *in vivo* data that the average maximum rate of white matter tract elongation in a mammal during development is approximately 100 μm per hour (Smith et al., 2001).

When mechanical tension is applied for an extended period, the initial hours of tension application are critical for growth cone morphology. Noticeably, stretching axons with a low initial rate and subsequently accelerating to a higher rate is more effective than stretching axons with a high constant rate throughout the application time (Pfister et al., 2004, Wang and Kuhl, 2019, Smith et al., 2001). Neurons initially react to the external tension by retracting their growth cones, so detachment or disconnection of axons may occur if the stretching rate is too much from the beginning. The gradual increase of stretch rate offers neurons an adaptive period to produce or rearrange their cytoskeleton to support axon elongation without disrupting cell viability. Figure 5.3 summarises maximum neurite lengths under mechanical tension at different time points from all available published results using mechanical tension application models to date. The grey area indicates the range of stretch rate that yields long axons with healthy morphology after being stretched. The rate of axon elongation under mechanical tension application (i.e., the slope of the grey line) was higher than the spontaneous axonal growth rate without any external stimulation (approximately 1-2 mm/day).

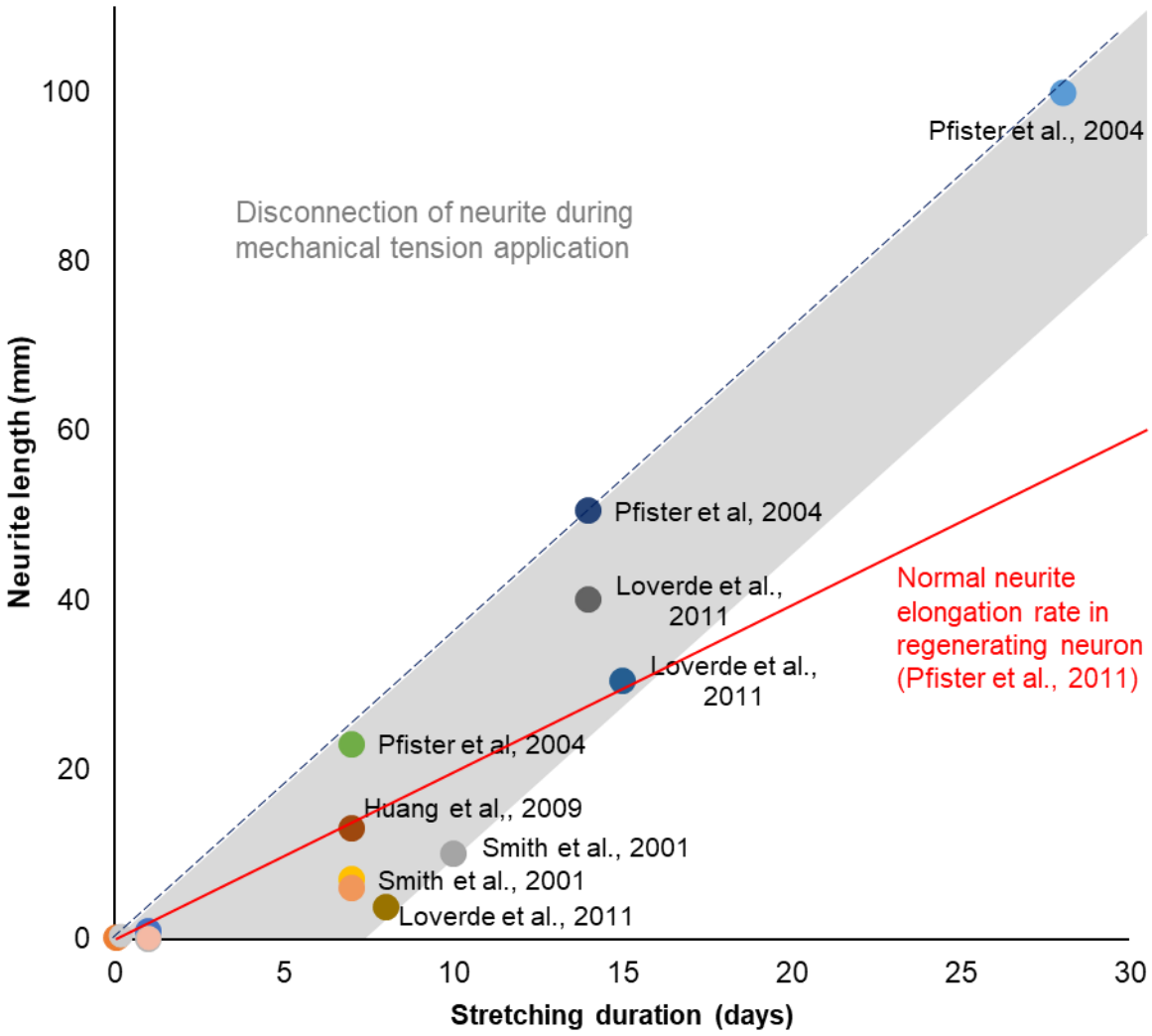

Figure 5.3 Neurite length (mm) corresponding to stretch duration (days) reported in previous literature. *The literature search was performed in September 2021 with similar methods to Table 5.2. Literatures reporting neurite length longer than 1 mm after stretching were selectively labelled. The red line represents the rate of neurite growth in regenerating neurons without external stimulation. The blue dotted line is a boundary where neurites begin to be torn away or disconnect from towing substrate.*

One dyne is defined as a magnitude of applied force that increases the velocity of a one-gram mass by one centimetre per second. Peripheral neurons begin elongating longer neurites when the tension exceeds 100-200 μdynes (Lamoureux et al., 1992, Zheng et al., 1991), while neurons in the brain have a lower threshold of approximately 20-40 μdynes. The unit is more convenient than the others when investigating cell sensitivity and response at different magnitudes of force. Dyne units cannot be directly converted to velocity rate (μm/hr) by simply calculating with the mass because accurate mass measurement of living neurons is difficult. Instead, researchers use sensitivity as a constant value of each specific cell to demonstrate the relationship between stretch velocity and magnitude of force. Sensitivity equals stretch velocity divided by magnitude of force in dynes, and each type of cell has different sensitivity. Most cells in the nervous system have sensitivity ranged between 0.5 and 5 μm per hour per μdyne of applied force with a mean value of approximately 1 μm per hour per μdyne of applied force (Chada et al., 1997, Lamoureux et al., 1992, Zheng et al., 1991). The sensitivity range of cells in the nervous system reflects their high flexibility, compared to cells in other biological systems, in responding and adjusting their morphology corresponding to an external force.

The percentage of strain is a measurement of a change in axon length divided by the original length in a period of time. It can be calculated from the velocity rate (μm/hr) only if the original length of axons before mechanical tension is applied. Neurons can maintain normal morphology and cellular activities without disconnection when the strain is lower than 18% (Loverde and Pfister, 2015). However, this method is more widely used in studies of nerve injury models than in stretch growth experiments.

5.1.4 TaeNT as a substrate for applying force to 3-dimensional neural cell culture

Although applying mechanical tension to neuronal cells for growth response was introduced by Paul Weiss and then continuously researched since 1934, only a few methods and protocols are recently available in the scientific literature, and none has been commercialised. The relatively slow progress is possibly correlated to a limitation in the translational application as clinical uses of mechanical tension application in tissue engineering have not been reported.

Most mechanical protocols for stretching neurons have utilised an overlapping membranes technique to attach and pull neurons through a towing bar (Huang et al., 2009, Loverde et al., 2011a, Pfister et al., 2004, Smith et al., 2001, Xu et al., 2014). According to the literature review in Table 5.2, all of the existing mechanical tension application models used a cell stretching system through the 2-dimensional (2D) substrate where a monolayer of neurons adhered to the surface of the elastic substrate and mechanical tension was applied to the cells by inducing expanding or bending deformation of the substrate. Applying a mechanical tensile force to neural cells through a 3-dimensional (3D) cell culture system became an increasingly interesting approach in the tissue engineering field because a 3D engineered microenvironment can closely mimic *in vivo* conditions for cell culture so that cells can express a native response to stimuli (Huang et al., 2017). The approach also enabled multiple dimensional stretching or creating a substrate with a gradient of stiffness for cell stretching (Caliari et al., 2016, Riehl et al., 2012). In this chapter, indirect stretching in a 3D co-culture system was proposed as a new method to improve the effectiveness of using mechanical tension to induce long neurites. The TaeNT using rat tail collagen type I became a substrate for 3D cell culture. The stretch force was transmitted to the embedded cells through deforming the hydrogel matrix.

Additionally, although previous research using mechanical tension has successfully stretched neural cells with long processes on acellular interfaces (Table 5.2), the alignment of neurites before applying mechanical tension occurs randomly on these substrates. Highly aligned Schwann cells in TaeNT enable neurons to elongate aligned neurites (as shown in Chapter 3), which might benefit a long-gap regenerative purpose when combined with mechanical tension application to extend their length. Since Schwann cells in collagen gels have been shown to help guide neurite outgrowth and produce neurotrophic factors for the long-term survival of neurons (Georgiou et al., 2015, Thompson and Buettner, 2004, Viader et al., 2011), a cellular hydrogel-based stretching system with aligned Schwann cells and supportive extracellular matrix was hypothesised to potentially improve viability and alignment of cells in the system during mechanical tension application.

5.1.5 Objectives of this chapter

This chapter mainly aimed to develop a protocol for mechanical tension application to induce stretch growth response for neural regeneration. TaeNT with aligned Schwann cells and neurons was proposed as a 3D cellular hydrogel-based substrate for the stretching system. Two hypotheses were formed accordingly: (1) TaeNT has a feasibility to provide an alternative platform to apply mechanical tension to neural cells for growth response, and (2) mechanical tension application using the developed model enhances neurite elongation. The protocols developed in this chapter were aimed to be easy to set up and cost-effective by minimising manufactured components. All aspects of the protocols should be available in a typical cell culture laboratory to enable adoption and reproducing by other groups, and should be suitable for future scale-up in a commercial or healthcare environment.

Three culture protocols to apply stretch force to the cells were developed in this chapter, starting from adapting an existing mould for manual stretch to developing a 3D printed mould connected to a linear actuator where the optimisation of mould fabrication parameters was also described. Each protocol contains multiple trials and troubleshooting, so a series of protocol development notes for each protocol are summarised. The result section of this chapter consists of the design concept description, protocol diagram, figures of an experimental setup, and a table describing protocol development.

To examine its efficacy in applying mechanical stretch, each protocol was initially tested with an acellular hydrogel with culture medium to assess gel setting and liquid leakage. After troubleshooting, the improved protocols were subsequently tested with TaeNT containing only Schwann cells to determine whether the protocol was suitable for use with cells. Only the protocol that could maintain Schwann cell alignment after stretching was finally tested with TaeNT containing both Schwann cells and neurons.

The last section of the chapter includes preliminary results of using the developed protocol to apply stretch force to TaeNT with Schwann cells and neurons. The cell morphology and alignment corresponding to applied stretch force was visualised and discussed.

Note that the source of neurons used in this chapter was not motor neurons that were primarily used in TaeNT as in Chapter 3. Most previous studies on mechanical tension application in neuronal cells have used DRG neurons (Bray, 1984, Dennerll et al., 1989, Huang et al., 2009, Loverde et al., 2011b, Pfister et al., 2004, Smith et al., 2001, Xu et al., 2014). By using DRG neurons in the protocol development here, the results from refined protocols could be compared easily to those from previously reported approaches. Motor neurons will be used in future work after finalising the protocol for mechanical tension application to TaeNT constructs.

5.2 Results

5.2.1 Protocol 1- Existing TaeNT mould and Daedal Positioning Systems (DPS) with manual stretching

Preliminary protocols were designed by adapting available materials in the laboratory, and using a simple manual method to apply mechanical tension. The Delrin mould was the 4-ml TaeNT mould with an external dimension of 6.5 x 4.5 x 2 cm (Figure 5.4). After 24-hour incubation of collagen gel containing Schwann cells when gel contraction was observed, tethering mesh at both ends were gently lifted from the mould cavity and placed on the upper edge close to the mould cavity to generate the stretch force with the longitudinal displacement of 0.5 cm to the cellular gel. Parafilm was patched on the tethering mesh and the upper edge of the mould after lifting in order to hold the mesh at the new position.

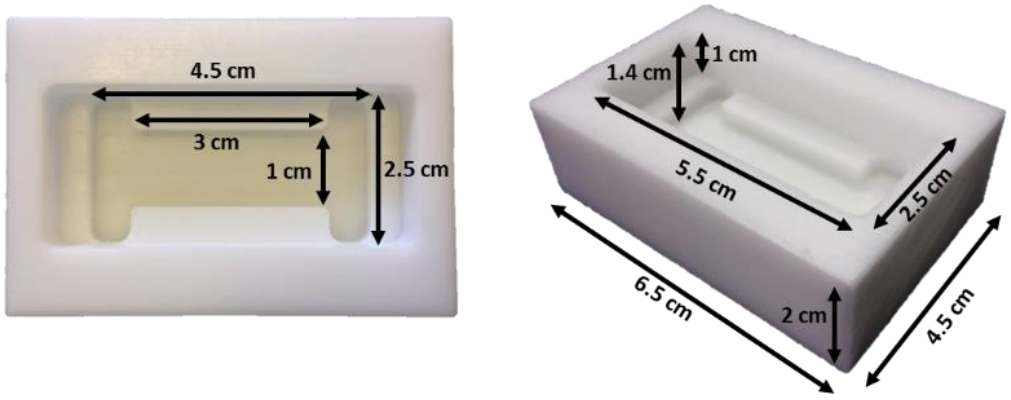

Figure 5.4 Dimensions of the Delrin mould used to make the 4-ml TaeNT.

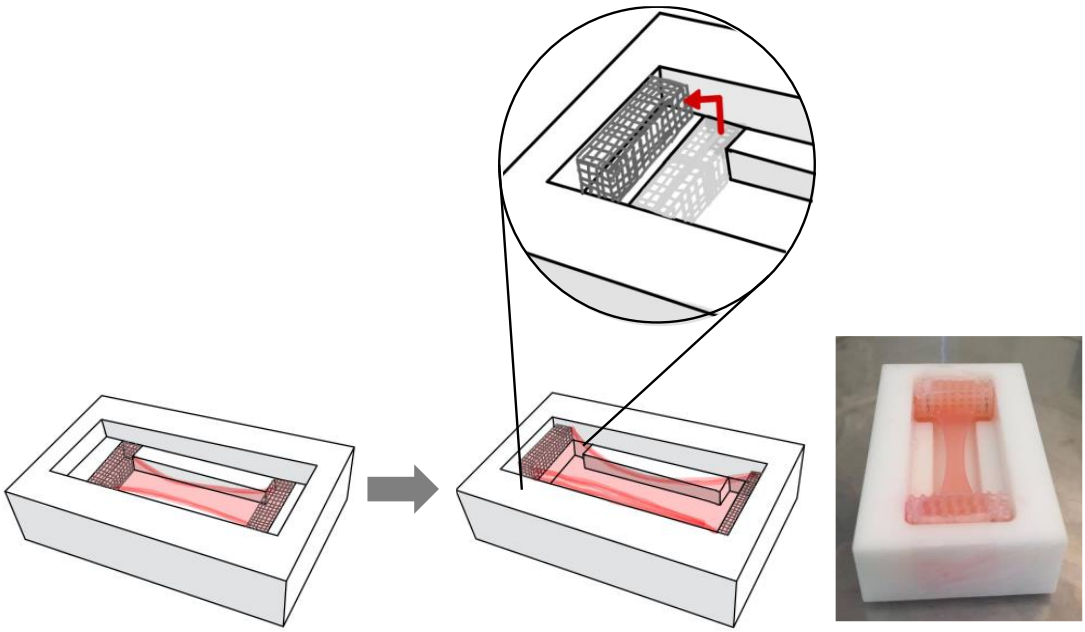

Figure 5.5 Design diagram of preliminary protocol on mechanical tension applying to TaeNT containing Schwann cells. *Stretch force was applied to the TaeNT by lifting both tethering mesh inserts to the upper edge, increasing the longitudinal length of the gel by 0.5 cm at each side. The rightmost figure showed the final process of the actual experiment after the gel was lifted without detachment of the gel from the tethering mesh.*

However, the protocol could not provide a reliable method because the tethering mesh could not be kept in place easily at the upper edge of the mould, even using a parafilm patch. An additional compartment was required to hold the tethering mesh upright at the desired position. After a series of refinements and optimisation, the protocol was modified to use 2 different Delrin moulds: a setting mould and a stretching mould. Similar to the original version, the ‘setting mould’ had an H-shaped cavity that allows collagen gels with Schwann cells to set and form anisotropic tissue-like structure when assembled with tethering mesh at each end of the cavity. The ‘stretching mould’ has a large rectangular cavity whose width is equal to that of the setting mould, and cavity length is longer than the length of the gel in a setting mould.

After the series of problem-solving and protocol development shown in Table 5.3, the final design of the first protocol was refined for 3 ml collagen gels consisting of 80% v/v type I rat tail collagen, 10% v/v 10X minimum essential medium, and 10% v/v cell suspension. F7 Schwann cells with the density of 2 million cells per 1 ml of gel were cultured on parafilm placed in the Delrin mould. Nylon tethering mesh inserts were assembled with medical-grade 0.25 mm stainless steel wire, and placed at each end of a mould. Another 0.9 mm stainless steel wire was attached to the tethering mesh and projected out of the mould, parallel to the longitudinal direction (Figure 5.6). To apply mechanical tension, the gel with the attached tethering mesh and wire was gently transferred from a setting mould to a stretching mould placed on a linear slide of the Daedal Positioning System (DPS). The thicker stainless steel wire was adhered to a side pillar on the DPS to fix one end of the gel in the same position. By adjusting the displacement roller of the DPS, the gel was stretched by moving the mould away from the pillar where one end of the gel was fixed. Each roller adjustment could stretch the gel by a distance range of 1 mm. The stretched gel was incubated for 24 hours, and the cell morphology in the gel was examined by immunofluorescence staining.

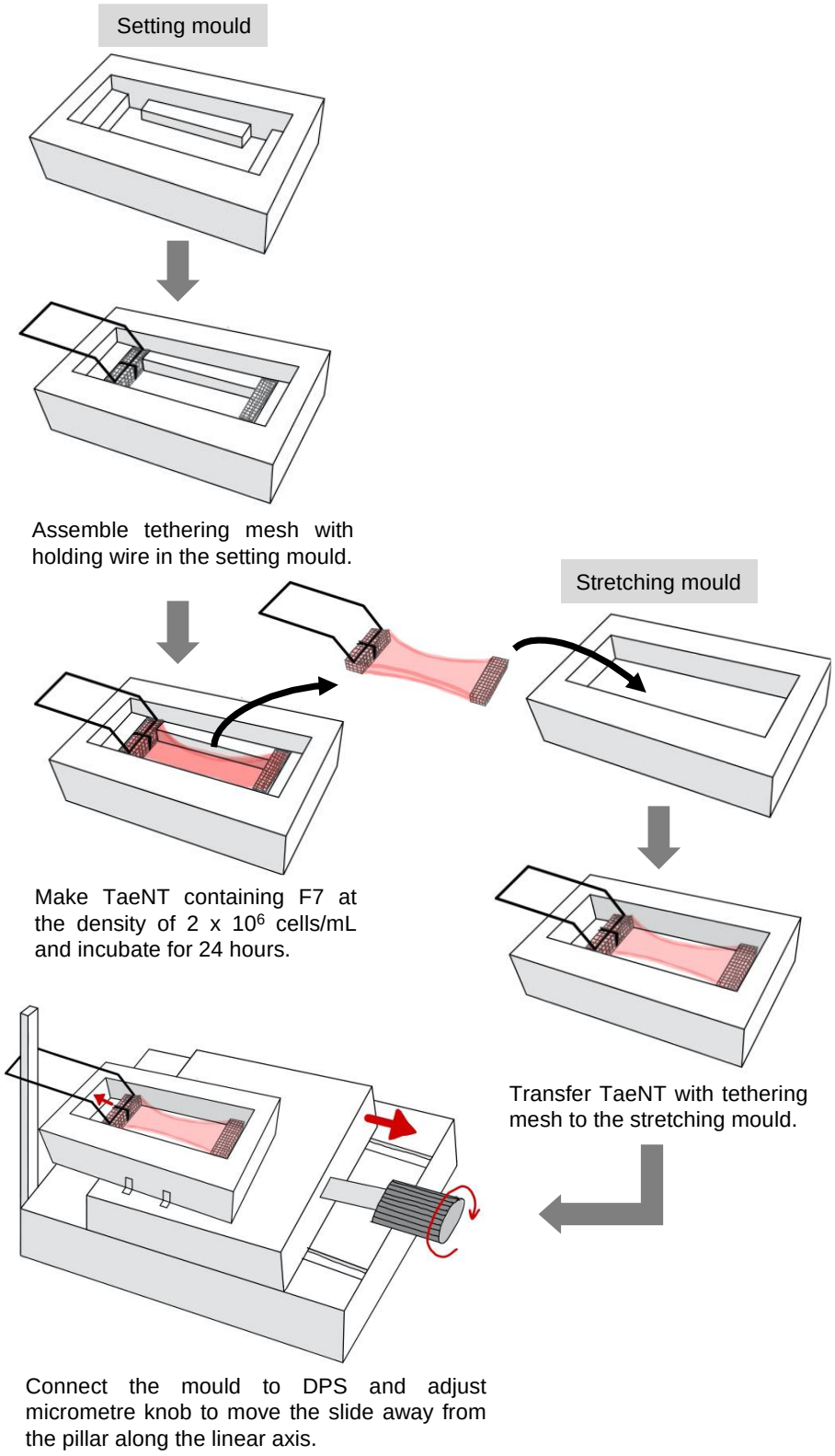

Figure 5.6 Design diagram of Protocol 1 on mechanical tension applying to TaeNT containing Schwann cells. *TaeNT was transferred from the setting mould to the stretching mould connecting to Daedal Positioning System (DPS), where stretch force was applied by moving the mould away while attaching one end of the tethering mesh with a fixed pillar.*

Issue Considered	Protocol Development
1. Volume of collagen gel in the setting mould The maximum volume that the gel cavity can contain is up to 4 ml, but a 4ml gel is too heavy to be lifted clear of the mould without breaking under its own weight. A lower volume of gel was thus considered.	Various volumes of collagen gel were filled into the gel cavity and gently lifted after it set. The detachment of gel from tethering mesh while lifting was reduced when the gel volume was less than 4 ml. On the other hand, collagen gels with volume less than 2 ml were too thin and had poor attachment to the tethering mesh. Thus, a volume of 3 ml was selected as optimal.
2. Cell density in collagen gel The original protocol of TaeNT used F7 Schwann cells at the density of 4 x 10^6 cells/ml to enable rapid contraction and alignment. There was a disadvantage for long-term culture as sustained contraction causes gel breakage. A lower density of F7 Schwann cells was therefore investigated.	F7 Schwann cells density of 1, 2, and 3 x 10^6 cells/ml of collagen gel was investigated. The density of 2 x 10^6 cells/ml was the minimum density where gel contraction can be clearly observed after 24 hours. Additionally, the contraction free-floating gels was more than 60% when the density is higher than 2 x 10^6 cells/ml. Free-floating gel contraction of 60% was previously determined to be the minimum amount to produce reliable alignment throughout the middle and side zones of tethered gels (O'Rourke et al., 2015). Therefore, a density of 2 x 10^6 cells/ml was selected as optimal.

Issue Considered	Protocol Development
3. Method for moving collagen gel from setting mould to stretching mould without gel detachment from tethering mesh	To transfer a gel from a setting mould, culture media was removed, and the tethering mesh at both ends were lifted directly. In order to keep the gel attached to the tethering mesh, the gel needs a liftable base to support its weight. Parafilm was placed under the gel to prevent detachment when lifting.
4. Method to control stretching displacement The displacement of stretching was considered as one of the protocol's important variables, so it should be measurable and adjustable.	The gel in a stretching mould was connected via its tethering mesh to the DPS, which provides precise linear positioning control by adjusting a micrometre knob to move the slide away from the pillar along the linear axis. By adjusting the displacement roller of the DPS with the resolution of 1 mm, the gel can be stretched with controlled strain.
5. Integration between gels and tethering mesh	Five layers of nylon mesh fit well with the width of mould cavity and are tied together using thin stainless steel wire. In order to facilitate integration between the gel and tethering mesh, the tying wire should be slightly loosened leaving enough spaces for the gel to penetrate into the bars.

Table 5.3 Considered issues for the design and improvement of Protocol 1. *The series of protocol testing and troubleshooting was used to refine the final version of the protocol in Figure 5.6.*

Despite several protocol refinements, the first protocol still failed to consistently support gel attachment to the tethering mesh when applying mechanical stretching to the collagen gels. The critical limitation of the protocol occurred during the gel transfer from one mould to another. During the transfer, the total length of the gel could change, and the tethering could be disrupted. Besides, gel detachment was usually observed during stretching.

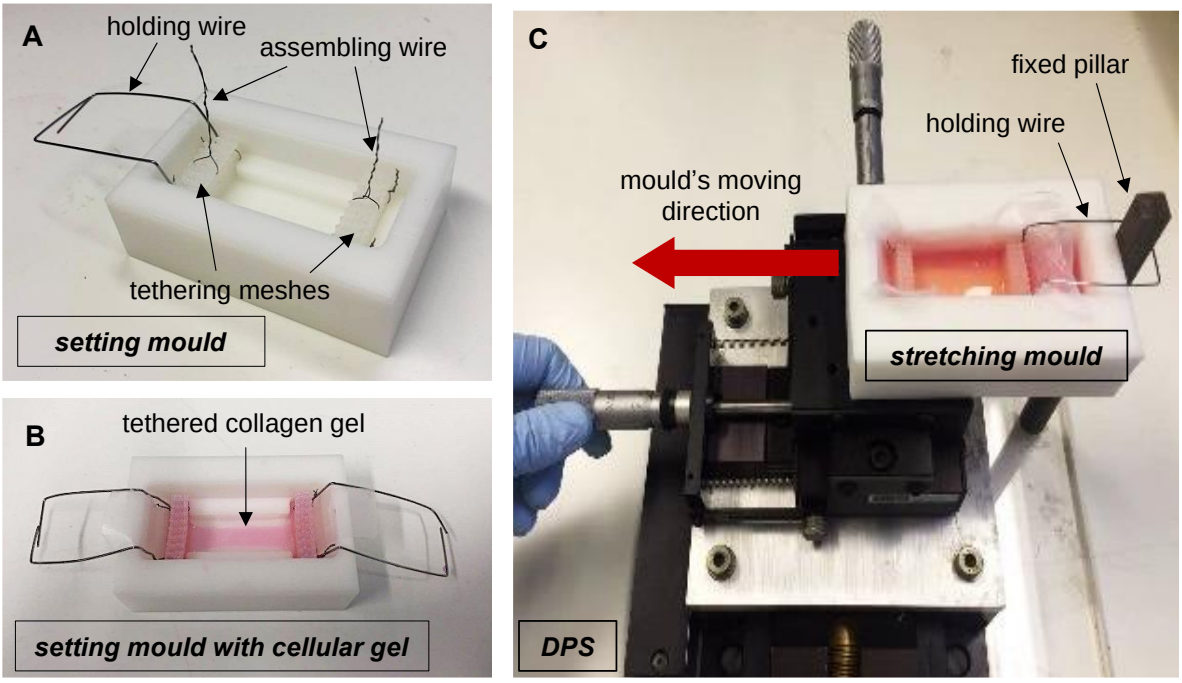

Figure 5.7 Experiment using Protocol 1. *(A) The setting mould with assembled tethering mesh and holding wire. (B) TaeNT in the setting mould with medium culture. (C) Medium removal of TaeNT after 24 hours. (D) TaeNT with culture medium in the stretching mould connecting to DPS.*

5.2.2 Optimisation of parameters for 3D printed mould

In order to overcome the limitation of transferring gel from one mould to another, a new mould was designed with AutoCAD software, and 3D printing technology was used to fabricate an individual mould as a preliminary customised prototype for mechanical tension application. The new moulds were designed to be partially similar to the 1 ml-TaeNT mould (described in Section 2.2.5) with an additional compartment to enable applying stretch force to the gel, and then 3D-printed by Ultimaker 2 printer with PolyMax™ PLA filament. Each mould design was described along with its stretching protocol in the following sections (Section 5.2.3 and 5.2.4)

The optimisation of 3D printing parameters was aimed to balance the quality of the mould with the cost and time used to print. The mould should also be lightweight but dense enough to prevent any fluid leakage. The parameter values from the compatible range specified in the printer manual were sequentially considered, and the optimal value was selected through the optimised determination of each printing parameter (Table 5.4).

Parameter	Compatible Range	Optimised Determination	Optimised value
Quality			
Layer height	0.06 - 0.25 mm	Select the smallest value for the highest resolution.	0.06 mm
Shell thickness	multiple of 0.4 mm	Print 3 moulds with the shell thickness of 0.4, 0.8, and 1.2 mm, and test by filling water into each printed moulds; the minimum value that could print a non-leakage mould was selected.	0.8 mm
Enable retraction	Yes/ No	Enable the retraction to eliminate excessive stringing on the printed mould when moving over non-printed area.	Yes
Fill			
Bottom/top thickness	multiple of layer height	Select the round number close to the shell thickness (0.8 mm) from the multiples of the selected layer height (0.06 mm) to create a compatible strong structure.	0.6 mm
Fill density	0 – 100% (hollow to solid)	Since the shell thickness was already selected to be enough to print a mould without liquid leakage, the fill density could be minimised to reduce the weight. 20% was selected for pieces of normal use with medium strength and low/medium loads.	20%

Parameter	Compatible Range	Optimised Determination	Optimised value
Speed and temperature			
Print speed	< 150 mm/s	Select the slowest range of speed for good printing quality where the total printing time do not exceed 8 hours in total.	80-100 mm/s
Support			
Support type	None/ Touching buildplate/ Everywhere	The mould design had no overhanging structure that required structural support during the printing.	None
Platform adhesion type	None/ Brim/ Raft	The mould design has large touching area to the buildplate that required no additional adhesion.	None
Machine			
Nozzle size	-	Depend on machine specification (automatically set)	0.4 mm

Table 5.4 Optimisation of 3D printing parameter to fabricate TaeNT mould and its components for mechanical tension application.

5.2.3 Protocol 2 - 3D printed mould with manual stretching using notches

In order to overcome the limitations on gel detachment noted in Protocol 1, the following design consisted of only one mould performing as both a setting mould and a stretching mould. The customised mould was aimed to be use for discrete stretching in Protocol 2, where the mechanical tension was periodically applied to the gel at a fixed displacement. The final design was a customised 3D-printed PLA mould with a longer-length cavity and 5 notches to support the tethering mesh positioning at one end (Figure 5.8). Each notch was 1 mm long and they were spaced 1 mm apart from each other.

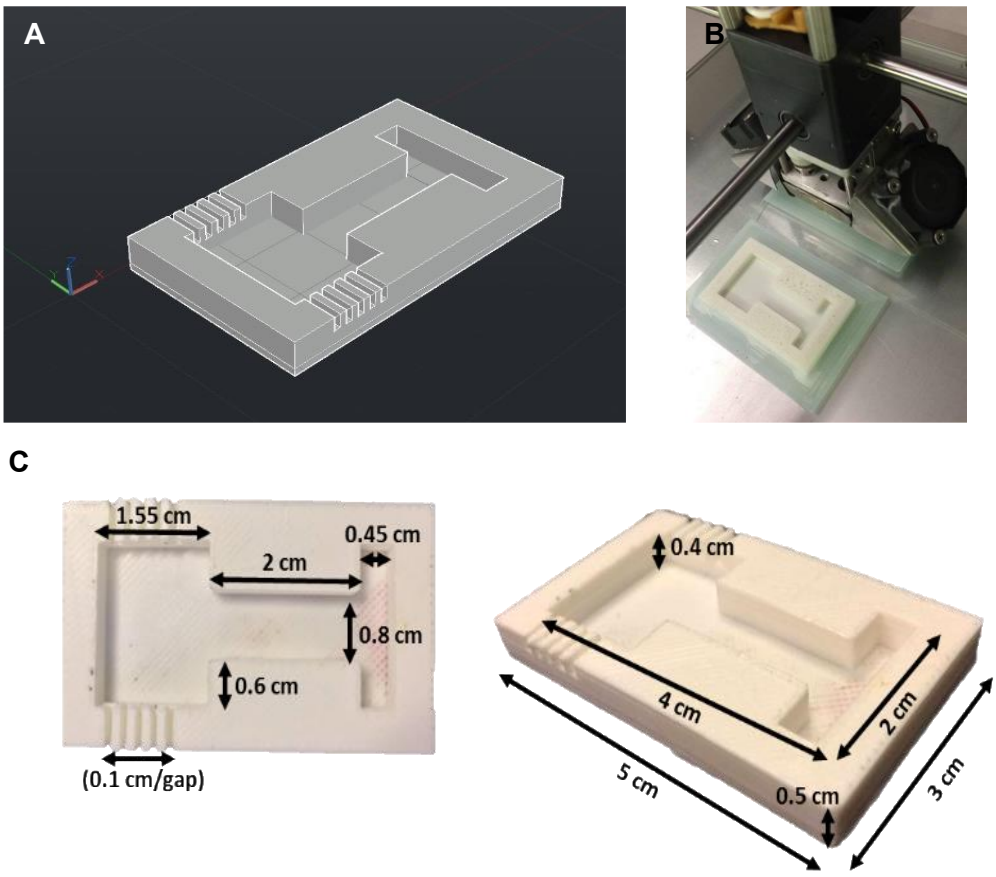

Figure 5.8 Fabrication of TaeNT mould for Protocol 2. *The protocol was described in Section 5.2.3. (A) The mould was designed by AutoCAD software, and then (B) printed by Ultimaker 2 printing. (C) Dimension of TaeNT mould for Protocol 2.*

To assemble the mould, a medical-grade stainless steel tape was cut into a flat T-shape wing whose sides fitted into the mould's notches to fix the tethering mesh in position. 1.5 ml collagen gels were set in the mould and integrated with three tethering mesh layers. A polysiloxane block was placed behind the T-shaped stainless steel wing to prevent gel leakage and removed after the gel set (Figure 5.10).

After the series of problem-solving and protocol development shown in Table 5.5, the final design of the first protocol was refined for 1 ml collagen gels consisting of 80% v/v type I rat tail collagen, 10% v/v 10X minimum essential medium, and 10% v/v cell suspension containing F7 Schwann cells. After incubating the cellular gel at 37°C, 5% CO_2 for 24 hours, DRG cultures were seeded on top of the gels and FBS-supplemented DMEM was added after leaving cells to attach for 1 hour. Stretch tension was applied to the gel by moving the T-shape stainless steel wing at one end of the gel to another further notch. The stretched gel was incubated for 3 days and subsequently fixed in 4% paraformaldehyde for immunofluorescence staining. The morphology of cells inside the gel was investigated by immunostaining images shown in Section 5.2.6

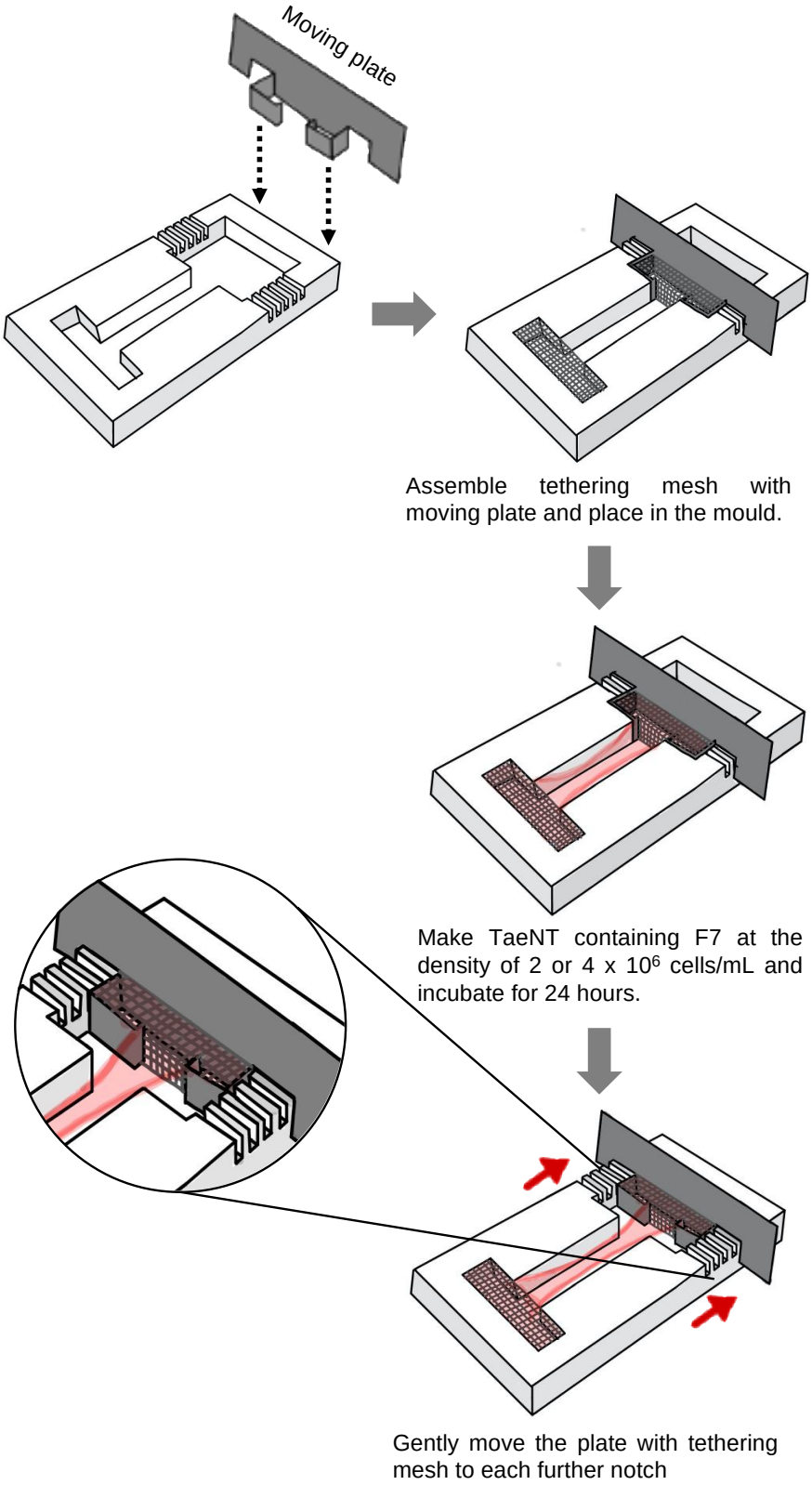

Figure 5.9 Design diagram of Protocol 2 on mechanical tension applying to TaeNT containing Schwann cells. *Tethering mesh was attached to the moving plate, which was subsequently moved to each further notch to apply stretch force to the gel.*

Issue Considered	Protocol Development
1. Volume of collagen gel and density of cells in the setting mould	The volume of collagen gel and density of F7 Schwann cells was similar to the TaeNT protocol described in Chapter 2: 1 ml of collagen gel with 4 x 10^6 F7 Schwann cells. However, a density of 2 x 10^6 cells/ml was also investigated because cells in TaeNT were expected to be cultured for a long time, where too much contraction in dense cellular gels would break the gel/tethering or affect cell morphology. The morphology of cells at different initial cell density after 3 and 7 days of incubation was investigated in Section 5.2.5.
2. Attachment of gels to the tethering mesh while moving the plate to a further notch Besides slow and gentle handling of tethering mesh by a curved tip tweezer, the integration of the collagen gel to the tethering mesh was a crucial feature to prevent the gel from detaching from the tethering mesh.	The integration of the gel and tethering mesh could be improved by pre-integrating the mesh before the gel was set. 100 µl gel was added at 4 °C to soak the tethering mesh at each end of the mould, and then the remaining gel was added to the remaining mould cavity before setting at 37°C. This resulted in better integration of the whole gel and the tethering mesh.

Issue Considered	Protocol Development
3. Method to control stretching displacement The stretch force was applied to the gel by manually lifting and pulling back, so it was difficult to control as the displacement was in 2 dimensions.	In order to minimise the displacement error, the notches in one end of the mould were designed to have a constant length, and the whole mould was printed with an optimised resolution. Each notch was 1 mm away from each other, and its height and length were 4 and 1 mm, respectively, resulting in the total longitudinal length of 2 mm for each displacement of tethering mesh.

Table 5.5 Considered issues for the design and improvement of Protocol 2. *The series of protocol testing and troubleshooting was used to refine the final version of the protocol in Figure 5.9.*

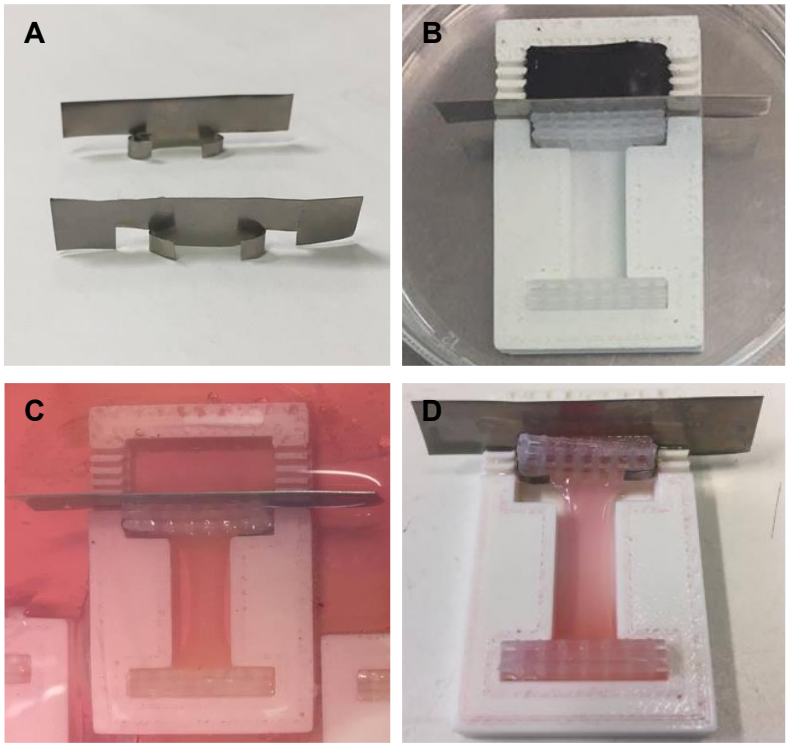

Figure 5.10 Experiment using Protocol 2*. (A) Stainless steel moving plate. (B) The mould assembling with a moving plate, tethering mesh, and a leakage block for TaeNT making. (C) TaeNT in the mould after 24 hours. (D) TaeNT after the stretch force was applied through the moving plate.*

5.2.4 Protocol 3 - 3D printed mould with gradual automatic stretching by a linear actuator

In order to develop a final protocol for mechanical tension application, limitations from all previous protocols were considered and overcome. Similar to Protocol 2, the protocol in Protocol 3 used only one mould in which the gel would be formed and continuously stretched with a range of 20 mm. Tethering mesh was gradually pulled along a longer cavity length of one end connected to a linear actuator. The first version of the mould for Protocol 3 was a mould in a 4-cm box with a lid to cover the culture system (Figure 5.11). Although the enclosed mould could prevent contamination, it was difficult to monitor the gel and cells inside during mechanical tension application, so the design was refined to be a mould without coverage and the mould cavity had no bottom making it easier to observe gel contraction (Figure 5.12). The height of the mould's wall was sufficient for adding culture medium to the gel. Additional components for the mould were tethering bars used to connect tethering mesh to the linear actuator: one set of bars was placed to hold tethering mesh in the mould cavity, and the larger bar was used to connect the smaller bars to the linear actuator.

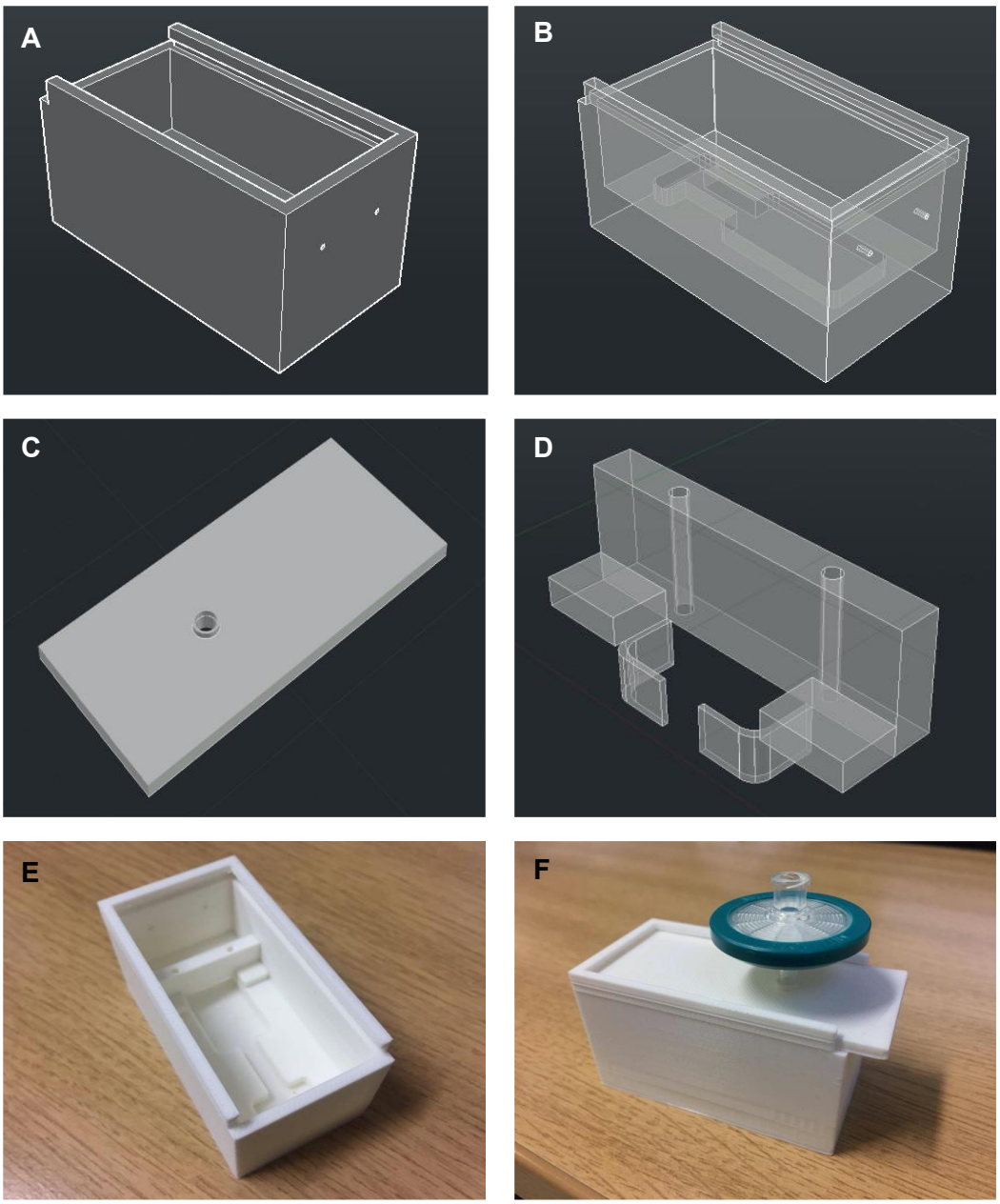

Figure 5.11 Fabrication of TaeNT mould for Protocol 3 (1st version). *(A), (B), (C), (D) The mould and its components were designed by AutoCAD software. (E) The printed mould chamber, and (F) a lid with a filter for gas exchange.*

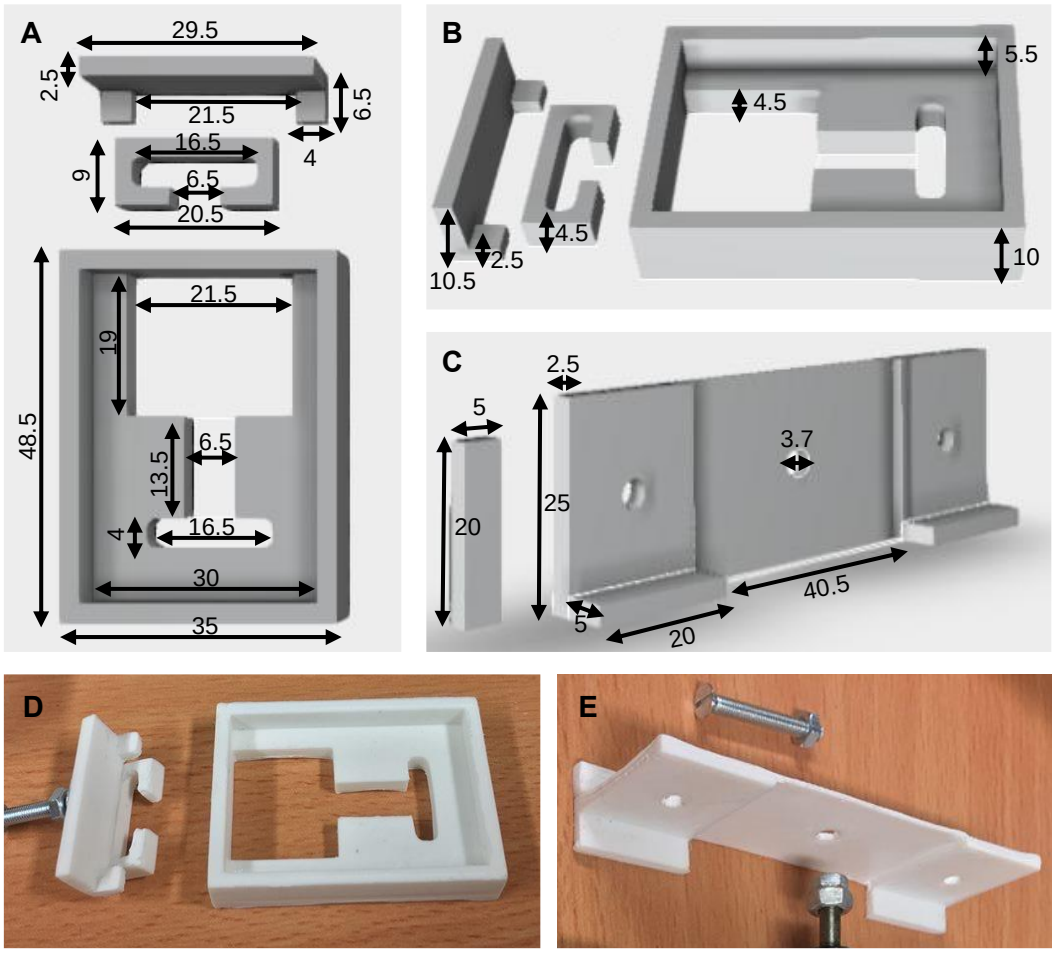

Figure 5.12 Fabrication of TaeNT mould for Protocol 3 (final version). *The protocol was described in Section 5.2.4. Measurement unit = mm. (A), (B), (C)The mould and its components with the dimension was designed by AutoCAD software. (D) The printed mould with an inner tethering bar, and (E) an external tethering bar for connecting the culture mould to a linear actuator.*

Gradual stretching with a smaller displacement stop is presumably another key to solve the detachment issue of the mechanical tension protocol in the project. The final protocol involved using an electrical linear actuator to apply automatic stretching to the gel in the mould, which provided more consistency and accuracy in terms of rate and displacement. The linear actuator specification is shown in Table 5.6.

The series of problem-solving and protocol development for the final refined design were shown in Table 5.7, and the complete system was set up and tested with acellular collagen gel (Figure 5.14C). After sterilisation, the mould and all components were assembled using screws (Figure 5.14B). Parafilm was placed at the bottom of the mould. The gels were added in the mould and integrated with three layers of tethering mesh. After incubating for 24 hours, tethering mesh at one end was gradually pulled along an extended cavity using the linear actuator.

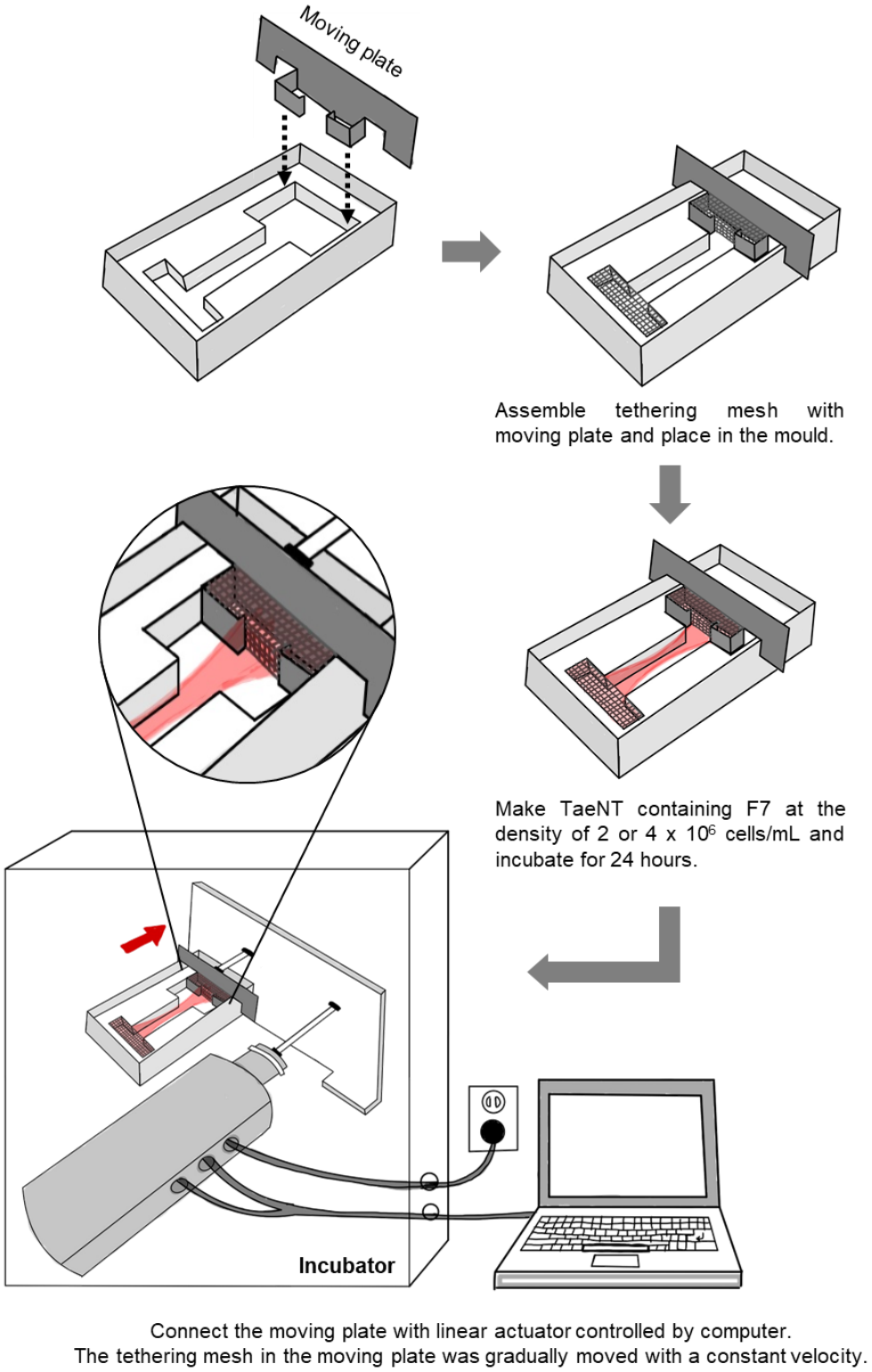

Figure 5.13 Design diagram of Protocol 3 on mechanical tension applying to TaeNT containing Schwann cells. *The moving plate containing tethering mesh was connected to a linear actuator controlled by a computer outside an incubator. Stretch force was gradually applied with a small magnitude by moving the tethering mesh away from the other side.*

Specification	Value
Built-in controller	Yes
Travel range	13 mm
Accuracy	24 µm
Speed	0.0009302 – 4 mm/s
Interface	RS-232
Power Supply	12-16 VDC
Motor type	Stepper (2 phase)
Manual Control	Yes
Temperature	0 – 50 C

Table 5.6 Specification of the miniature linear actuator (T-LA13A-KT03U) to control the mechanical tension application in TaeNT containing neural cells.

Considered Issues	Protocol Development
1. Volume of collagen gel and density of cells in the setting mould	Similar to that of Protocol 2 in Table 5.5
2. Method to control stretching displacement	In order to overcome a limitation in precise displacement due to manual stretching, a linear actuator was used to allow automatic stretch with a small and continuous displacement. The specification of the linear actuator was mentioned in Table 5.6, where the linear actuator was selected by considering travel range, accuracy, and moving speed. The mould and tethering mesh were connected to the linear actuator through a moving bar and fixed with screws that could be removed to separate all compartments for cleaning. The mould was connected to the linear actuator in a large glass container inside an incubator. Three cable plugs were connected to the linear actuator: input cable, output cable, and power supply. The input and output plug could be combined and connected to a computer outside the incubator.

Considered Issues	Protocol Development
3. Determining and setting a stretching velocity to command the linear actuator.	The stretching velocity was calculated from the stretching rate reported in previous literature: DRG neurons can bear an increasing stretching rate from 41.7 to 166.7 μm per hour (Pfister et al., 2004). Thus, the command for the linear actuator would be as following. • Step = 0.5-3 μm per step every minute • Total rate = 1-4 mm per day (40-160 μm per hour)
4. Duration of stretching	Schwann cells and neurons were co-cultured with the applied stretch force for 3 and 7 days to compare the result of direct stretching at a similar time course from other related literature.

Table 5.7 Considered issues for the design and improvement of Protocol 3. *The series of protocol testing and troubleshooting was used to refine the final version of the protocol in Figure 5.13.*

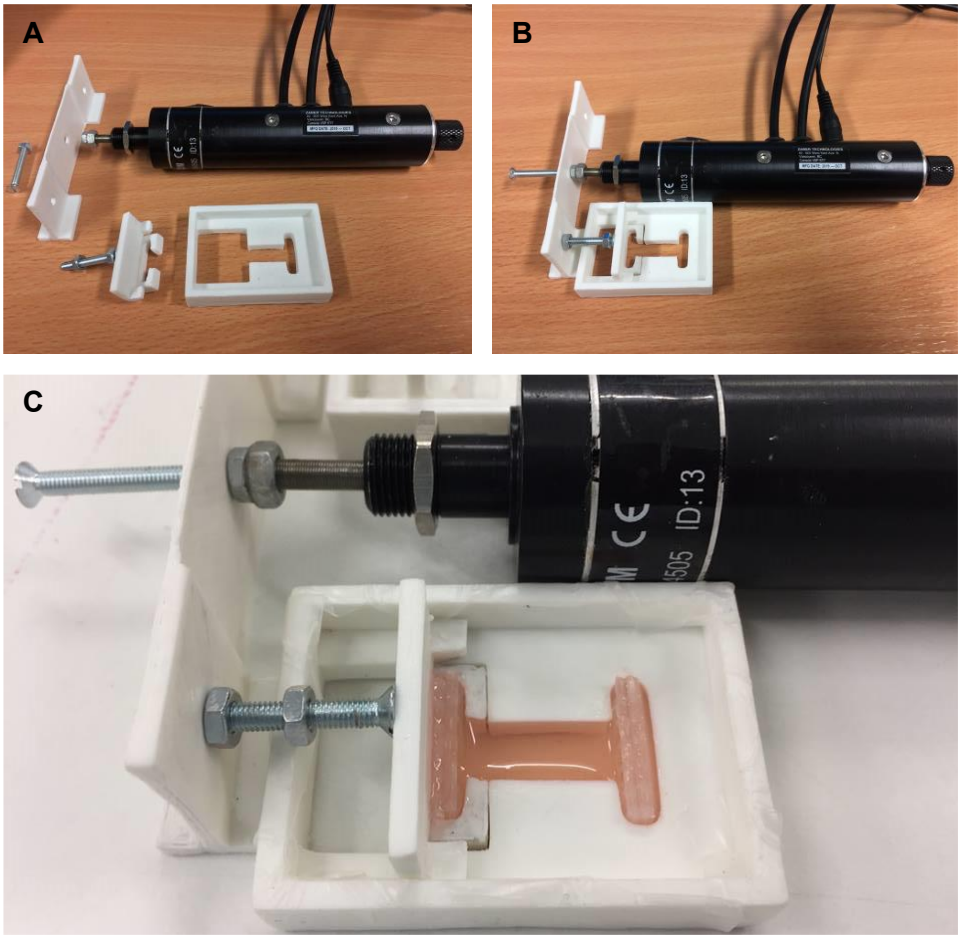

Figure 5.14 Experiment using Protocol 3. *(A) The mould and its separate components. (B) Assembly of mould for TaeNT casting and linear actuator. (C) Protocol testing with acellular collagen gel.*

5.2.5 Longer term culture of F7 Schwann cells in TaeNT

The time course to incubate cells after applying stretch force was set to 3 and 7 days to make the results comparable to previous literature (Huang et al., 2009, Li et al., 2016, Pfister et al., 2004, Smith et al., 2001). Before testing stretching protocols, the influence of long-term culture on the morphology and alignment of F7 Schwann cells in TaeNT was investigated.

The hydrogel was immunostained for S100 (red) and Hoechst 33342 (blue) with F7 Schwann cells cultured at 2 seeding densities for 2 days. The fluorescent immunostaining showed that cell density increased with time, and cell alignment was observed in all culture conditions, where the majority of cells were elongated (Figure 5.15). At 3 days, there was no distinct difference between the cells at different initial densities. At 7 days, cell alignment was clearly observed at the density of 2×10^6 cells/ml. Less aligned and highly aggregated cells were found in the gel with seeding density 4×10^6 cells/ml after 7 days, and it was difficult to determine the organisation of the cells because they were too dense.

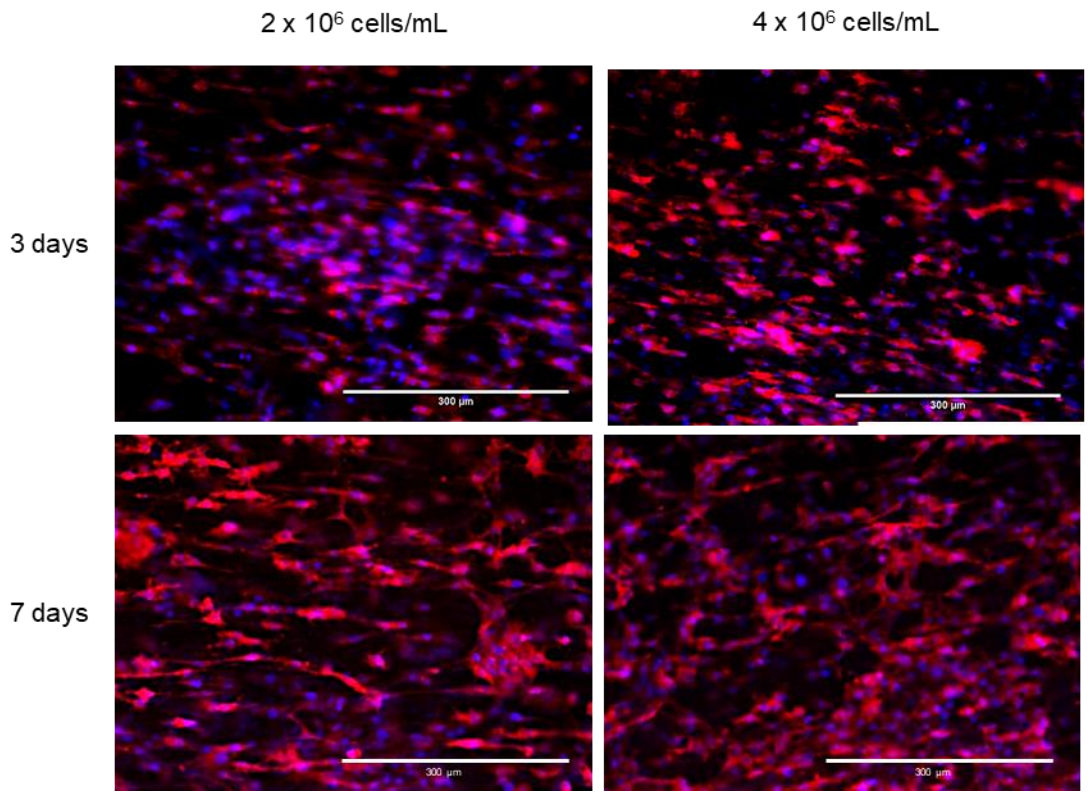

Figure 5.15 Morphology of F7 Schwann cells in TaeNT after 3 and 7 days. *Representatiive fluorescence micrographs showing immunostaining for S100 (red) and Hoechst 33342 (blue) in F7 Schwann cells cultured at two different seeding densities for the two different durations. Scale bar = 300 µm.*

5.2.6 Morphology of cells in TaeNT after mechanical tension application

The protocols designed in the previous sections were preliminarily tested with F7 Schwann cells and DRG neurons. After applying mechanical tension to the cellular hydrogel, the whole gel was fixed and immunostained to visualise the morphology and alignment of cells following strain.

Gel contraction and cell morphology was observed in TaeNT containing F7 Schwann cells before applying the mechanical tension (Figure 5.15). However, immunostaining for S-100 showed that F7 Schwann cells, in gels stretched using Protocol 1, did not exhibit alignment although the whole gel remained in the contracted shape (Figure 5.16). Cells in the hydrogel lost their spindle-like Schwan cell shape and did not aggregate in the culture.

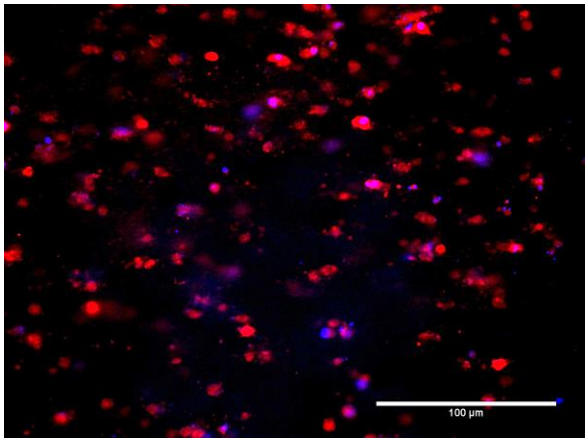

Figure 5.16 Morphology of cells in TaeNT after mechanical tension application by Protocol 1. *Immunostaining for S100 (red) and Hoechst 33342 (blue) of F7 Schwann cells after the stretch force was applied using Protocol 1. Scale bar = 100 µm.*

On the other hand, the alignment of F7 Schwann cells along the main axis of the gels was preserved in Protocol 2. Fluorescence images showed that DRG and F7 Schwann cells survived with normal morphology and had visible elongated neurites after 3 days following a single stretch of 2-mm displacement. (Figure 5.17). A number of DRG neurons were found at the edge of the gels which had elongated thin neurites. The spindle-like shape of F7 Schwann cells with an initial cell density of 2 x 10^6 cells/ml was observed more clearly than those with the higher initial cell density (Figure 5.17A). From the observation, the morphology and alignment of Schwann cells and DRG neurites were similar to those before mechanical tension was applied at similar duration. The immunostaining images of Schwann cells and neurites in TaeNT without mechanical tension was previously shown in Figure 3.3 in Chapter 3.

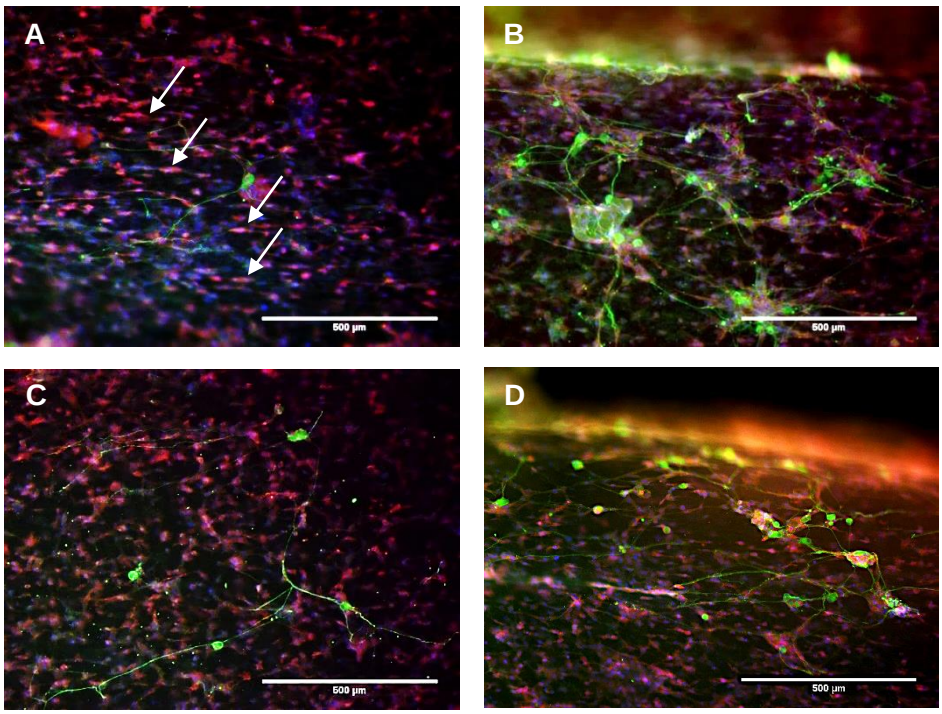

Figure 5.17 Morphology of F7 Schwann cells and DRG neurons seeding on top after stretch force was applied to by Protocol 2. *Immunostaining for S100 (red), Hoechst33342 (blue), GFP+ (green). The seeding density of F7 Schwann cells was (A, B) 2 x 10^6 cells/ml and (C, D) 4 x 10^6 cells/ml. Tethering mesh was moved to another notch for one time with the length of 2 mm. (A, C) The alignment of F7 Schwann cells and neurite elongation of DRG neurons at the middle and (B, D) at the edge of the TaeNT. The white arrows indicated spindle-like shape of Schwann cells due to the alignment. Scale bar = 500 µm.*

5.3 Discussion

With a suitable range of magnitude and appropriate culture protocols, neurons and glial cells respond to mechanical stimulation through growth (Pfister et al., 2004, Katiyar et al., 2016, Tricaud, 2018, Bray, 1984). The application of stretch force to neuronal cultures for tissue engineering should be designed to maintain neuronal morphology and function (e.g., survival, network formation, and cell interaction, before and during and after the application of strain).

The mechanical tension protocols proposed in this chapter have been preliminarily developed using the TaeNT substrate, where a whole tethered hydrogel containing aligned Schwann cells and neurons was stretched to apply a mechanical strain to the entire engineered tissue. The protocols explored alternative methods for applying a mechanical tensile force to neural cells through a 3-dimensional cell culture system. It was the first non-direct contact approach reported for mechanical tension application in neural cultures. A similar technique where mechanical tension was indirectly applied to cells through collagen gels has been reported using other cell types such as myoblasts and fibroblasts (Cheema et al., 2005, Eastwood et al., 1996). Those protocols also utilised tethering mesh, to attach collagen gels to a culture force monitor (CFM) and a computer-controlled mechanical bioreactor. The non-direct contact protocol has advantages in low risk of contamination in susceptible cells (Kamble et al., 2016). The 3D-printed mould and its connecting components were also low-cost components allowing reproducing in other laboratories. Plus, cellular support from Schwann cells is also another distinctive feature of the protocols proposed here since previously reported protocols for mechanical tension application in neurons have not involved co-culture with glial cells.

The use of the fully-hydrated hydrogel system should also be beneficial in cell stretching approaches, providing a more natural tissue-like environment than monolayer

systems and helping to retain cells and support cell viability. In cell-based therapy application, hydrogels have been used as a mechanical support that provided protection to injected cells (Burdick et al., 2016, Wagner et al., 2014). It has also been suggested that hydrogels have non-linear strain stiffening properties enabling long-range transmission of applied mechanical force, maintaining tissue integrity, and shielding cells from overstretching (Sopher et al., 2018, Wang et al., 2014, Wen and Janmey, 2013).

The manual stretching was tested in Protocols 1-2. In the cell culture with Protocol 2, immunofluorescent images showed alignment of F7 Schwann cells and healthy morphology of DRG neurons with extended neurites after 3 days of culture, implying that mechanical tension application does not negatively affect the viability of neurons in this system. Even with the displacement step of 2 mm, the normal morphology of neurons and Schwann cells in the stretched hydrogel were still observed. The unbroken gel and cells with normal morphology indicate that this simple manual stretching approach could be feasible in extending engineered tissue constructs. Further work should build on this preliminary investigation, exploring the limits of strain and rate of extension and their effects on cell viability and neurite growth.

The stretching system controlled by a linear actuator in Protocol 3 was not tested with cell culture due to insufficient experimental time in the project. Nevertheless, it has been verified that Protocol 3 could be used to stretch an acellular fully-hydrated collagen gel with a controlled length of up to 3 µm per each stretching step without loss of gel integration from the tethering meshes. The result from cell culture testing in Protocol 2, whose strain rate is higher, could give supportive evidence for the similar results in Protocol 3. Healthy cell morphology and elongated neurites were hypothesised to be observed in Protocol 3. Future work is needed to verify the hypothesis and to further investigate the potential of the protocol to improve neurite elongation.

What was extensively learned throughout the protocol development journey for the 3D cell stretching approach (Table 5.3, 5.5, 5.7) was additional design considerations which were different to the 2D conventional approach. Although the concern about adhesion between cell and substrate was eliminated, a different challenge in hydrogel integration with tethering bars is present in the 3D stretching system. To develop a mechanical tension protocol, reliable attachment of tethered gels to a movable bar without detachment when the gel is stretched became a key consideration.

In Protocol 1, manual force applied to the gel when lifted and transferred from one mould to another caused regular detachment of the gel from the tethering mesh. Less frequent detachment of gels was observed in Protocol 2 because the handling was reduced by using only one mould. Thus, despite an effort to minimise undesired tensile force to the hydrogel during carrying, it should be noted in protocol development that the cell culture system should not include relocation of cellular hydrogel once cells were encapsulated in the hydrogel. F7 Schwann cells in the gel lost the alignment following the disintegration of collagen gel and tethering mesh as shown in cellular testing with Protocol 1.

Despite refining the protocol to avoid the need to transfer gels between moulds, the tethering of the ends of the gel was still a limitation of this approach. Working with fully-hydrated gels on applying mechanical tension to neurons also has challenges, such as the integration between gels and tethering mesh: the gel could be easily detached from the tethering mesh while the towing bar was moving, leading to the loss of cell alignment in the gel. It has also been reported by others that hydrogels used for the 3D stretching systems are difficult to anchor with conventional clamps due to susceptibility to slippage or breakage during stretching (Galie and Stegemann, 2011, Tomei et al., 2009). The protocol investigation in this chapter demonstrated that soaking tethering meshes with cold collagen solution improved subsequent gel integration with the tethering bar, but the strength of the attachment was still insufficient to ensure there was never detachment during gel stretching.

Further improvements to gel integration with tethering bars may include chemical crosslinking to strengthen gel attachment (Mihic et al., 2014, Pang et al., 2010, Yuk et al., 2019). An alternative method could involve changing the shape, for example, ring-like hydrogel tissue constructs could provide better tethering security (Asnes et al., 2006, Lee et al., 2012b, Rinoldi et al., 2019).

Other important considerations in stretching protocols in this chapter were cell density in TaeNT and system controllability. For long-term culture, the minimum initial density for contraction-mediated alignment of cells is crucial to consider as the cell density will increase by time. If the density is too high, there will be too much tension and the gel will detach. Schwann cells with high density in long-term culture can contract and consequently deform the gel.

Taking both challenges mentioned above into consideration, the future direction of mechanical tension application for neuronal stretch growth should involve an alternative approach to overcome the challenges. The RAFT-stabilisation process might be one of the solutions as it produces a stiffer collagen matrix by the fluid removal process on the fully-hydrated collagen gel enabling the stabilised gel to be clamped and manipulated more easily. The method was previously used to fabricate an engineered neural tissue (EngNT) (Figure 1.9), producing a stable tissue-like biomaterial with aligned cellular and extracellular matrix architecture associated with a nerve graft (Georgiou et al., 2013). Figure 5.18 represents a new suggested design diagram of an additional protocol concept on mechanical tension applying to DRG neurites on engineered neural tissue (EngNT) containing aligned Schwann cells. The approach simplifies the method by removing the use of a mould in the stretching process, and only a clamp or moving bar is needed to connect the gel to the actuator. The same linear actuator used in Protocol 3 can also be used as the range of stretching is the same. The protocol combines the EngNT concept with a 2D stretching approach using two overlapping membranes (Huang et al., 2009, Pfister et al.,

2004). DRG explant will be placed to elongate neurite across two overlapping EngNT moving apart from each other to induce a stretch force to the attached neurites. Compared to the previous monolayer stretching approaches, the protocol would provide a cellular substrate containing aligned Schwann cells to support the elongated neurons, and this cellular support might be beneficial to the stretching system.

Overall, this chapter has modified the TaeNT containing aligned Schwann cells and neurons to be a cellular hydrogel-based substrate for the stretching system. The approach combined the use of a supportive co-culture system with mechanical tension application in neural cells, providing new protocols that can expand the stretching range for a healthy neurite elongation. Understanding the design concept of existing stretching protocols and the development considerations of the new approach could help overcome the limitations of mechanical tension application to neural cells. Moving toward translational research, the neuronal growth within a novel 3D construct combined with mechanical stretching provides an innovative new approach for nerve regeneration where the engineered living scaffold containing long neuronal extensions could potentially be of benefit in long gap repair.

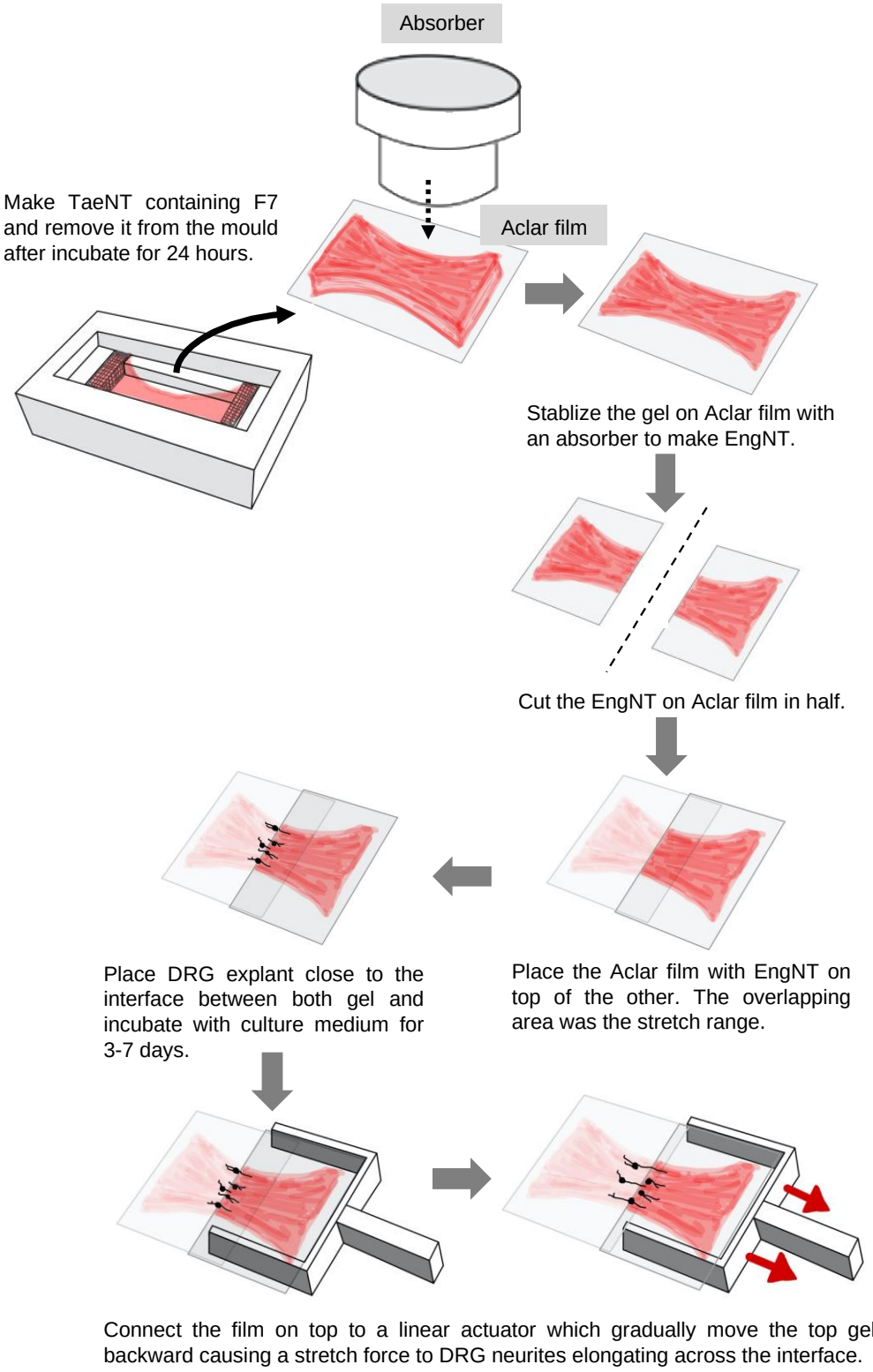

Figure 5.18 Design diagram of an additional protocol concept on mechanical tension applying to DRG neurites on EngNT containing Schwann cells. *EngNT cut in half and pieces placed next to one to another. DRG explant placed close to the interface resulting in neurite elongation across the interface. Stretch force applied directly to the neurites by moving the EngNT on top away from the other.*

CHAPTER 6

Conclusions and proposed future work

6.1 Overall summary and conclusion

Peripheral nerve injury has a tremendous negative impact on a patient's well-being, with functional recovery from nerve repair remaining a clinical challenge, especially when the injured site is very proximal, leaving a long distal distance to regenerate. The delay in reinnervation following Wallerian degeneration results in a high chance of muscle atrophy, even when the 'gold standard' autograft is used. Engineered neural tissue has been one of the promising Advanced Therapy Medicinal Product (ATMP) approaches showing potential to overcome limitations of long-distance nerve regeneration. This research project has introduced and developed tethered aligned engineered neural tissue (TaeNT) as a living scaffold containing highly aligned Schwann cells and elongated neurons in fully-hydrated tethered collagen gels, with a hypothesis that it would improve functional recovery by accelerating nerve gap functional re-connection instead of only supporting regenerating host axons.

Throughout previous chapters, the regenerative potential of TaeNT was examined through studying various attributes. Firstly, Chapter 3 demonstrated the basic but essential properties of the construct in supporting neurite elongation and crossing of the transplant interface. After culture medium testing, the NG108-15 motor neuron-like cell line was co-cultured with TaeNT containing aligned F7 Schwann cells. The aligned F7 Schwann cells in TaeNT resembled the structure of the Bands of Büngner, upon which the NG108-15 neurites could elongate and align. The subsequent *in vivo* studies used a self-organising collagen guidance conduit for transplantation of a tethered aligned collagen-based culture system

containing neurons and Schwann cells into rat sciatic nerve. The density of Schwann cells and ratio of neurons to Schwann cells were optimised before transplanting into a 10-mm rat sciatic nerve gap for 3 weeks. By cross-sectioning both proximal and distal interfaces between host tissue and transplanted conduit, the spatial interactions of host and transplanted cells were determined through the distribution of both cell populations. The host and transplanted neurites could elongate across the transplant interface without disruption as the number of neurites across both interfaces remained steady. Both *in vitro* and *in vivo* examination showed that TaeNT can be a suitable substrate for transplanted neurons as it can support neurite elongation, alignment, and interface-crossing behaviour.

Apart from neurite guidance, the behaviours of supporting glial cells were also considered as influential in nerve regeneration, so the nature and consequence of the interaction between host and transplanted glial cells were investigated in Chapter 4. The distribution, migration, and alignment of both cell populations contribute to maintaining tissue organisation and homeostasis, influencing neurite elongation. The cell source was extended from Schwann cell lines to include glial cells dissociated from primary DRG culture, which was optimised by extending incubating time to enrich glial cell proportion to more than 80% in the culture.

The interaction of glial cells from two different sources was preliminarily examined in a 3D culture interface model, where the ability of each cell population to migrate across the interface was demonstrated. The following *in vitro* experiment in TaeNT showed that endogenous (cells cultured in TaeNT) and exogenous glial cells (cells seeded on TaeNT) did not disrupt the migration and orientation of each other. These *in vitro* experiments consequently led to an investigation of glial cell interaction *in vivo*. The repaired nerves from the transplantation procedure in Chapter 3 were longitudinally sectioned and glial cell distribution and orientation was quantified. The transplanted glial cells were shown to survive

and be aligned at 3 weeks, with host glial cells migrating into the conduit through both nerve stumps.

The work in Chapter 3 and 4 provided a new understanding of the interaction of host and transplanted cells in terms of both neurons and supporting glial cells. The interaction between transplanted cells and host tissue leads to a regeneration-supportive response, reflecting the regenerative potential of TaeNT as an engineered neural tissue approach that could be tested in future work to enhance peripheral nerve regeneration in long-distance injury.

Chapter 5 portrayed an engineering journey to develop an additional system to further improve the scalability and regenerative potential of living scaffolds by inducing longer neurite growth inside the construct. In an attempt to induce longer neurite growth, TaeNT was proposed as a cellular hydrogel-based substrate that could be modified and combined with mechanical tension application using a specific 3D-printed mould developed to stretch the cellular gels in a controlled manner. A series of newly designed protocols for mechanical tension application to induce growth response for enhanced neural regeneration was developed and discussed correspondingly. The design considerations of the 3D cell stretching approach learned throughout the chapter included reliable attachment and integration between the hydrogel and movable bars, initial cell density in TaeNT, and system controllability. Engineering development of a stretching protocol for TaeNT with preliminary tests on cell morphology showed the potential of combining mechanical tension application with TaeNT to induce longer neurite elongation. While still at an early stage of testing, this is considered the first hydrogel-based protocol that has been developed to apply an indirect stretch growth to neural cells in 3D co-culture. This is distinct from previous studies since the movable bar was integrated with the tethered gel containing elongated neurons in engineered tissue, rather than relying on a direct attachment to isolated neurons in monolayer culture.

In conclusion, in addition to the established cellular-based scaffolds using Schwann cells in a tethered hydrogel, populating the construct with neurons exhibiting long neurite extensions was a key feature to explore in improving the functional recovery of long-distance nerve regeneration. The novel concept imitated axon elongation during development, where a pioneer axon formed a tract to guide the following axons (Struzyna et al., 2015). The study of axon elongation in the TaeNT in this project strengthened supportive evidence for an important role of Schwann cells in nerve regeneration in which the presence of Schwann cells increases neurite outgrowth and promotes directional guidance to elongating neurites (Georgiou et al., 2013, Georgiou et al., 2015, Hadlock et al., 2000, Martens et al., 2014, Thompson and Buettner, 2006). The supportive cell interaction was observed in the transplantation of TaeNT. Host neurites could enter the conduit as well as into an acellular hydrogel conduit (Du et al., 2017, McGrath et al., 2010, Meyer et al., 2016, Wu et al., 2017), and living scaffolds with other types of cells (Huang et al., 2009, Georgiou et al., 2013, Lee et al., 2017, Flachsbarth et al., 2014). Plus, the transplanted neurites could also penetrate host tissue without disruption with more neurites at the proximal site corresponding to the distribution of migrating Schwann cells reported here and previously (Chen et al., 2019). Host glial cells migrated into the conduit as well as into an acellular conduit (Bryan et al., 1999, Chen et al., 2019, Parrinello et al., 2010, Cattin et al., 2015, Dun and Parkinson, 2020) and interacted with transplanted glial cells by aligning in a similar pattern. Furthermore, the TaeNT is a feasible way to provide an alternative platform to apply mechanical tension to neural cells for growth response. In the light of previous stretching models with long neurites (Bray, 1984, Huang et al., 2009, Li et al., 2016, Loverde et al., 2011, Pfister et al., 2004, Smith et al., 2001), key considerations in designing stretching protocols were reviewed to develop the first non-direct contact approach with TaeNT modifications. Taking all attributes together, the findings represent the initial development and investigation of an engineered living scaffold containing neurons and Schwann cells suitable for stretch-growth with

potential to provide elongated functional replacement nerve tissue. The new technology, TaeNT, introduced in this project, could be considered promising as a new way to generate tissue engineered nerve grafts for peripheral nerve regeneration.

6.2 Proposed future work

6.2.1 TaeNT protocol optimisation

Like other tissue engineered constructs, developing TaeNT includes several choices in terms of selecting cells, materials, and techniques. This research project has studied TaeNT using only a few specific sources of cells and techniques, so expanding the variety to determine the best protocol for engineering TaeNT with optimal efficacy and practicality is recommended. Future work to enhance translational potential includes the study of therapeutic cells to culture in TaeNT, such as differentiated stem cells. Currently, the use of tissue-specific cells in clinical applications is less prevalent compared to stem cells. According to the ClinicalTrials.gov database, less than 20 neural cell-based therapies are currently active for clinical trials, and all are still at phase I or II. The vast majority of cell-based therapies use mesenchymal stem cells, and some of them are at Phase III intended eventually for use in the neurology field. The clinical trial databases therefore indicate that differentiated stem cells might be a suitable current therapeutic source of cells for TaeNT when aiming to accelerate the research to the translational stage. For example, CTX0E03 was a source of GMP-certified human neural stem cell line which can be derived to many specific types of cells for transplantations (Yoon et al., 2020, Stevanato et al., 2015, O'Rourke et al., 2018). The transplantation of stem cell-derived motor neuron progenitors was reported to be one of potential treatments for diseases related to motor neuron loss, such as Amyotrophic latera sclerosis (ALS), spinal muscular atrophy (SMA), and spinal cord injury (SCI). The transplanted human neural stem cells, even without a scaffold, were found

to promote functional improvement to the system regardless of the presence of functional integration because it promoted regeneration of injured neurites by secreting growth factors, such as NGF, GDNF, NT-3, and BDNF (Lu et al., 2003, Rossi et al., 2010, Lu et al., 2011). The differentiation can generate various subtypes of motor neurons with unique motor neuron markers and electrophysiological activity (Amoroso et al., 2013, Du et al., 2015, Goparaju et al., 2017, Maury et al., 2015).

Moreover, combinations of neurons with different regeneration-supporting cells, other than Schwann cells, could also be studied with the TaeNT and stretch-growth approach. For instance, tissue-engineered constructs containing aligned endothelial cells, previously proposed as another candidate to treat peripheral nerve injury (Muangsanit et al., 2021), could potentially be modified for stretching to test whether the mechanical effect could improve axonal regeneration and simultaneous vascularisation.

6.2.2 Functional integration of TaeNT and host tissue

Investigating the integration of host and transplanted cells is a crucial step to determine the effectiveness of TaeNT for future clinical use. In addition to secreting various supportive growth factors, transplanted neurons should be able to integrate to the host tissue to optimise the efficacy of the nerve regeneration. TaeNT would not completely bridge the nerve gap unless the integration at the interfaces between the transplanted conduit and nerve stumps is sufficient to allow axonal communication to be established with the distal muscle.

This project has demonstrated spatial integration by measuring the number and distribution of host and transplanted neurites elongating across the conduit interface. The spatial integration between transplanted neurons in engineered tissue constructs and the host tissue was also reported in previous literature (Huang et al., 2009, Katiyar et al., 2020).

However, the spatial or structural integration of neurites could not imply the functional integration and electrical activity of TaeNT and host tissue. The verification of spatial integration only provides supportive evidence to hypothesise that the connection has a positive tendency to exhibit patterns of functional connectivity.

The functional integration of transplanted and host neurons was extensively investigated in CNS research as it is one of the fundamental principles in brain organisation and plasticity (Falkner et al., 2016, Jgamadze et al., 2012, Wernig et al., 2004). In the PNS, elongating neurites also connect to the other parts of the body and relay signals back and forth to maintain communications between the nervous system and the target tissue. The absence of functional integration between peripheral nerves and muscle for extended time leads to neurogenic muscle atrophy as muscle contraction is eliminated without signal transmission from the nerve. In clinical practice, various coaptation techniques have been consequently applied to delay the atrophy by creating a temporary connection between the injured nerve and a healthy adjacent nerve (Kelly et al., 2007, Shea et al., 2014, von Guionneau et al., 2020). The need of coaptation is one of practical examples underlining the importance of maintaining functional integration of neurites and the target tissue.

Therefore, further *in vivo* experiments should include functional tests or electrophysiological tests to verify functional integration. Gastrocnemius muscle harvest and analysis would also be additionally helpful to determine a degree of functional recovery following sciatic nerve injury. Through these post-transplantation functional analyses, several interface-related questions and hypotheses could be consequently studied (e.g., how long it takes to functionally transmit neuronal signals through the transplanted construct to distal muscle after long-distance nerve injury, and whether it is more time-efficient than waiting for host neurite regeneration through an autograft).

6.2.3 Preservation protocol for clinical applications

The practical use of TaeNT in a clinic would be in the form of an ‘off-the-shelf’ construct, where a tissue engineered conduit containing living allogeneic cells had already been manufactured (GMP-certified) ready for immediate transplantation into an injured peripheral nerve. Clinical-grade cells could be cultured and stretched in biocompatible collagen gels with TaeNT approach, and then transplanted with an immunosuppressive therapy to avoid rejection. The use of allogeneic GMP-certified cells and 3D-printed stretching protocol provides high reproducibility of the building construct (Kang et al., 2022, Hodges et al., 2007, O'Rourke et al., 2018).

To make an off-the-shelf construct for clinical application, biopreservation of TaeNT is required, to allow time for the construct to be stored and shipped from the manufacturing facility to the clinic. Different construct preservation techniques as well as the optimal temperature and maximum storage duration that do not disrupt cellular and extracellular components and structure in the construct could be explored. Similar living scaffolds with aligned axon tracts like TENGs can be stored at 4 °C for 28 days and still maintain equivalent pro-regenerative properties to fresh TENGs (Shultz et al., 2021). EngNT containing highly aligned Schwann cells has been shown to withstand freezing at 4 °C and liquid nitrogen by using a specific mixture of media (Day et al., 2017). The long-term preservation of neuron-containing TaeNT approach should also be investigated to a similar extent.

REFERENCES

ABRAHAM, J. A., LINNARTZ, C., DREISSEN, G., SPRINGER, R., BLASCHKE, S., RUEGER, M. A., FINK, G. R., HOFFMANN, B. & MERKEL, R. 2019. Directing Neuronal Outgrowth and Network Formation of Rat Cortical Neurons by Cyclic Substrate Stretch. Langmuir, 35, 7423-7431.

ADAMS, R. D., RENDELL, S. R., COUNTS, L. R., PAPKE, J. B., WILLITS, R. K. & HARKINS, A. B. 2014. Electrical and neurotrophin enhancement of neurite outgrowth within a 3D collagen scaffold. Ann Biomed Eng, 42, 1282-91.

ALI, S. A., ROSKO, A. J., HANKS, J. E., STEBBINS, A. W., ALKHALILI, O., HOGIKYAN, N. D., FELDMAN, E. L. & BRENNER, M. J. 2019. Effect of Motor versus Sensory Nerve Autografts on Regeneration and Functional Outcomes of Rat Facial Nerve Reconstruction. Sci Rep, 9, 8353.

AMOROSO, M. W., CROFT, G. F., WILLIAMS, D. J., O'KEEFFE, S., CARRASCO, M. A., DAVIS, A. R., ROYBON, L., OAKLEY, D. H., MANIATIS, T., HENDERSON, C. E. & WICHTERLE, H. 2013. Accelerated high-yield generation of limb-innervating motor neurons from human stem cells. J Neurosci, 33, 574-86.

ANAVA, S., GREENBAUM, A., BEN JACOB, E., HANEIN, Y. & AYALI, A. 2009. The regulative role of neurite mechanical tension in network development. Biophys J, 96, 1661-70.

ANDREWS, A. M., LUTTON, E. M., MERKEL, S. F., RAZMPOUR, R. & RAMIREZ, S. H. 2016. Mechanical Injury Induces Brain Endothelial-Derived Microvesicle Release: Implications for Cerebral Vascular Injury during Traumatic Brain Injury. Front Cell Neurosci, 10, 43.

ARMSTRONG, S. J., WIBERG, M., TERENGHI, G. & KINGHAM, P. J. 2007. ECM molecules mediate both Schwann cell proliferation and activation to enhance neurite outgrowth. Tissue Eng, 13, 2863-70.

ARMSTRONG, S. J., WIBERG, M., TERENGHI, G. & KINGHAM, P. J. 2008. Laminin activates NF-kappaB in Schwann cells to enhance neurite outgrowth. Neurosci Lett, 439, 42-6.

AROLD, S. P., WONG, J. Y. & SUKI, B. 2007. Design of a new stretching apparatus and the effects of cyclic strain and substratum on mouse lung epithelial-12 cells. Ann Biomed Eng, 35, 1156-64.

ARSLANTUNALI, D., DURSUN, T., YUCEL, D., HASIRCI, N. & HASIRCI, V. 2014. Peripheral nerve conduits: technology update. Med Devices (Auckl), 7, 405-24.

ARTHUR-FARRAJ, P. J., LATOUCHE, M., WILTON, D. K., QUINTES, S., CHABROL, E., BANERJEE, A., WOODHOO, A., JENKINS, B., RAHMAN, M., TURMAINE, M., WICHER, G. K., MITTER, R., GREENSMITH, L., BEHRENS, A., RAIVICH, G., MIRSKY, R. & JESSEN, K. R. 2012. c-Jun reprograms Schwann cells of injured nerves to generate a repair cell essential for regeneration. Neuron, 75, 633-47.

ASNES, C. F., MARQUEZ, J. P., ELSON, E. L. & WAKATSUKI, T. 2006. Reconstitution of the Frank-Starling mechanism in engineered heart tissues. Biophys J, 91, 1800-10.

ASSOULINE, J. G., BOSCH, E. P. & LIM, R. 1983. Purification of rat Schwann cells from cultures of peripheral nerve: an immunoselective method using surfaces coated with anti-immunoglobulin antibodies. Brain Res, 277, 389-92.

ATHAMNEH, A. I. M., HE, Y., LAMOUREUX, P., FIX, L., SUTER, D. M. & MILLER, K. E. 2017. Neurite elongation is highly correlated with bulk forward translocation of microtubules. Sci Rep, 7, 7292.

AVRAHAM, O., DENG, P. Y., JONES, S., KURUVILLA, R., SEMENKOVICH, C. F., KLYACHKO, V. A. & CAVALLI, V. 2020. Satellite glial cells promote regenerative growth in sensory neurons. Nat Commun, 11, 4891.

BALGUDE, A. P., YU, X., SZYMANSKI, A. & BELLAMKONDA, R. V. 2001. Agarose gel stiffness determines rate of DRG neurite extension in 3D cultures. Biomaterials, 22, 1077-84.

BEAUDET, M. J., YANG, Q., CADAU, S., BLAIS, M., BELLENFANT, S., GROS-LOUIS, F. & BERTHOD, F. 2015. High yield extraction of pure spinal motor neurons, astrocytes and microglia from single embryo and adult mouse spinal cord. Sci Rep, 5, 16763.

BENITO, C., DAVIS, C. M., GOMEZ-SANCHEZ, J. A., TURMAINE, M., MEIJER, D., POLI, V., MIRSKY, R. & JESSEN, K. R. 2017. STAT3 Controls the Long-Term Survival and Phenotype of Repair Schwann Cells during Nerve Regeneration. J Neurosci, 37, 4255-4269.

BERGMEISTER, K. D., GROSSE-HARTLAGE, L., DAESCHLER, S. C., RHODIUS, P., BOCKER, A., BEYERSDORFF, M., KERN, A. O., KNESER, U. & HARHAUS, L. 2020. Acute and long-term costs of 268 peripheral nerve injuries in the upper extremity. PLoS One, 15, e0229530.

BERROCAL, Y. A., ALMEIDA, V. W., GUPTA, R. & LEVI, A. D. 2013. Transplantation of Schwann cells in a collagen tube for the repair of large, segmental peripheral nerve defects in rats. J Neurosurg, 119, 720-32.

BHANG, S. H., LIM, J. S., CHOI, C. Y., KWON, Y. K. & KIM, B. S. 2007. The behavior of neural stem cells on biodegradable synthetic polymers. J Biomater Sci Polym Ed, 18, 223-39.

BHATHEJA, K. & FIELD, J. 2006. Schwann cells: origins and role in axonal maintenance and regeneration. Int J Biochem Cell Biol, 38, 1995-9.

BIAZAR, E. & HEIDARI KESHEL, S. 2013. A nanofibrous PHBV tube with Schwann cell as artificial nerve graft contributing to rat sciatic nerve regeneration across a 30-mm defect bridge. Cell Commun Adhes, 20, 41-9.

BIRLING, M. C. & PRICE, J. 1995. Influence of growth factors on neuronal differentiation. Curr Opin Cell Biol, 7, 878-84.

BLESCH, A., LU, P., TSUKADA, S., ALTO, L. T., ROET, K., COPPOLA, G., GESCHWIND, D. & TUSZYNSKI, M. H. 2012. Conditioning lesions before or after spinal cord injury recruit broad genetic mechanisms that sustain axonal regeneration: superiority to camp-mediated effects. Exp Neurol, 235, 162-73.

BOJIC, S., MURRAY, A., BENTLEY, B. L., SPINDLER, R., PAWLIK, P., CORDEIRO, J. L., BAUER, R. & DE MAGALHAES, J. P. 2021. Winter is coming: the future of cryopreservation. BMC Biol, 19, 56.

BOONEN, K. J., LANGELAAN, M. L., POLAK, R. B., VAN DER SCHAFT, D. W., BAAIJENS, F. P. & POST, M. J. 2010. Effects of a combined mechanical stimulation protocol: Value for skeletal muscle tissue engineering. J Biomech, 43, 1514-21.

BOTTENSTEIN, J. E. & SATO, G. H. 1979. Growth of a rat neuroblastoma cell line in serum-free supplemented medium. Proc Natl Acad Sci U S A, 76, 514-7.

BOZKURT, A., BOECKER, A., TANK, J., ALTINOVA, H., DEUMENS, R., DABHI, C., TOLBA, R., WEIS, J., BROOK, G. A., PALLUA, N. & VAN NEERVEN, S. G. A.

2016. Efficient bridging of 20 mm rat sciatic nerve lesions with a longitudinally micro-structured collagen scaffold. Biomaterials, 75, 112-122.

BOZKURT, A., DEUMENS, R., BECKMANN, C., OLDE DAMINK, L., SCHUGNER, F., HESCHEL, I., SELLHAUS, B., WEIS, J., JAHNEN-DECHENT, W., BROOK, G. A. & PALLUA, N. 2009. *In vitro* cell alignment obtained with a Schwann cell enriched microstructured nerve guide with longitudinal guidance channels. Biomaterials, 30, 169-79.

BRAY, D. 1979. Mechanical Tension Produced by Nerve-Cells in Tissue-Culture. Journal of Cell Science, 37, 391-410.

BRAY, D. 1984. Axonal growth in response to experimentally applied mechanical tension. Dev Biol, 102, 379-89.

BROCKES, J. P. & RAFF, M. C. 1979. Studies on cultured rat Schwann cells. II. Comparison with a rat Schwann cell line. In Vitro, 15, 772-8.

BROCKES, J. P., FIELDS, K. L. & RAFF, M. C. 1979. Studies on cultured rat Schwann cells. I. Establishment of purified populations from cultures of peripheral nerve. Brain Res, 165, 105-18.

BROWN, J. P., FINLEY, V. G. & KUO, C. K. 2014. Embryonic mechanical and soluble cues regulate tendon progenitor cell gene expression as a function of developmental stage and anatomical origin. J Biomech, 47, 214-22.

BRYAN, D. J., WANG, K. K. & SUMMERHAYES, C. 1999. Migration of schwann cells in peripheral-nerve regeneration. J Reconstr Microsurg, 15, 591-6.

BUNTING, S., DI SILVIO, L., DEB, S. & HALL, S. 2005. Bioresorbable glass fibres facilitate peripheral nerve regeneration. J Hand Surg Br, 30, 242-7.

BURDICK, J. A., MAUCK, R. L. & GERECHT, S. 2016. To Serve and Protect: Hydrogels to Improve Stem Cell-Based Therapies. Cell Stem Cell, 18, 13-5.

BURNETT, M. G. & ZAGER, E. L. 2004. Pathophysiology of peripheral nerve injury: a brief review. Neurosurg Focus, 16, E1.

BUSIS, N. A., DANIELS, M. P., BAUER, H. C., PUDIMAT, P. A., SONDEREGGER, P., SCHAFFNER, A. E. & NIRENBERG, M. 1984. Three cholinergic neuroblastoma hybrid cell lines that form few synapses on myotubes are deficient in acetylcholine

receptor aggregation molecules and large dense core vesicles. Brain Res, 324, 201-10.

CALIARI, S. R., VEGA, S. L., KWON, M., SOULAS, E. M. & BURDICK, J. A. 2016. Dimensionality and spreading influence MSC YAP/TAZ signaling in hydrogel environments. Biomaterials, 103, 314-323.

CAPUANO, A., DE CORATO, A., LISI, L., TRINGALI, G., NAVARRA, P. & DELLO RUSSO, C. 2009. Proinflammatory-activated trigeminal satellite cells promote neuronal sensitization: relevance for migraine pathology. Mol Pain, 5, 43.

CARLSON, K. B., SINGH, P., FEASTER, M. M., RAMNARAIN, A., PAVLIDES, C., CHEN, Z. L., YU, W. M., FELTRI, M. L. & STRICKLAND, S. 2011. Mesenchymal stem cells facilitate axon sorting, myelination, and functional recovery in paralyzed mice deficient in Schwann cell-derived laminin. Glia, 59, 267-77.

CARMONA-FONTAINE, C., MATTHEWS, H. K., KURIYAMA, S., MORENO, M., DUNN, G. A., PARSONS, M., STERN, C. D. & MAYOR, R. 2008. Contact inhibition of locomotion *in vivo* controls neural crest directional migration. Nature, 456, 957-61.

CASTILLO, C., NORCINI, M., MARTIN HERNANDEZ, L. A., CORREA, G., BLANCK, T. J. & RECIO-PINTO, E. 2013. Satellite glia cells in dorsal root ganglia express functional NMDA receptors. Neuroscience, 240, 135-46.

CATTIN, A. L., BURDEN, J. J., VAN EMMENIS, L., MACKENZIE, F. E., HOVING, J. J., GARCIA CALAVIA, N., GUO, Y., MCLAUGHLIN, M., ROSENBERG, L. H., QUEREDA, V., JAMECNA, D., NAPOLI, I., PARRINELLO, S., ENVER, T., RUHRBERG, C. & LLOYD, A. C. 2015. Macrophage-Induced Blood Vessels Guide Schwann Cell-Mediated Regeneration of Peripheral Nerves. Cell, 162, 1127-39.

CHADA, S., LAMOUREUX, P., BUXBAUM, R. E. & HEIDEMANN, S. R. 1997. Cytomechanics of neurite outgrowth from chick brain neurons. J Cell Sci, 110 (Pt 10), 1179-86.

CHAN, B. P., LI, C. H., AU-YEUNG, K. L., SZE, K. Y. & NGAN, A. H. 2008. A microplate compression method for elastic modulus measurement of soft and viscoelastic collagen microspheres. Ann Biomed Eng, 36, 1254-67.

CHAUDHURI, O. 2017. Viscoelastic hydrogels for 3D cell culture. Biomater Sci, 5, 1480-1490.

CHEEMA, U., BROWN, R., MUDERA, V., YANG, S. Y., MCGROUTHER, G. & GOLDSPINK, G. 2005. Mechanical signals and IGF-I gene splicing *in vitro* in relation to development of skeletal muscle. J Cell Physiol, 202, 67-75.

CHEN, B., CHEN, Q., PARKINSON, D. B. & DUN, X. P. 2019. Analysis of Schwann Cell Migration and Axon Regeneration Following Nerve Injury in the Sciatic Nerve Bridge. Front Mol Neurosci, 12, 308.

CHEN, W., XIAO, S., WEI, Z., DENG, C., NIE, K. & WANG, D. 2019. Schwann Cell-Like Cells Derived from Human Amniotic Mesenchymal Stem Cells Promote Peripheral Nerve Regeneration through a MicroRNA-214/c-Jun Pathway. Stem Cells Int, 2019, 2490761.

CHENG, C. W., SOLORIO, L. D. & ALSBERG, E. 2014. Decellularized tissue and cell-derived extracellular matrices as scaffolds for orthopaedic tissue engineering. Biotechnol Adv, 32, 462-84.

CHRISTOPHER, G. F., YOO, J. M., DAGALAKIS, N., HUDSON, S. D. & MIGLER, K. B. 2010. Development of a MEMS based dynamic rheometer. Lab Chip, 10, 2749-57.

CLINICALGATE. (2015). The neuromuscular junction. [Online image] Available at: https://clinicalgate.com/infections-of-the-nervous-system-and-senses/ [Accessed 04/01/22].

CORFAS, G., VELARDEZ, M. O., KO, C. P., RATNER, N. & PELES, E. 2004. Mechanisms and roles of axon-Schwann cell interactions. J Neurosci, 24, 9250-60.

CUI, L., JIANG, J., WEI, L., ZHOU, X., FRASER, J. L., SNIDER, B. J. & YU, S. P. 2008. Transplantation of embryonic stem cells improves nerve repair and functional recovery after severe sciatic nerve axotomy in rats. Stem Cells, 26, 1356-65.

CUI, Y., HAMEED, F. M., YANG, B., LEE, K., PAN, C. Q., PARK, S. & SHEETZ, M. 2015. Cyclic stretching of soft substrates induces spreading and growth. Nat Commun, 6, 6333.

DAS, S., SHARMA, M., SAHARIA, D., SARMA, K. K., SARMA, M. G., BORTHAKUR, B. B. & BORA, U. 2015. *In vivo* studies of silk based gold nano-composite conduits for functional peripheral nerve regeneration. Biomaterials, 62, 66-75.

DAVIES, A. M. 2000. Neurotrophins: neurotrophic modulation of neurite growth. Curr Biol, 10, R198-200.

DAVIS, G. E., SKAPER, S. D., MANTHORPE, M., MOONEN, G. & VARON, S. 1984. Fetal calf serum-mediated inhibition of neurite growth from ciliary ganglion neurons *in vitro*. J Neurosci Res, 12, 29-39.

DAY, A. G. E., BHANGRA, K. S., MURRAY-DUNNING, C., STEVANATO, L. & PHILLIPS, J. B. 2017. The Effect of Hypothermic and Cryogenic Preservation on Engineered Neural Tissue. Tissue Eng Part C Methods, 23, 575-582.

DE ROOIJ, R., MILLER, K. E. & KUHL, E. 2017. Modeling molecular mechanisms in the axon. Comput Mech, 59, 523-537.

DE VINCENTIIS, S., FALCONIERI, A., MICKOLEIT, F., CAPPELLO, V., SCHULER, D. & RAFFA, V. 2021. Induction of Axonal Outgrowth in Mouse Hippocampal Neurons via Bacterial Magnetosomes. Int J Mol Sci, 22.

DELGADILLO, J. O. V., DELORME, S., EL-AYOUBI, R., DIRADDO, R. & HATZIKIRIAKOS, S. G. 2010. Effect of freezing on the passive mechanical properties of arterial samples. Journal of Biomedical Science and Engineering, 03, 645-652.

DENNERLL, T. J., LAMOUREUX, P., BUXBAUM, R. E. & HEIDEMANN, S. R. 1989. The cytomechanics of axonal elongation and retraction. J Cell Biol, 109, 3073-83.

DEVIREDDY, R. V., NEIDERT, M. R., BISCHOF, J. C. & TRANQUILLO, R. T. 2003. Cryopreservation of collagen-based tissue equivalents. I. Effect of freezing in the absence of cryoprotective agents. Tissue Eng, 9, 1089-100.

DI SUMMA, P. G., KALBERMATTEN, D. F., PRALONG, E., RAFFOUL, W., KINGHAM, P. J. & TERENGHI, G. 2011. Long-term *in vivo* regeneration of peripheral nerves through bioengineered nerve grafts. Neuroscience, 181, 278-91.

DILLON, G. P., YU, X., SRIDHARAN, A., RANIERI, J. P. & BELLAMKONDA, R. V. 1998. The influence of physical structure and charge on neurite extension in a 3D hydrogel scaffold. J Biomater Sci Polym Ed, 9, 1049-69.

DORON-MANDEL, E., FAINZILBER, M. & TERENZIO, M. 2015. Growth control mechanisms in neuronal regeneration. FEBS Lett, 589, 1669-77.

DU, J., LIU, J., YAO, S., MAO, H., PENG, J., SUN, X., CAO, Z., YANG, Y., XIAO, B., WANG, Y., TANG, P. & WANG, X. 2017. Prompt peripheral nerve regeneration induced by a hierarchically aligned fibrin nanofiber hydrogel. Acta Biomater, 55, 296-309.

DU, Z. W., CHEN, H., LIU, H., LU, J., QIAN, K., HUANG, C. L., ZHONG, X., FAN, F. & ZHANG, S. C. 2015. Generation and expansion of highly pure motor neuron progenitors from human pluripotent stem cells. Nat Commun, 6, 6626.

DUBEY, N., LETOURNEAU, P. C. & TRANQUILLO, R. T. 1999. Guided neurite elongation and schwann cell invasion into magnetically aligned collagen in simulated peripheral nerve regeneration. Exp Neurol, 158, 338-50.

DUN, X. P. & PARKINSON, D. B. 2020. Classic axon guidance molecules control correct nerve bridge tissue formation and precise axon regeneration. Neural Regen Res, 15, 6-9.

EAST, E., DE OLIVEIRA, D. B., GOLDING, J. P. & PHILLIPS, J. B. 2010. Alignment of astrocytes increases neuronal growth in three-dimensional collagen gels and is maintained following plastic compression to form a spinal cord repair conduit. Tissue Eng Part A, 16, 3173-84.

EAST, E., GOLDING, J. P. & PHILLIPS, J. B. 2012. Engineering an integrated cellular interface in three-dimensional hydrogel cultures permits monitoring of reciprocal astrocyte and neuronal responses. Tissue Eng Part C Methods, 18, 526-36.

EASTWOOD, M., MCGROUTHER, D. A. & BROWN, R. A. 1998. Fibroblast responses to mechanical forces. Proc Inst Mech Eng H, 212, 85-92.

EASTWOOD, M., PORTER, R., KHAN, U., MCGROUTHER, G. & BROWN, R. 1996. Quantitative analysis of collagen gel contractile forces generated by dermal fibroblasts and the relationship to cell morphology. J Cell Physiol, 166, 33-42.

EHRLICHER, A., BETZ, T., STUHRMANN, B., GOGLER, M., KOCH, D., FRANZE, K., LU, Y. & KAS, J. 2007. Optical neuronal guidance. Methods Cell Biol, 83, 495-520.

ELLIS, A. & BENNETT, D. L. 2013. Neuroinflammation and the generation of neuropathic pain. Br J Anaesth, 111, 26-37.

ENGLAND, S., HEBLICH, F., JAMES, I. F., ROBBINS, J. & DOCHERTY, R. J. 2001. Bradykinin evokes a Ca2+-activated chloride current in non-neuronal cells isolated from neonatal rat dorsal root ganglia. J Physiol, 530, 395-403.

ERBA, P., MANTOVANI, C., KALBERMATTEN, D. F., PIERER, G., TERENGHI, G. & KINGHAM, P. J. 2010. Regeneration potential and survival of transplanted undifferentiated adipose tissue-derived stem cells in peripheral nerve conduits. J Plast Reconstr Aesthet Surg, 63, e811-7.

EVANS, E. B., BRADY, S. W., TRIPATHI, A. & HOFFMAN-KIM, D. 2018. Schwann cell durotaxis can be guided by physiologically relevant stiffness gradients. Biomaterials Research, 22, 14.

FALKNER, S., GRADE, S., DIMOU, L., CONZELMANN, K. K., BONHOEFFER, T., GOTZ, M. & HUBENER, M. 2016. Transplanted embryonic neurons integrate into adult neocortical circuits. Nature, 539, 248-253.

FANSA, H., KEILHOFF, G., PLOGMEIER, K., FRERICHS, O., WOLF, G. & SCHNEIDER, W. 1999. Successful implantation of Schwann cells in acellular muscles. J Reconstr Microsurg, 15, 61-5.

FAZAL, S. V., GOMEZ-SANCHEZ, J. A., WAGSTAFF, L. J., MUSNER, N., OTTO, G., JANZ, M., MIRSKY, R. & JESSEN, K. R. 2017. Graded Elevation of c-Jun in Schwann Cells *In Vivo*: Gene Dosage Determines Effects on Development, Remyelination, Tumorigenesis, and Hypomyelination. J Neurosci, 37, 12297-12313.

FLACHSBARTH, K., KRUSZEWSKI, K., JUNG, G., JANKOWIAK, W., RIECKEN, K., WAGENFELD, L., RICHARD, G., FEHSE, B. & BARTSCH, U. 2014. Neural stem cell-based intraocular administration of ciliary neurotrophic factor attenuates the loss of axotomized ganglion cells in adult mice. Invest Ophthalmol Vis Sci, 55, 7029-39.

FOGLI, B., CORTHOUT, N., KERSTENS, A., BOSSE, F., KLIMASCHEWSKI, L., MUNCK, S. & SCHWEIGREITER, R. 2019. Imaging axon regeneration within synthetic nerve conduits. Sci Rep, 9, 10095.

FORNARO, M., MARCUS, D., RATTIN, J. & GORAL, J. 2021. Dynamic Environmental Physical Cues Activate Mechanosensitive Responses in the Repair Schwann Cell Phenotype. Cells, 10.

FORNASARI, B. E., EL SOURY, M., NATO, G., FUCINI, A., CARTA, G., RONCHI, G., CROSIO, A., PERROTEAU, I., GEUNA, S., RAIMONDO, S. & GAMBAROTTA, G. 2020. Fibroblasts Colonizing Nerve Conduits Express High Levels of Soluble Neuregulin1, a Factor Promoting Schwann Cell Dedifferentiation. Cells, 9.

FRAZIER, C., ANDERSON, D., WALL, M. E., SUMANASINGHE, R. & BANES, A. J. 2017. Quantification of strain at the membrane level. StageFlexer Tech Report, 4, Flexcell international corporation.

FU, S. Y. & GORDON, T. 1997. The cellular and molecular basis of peripheral nerve regeneration. Mol Neurobiol, 14, 67-116.

FUKAZAWA, T., MATSUMOTO, M., IMURA, T., KHALESI, E., KAJIUME, T., KAWAHARA, Y., TANIMOTO, K. & YUGE, L. 2013. Electrical stimulation accelerates neuromuscular junction formation through ADAM19/neuregulin/ErbB signaling *in vitro*. Neurosci Lett, 545, 29-34.

FUNG, Y. C. 1993. Biomechanics : mechanical properties of living tissues, New York, Springer-Verlag.

GALIE, P. A. & STEGEMANN, J. P. 2011. Simultaneous application of interstitial flow and cyclic mechanical strain to a three-dimensional cell-seeded hydrogel. Tissue Eng Part C Methods, 17, 527-36.

GAO, D. & CRITSER, J. K. 2000. Mechanisms of cryoinjury in living cells. ILAR J, 41, 187-96.

GEORGE, R. & GRIFFIN, J. W. 1994. Delayed macrophage responses and myelin clearance during Wallerian degeneration in the central nervous system: the dorsal radiculotomy model. Exp Neurol, 129, 225-36.

GEORGIOU, M., BUNTING, S. C., DAVIES, H. A., LOUGHLIN, A. J., GOLDING, J. P. & PHILLIPS, J. B. 2013. Engineered neural tissue for peripheral nerve repair. Biomaterials, 34, 7335-43.

GEORGIOU, M., GOLDING, J. P., LOUGHLIN, A. J., KINGHAM, P. J. & PHILLIPS, J. B. 2015. Engineered neural tissue with aligned, differentiated adipose-derived stem cells promotes peripheral nerve regeneration across a critical sized defect in rat sciatic nerve. Biomaterials, 37, 242-51.

GHAHARY, A., MCPHERSON, P. S. & CHENG, K. W. 1989. A serum factor inducing neurite retraction of morphologically differentiated neuroblastoma x glioma NG108-15 cells. J Cell Sci, 92 (Pt 2), 251-6.

GILMOUR, D., KNAUT, H., MAISCHEIN, H. M. & NUSSLEIN-VOLHARD, C. 2004. Towing of sensory axons by their migrating target cells *in vivo*. Nat Neurosci, 7, 491-2.

GINGRAS, M., GAGNON, V., MINOTTI, S., DURHAM, H. D. & BERTHOD, F. 2007. Optimized protocols for isolation of primary motor neurons, astrocytes and microglia from embryonic mouse spinal cord. J Neurosci Methods, 163, 111-8.

GLITSCH, M. D. 2008. Calcium influx through N-methyl-D-aspartate receptors triggers GABA release at interneuron-Purkinje cell synapse in rat cerebellum. Neuroscience, 151, 403-9.

GOMEZ-SANCHEZ, J. A., PILCH, K. S., VAN DER LANS, M., FAZAL, S. V., BENITO, C., WAGSTAFF, L. J., MIRSKY, R. & JESSEN, K. R. 2017. After Nerve Injury, Lineage Tracing Shows That Myelin and Remak Schwann Cells Elongate Extensively and Branch to Form Repair Schwann Cells, Which Shorten Radically on Remyelination. J Neurosci, 37, 9086-9099.

GONCALVES, M. B., BOYLE, J., WEBBER, D. J., HALL, S., MINGER, S. L. & CORCORAN, J. P. 2005. Timing of the retinoid-signalling pathway determines the expression of neuronal markers in neural progenitor cells. Dev Biol, 278, 60-70.

GOPARAJU, S. K., KOHDA, K., IBATA, K., SOMA, A., NAKATAKE, Y., AKIYAMA, T., WAKABAYASHI, S., MATSUSHITA, M., SAKOTA, M., KIMURA, H., YUZAKI, M., KO, S. B. & KO, M. S. 2017. Rapid differentiation of human pluripotent stem cells into functional neurons by mRNAs encoding transcription factors. Sci Rep, 7, 42367.

GORDON, J., AMINI, S. & WHITE, M. K. 2013. General overview of neuronal cell culture. Methods Mol Biol, 1078, 1-8.

GOTZ, M. & BOCCHI, R. 2021. Neuronal replacement: Concepts, achievements, and call for caution. Curr Opin Neurobiol, 69, 185-192.

GRABER, D. J. & HARRIS, B. T. 2013. Purification and culture of spinal motor neurons from rat embryos. Cold Spring Harb Protoc, 2013, 319-26.

GRECO, S. J. & RAMESHWAR, P. 2008. Microenvironmental considerations in the application of human mesenchymal stem cells in regenerative therapies. Biologics, 2, 699-705.

GRIFFIN, M. T., LAW, P. Y. & LOH, H. H. 1985. Neuroblastoma X glioma NG108-15 hybrid cells cultured in a serum-free chemically defined medium: effects on acute and chronic opiate regulation of adenylate cyclase activity. Brain Res, 360, 370-3.

GSTRAUNTHALER, G. 2003. Alternatives to the use of fetal bovine serum: serum-free cell culture. ALTEX, 20, 275-81.

GUENARD, V., KLEITMAN, N., MORRISSEY, T. K., BUNGE, R. P. & AEBISCHER, P. 1992. Syngeneic Schwann cells derived from adult nerves seeded in semipermeable

guidance channels enhance peripheral nerve regeneration. J Neurosci, 12, 3310-20.

GUTMANN, E. 1945. Functional regeneration of peripheral nerves. Notes Czechoslov Med Assoc G B, 49-57.

HADJIPANAYI, E., ANANTA, M., BINKOWSKI, M., STREETER, I., LU, Z., CUI, Z. F., BROWN, R. A. & MUDERA, V. 2011. Mechanisms of structure generation during plastic compression of nanofibrillar collagen hydrogel scaffolds: towards engineering of collagen. J Tissue Eng Regen Med, 5, 505-19.

HADLOCK, T., SUNDBACK, C., HUNTER, D., CHENEY, M. & VACANTI, J. P. 2000. A polymer foam conduit seeded with Schwann cells promotes guided peripheral nerve regeneration. Tissue Eng, 6, 119-27.

HAQ, F., KEITH, C. & ZHANG, G. 2006. Neurite development in PC12 cells on flexible micro-textured substrates under cyclic stretch. Biotechnol Prog, 22, 133-40.

HARKINS, J., ARSENAULT, M., SCHLESINGER, K. & KATES, J. 1972. Induction of neuronal functions: acetylcholine-induced acetylcholinesterase activity in mouse neuroblastoma cells. Proc Natl Acad Sci U S A, 69, 3161-4.

HEIDEMANN, S. R. & BRAY, D. 2015. Tension-driven axon assembly: a possible mechanism. Front Cell Neurosci, 9, 316.

HEO, Y. J., KAN, T., IWASE, E., MATSUMOTO, K. & SHIMOYAMA, I. 2013. Stretchable cell culture platforms using micropneumatic actuators. Micro & Nano Letters, 8, 865-868.

HODGES, H., POLLOCK, K., STROEMER, P., PATEL, S., STEVANATO, L., REUTER, I. & SINDEN, J. 2007. Making stem cell lines suitable for transplantation. Cell Transplant, 16, 101-15.

HONGPAISAN, J. 2000. Inhibition of proliferation of contaminating fibroblasts by D-valine in cultures of smooth muscle cells from human myometrium. Cell Biol Int, 24, 1-7.

HONKANEN, H., LAHTI, O., NISSINEN, M., MYLLYLA, R. M., KANGAS, S., PAIVALAINEN, S., ALANNE, M. H., PELTONEN, S., PELTONEN, J. & HEAPE, A. M. 2007. Isolation, purification and expansion of myelination-competent, neonatal mouse Schwann cells. Eur J Neurosci, 26, 953-64.

HUANG, G., LI, F., ZHAO, X., MA, Y., LI, Y., LIN, M., JIN, G., LU, T. J., GENIN, G. M. & XU, F. 2017. Functional and Biomimetic Materials for Engineering of the Three-Dimensional Cell Microenvironment. Chem Rev, 117, 12764-12850.

HUANG, J. H., CULLEN, D. K., BROWNE, K. D., GROFF, R., ZHANG, J., PFISTER, B. J., ZAGER, E. L. & SMITH, D. H. 2009. Long-term survival and integration of transplanted engineered nervous tissue constructs promotes peripheral nerve regeneration. Tissue Eng Part A, 15, 1677-85.

HUANG, Y. & NGUYEN, N. T. 2013. A polymeric cell stretching device for real-time imaging with optical microscopy. Biomed Microdevices, 15, 1043-54.

HUH, D., MATTHEWS, B. D., MAMMOTO, A., MONTOYA-ZAVALA, M., HSIN, H. Y. & INGBER, D. E. 2010. Reconstituting organ-level lung functions on a chip. Science, 328, 1662-8.

ISAACS, J. & BROWNE, T. 2014. Overcoming short gaps in peripheral nerve repair: conduits and human acellular nerve allograft. Hand (N Y), 9, 131-7.

ISAACS, J., MALLU, S., YAN, W. & LITTLE, B. 2014. Consequences of oversizing: nerve-to-nerve tube diameter mismatch. J Bone Joint Surg Am, 96, 1461-7.

JAIN, M., RAJAN, R., HYON, S. H. & MATSUMURA, K. 2014. Hydrogelation of dextran-based polyampholytes with cryoprotective properties via click chemistry. Biomater Sci, 2, 308-317.

JANG, T. H., PARK, S. C., YANG, J. H., KIM, J. Y., SEOK, J. H., PARK, U. S., CHOI, C. W., LEE, S. R. & HAN, J. 2017. Cryopreservation and its clinical applications. Integr Med Res, 6, 12-18.

JESSEN, K. R. & MIRSKY, R. 2008. Negative regulation of myelination: relevance for development, injury, and demyelinating disease. Glia, 56, 1552-65.

JESSEN, K. R. & MIRSKY, R. 2016. The repair Schwann cell and its function in regenerating nerves. J Physiol, 594, 3521-31.

JESSEN, K. R., MIRSKY, R. & LLOYD, A. C. 2015. Schwann Cells: Development and Role in Nerve Repair. Cold Spring Harb Perspect Biol, 7, a020487.

JGAMADZE, D., BERGEN, J., STONE, D., JANG, J. H., SCHAFFER, D. V., ISACOFF, E. Y. & PAUTOT, S. 2012. Colloids as mobile substrates for the implantation and

integration of differentiated neurons into the mammalian brain. PLoS One, 7, e30293.

JIANG, Y., WANG, Y. & TANG, G. 2016. Cyclic tensile strain promotes the osteogenic differentiation of a bone marrow stromal cell and vascular endothelial cell co-culture system. Arch Biochem Biophys, 607, 37-43.

JIN, Y. Q., LIU, W., HONG, T. H. & CAO, Y. 2008. Efficient Schwann cell purification by differential cell detachment using multiplex collagenase treatment. J Neurosci Methods, 170, 140-8.

KADOYAMA, K., TAKAHASHI, Y., HIGASHIDA, H., TANABE, T. & YOSHIMOTO, T. 2001. Cyclooxygenase-2 stimulates production of amyloid beta-peptide in neuroblastoma x glioma hybrid NG108-15 cells. Biochem Biophys Res Commun, 281, 483-90.

KAMBLE, H., BARTON, M. J., JUN, M., PARK, S. & NGUYEN, N. T. 2016. Cell stretching devices as research tools: engineering and biological considerations. Lab Chip, 16, 3193-203.

KANG, H., TIAN, L. & THOMPSON, W. 2003. Terminal Schwann cells guide the reinnervation of muscle after nerve injury. J Neurocytol, 32, 975-85.

KANG, N. U., LEE, S. J. & GWAK, S. J. 2022. Fabrication Techniques of Nerve Guidance Conduits for Nerve Regeneration. Yonsei Med J, 63, 114-123.

KAPPOS, E. A., ENGELS, P. E., TREMP, M., MEYER ZU SCHWABEDISSEN, M., DI SUMMA, P., FISCHMANN, A., VON FELTEN, S., SCHERBERICH, A., SCHAEFER, D. J. & KALBERMATTEN, D. F. 2015. Peripheral Nerve Repair: Multimodal Comparison of the Long-Term Regenerative Potential of Adipose Tissue-Derived Cells in a Biodegradable Conduit. Stem Cells Dev, 24, 2127-41.

KARABEKMEZ, F. E., DUYMAZ, A. & MORAN, S. L. 2009. Early clinical outcomes with the use of decellularized nerve allograft for repair of sensory defects within the hand. Hand (N Y), 4, 245-9.

KARIMI, M., BIAZAR, E., KESHEL, S. H., RONAGHI, A., DOOSTMOHAMADPOUR, J., JANFADA, A. & MONTAZERI, A. 2014. Rat sciatic nerve reconstruction across a 30 mm defect bridged by an oriented porous PHBV tube with Schwann cell as artificial nerve graft. ASAIO J, 60, 224-33.

KATIYAR, K. S., STRUZYNA, L. A., MORAND, J. P., BURRELL, J. C., CLEMENTS, B., LAIMO, F. A., BROWNE, K. D., KOHN, J., ALI, Z., LEDEBUR, H. C., SMITH, D. H.

& CULLEN, D. K. 2020. Tissue Engineered Axon Tracts Serve as Living Scaffolds to Accelerate Axonal Regeneration and Functional Recovery Following Peripheral Nerve Injury in Rats. Front Bioeng Biotechnol, 8, 492.

KATIYAR, K. S., WINTER, C. C., STRUZYNA, L. A., HARRIS, J. P. & CULLEN, D. K. 2016. Mechanical elongation of astrocyte processes to create living scaffolds for nervous system regeneration. J Tissue Eng Regen Med.

KELLY, E. J., JACOBY, C., TERENGHI, G., MENNEN, U., LJUNGBERG, C. & WIBERG, M. 2007. End-to-side nerve coaptation: a qualitative and quantitative assessment in the primate. J Plast Reconstr Aesthet Surg, 60, 1-12

KIM, H. S., SONG, M., KIM, E., RYU, S. H. & SUH, P. G. 2003. Dexamethasone differentiates NG108-15 cells through cyclooxygenase 1 induction. Exp Mol Med, 35, 203-10.

KIM, J. & KIM, H. A. 2018. Isolation and Expansion of Schwann Cells from Transgenic Mouse Models. Methods Mol Biol, 1739, 39-48.

KIM, S. M., LEE, S. K. & LEE, J. H. 2007. Peripheral nerve regeneration using a three dimensionally cultured schwann cell conduit. J Craniofac Surg, 18, 475-88.

KIM, Y. M., KANG, Y. G., PARK, S. H., HAN, M. K., KIM, J. H., SHIN, J. W. & SHIN, J. W. 2017. Effects of mechanical stimulation on the reprogramming of somatic cells into human-induced pluripotent stem cells. Stem Cell Res Ther, 8, 139.

KINGHAM, P. J., KALBERMATTEN, D. F., MAHAY, D., ARMSTRONG, S. J., WIBERG, M. & TERENGHI, G. 2007. Adipose-derived stem cells differentiate into a Schwann cell phenotype and promote neurite outgrowth *in vitro*. Exp Neurol, 207, 267-74.

KINGHAM, P. J., MANTOVANI, C. & TERENGHI, G. 2009. Notch independent signalling mediates Schwann cell-like differentiation of adipose derived stem cells. Neurosci Lett, 467, 164-8.

KOMIYAMA, T., NAKAO, Y., TOYAMA, Y., ASOU, H., VACANTI, C. A. & VACANTI, M. P. 2003. A novel technique to isolate adult Schwann cells for an artificial nerve conduit. J Neurosci Methods, 122, 195-200.

KOWTHA, V. C., BRYANT, H. J., KRAUTHAMER, V., IWASA, K. H. & STENGER, D. A. 1996. Spontaneous firing of NG108-15 cells induced by transient exposure to ammonium chloride. Cell Mol Neurobiol, 16, 1-9.

KOWTHA, V. C., QUONG, J. N., BRYANT, H. J. & STENGER, D. A. 1993. Comparative electrophysiological properties of NG108-15 cells in serum-containing and serum-free media. Neurosci Lett, 164, 129-33.

KRAMER, R., BUCAY, N., KANE, D. J., MARTIN, L. E., TARPLEY, J. E. & THEILL, L. E. 1996. Neuregulins with an Ig-like domain are essential for mouse myocardial and neuronal development. Proc Natl Acad Sci U S A, 93, 4833-8.

KRAUS, D., BOYLE, V., LEIBIG, N., STARK, G. B. & PENNA, V. 2015. The Neuro-spheroid--A novel 3D *in vitro* model for peripheral nerve regeneration. J Neurosci Methods, 246, 97-105.

KREUTZER, J., IKONEN, L., HIRVONEN, J., PEKKANEN-MATTILA, M., AALTO-SETALA, K. & KALLIO, P. 2014. Pneumatic cell stretching system for cardiac differentiation and culture. Med Eng Phys, 36, 496-501.

KRYSTOSEK, A. 1989. Conversion to the terminally differentiated state during treatment of NG108-15 neural tumor cells with 1-beta-D-arabinofuranosylcytosine in defined medium. Cancer Res, 49, 450-8.

KWIATKOWSKI, J. L., RUTKOWSKI, J. L., YAMASHIRO, D. J., TENNEKOON, G. I. & BRODEUR, G. M. 1998. Schwann cell-conditioned medium promotes neuroblastoma survival and differentiation. Cancer Res, 58, 4602-6.

LAGO, N., CASAS, C., MUIR, E. M., ROGERS, J. & NAVARRO, X. 2009. Effects of Schwann cell transplants in an experimental nerve amputee model. Restor Neurol Neurosci, 27, 67-78.

LAMOUREUX, P., RUTHEL, G., BUXBAUM, R. E. & HEIDEMANN, S. R. 2002. Mechanical tension can specify axonal fate in hippocampal neurons. Journal of Cell Biology, 159, 499-508.

LAMOUREUX, P., ZHENG, J., BUXBAUM, R. E. & HEIDEMANN, S. R. 1992. A cytomechanical investigation of neurite growth on different culture surfaces. J Cell Biol, 118, 655-61.

LANGLEY, J. N. & ANDERSON, H. K. 1904. On autogenetic regeneration in the nerves of the limbs. J Physiol, 31, 418-28.

LEBLANC, S. E., SRINIVASAN, R., FERRI, C., MAGER, G. M., GILLIAN-DANIEL, A. L., WRABETZ, L. & SVAREN, J. 2005. Regulation of cholesterol/lipid biosynthetic

genes by Egr2/Krox20 during peripheral nerve myelination. J Neurochem, 93, 737-48.

LEE, D. C., CHEN, J. H., HSU, T. Y., CHANG, L. H., CHANG, H., CHI, Y. H. & CHIU, I. M. 2017. Neural stem cells promote nerve regeneration through IL12-induced Schwann cell differentiation. Mol Cell Neurosci, 79, 1-11.

LEE, H., SHAMY, G. A., ELKABETZ, Y., SCHOFIELD, C. M., HARRSION, N. L., PANAGIOTAKOS, G., SOCCI, N. D., TABAR, V. & STUDER, L. 2007. Directed differentiation and transplantation of human embryonic stem cell-derived motoneurons. Stem Cells, 25, 1931-9.

LEE, J. Y., GIUSTI, G., FRIEDRICH, P. F., ARCHIBALD, S. J., KEMNITZER, J. E., PATEL, J., DESAI, N., BISHOP, A. T. & SHIN, A. Y. 2012. The effect of collagen nerve conduits filled with collagen-glycosaminoglycan matrix on peripheral motor nerve regeneration in a rat model. J Bone Joint Surg Am, 94, 2084-91.

LEE, S. L., NEKOUZADEH, A., BUTLER, B., PRYSE, K. M., MCCONNAUGHEY, W. B., NATHAN, A. C., LEGANT, W. R., SCHAEFER, P. M., PLESS, R. B., ELSON, E. L. & GENIN, G. M. 2012. Physically-induced cytoskeleton remodeling of cells in three-dimensional culture. PLoS One, 7, e45512.

LEE, Y. S., WU, S., ARINZEH, T. L. & BUNGE, M. B. 2017. Transplantation of Schwann Cells Inside PVDF-TrFE Conduits to Bridge Transected Rat Spinal Cord Stumps to Promote Axon Regeneration Across the Gap. J Vis Exp.

LEMES, J. B. P., DE CAMPOS LIMA, T., SANTOS, D. O., NEVES, A. F., DE OLIVEIRA, F. S., PARADA, C. A. & DA CRUZ LOTUFO, C. M. 2018. Participation of satellite glial cells of the dorsal root ganglia in acute nociception. Neurosci Lett, 676, 8-12.

LESTANOVA, Z., BACOVA, Z., KISS, A., HAVRANEK, T., STRBAK, V. & BAKOS, J. 2016. Oxytocin Increases Neurite Length and Expression of Cytoskeletal Proteins Associated with Neuronal Growth. J Mol Neurosci, 59, 184-92.

LEVENTAL, I., GEORGES, P. C. & JANMEY, P. A. 2007. Soft biological materials and their impact on cell function. Soft Matter, 3, 299-306.

LEVI, A. D., BURKS, S. S., ANDERSON, K. D., DIDIDZE, M., KHAN, A. & DIETRICH, W. D. 2016. The Use of Autologous Schwann Cells to Supplement Sciatic Nerve Repair With a Large Gap: First in Human Experience. Cell Transplant, 25, 1395-403.

LI, X., XU, Q., WANG, Y., CHEN, F. & HE, J. 2016. Development of a new miniaturized bioreactor for axon stretch growth. J Integr Neurosci, 15, 365-380.

LI, Y., YU, Z., MEN, Y., CHEN, X. & WANG, B. 2018. Laminin-chitosan-PLGA conduit co-transplanted with Schwann and neural stem cells to repair the injured recurrent laryngeal nerve. Exp Ther Med, 16, 1250-1258.

LIU, B., QU, M. J., QIN, K. R., LI, H., LI, Z. K., SHEN, B. R. & JIANG, Z. L. 2008. Role of cyclic strain frequency in regulating the alignment of vascular smooth muscle cells *in vitro*. Biophys J, 94, 1497-507.

LIU, B., XIN, W., TAN, J. R., ZHU, R. P., LI, T., WANG, D., KAN, S. S., XIONG, D. K., LI, H. H., ZHANG, M. M., SUN, H. H., WAGSTAFF, W., ZHOU, C., WANG, Z. J., ZHANG, Y. G. & HE, T. C. 2019. Myelin sheath structure and regeneration in peripheral nerve injury repair. Proc Natl Acad Sci U S A, 116, 22347-22352.

LIU, W., REN, Y., BOSSERT, A., WANG, X., DAYAWANSA, S., TONG, J., HE, X., SMITH, D. H., GELBARD, H. A. & HUANG, J. H. 2012. Allotransplanted neurons used to repair peripheral nerve injury do not elicit overt immunogenicity. PLoS One, 7, e31675.

LIU, W., YIN, L., YAN, X., CUI, J., LIU, W., RAO, Y., SUN, M., WEI, Q. & CHEN, F. 2017. Directing the Differentiation of Parthenogenetic Stem Cells into Tenocytes for Tissue-Engineered Tendon Regeneration. Stem Cells Transl Med, 6, 196-208.

LOPERENA, R. & HARRISON, D. G. 2017. Oxidative Stress and Hypertensive Diseases. Med Clin North Am, 101, 169-193.

LORSCH, J. R., COLLINS, F. S. & LIPPINCOTT-SCHWARTZ, J. 2014. Cell Biology. Fixing problems with cell lines. Science, 346, 1452-3.

LOVERDE, J. R. & PFISTER, B. J. 2015. Developmental axon stretch stimulates neuron growth while maintaining normal electrical activity, intracellular calcium flux, and somatic morphology. Front Cell Neurosci, 9, 308.

LOVERDE, J. R., OZOKA, V. C., AQUINO, R., LIN, L. & PFISTER, B. J. 2011a. Live Imaging of Axon Stretch Growth in Embryonic and Adult Neurons. Journal of Neurotrauma, 28, 2389-2403.

LOVERDE, J. R., TOLENTINO, R. E. & PFISTER, B. J. 2011b. Axon stretch growth: the mechanotransduction of neuronal growth. J Vis Exp.

LOZANO, A. M., SCHMIDT, M. & ROACH, A. 1995. A convenient *in vitro* assay for the inhibition of neurite outgrowth by adult mammalian CNS myelin using immortalized neuronal cells. J Neurosci Methods, 63, 23-8.

LU, P., JONES, L. L., SNYDER, E. Y. & TUSZYNSKI, M. H. 2003. Neural stem cells constitutively secrete neurotrophic factors and promote extensive host axonal growth after spinal cord injury. Exp Neurol, 181, 115-29.

LU, S. J., LEE, R. J., NAPOLI, C., OH, S., KIMBREL, E. A. & FENG, Q. 2011. The Promise and Therapeutic Potential of Human ES and iPS Cells. Stem Cells Int, 2011, 959275.

LU, Y. B., FRANZE, K., SEIFERT, G., STEINHAUSER, C., KIRCHHOFF, F., WOLBURG, H., GUCK, J., JANMEY, P., WEI, E. Q., KAS, J. & REICHENBACH, A. 2006. Viscoelastic properties of individual glial cells and neurons in the CNS. Proc Natl Acad Sci U S A, 103, 17759-64.

M, F. G., M, M., S, H. & KHAN, W. S. 2014. Peripheral nerve injury: principles for repair and regeneration. Open Orthop J, 8, 199-203.

MACDONALD, S. C., FLEETWOOD, I. G., HOCHMAN, S., DODD, J. G., CHENG, G. K., JORDAN, L. M. & BROWNSTONE, R. M. 2003. Functional motor neurons differentiating from mouse multipotent spinal cord precursor cells in culture and after transplantation into transected sciatic nerve. J Neurosurg, 98, 1094-103.

MACKINNON, S. E. 1989. New directions in peripheral nerve surgery. Ann Plast Surg, 22, 257-73.

MAGGIORE, J. C., BURRELL, J. C., BROWNE, K. D., KATIYAR, K. S., LAIMO, F. A., ALI, Z. S., KAPLAN, H. M., ROSEN, J. M. & CULLEN, D. K. 2020. Tissue engineered axon-based "living scaffolds" promote survival of spinal cord motor neurons following peripheral nerve repair. J Tissue Eng Regen Med, 14, 1892-1907.

MAHMOOD ALABED, E. A., ENGEL, M., YAMAUCHI, Y., HOSSAIN, M. S. A., & OOI, L. 2019. DC and AC magnetic fields increase neurite outgrowth of SH-SY5Y neuroblastoma cells with and without retinoic acid. RSC Advances, 9, no. 31, 17717-17725. https://doi.org/10.1039/c9ra02001b

MANENT, J., OGUIEVETSKAIA, K., BAYER, J., RATNER, N. & GIOVANNINI, M. 2003. Magnetic cell sorting for enriching Schwann cells from adult mouse peripheral nerves. J Neurosci Methods, 123, 167-73.

MARELLI, B., GHEZZI, C. E., JAMES-BHASIN, M. & NAZHAT, S. N. 2015. Fabrication of injectable, cellular, anisotropic collagen tissue equivalents with modular fibrillar densities. Biomaterials, 37, 183-93.

MARTENS, W., SANEN, K., GEORGIOU, M., STRUYS, T., BRONCKAERS, A., AMELOOT, M., PHILLIPS, J. & LAMBRICHTS, I. 2014. Human dental pulp stem cells can differentiate into Schwann cells and promote and guide neurite outgrowth in an aligned tissue-engineered collagen construct *in vitro*. FASEB J, 28, 1634-43.

MARTINI, R., FISCHER, S., LOPEZ-VALES, R. & DAVID, S. 2008. Interactions between Schwann cells and macrophages in injury and inherited demyelinating disease. Glia, 56, 1566-77.

MATSUSE, D., KITADA, M., KOHAMA, M., NISHIKAWA, K., MAKINOSHIMA, H., WAKAO, S., FUJIYOSHI, Y., HEIKE, T., NAKAHATA, T., AKUTSU, H., UMEZAWA, A., HARIGAE, H., KIRA, J. & DEZAWA, M. 2010. Human umbilical cord-derived mesenchymal stromal cells differentiate into functional Schwann cells that sustain peripheral nerve regeneration. J Neuropathol Exp Neurol, 69, 973-85.

MATSUSHITA, K., WANG, W., ITOH, S., DOMON, T., FUNAHASHI, M. & TOTSUKA, Y. 2012. Dental pulp can be a good candidate for nerve grafting in a xeno-graft model. J Neurosci Methods, 205, 246-51.

MATURANA, L. G., ZANON, R. G., PIERUCCI, A., VIDAL, B. C. & OLIVEIRA, A. L. 2011. Supraorganized collagen enhances Schwann cell reactivity and organization *in vitro*. Braz J Med Biol Res, 44, 682-7.

MAURITZ, C., GROTHE, C. & HAASTERT, K. 2004. Comparative study of cell culture and purification methods to obtain highly enriched cultures of proliferating adult rat Schwann cells. J Neurosci Res, 77, 453-61.

MAURY, Y., COME, J., PISKOROWSKI, R. A., SALAH-MOHELLIBI, N., CHEVALEYRE, V., PESCHANSKI, M., MARTINAT, C. & NEDELEC, S. 2015. Combinatorial analysis of developmental cues efficiently converts human pluripotent stem cells into multiple neuronal subtypes. Nat Biotechnol, 33, 89-96.

MAY, F., BUCHNER, A., MATIASEK, K., SCHLENKER, B., STIEF, C. & WEIDNER, N. 2016. Recovery of erectile function comparing autologous nerve grafts, unseeded conduits, Schwann-cell-seeded guidance tubes and GDNF-overexpressing Schwann cell grafts. Dis Model Mech, 9, 1507-1511.

MAZZUOLI-WEBER, G. & SCHEMANN, M. 2015. Mechanosensitivity in the enteric nervous system. Front Cell Neurosci, 9, 408.

MCGRATH, A. M., NOVIKOVA, L. N., NOVIKOV, L. N. & WIBERG, M. 2010. BD PuraMatrix peptide hydrogel seeded with Schwann cells for peripheral nerve regeneration. Brain Res Bull, 83, 207-13.

MEINERS, S., MERCADO, M. L., NUR-E-KAMAL, M. S. & GELLER, H. M. 1999. Tenascin-C contains domains that independently regulate neurite outgrowth and neurite guidance. J Neurosci, 19, 8443-53.

MEYER, C., STENBERG, L., GONZALEZ-PEREZ, F., WROBEL, S., RONCHI, G., UDINA, E., SUGANUMA, S., GEUNA, S., NAVARRO, X., DAHLIN, L. B., GROTHE, C. & HAASTERT-TALINI, K. 2016. Chitosan-film enhanced chitosan nerve guides for long-distance regeneration of peripheral nerves. Biomaterials, 76, 33-51.

MEYER, D., YAMAAI, T., GARRATT, A., RIETHMACHER-SONNENBERG, E., KANE, D., THEILL, L. E. & BIRCHMEIER, C. 1997. Isoform-specific expression and function of neuregulin. Development, 124, 3575-86.

MIHIC, A., LI, J., MIYAGI, Y., GAGLIARDI, M., LI, S. H., ZU, J., WEISEL, R. D., KELLER, G. & LI, R. K. 2014. The effect of cyclic stretch on maturation and 3D tissue formation of human embryonic stem cell-derived cardiomyocytes. Biomaterials, 35, 2798-808.

MIN, Q., PARKINSON, D. B. & DUN, X. P. 2021. Migrating Schwann cells direct axon regeneration within the peripheral nerve bridge. Glia, 69, 235-254.

MIRFEIZI, L., STRATTON, J. A., KUMAR, R., SHAH, P., AGABALYAN, N., STYKEL, M. G., MIDHA, R., BIERNASKIE, J. & KALLOS, M. S. 2017. Serum-free bioprocessing of adult human and rodent skin-derived Schwann cells: implications for cell therapy in nervous system injury. J Tissue Eng Regen Med, 11, 3385-3397.

MISHRA, A. K., CAMPANALE, J. P., MONDO, J. A. & MONTELL, D. J. 2019. Cell interactions in collective cell migration. Development, 146.

MOHAMMADI, R., AZIZI, S., DELIREZH, N., HOBBENAGHI, R., AMINI, K. & MALEKKHETABI, P. 2012. The use of undifferentiated bone marrow stromal cells for sciatic nerve regeneration in rats. Int J Oral Maxillofac Surg, 41, 650-6.

MOKARRAM, N. & BELLAMKONDA, R. V. 2011. Overcoming endogenous constraints on neuronal regeneration. IEEE Trans Biomed Eng, 58, 1900-6.

MOKARRAM, N., MERCHANT, A., MUKHATYAR, V., PATEL, G. & BELLAMKONDA, R. V. 2012. Effect of modulating macrophage phenotype on peripheral nerve repair. Biomaterials, 33, 8793-801.

MORRISSEY, T. K., KLEITMAN, N. & BUNGE, R. P. 1991. Isolation and functional characterization of Schwann cells derived from adult peripheral nerve. J Neurosci, 11, 2433-42.

MOSAHEBI, A., WIBERG, M. & TERENGHI, G. 2003. Addition of fibronectin to alginate matrix improves peripheral nerve regeneration in tissue-engineered conduits. Tissue Eng, 9, 209-18.

MOSSER, D. M. & EDWARDS, J. P. 2008. Exploring the full spectrum of macrophage activation. Nat Rev Immunol, 8, 958-69.

MOUTINHO, V., D'ANGELICA, M. & KINGHAM, P. 2017. Chapter 98D - Cryotherapy and ethanol injection. In: JARNAGIN, W. R. (ed.) Blumgart's surgery of the liver, biliary tract, and pancreas. Sixth edition. ed.

MUANGSANIT, P., DAY, A., DIMIOU, S., ATAC, A. F., KAYAL, C., PARK, H., NAZHAT, S. N. & PHILLIPS, J. B. 2020. Rapidly formed stable and aligned dense collagen gels seeded with Schwann cells support peripheral nerve regeneration. J Neural Eng, 17, 046036.

MUANGSANIT, P., ROBERTON, V., COSTA, E. & PHILLIPS, J. B. 2021. Engineered aligned endothelial cell structures in tethered collagen hydrogels promote peripheral nerve regeneration. Acta Biomater, 126, 224-237.

MUDERA, V. C., PLEASS, R., EASTWOOD, M., TARNUZZER, R., SCHULTZ, G., KHAW, P., MCGROUTHER, D. A. & BROWN, R. A. 2000. Molecular responses of human dermal fibroblasts to dual cues: contact guidance and mechanical load. Cell Motil Cytoskeleton, 45, 1-9.

NAMGUNG, U. 2014. The role of Schwann cell-axon interaction in peripheral nerve regeneration. Cells Tissues Organs, 200, 6-12.

NASCIMENTO, D. S., CASTRO-LOPES, J. M. & MOREIRA NETO, F. L. 2014. Satellite glial cells surrounding primary afferent neurons are activated and proliferate during monoarthritis in rats: is there a role for ATF3? PLoS One, 9, e108152.

NHS ENGLAND AND NHS IMPROVEMENT. (2020). NHS Diagnostic Waiting Times and Activity Data, September 2020 Monthly Report. [online] NHS England. Available at:

https://www.england.nhs.uk/statistics/wp-content/uploads/sites/2/2020/12/DWTA-Report-October-2020.pdf [Accessed 04/01/22].

NIRMALANANDHAN, V. S., LEVY, M. S., HUTH, A. J. & BUTLER, D. L. 2006. Effects of cell seeding density and collagen concentration on contraction kinetics of mesenchymal stem cell-seeded collagen constructs. Tissue Eng, 12, 1865-72.

O'MALLEY, J. P., WARAN, M. T. & BALICE-GORDON, R. J. 1999. *In vivo* observations of terminal Schwann cells at normal, denervated, and reinnervated mouse neuromuscular junctions. J Neurobiol, 38, 270-86.

O'ROURKE, C., DAY, A. G. E., MURRAY-DUNNING, C., THANABALASUNDARAM, L., COWAN, J., STEVANATO, L., GRACE, N., CAMERON, G., DRAKE, R. A. L., SINDEN, J. & PHILLIPS, J. B. 2018. An allogeneic 'off the shelf' therapeutic strategy for peripheral nerve tissue engineering using clinical grade human neural stem cells. Sci Rep, 8, 2951.

O'ROURKE, C., DRAKE, R. A., CAMERON, G. W., LOUGHLIN, A. J. & PHILLIPS, J. B. 2015. Optimising contraction and alignment of cellular collagen hydrogels to achieve reliable and consistent engineered anisotropic tissue. J Biomater Appl, 30, 599-607.

O'TOOLE, M., LAMOUREUX, P. & MILLER, K. E. 2008. A physical model of axonal elongation: force, viscosity, and adhesions govern the mode of outgrowth. Biophys J, 94, 2610-20.

PALAZZOLO, G., HORVATH, P. & ZENOBI-WONG, M. 2012. The flavonoid isoquercitrin promotes neurite elongation by reducing RhoA activity. PLoS One, 7, e49979.

PAN, C., KUMAR, C., BOHL, S., KLINGMUELLER, U. & MANN, M. 2009. Comparative proteomic phenotyping of cell lines and primary cells to assess preservation of cell type-specific functions. Mol Cell Proteomics, 8, 443-50.

PANG, Q., ZU, J. W., SIU, G. M. & LI, R. K. 2010. Design and development of a novel biostretch apparatus for tissue engineering. J Biomech Eng, 132, 014503.

PARK, B. W., KANG, D. H., KANG, E. J., BYUN, J. H., LEE, J. S., MAENG, G. H. & RHO, G. J. 2012. Peripheral nerve regeneration using autologous porcine skin-derived mesenchymal stem cells. J Tissue Eng Regen Med, 6, 113-24.

PARRINELLO, S., NAPOLI, I., RIBEIRO, S., WINGFIELD DIGBY, P., FEDOROVA, M., PARKINSON, D. B., DODDRELL, R. D., NAKAYAMA, M., ADAMS, R. H. & LLOYD,

A. C. 2010. EphB signaling directs peripheral nerve regeneration through Sox2-dependent Schwann cell sorting. Cell, 143, 145-55.

PAVIOLO, C., HAYCOCK, J. W., YONG, J., YU, A., STODDART, P. R. & MCARTHUR, S. L. 2013. Laser exposure of gold nanorods can increase neuronal cell outgrowth. Biotechnol Bioeng, 110, 2277-91.

PEARSE, D. D., BASTIDAS, J., IZABEL, S. S. & GHOSH, M. 2018. Schwann Cell Transplantation Subdues the Pro-Inflammatory Innate Immune Cell Response after Spinal Cord Injury. Int J Mol Sci, 19.

PEDROSA, S. S., CASEIRO, A. R., SANTOS, J. D., MAURÍCIO, A. C. 2017. 'Scaffolds for Peripheral Nerve Regeneration, the Importance of *In Vitro* and *In Vivo* Studies for the Development of Cell-Based Therapies and Biomaterials: State of the Art', in F. Baino (ed.), Scaffolds in Tissue Engineering - Materials, Technologies and Clinical Applications, IntechOpen, London. 10.5772/intechopen.69540.PFISTER, B. J., GORDON, T., LOVERDE, J. R., KOCHAR, A. S., MACKINNON, S. E. & CULLEN, D. K. 2011. Biomedical engineering strategies for peripheral nerve repair: surgical applications, state of the art, and future challenges. *Crit Rev Biomed Eng,* 39, 81-124.

PFISTER, B. J., HUANG, J. H., KAMESWARAN, N., ZAGER, E. L. & SMITH, D. H. 2007. Neural engineering to produce *in vitro* nerve constructs and neurointerface. Neurosurgery, 60, 137-41; discussion 141-2.

PFISTER, B. J., IWATA, A., MEANEY, D. F. & SMITH, D. H. 2004. Extreme stretch growth of integrated axons. J Neurosci, 24, 7978-83.

PHILLIPS, J. B. & BROWN, R. 2011. Micro-structured materials and mechanical cues in 3D collagen gels. Methods Mol Biol, 695, 183-96.

PHILLIPS, J. B., BUNTING, S. C., HALL, S. M. & BROWN, R. A. 2005. Neural tissue engineering: a self-organizing collagen guidance conduit. Tissue Eng, 11, 1611-7.

POLLEUX, F. & SNIDER, W. 2010. Initiating and growing an axon. Cold Spring Harb Perspect Biol, 2, a001925.

PRAGER-KHOUTORSKY, M. & SPIRA, M. E. 2009. Neurite retraction and regrowth regulated by membrane retrieval, membrane supply, and actin dynamics. Brain Res, 1251, 65-79.

PUROHIT, P. K. & SMITH, D. H. 2016. A model for stretch growth of neurons. Journal of Biomechanics, 49, 3934-3942.

QUIGLEY, A. F., BULLUSS, K. J., KYRATZIS, I. L., GILMORE, K., MYSORE, T., SCHIRMER, K. S., KENNEDY, E. L., O'SHEA, M., TRUONG, Y. B., EDWARDS, S. L., PEETERS, G., HERWIG, P., RAZAL, J. M., CAMPBELL, T. E., LOWES, K. N., HIGGINS, M. J., MOULTON, S. E., MURPHY, M. A., COOK, M. J., CLARK, G. M., WALLACE, G. G. & KAPSA, R. M. 2013. Engineering a multimodal nerve conduit for repair of injured peripheral nerve. J Neural Eng, 10, 016008.

RAIVICH, G. & KREUTZBERG, G. W. 1993. Peripheral nerve regeneration: role of growth factors and their receptors. Int J Dev Neurosci, 11, 311-24.

RAJAGOPALAN, J., TOFANGCHI, A. & MT, A. S. 2010. Drosophila neurons actively regulate axonal tension *in vivo*. Biophys J, 99, 3208-15.

RAMON-CUETO, A., PLANT, G. W., AVILA, J. & BUNGE, M. B. 1998. Long-distance axonal regeneration in the transected adult rat spinal cord is promoted by olfactory ensheathing glia transplants. J Neurosci, 18, 3803-15.

RAYNER, M. L. D., LARANJEIRA, S., EVANS, R. E., SHIPLEY, R. J., HEALY, J. & PHILLIPS, J. B. 2018. Developing an *In Vitro* Model to Screen Drugs for Nerve Regeneration. Anat Rec (Hoboken), 301, 1628-1637.

RECKNOR, J. B., SAKAGUCHI, D. S. & MALLAPRAGADA, S. K. 2006. Directed growth and selective differentiation of neural progenitor cells on micropatterned polymer substrates. Biomaterials, 27, 4098-108.

REDDEN, R. A. & DOOLIN, E. J. 2003. Collagen crosslinking and cell density have distinct effects on fibroblast-mediated contraction of collagen gels. Skin Res Technol, 9, 290-3.

RIBEIRO-RESENDE, V. T., KOENIG, B., NICHTERWITZ, S., OBERHOFFNER, S. & SCHLOSSHAUER, B. 2009. Strategies for inducing the formation of bands of Bungner in peripheral nerve regeneration. Biomaterials, 30, 5251-9.

RICHNER, M., ULRICHSEN, M., ELMEGAARD, S. L., DIEU, R., PALLESEN, L. T. & VAEGTER, C. B. 2014. Peripheral nerve injury modulates neurotrophin signaling in the peripheral and central nervous system. Mol Neurobiol, 50, 945-70.

RIEHL, B. D., PARK, J. H., KWON, I. K. & LIM, J. Y. 2012. Mechanical stretching for tissue engineering: two-dimensional and three-dimensional constructs. Tissue Eng Part B Rev, 18, 288-300.

RINOLDI, C., COSTANTINI, M., KIJENSKA-GAWRONSKA, E., TESTA, S., FORNETTI, E., HELJAK, M., CWIKLINSKA, M., BUDA, R., BALDI, J., CANNATA, S., GUZOWSKI, J., GARGIOLI, C., KHADEMHOSSEINI, A. & SWIESZKOWSKI, W. 2019. Tendon Tissue Engineering: Effects of Mechanical and Biochemical Stimulation on Stem Cell Alignment on Cell-Laden Hydrogel Yarns. Adv Healthc Mater, 8, e1801218.

ROSNER, B. I., HANG, T. & TRANQUILLO, R. T. 2005. Schwann cell behavior in three-dimensional collagen gels: evidence for differential mechano-transduction and the influence of TGF-beta 1 in morphological polarization and differentiation. Exp Neurol, 195, 81-91.

ROSSI, S. L., NISTOR, G., WYATT, T., YIN, H. Z., POOLE, A. J., WEISS, J. H., GARDENER, M. J., DIJKSTRA, S., FISCHER, D. F. & KEIRSTEAD, H. S. 2010. Histological and functional benefit following transplantation of motor neuron progenitors to the injured rat spinal cord. PLoS One, 5, e11852.

ROSSO, G., LIASHKOVICH, I., GESS, B., YOUNG, P., KUN, A. & SHAHIN, V. 2014. Unravelling crucial biomechanical resilience of myelinated peripheral nerve fibres provided by the Schwann cell basal lamina and PMP22. Sci Rep, 4, 7286.

ROTH, K. B., NEEVES, K. B., SQUIER, J. & MARR, D. W. 2015. Imaging of a linear diode bar for an optical cell stretcher. Biomed Opt Express, 6, 807-14.

SANEN, K., MARTENS, W., GEORGIOU, M., AMELOOT, M., LAMBRICHTS, I. & PHILLIPS, J. 2017. Engineered neural tissue with Schwann cell differentiated human dental pulp stem cells: potential for peripheral nerve repair? J Tissue Eng Regen Med, 11, 3362-3372.

SANTIAGO-TOLEDO, G., GEORGIOU, M., DOS REIS, J., ROBERTON, V. H., VALINHAS, A., WOOD, R. C., PHILLIPS, J. B., MASON, C., LI, D., LI, Y., SINDEN, J. D., CHOI, D., JAT, P. S. & WALL, I. B. 2019. Generation of c-MycER(TAM)-transduced human late-adherent olfactory mucosa cells for potential regenerative applications. Sci Rep, 9, 13190.

SCHNEIDER, C. A., RASBAND, W. S. & ELICEIRI, K. W. 2012. NIH Image to ImageJ: 25 years of image analysis. Nat Methods, 9, 671-5.

SEDDON, H. J. 1942. A Classification of Nerve Injuries. Br Med J, 2, 237-9.

SHAO, Y., MANN, J. M., CHEN, W. & FU, J. 2014. Global architecture of the F-actin cytoskeleton regulates cell shape-dependent endothelial mechanotransduction. Integr Biol (Camb), 6, 300-11.

SHEA, J. E., GARLICK, J. W., SALAMA, M. E., MENDENHALL, S. D., MORAN, L. A. & AGARWAL, J. P. 2014. Side-to-side nerve bridges reduce muscle atrophy after peripheral nerve injury in a rodent model. J Surg Res, 187, 350-8.

SHEU, J. Y., KULHANEK, D. J. & ECKENSTEIN, F. P. 2000. Differential patterns of ERK and STAT3 phosphorylation after sciatic nerve transection in the rat. Exp Neurol, 166, 392-402.

SHIMIZU, K., SHUNORI, A., MORIMOTO, K., HASHIDA, M. & KONISHI, S. 2011. Development of a biochip with serially connected pneumatic balloons for cell-stretching culture. Sensors and Actuators B: Chemical, 156, 486-493.

SHULTZ, R. B., KATIYAR, K. S., LAIMO, F. A., BURRELL, J. C., BROWNE, K. D., ALI, Z. S. & CULLEN, D. K. 2021. Biopreservation of living tissue engineered nerve grafts. J Tissue Eng, 12, 20417314211032488.

SHVARTSMAN, D., STORRIE-WHITE, H., LEE, K., KEARNEY, C., BRUDNO, Y., HO, N., CEZAR, C., MCCANN, C., ANDERSON, E., KOULLIAS, J., TAPIA, J. C., VANDENBURGH, H., LICHTMAN, J. W. & MOONEY, D. J. 2014. Sustained delivery of VEGF maintains innervation and promotes reperfusion in ischemic skeletal muscles via NGF/GDNF signaling. Mol Ther, 22, 1243-1253.

SIEMIONOW, M. & BRZEZICKI, G. 2009. Chapter 8: Current techniques and concepts in peripheral nerve repair. Int Rev Neurobiol, 87, 141-72.

SINIS, N., SCHALLER, H. E., SCHULTE-EVERSUM, C., SCHLOSSHAUER, B., DOSER, M., DIETZ, K., ROSNER, H., MULLER, H. W. & HAERLE, M. 2005. Nerve regeneration across a 2-cm gap in the rat median nerve using a resorbable nerve conduit filled with Schwann cells. J Neurosurg, 103, 1067-76.

SMALHEISER, N. R. 1989. Analysis of slow-onset neurite formation in NG108-15 cells: implications for a unified model of neurite elongation. Brain Res Dev Brain Res, 45, 49-57.

SMITH, D. H., WOLF, J. A. & MEANEY, D. F. 2001. A new strategy to produce sustained growth of central nervous system axons: continuous mechanical tension. Tissue Eng, 7, 131-9.

SOPHER, R. S., TOKASH, H., NATAN, S., SHARABI, M., SHELAH, O., TCHAICHEEYAN, O. & LESMAN, A. 2018. Nonlinear Elasticity of the ECM Fibers Facilitates Efficient Intercellular Communication. Biophys J, 115, 1357-1370.

SORRELL, J. M. & CAPLAN, A. I. 2009. Fibroblasts-a diverse population at the center of it all. Int Rev Cell Mol Biol, 276, 161-214.

SPIEGEL, I. & PELES, E. 2009. A novel method for isolating Schwann cells using the extracellular domain of Necl1. J Neurosci Res, 87, 3288-96.

STEVANATO, L., HICKS, C. & SINDEN, J. D. 2015. Differentiation of a Human Neural Stem Cell Line on Three Dimensional Cultures, Analysis of MicroRNA and Putative Target Genes. J Vis Exp.

STEWART, H. J., TURNER, D., JESSEN, K. R. & MIRSKY, R. 1997. Expression and regulation of alpha1beta1 integrin in Schwann cells. J Neurobiol, 33, 914-28.

STRATTON, J. A. & SHAH, P. T. 2016. Macrophage polarization in nerve injury: do Schwann cells play a role? Neural Regen Res, 11, 53-7.

STRATTON, J. A., SHAH, P. T., KUMAR, R., STYKEL, M. G., SHAPIRA, Y., GROCHMAL, J., GUO, G. F., BIERNASKIE, J. & MIDHA, R. 2016. The immunomodulatory properties of adult skin-derived precursor Schwann cells: implications for peripheral nerve injury therapy. Eur J Neurosci, 43, 365-75.

STRAUCH, B., RODRIGUEZ, D. M., DIAZ, J., YU, H. L., KAPLAN, G. & WEINSTEIN, D. E. 2001. Autologous Schwann cells drive regeneration through a 6-cm autogenous venous nerve conduit. J Reconstr Microsurg, 17, 589-95; discussion 596-7.

STRUZYNA, L. A., HARRIS, J. P., KATIYAR, K. S., CHEN, H. I. & CULLEN, D. K. 2015. Restoring nervous system structure and function using tissue engineered living scaffolds. Neural Regen Res, 10, 679-85.

STRUZYNA, L. A., WOLF, J. A., MIETUS, C. J., ADEWOLE, D. O., CHEN, H. I., SMITH, D. H. & CULLEN, D. K. 2015. Rebuilding Brain Circuitry with Living Micro-Tissue Engineered Neural Networks. Tissue Eng Part A, 21, 2744-56.

SUDHOF, T. C. 2012. Calcium control of neurotransmitter release. Cold Spring Harb Perspect Biol, 4, a011353.

SUTER, D. M. & MILLER, K. E. 2011. The emerging role of forces in axonal elongation. Progress in Neurobiology, 94, 91-101.

SUTO, K., URABE, K., NARUSE, K., UCHIDA, K., MATSUURA, T., MIKUNI-TAKAGAKI, Y., SUTO, M., NEMOTO, N., KAMIYA, K. & ITOMAN, M. 2012. Repeated freeze-thaw cycles reduce the survival rate of osteocytes in bone-tendon constructs without affecting the mechanical properties of tendons. Cell Tissue Bank, 13, 71-80.

SUZUKI, K., SUZUKI, Y., TANIHARA, M., OHNISHI, K., HASHIMOTO, T., ENDO, K. & NISHIMURA, Y. 2000. Reconstruction of rat peripheral nerve gap without sutures using freeze-dried alginate gel. J Biomed Mater Res, 49, 528-33.

TAYLOR, C. A., BRAZA, D., RICE, J. B. & DILLINGHAM, T. 2008. The incidence of peripheral nerve injury in extremity trauma. Am J Phys Med Rehabil, 87, 381-5.

THOMPSON, D. M. & BUETTNER, H. M. 2004. Oriented Schwann cell monolayers for directed neurite outgrowth. Ann Biomed Eng, 32, 1120-30.

THOMPSON, D. M. & BUETTNER, H. M. 2006. Neurite outgrowth is directed by schwann cell alignment in the absence of other guidance cues. Ann Biomed Eng, 34, 161-8.

THOMPSON, J. C. 2016. Netter's concise orthopaedic anatomy, Philadelphia, PA, Saunders Elsevier.

THONHOFF, J. R., OJEDA, L. & WU, P. 2009. Stem cell-derived motor neurons: applications and challenges in amyotrophic lateral sclerosis. Curr Stem Cell Res Ther, 4, 178-99.

THORNTON, M. R., MANTOVANI, C., BIRCHALL, M. A. & TERENGHI, G. 2005. Quantification of N-CAM and N-cadherin expression in axotomized and crushed rat sciatic nerve. J Anat, 206, 69-78.

TOHDA, C. & JACOBOWITZ, D. M. 1999. The function and expression of sproutin, a novel neurite outgrowth factor. Neuroreport, 10, 2089-94.

TOHILL, M. P., MANN, D. J., MANTOVANI, C. M., WIBERG, M. & TERENGHI, G. 2004. Green fluorescent protein is a stable morphological marker for schwann cell transplants in bioengineered nerve conduits. Tissue Eng, 10, 1359-67.

TOMEI, A. A., BOSCHETTI, F., GERVASO, F. & SWARTZ, M. A. 2009. 3D collagen cultures under well-defined dynamic strain: a novel strain device with a porous elastomeric support. Biotechnol Bioeng, 103, 217-25.

TOMITA, K., MADURA, T., SAKAI, Y., YANO, K., TERENGHI, G. & HOSOKAWA, K. 2013. Glial differentiation of human adipose-derived stem cells: implications for cell-based transplantation therapy. Neuroscience, 236, 55-65.

TONG, L., JI, L., WANG, Z., TONG, X., ZHANG, L. & SUN, X. 2010. Differentiation of neural stem cells into Schwann-like cells *in vitro*. Biochem Biophys Res Commun, 401, 592-7.

TONGTAKO, W., LEHMBECKER, A., WANG, Y., HAHN, K., BAUMGARTNER, W. & GERHAUSER, I. 2017. Canine dorsal root ganglia satellite glial cells represent an exceptional cell population with astrocytic and oligodendrocytic properties. Sci Rep, 7, 13915.

TORIGOE, K., TANAKA, H. F., TAKAHASHI, A., AWAYA, A. & HASHIMOTO, K. 1996. Basic behavior of migratory Schwann cells in peripheral nerve regeneration. Exp Neurol, 137, 301-8.

TREMBLAY, D., CHAGNON-LESSARD, S., MIRZAEI, M., PELLING, A. E. & GODIN, M. 2014. A microscale anisotropic biaxial cell stretching device for applications in mechanobiology. Biotechnol Lett, 36, 657-65.

TREMP, M., MEYER ZU SCHWABEDISSEN, M., KAPPOS, E. A., ENGELS, P. E., FISCHMANN, A., SCHERBERICH, A., SCHAEFER, D. J. & KALBERMATTEN, D. F. 2015. The regeneration potential after human and autologous stem cell transplantation in a rat sciatic nerve injury model can be monitored by MRI. Cell Transplant, 24, 203-11.

TREPAT, X., CHEN, Z. & JACOBSON, K. 2012. Cell migration. Compr Physiol, 2, 2369-92.

TRICAUD, N. 2018. Myelinating Schwann Cell Polarity and Mechanically-Driven Myelin Sheath Elongation. Frontiers in Cellular Neuroscience, 11.

UEMURA, T., IKEDA, M., TAKAMATSU, K., YOKOI, T., OKADA, M. & NAKAMURA, H. 2014. Long-term efficacy and safety outcomes of transplantation of induced pluripotent stem cell-derived neurospheres with bioabsorbable nerve conduits for peripheral nerve regeneration in mice. Cells Tissues Organs, 200, 78-91.

URBANCHEK, M. G., KUNG, T. A., FROST, C. M., MARTIN, D. C., LARKIN, L. M., WOLLSTEIN, A. & CEDERNA, P. S. 2016. Development of a Regenerative Peripheral Nerve Interface for Control of a Neuroprosthetic Limb. Biomed Res Int, 2016, 5726730.

VAEGTER, C. B. 2014. Neurotrophins and their receptors in satellite glial cells following nerve injury. Neural Regen Res, 9, 2038-9.

VECTORMINE. (2018). Peripheral nervous system, medical vector illustration diagram with full body nerve scheme. [Online image] Available at: https://depositphotos.com/187186576/stock-illustration-peripheral-nervous-system-medical-vector.html [Accessed 04/01/22].

VIADER, A., GOLDEN, J. P., BALOH, R. H., SCHMIDT, R. E., HUNTER, D. A. & MILBRANDT, J. 2011. Schwann cell mitochondrial metabolism supports long-term axonal survival and peripheral nerve function. J Neurosci, 31, 10128-40.

VILLA, G., FUMAGALLI, M., VERDERIO, C., ABBRACCHIO, M. P. & CERUTI, S. 2010. Expression and contribution of satellite glial cells purinoceptors to pain transmission in sensory ganglia: an update. Neuron Glia Biol, 6, 31-42.

VON GUIONNEAU, N., SARHANE, K. A., BRANDACHER, G., HETTIARATCHY, S., BELZBERG, A. J. & TUFFAHA, S. 2020. Mechanisms and outcomes of the supercharged end-to-side nerve transfer: a review of preclinical and clinical studies. J Neurosurg, 134, 1590-1598.

WAGNER, M. A., MARKS, W. H. & BHATIA, S. K. 2014. Hydrogel encapsulation to improve cell viability during syringe needle flow. J Long Term Eff Med Implants, 24, 151-62.

WANG, H. K., WANG, Y. X., XUE, C. B., LI, Z. M., HUANG, J., ZHAO, Y. H., YANG, Y. M. & GU, X. S. 2016. Angiogenesis in tissue-engineered nerves evaluated objectively using MICROFIL perfusion and micro-CT scanning. Neural Regen Res, 11, 168-73.

WANG, H., ABHILASH, A. S., CHEN, C. S., WELLS, R. G. & SHENOY, V. B. 2014. Long-range force transmission in fibrous matrices enabled by tension-driven alignment of fibers. Biophys J, 107, 2592-603.

WANG, L. M. & KUHL, E. 2019. Viscoelasticity of the axon limits stretch-mediated growth. Computational Mechanics, 65, 587.

WANG, X. B., MA, W., LUO, T., YANG, J. W., WANG, X. P., DAI, Y. F., GUO, J. H. & LI, L. Y. 2019. A novel primary culture method for high-purity satellite glial cells derived from rat dorsal root ganglion. Neural Regen Res, 14, 339-345.

WANNER, I. B. & WOOD, P. M. 2002. N-cadherin mediates axon-aligned process growth and cell-cell interaction in rat Schwann cells. J Neurosci, 22, 4066-79.

WEI, Y., ZHOU, J., ZHENG, Z., WANG, A., AO, Q., GONG, Y. & ZHANG, X. 2009. An improved method for isolating Schwann cells from postnatal rat sciatic nerves. Cell Tissue Res, 337, 361-9.

WEINBERGER, F., MANNHARDT, I. & ESCHENHAGEN, T. 2017. Engineering Cardiac Muscle Tissue: A Maturating Field of Research. Circ Res, 120, 1487-1500.

WEISS, P. 1934. *In vitro* experiments on the factors determining the course of the outgrowing nerve fiber. Journal of Experimental Zoology, 68, 393-448.

WEISS, P. 1945. Experiments on cell and axon orientation *in vitro*; the role of colloidal exudates in tissue organization. J Exp Zool, 100, 353-86.

WEISS, P. A. 1941. Nerve patterns: the mechanics of nerve growth, [United States], [publisher not identified].

WEN, Q. & JANMEY, P. A. 2013. Effects of non-linearity on cell-ECM interactions. Exp Cell Res, 319, 2481-9.

WENG, S., SHAO, Y., CHEN, W. & FU, J. 2016. Mechanosensitive subcellular rheostasis drives emergent single-cell mechanical homeostasis. Nat Mater, 15, 961-967.

WERNIG, M., BENNINGER, F., SCHMANDT, T., RADE, M., TUCKER, K. L., BUSSOW, H., BECK, H. & BRUSTLE, O. 2004. Functional integration of embryonic stem cell-derived neurons *in vivo*. J Neurosci, 24, 5258-68.

WILLIAMS, L. R., LONGO, F. M., POWELL, H. C., LUNDBORG, G. & VARON, S. 1983. Spatial-temporal progress of peripheral nerve regeneration within a silicone chamber: parameters for a bioassay. J Comp Neurol, 218, 460-70.

WOLPOWITZ, D., MASON, T. B., DIETRICH, P., MENDELSOHN, M., TALMAGE, D. A. & ROLE, L. W. 2000. Cysteine-rich domain isoforms of the neuregulin-1 gene are required for maintenance of peripheral synapses. Neuron, 25, 79-91.

WU, G., LU, Z. H., OBUKHOV, A. G., NOWYCKY, M. C. & LEDEEN, R. W. 2007. Induction of calcium influx through TRPC5 channels by cross-linking of GM1 ganglioside

associated with alpha5beta1 integrin initiates neurite outgrowth. J Neurosci, 27, 7447-58.

WU, X., HE, L., LI, W., LI, H., WONG, W. M., RAMAKRISHNA, S. & WU, W. 2017. Functional self-assembling peptide nanofiber hydrogel for peripheral nerve regeneration. Regen Biomater, 4, 21-30.

XIAO, J., DUAN, H., LIU, Z., WU, Z., LAN, Y., ZHANG, W., LI, C., CHEN, F., ZHOU, Q., WANG, X., HUANG, J. & WANG, Z. 2011. Construction of the recellularized corneal stroma using porous acellular corneal scaffold. Biomaterials, 32, 6962-71.

XU, Q., CHEN, F., WANG, Y., LI, X. & HE, J. 2014. Development of a miniaturized bioreactor for neural culture and axon stretch growth. Conf Proc IEEE Eng Med Biol Soc, 2014, 1416-9.

YAMADA, K. M. & SIXT, M. 2019. Mechanisms of 3D cell migration. Nat Rev Mol Cell Biol, 20, 738-752.

YAMAMOTO, T., OSAKO, Y., ITO, M., MURAKAMI, M., HAYASHI, Y., HORIBE, H., IOHARA, K., TAKEUCHI, N., OKUI, N., HIRATA, H., NAKAYAMA, H., KURITA, K. & NAKASHIMA, M. 2016. Trophic Effects of Dental Pulp Stem Cells on Schwann Cells in Peripheral Nerve Regeneration. Cell Transplant, 25, 183-93.

YANG, F., MURUGAN, R., RAMAKRISHNA, S., WANG, X., MA, Y. X. & WANG, S. 2004. Fabrication of nano-structured porous PLLA scaffold intended for nerve tissue engineering. Biomaterials, 25, 1891-900.

YANNAS, I. V., TZERANIS, D. S., HARLEY, B. A. & SO, P. T. 2010. Biologically active collagen-based scaffolds: advances in processing and characterization. Philos Trans A Math Phys Eng Sci, 368, 2123-39.

YI, S., TANG, X., YU, J., LIU, J., DING, F. & GU, X. 2017. Microarray and qPCR Analyses of Wallerian Degeneration in Rat Sciatic Nerves. Front Cell Neurosci, 11, 22.

YOON, Y., KIM, H. S., JEON, I., NOH, J. E., PARK, H. J., LEE, S., PARK, I. H., STEVANATO, L., HICKS, C., CORTELING, R., BARKER, R. A., SINDEN, J. D. & SONG, J. 2020. Implantation of the clinical-grade human neural stem cell line, CTX0E03, rescues the behavioral and pathological deficits in the quinolinic acid-lesioned rodent model of Huntington's disease. Stem Cells, 38, 936-947.

YOU, H., WEI, L., LIU, Y., OUDEGA, M., JIAO, S. S., FENG, S. N., CHEN, Y., CHEN, J. M. & LI, B. C. 2011. Olfactory ensheathing cells enhance Schwann cell-mediated

anatomical and functional repair after sciatic nerve injury in adult rats. Exp Neurol, 229, 158-67.

YUK, H., VARELA, C. E., NABZDYK, C. S., MAO, X., PADERA, R. F., ROCHE, E. T. & ZHAO, X. 2019. Dry double-sided tape for adhesion of wet tissues and devices. Nature, 575, 169-174.

ZALEWSKI, A. A. 1970. Effects of reinnervation on denervated skeletal muscle by axons of motor, sensory, and sympathetic neurons. Am J Physiol, 219, 1675-9.

ZHANG, Q. Y., ZHANG, Y. Y., XIE, J., LI, C. X., CHEN, W. Y., LIU, B. L., WU, X. A., LI, S. N., HUO, B., JIANG, L. H. & ZHAO, H. C. 2014. Stiff substrates enhance cultured neuronal network activity. Sci Rep, 4, 6215.

ZHANG, W., FANG, X., ZHANG, C., LI, W., WONG, W. M., XU, Y., WU, W. & LIN, J. 2017. Transplantation of embryonic spinal cord neurons to the injured distal nerve promotes axonal regeneration after delayed nerve repair. Eur J Neurosci, 45, 750-762.

ZHANG, W., HUANG, G. & XU, F. 2020. Engineering Biomaterials and Approaches for Mechanical Stretching of Cells in Three Dimensions. Front Bioeng Biotechnol, 8, 589590.

ZHANG, Z., YU, B., GU, Y., ZHOU, S., QIAN, T., WANG, Y., DING, G., DING, F. & GU, X. 2016. Fibroblast-derived tenascin-C promotes Schwann cell migration through beta1-integrin dependent pathway during peripheral nerve regeneration. Glia, 64, 374-85.

ZHAO, L., QU, W., WU, Y., MA, H. & JIANG, H. 2014. Dorsal root ganglion-derived Schwann cells combined with poly(lactic-co-glycolic acid)/chitosan conduits for the repair of sciatic nerve defects in rats. Neural Regen Res, 9, 1961-7.

ZHENG, J., LAMOUREUX, P., SANTIAGO, V., DENNERLL, T., BUXBAUM, R. E. & HEIDEMANN, S. R. 1991. Tensile regulation of axonal elongation and initiation. J Neurosci, 11, 1117-25.

ZHONG, Z. G., NODA, M., TAKAHASHI, H. & HIGASHIDA, H. 1999. Overexpression of rat synapsins in NG108-15 neuronal cells enhances functional synapse formation with myotubes. Neurosci Lett, 260, 93-6.